NOVEL SOLID FORMS OF ACTIVE PHARMACEUTICAL INGREDIENTS (APIs) AND THEIR PHYSICOCHEMICAL PROPERTIES
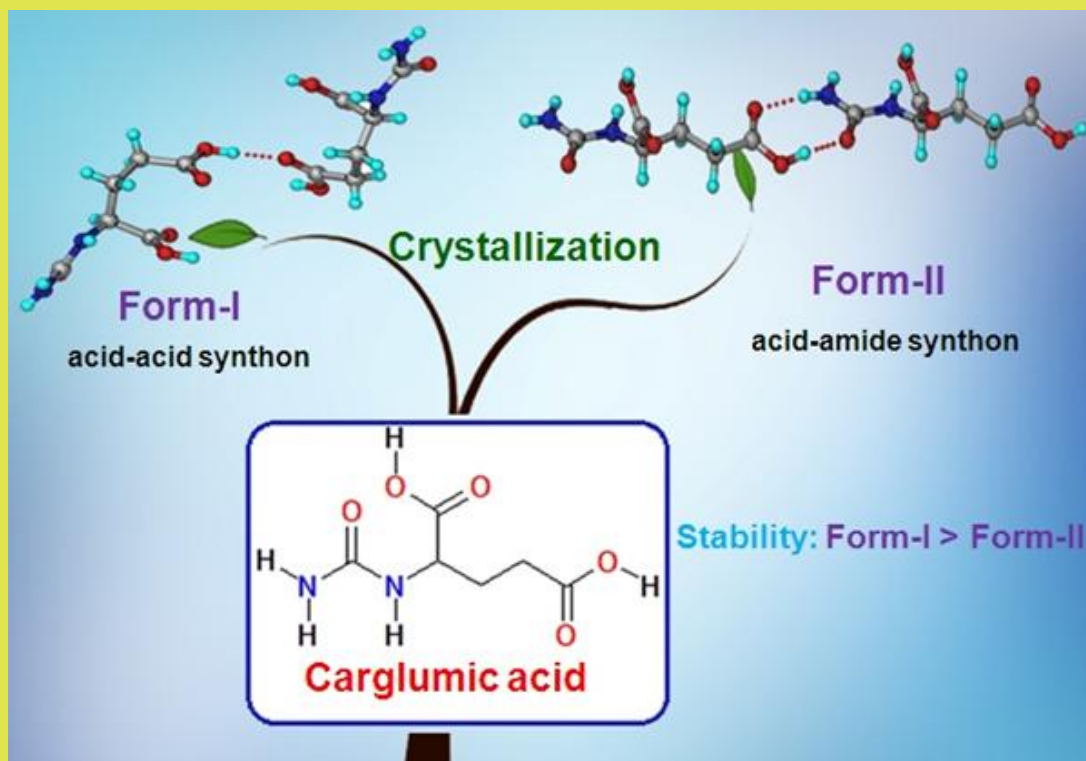
A Thesis Submitted during 2009-2015 to the
University of Hyderabad in partial fulfillment of
the Award of a Ph.D. Degree in Chemistry

By

D. Maddileti

School of Chemistry

University of Hyderabad

(P.O.) Central University, Gachibowli

Hyderabad-500046

Telangana State

India

Anti-hyperammonemic drug carglumic acid resulted in two polymorphs Form-I and Form-II. Crystal structure of Form-I is sustained by acid-acid catemer synthon whereas Form-II has acid-amide heterosynthon. Form-I is the thermodynamically stable form.

NOVEL SOLID FORMS OF ACTIVE PHARMACEUTICAL INGREDIENTS (APIs) AND THEIR PHYSICOCHEMICAL PROPERTIES

A Thesis Submitted during 2009-2015 to the University of Hyderabad in partial fulfillment of the Award of a Ph.D. Degree in Chemistry

By

D. Maddileti

School of Chemistry

University of Hyderabad

(P.O.) Central University, Gachibowli

Hyderabad-500046

Telangana State

India

DEDICATION

To

Amma & Nanna

CERTIFICATE

This is to certify that the thesis entitled **"Novel Solid Forms of Active Pharmaceutical Ingredients (APIs) and their Physicochemical Properties"** submitted by **D. Maddileti** bearing Regd. No. 09CHPH06 in partial fulfillment of the requirements for the award of Doctor of Philosophy in Chemistry is a bonafide work carried out by him under my supervision and guidance which is a plagiarism free thesis.

The thesis has not been submitted previously in part or in full to this or any other University or Institution for the award of any degree or diploma.

Prof. Ashwini Nangia   **Dean**

Signature of the Supervisor   School of Chemistry

DECLARATION

I, **D. Maddileti**, hereby declare that this thesis entitled **"Novel Solid Forms of Active Pharmaceutical Ingredients (APIs) and their Physicochemical Properties"** submitted by me under the guidance and supervision of **Professor Ashwini Nangia** is a bonafide research work which is also free from plagiarism. I also declare that it has not been submitted previously in part or in full to this University or any other University or Institution for the award of any degree or diploma. I hereby agree that my thesis can be deposited in Shodganga/INFLIBNET.

Hyderabad

Name: **D. Maddileti**

Date:

Signature:

Regd. No. 09CHPH06

ACKNOWLEDGEMENTS

SYNOPSIS

This thesis entitled "**Novel Solid Forms of Active Pharmaceutical Ingredients (APIs) and their Physicochemical Properties**" consists of seven chapters

CHAPTER ONE

Crystal Engineering and Pharmaceutical Solids

Traditionally, there have been three branches of chemistry: organic, physical, inorganic, with some arguments in favour of including analytical as a fourth branch of chemistry. An alternative and a fairly new classification is to divide chemistry into two broad areas: molecular (includes liquids and gases) and non-molecular chemistry (or solid state). In addition, solid-state supramolecular chemistry is a new and rapidly progressing field in chemistry, biology, physics and materials science. It is about the chemistry of molecular assemblies (beyond molecules) and of intermolecular interactions (non-covalent bonds). Within the realm of supramolecular chemistry a well-defined area is *crystal engineering*, devoted to the design and studies of crystals with desirable physical and chemical and mechanical properties. Pepinsky first introduced the term "*Crystal Engineering*" in 1955, it was implemented by Schmidt in the context of organic solid-state photochemical reactions around 1970, and the general meaning of the term was proposed by Desiraju (in 1989) as "*the understanding of intermolecular interactions in the context of crystal packing and the utilization of such understanding in the design of new solids with desired physical and chemical properties*". Crystal engineering is an interdisciplinary field dealing with the prediction and control of the structure and the functional properties of solids. Two popular strategies currently in vogue for crystal engineering studies in the context of pharmaceutical and materials applications are based on manipulation of hydrogen bonding and coordination polymers. Some of the key research areas within the realm of crystal engineering are catalysis, optical materials, conducting and magnetic materials, nanotechnology, electronic materials and sensors, nano and microporous materials, supramolecular devices, protein-receptor binding, molecular modeling, drug design and improving properties of existing APIs. Today, crystal engineering is popular among academic and industrial chemists for its ability to design novel pharmaceutical solid forms for improved drug development.

Poor aqueous solubility of emerging new chemical entities as well as older drug molecules, represent a barrier to solid oral dosage form development and optimal clinical performance. Depending on the design strategies and developmental procedures, a pharmaceutical solid may exist in a single or a multi-component form. Generally different solid forms such as polymorphs, amorphous forms, salts, cocrystals, hydrates/solvates etc. are used to modulate physicochemical properties of drug molecules. As there is no single solution to the problems arising from the physicochemical behavior of drug forms, it is absolutely essential to screen for all possible solid forms depending on the specific issue to be addressed. Multi component solids of a drug may be in the form of a 'Salt' where the components are held together by ionic interactions, or 'Hydrate/ Solvate' where the crystal lattice of parent molecule contains of water/solvent molecules. Conventionally salts and amorphous forms of the drug are prepared to address the issues associated with the drug, but amorphous forms have stability issues; salts can be hygroscopic and not all drug molecules form salts and synergism via a partner molecule is not possible. In this context, cocrystals offer a new methodology and API's can be modified into 'Cocrystals', a recently popularized multicomponent system where the stoichiometric components are solids at ambient conditions and are held together by non-covalent interactions. Polymorphism is the phenomenon wherein the same chemical compound exists in different crystalline forms without anymore change in chemical formula. Today, it is one of the most promising and well established branches of the solid-state chemistry because polymorphic forms of drugs may be entitled to independent patent protection if they show new and improved properties over the known crystal forms. With the growing importance of generic drugs in the market, the importance of the crystal engineering to the pharmaceutical industry is also expected to grow exponentially. Hence, diversity in the nature of pharmaceutical solid forms is essential because the pathological profile of a disease/infection might demand different formulations of a drug at various stages for effective treatment. This chapter deals with the brief description of crystal engineering principles and its consequence of application in various pharmaceutical solid forms. This is a preface to the other chapters of this thesis which deals with the discovery of novel pharmaceutical solid forms with improved physicochemical properties and superior material characteristics.

CHAPTER TWO

Soluble Cocrystals of Xanthine Oxidase Inhibitor Febuxostat

Febuxostat (2-(3-cyano-4-isobutyloxy)-phenyl-4-methyl-5-thiazolecarboxylic acid, hereafter FEB) is a non-purine selective inhibitor of xanthine oxidase which is used for the management of hyperuricemia in patients with gout. Gout is a disorder caused by the deposition of monosodium urate crystals in joints and tissues as a result of extracellular urate supersaturation. FEB is a BCS class II drug as per Biopharmaceutics Classification System (low solubility, high permeability) having low aqueous solubility of 12.9 mg/L and $D_0 = 25$ (i.e. practically insoluble in water). Several patents are reported on different crystalline forms of FEB, solvates and inorganic salts with Na, K, Li etc., but so far no attempts solid form screening have been performed to address the solubility issue. Our main focus was to address the solubility problems of FEB without compromising the stability by using crystal engineering principles. Here, improving the solubility of BCS class II drug FEB in neutral state without recourse to the obvious sodium salt of the carboxylic acid is necessary because the presence of Na^+ will lead to the precipitation of uric acid as sodium urate crystals, and such crystals cause acute pain at the joints. Thus, the alternative strategy is only with pharmaceutical cocrystals, which is usually a choice method for non-ionizable APIs, is the suitable method for FEB where in such special cases metal carboxylates cause side complications. We prepared pharmaceutical cocrystals of FEB with various GRAS molecules such as urea (URE), acetamide (ACT), nicotinamide (NIC), p-aminobenzoic acid (PABA), and saccharin (SAC) (see Scheme 1).
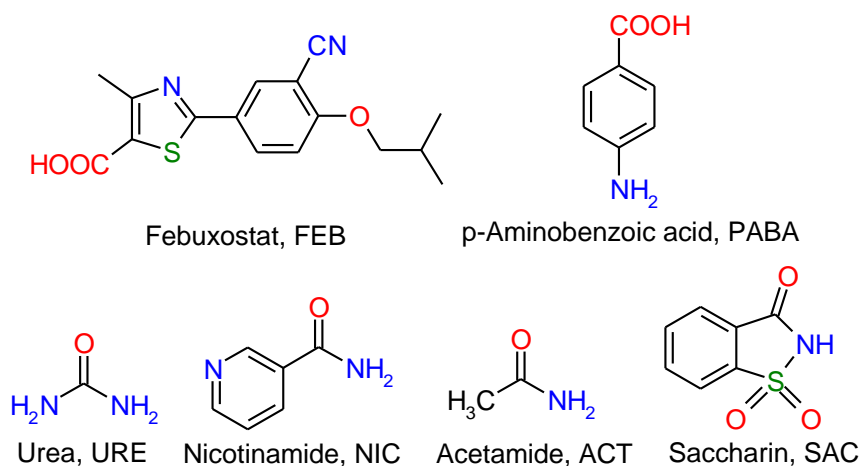
Scheme 1 Chemical Structures of Febuxostat and Coformers studied in this work.

All the new crystalline forms were characterized by solid state spectroscopy techniques, thermal analysis, and X-ray diffraction. The crystal structure of guest free form FEB contains O–H···N hydrogen bond (COOH···N≡C) instead of the expected acid–acid homodimer synthon with the carboxylic acid. The cocrystal structures are sustained by the cyclic synthons of acid–amide (FEB–URE, FEB–NIC) and acid–acid (FEB–PABA), where as FEB–ACT has no distinct ring motif in the crystal structure. The advantage of these cocrystals was ascertained through solubility and dissolution studies. Due to the poor solubility of FEB in aqueous medium, solubility and dissolution experiments were conducted in 60% EtOH–H$_2$O medium. Equilibrium solubility values of FEB cocrystals could not be determined in fact they were unstable in 60% EtOH–H$_2$O medium for 24 h. In dissolution study, all these cocrystals showed an improved dissolution rate compared to the parent drug FEB. As a result, the dissolution rates of cocrystals are in the order of FEB–ACT > FEB–NIC > FEB–PABA > FEB–SAC > FEB–URE > FEB guest free > FEB commercial material. The cocrystals were found to be stable in the solvent medium even after 4 h. The intrinsic dissolution rate curves are displayed in Figure 1.
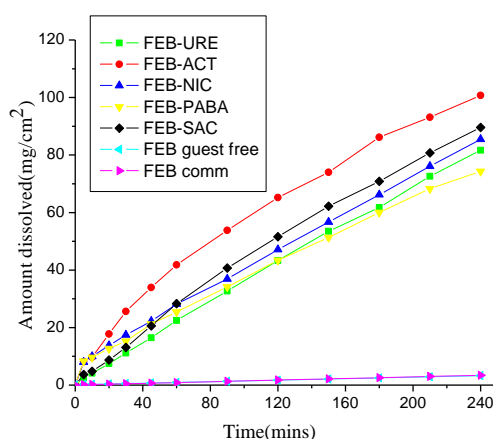
Figure 1 Dissolution curve of FEB cocrystals for 4 h duration.

The improvement in the solubility/dissolution of a drug must be accompanied with good physicochemical stability of the solid form. The physical form stability of FEB cocrystals was established under ICH conditions (accelerated) of 40 °C, 75% RH for 6 weeks. No hydrate formation or the dissociation of the cocrystals to the API and coformer in this study, except for except FEB-ACT. In this study, FEB–ACT showed the

fastest dissolving cocrystal (52.5 times compared to FEB) but it was found to be unstable under ICH conditions of 75% RH at 40 °C. Hence the second best candidate FEB–NIC cocrystal may be preferable for formulation because it is stable and has good dissolution rate (36.6 times faster than FEB). In this chapter we have highlighted that cocrystals represent a viable alternative method to solve the drug issues for an ionizable drug wherein salt formation is not an option for other reasons.

CHAPTER THREE

Tetramorphs of the Antibiotic Drug Trimethoprim: Characterization and Stability

Trimethoprim (hereafter TMP) is a well-known antifolate drug, used mainly in the treatment of urinary tract infections, which selectively inhibits the bacterial species of enzyme dihydrofolate reductase (DHFR). TMP is on the World Health Organization's List of Essential Medicines, a list of the most important medication needed in a basic health system. TMP was first approved by the FDA in combination with sulfamethoxazole (SMZ) in 1973. The combo-drug use has been declining due to reports of SMZ bone marrow toxicity, resistance and lack of greater efficacy in treating common urine and chest infections, and side effects of antibacterial sulfonamides. As a consequence the combination was restricted and following the availability of TMP alone. TMP is a Biopharmaceutics Classification System (BCS) class II drug with high permeability and low solubility (0.4 mg/mL) having dose number (D_0) of 2. In spite of thorough screening of TMP by many research groups for multicomponent systems only one guest free form was reported till today in the CSD, however Bettinetti et al reported three forms of TMP (Form I, Form II, Form III) and TMP hydrate. However, complete characterization, their structural analysis, and stability relationship were not yet been established. Through our comprehensive polymorph screening, we herein report four polymorphs (Forms 1, 2, 3, and 4) and a TMP hemihydrate which were obtained by various techniques such as anti-solvent method, dehydration, freeze drying and spray drying. Polymorphs 1 and 2 from our study matches with Forms I and II reported, and Forms 3 and 4 found to be novel forms in our study. All these forms were characterized by FT-IR, FT-Raman, differential scanning calorimetry (DSC), ^{15}N ss-NMR, Field emission scanning electron microscopy (FESEM), powder X-ray diffraction (PXRD),

and also dynamic vapor sorption (DVS). We were successful in getting the diffraction quality single crystals for Form 1 and Form 2, and crystal structures were determined by X-ray diffraction. Crystal structure analysis shows that both the structures were sustained by N–H⋯N_{arom} hydrogen bonds and the main difference was found to be R_2^2 (8) type I and type II motifs in Form 1, and R_2^2 (8) type III and R_3^2 (8) motifs in Form 2 (Figure 2).
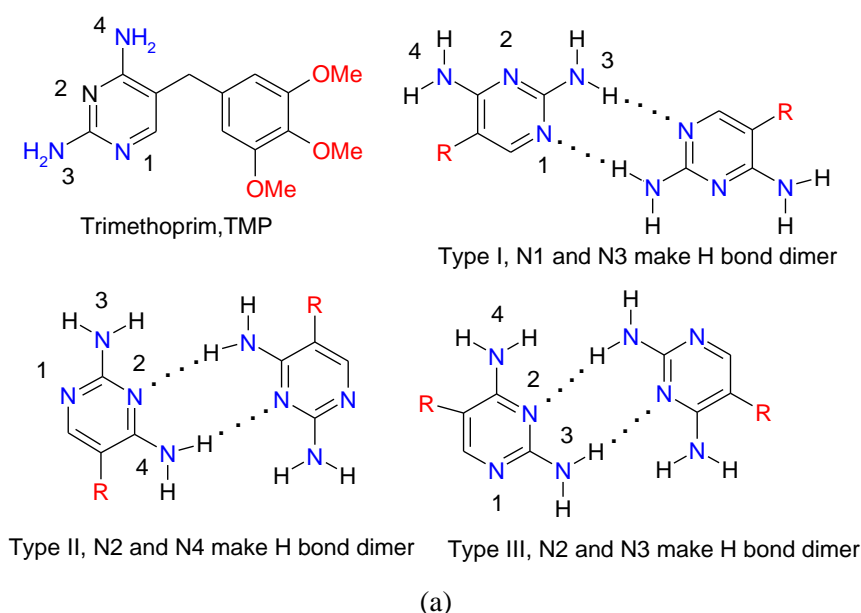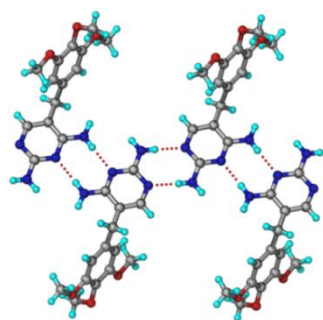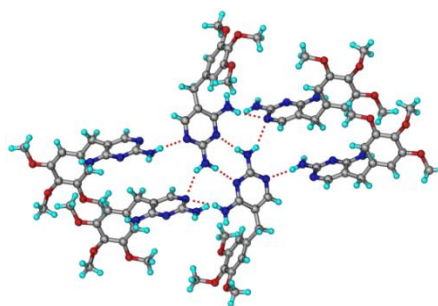
Figure 2 (a) Molecular structure of Trimethoprim and hydrogen bonded synthons types in polymorphs. (b) The ribbon H bond network of Form 1 sustained by type I and type II motifs. (c) Inversion related TMP molecules formed dimers through type III motif. The difference between the N–H⋯N dimer motifs I, II and III is the involvement of donor and acceptor groups and placement of R group with respect to the hydrogen-bonded dimer.

From structural analysis Form 1 and Form 2 classified as synthon and packing polymorphs and from Hirshfeld surface analysis major interactions were quantified and stability was rationalized between Forms 1 and 2. Further to know the morphology of the forms at the micro level we have recorded scanning electron microscopy (SEM). A thorough inspection of the SEM images indicated that the forms exhibit different morphologies specifically, Form-1 and 3 appeared as block and needle morphologies respectively at 20 μm range and Form-2 and 4 were found to be aggregated flat plate-type morphologies at 2 μm range (Figure 3). The morphologies of the Form-1 (block) and Form-2 (needle) in SEM images were in excellent match with those of the single crystals mounted for X-ray diffraction.

(a)   (b)

(c)   (d)
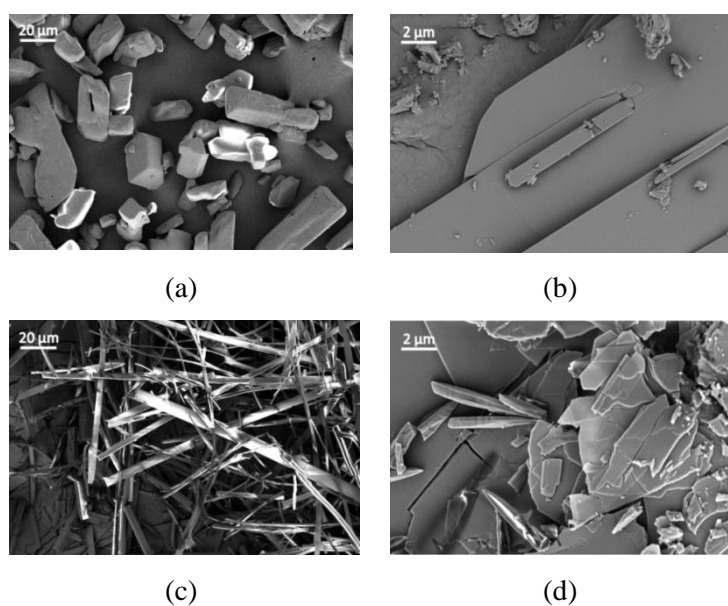
Figure 3 SEM images of the TMP forms (a) Form 1 (b) Form 2 (c) Form 3 (d) Form 4 to show the differences in morphology among the polymorphs.

DVS analysis revealed that all the TMP forms show negligible moisture uptake (< 0.3 %) even at high RH conditions (90%, 40 ºC). All the polymorphs were found to be stable for the test period of three months in accelerated ICH conditions of 40 ºC and 75% RH, except Form 3 which was converted into Form 2. From slurry and grinding experiments Form 2, Form 3 and Form 4 found to be metastable and Form 1 is stable form, and the stability order found to be Form 3 (least stable) < Form 4 < Form 2 < Form 1 (thermodynamic). Slurry, grinding, and thermal experiments suggest that TMP Form 1 is the most stable form for formulation.

CHAPTER FOUR

High Solubility Crystalline Pharmaceutical Forms of Blonanserin

Blonanserin (BLN) is a novel antipsychotic agent, having dopamine D2 and serotonin 5-HT2A receptor antagonist properties. It belongs to the series of 4-phenyl-2-(1-piperazinyl) pyridines, a second-generation antipsychotic agent which is used to treat schizophrenia. Schizophrenia is a heterogeneous devastating psychiatric disorder characterized by positive, negative, affective, and cognitive symptoms. BLN overcomes this drawbacks other drugs (such as haloperidol and chlorpromazine) in the treatment of both positive and negative symptoms of schizophrenia without extra-pyramidal symptoms. BLN is a basic drug molecule in Biopharmaceutics Classification System (BCS) Category II (low solubility, high permeability) with aqueous solubility of 0.033 mg/L. BLN form B was reported in patent CN101747272 (A) and a few organic and inorganic salts were mentioned in a US patent. Our literature survey suggested an opportunity to improve the solubility and dissolution of BLN by making salts and cocrystals of the drug. The drug was screened with several Generally Regarded As Safe (GRAS) molecules for salt and cocrystal forms (Scheme 2). Liquid-assisted grinding and solvent evaporative crystallization with GRAS coformers resulted in four salts ($BLNH^+$–SUC^-, $BLNH^+$–NIA^-, $BLNH^+$–TsO^- and $BLNH^+$–MSA^-), one salt hydrate ($BLNH^+$–MSA^-–H_2O), and one cocrystal (BLN–SBA). All the novel solid forms were characterized by thermal, spectroscopic and X-ray diffraction techniques. Single crystal structures were determined for all the solid forms and in the crystal structures proton transferred to the piperazine N_3 atom of BLN and sustained by N^+–$H \cdots O^-$ ionic H-bond, except in BLN–SBA which has neutral $COOH \cdots N$(tertiary amine) H-bond.
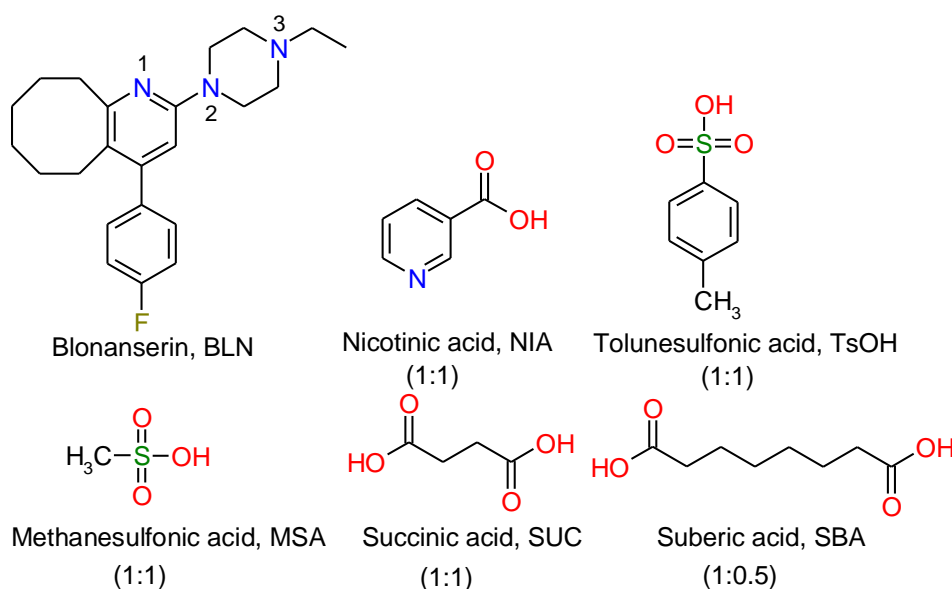
Scheme 2 Chemical structures of Blonanserin and coformers used in this study. The stoichiometry of API:coformer ratio is mentioned in brackets.

Solubility remains a major hurdle for BCS class II drugs (low solubility, high permeability) since bioavailability is limited by poor dissolution. Solubility and dissolution studies on BLN solid forms were conducted in 60% EtOH−water medium because the solubility of pure BLN in water is very low (0.033 mg/L), and in 60% EtOH−water 1.6 mg/mL. The solubility of the new solid forms in this study (measured at 24 h) was superior to that of the reference drug BLN. BLNH$^+$–MSA$^−$–H$_2$O exhibited the highest solubility (742.9 mg/mL, 464 times higher) and the second highest is BLNH$^+$–NIA$^−$ (408.2 mg/mL, 255 times higher). IDR experiments on BLN solid forms exhibited improved dissolution rate compared to the parent drug and were stable until the end of the IDR experimental conditions as confirmed by PXRD of the residue at 45-60 min (Figure 4). BLNH$^+$–MSA$^−$ salt was converted to its monohydrate form as expected. The extent of solid form dissolved over 30 min was BLNH$^+$–MSA$^−$–H$_2$O 74%, BLNH$^+$–MSA$^−$ 68%, BLNH$^+$–TsO$^−$ 65%, BLNH$^+$–SUC$^−$ 51%, BLNH$^+$–NIA$^−$ 38%, BLN–SBA 6%, BLN 0.5%. BLNH$^+$–MSA$^−$ salt exhibited faster dissolution for the first 23 min but dropped below BLNH$^+$–MSA$^−$–H$_2$O salt hydrate between 23-45 min (Figure 4), perhaps due to conversion of anhydrous BLNH$^+$–MSA$^−$ salt to the monohydrate salt. All the salts are faster dissolving compared to BLN–SBA cocrystal. The calculated IDR values of the

solid forms followed the order $BLNH^+–MSA^- > BLNH^+–MSA^-–H_2O > BLNH^+–NIA^- > BLNH^+–TsO^- > BLNH^+–SUC^- > BLN–SBA > BLN$.
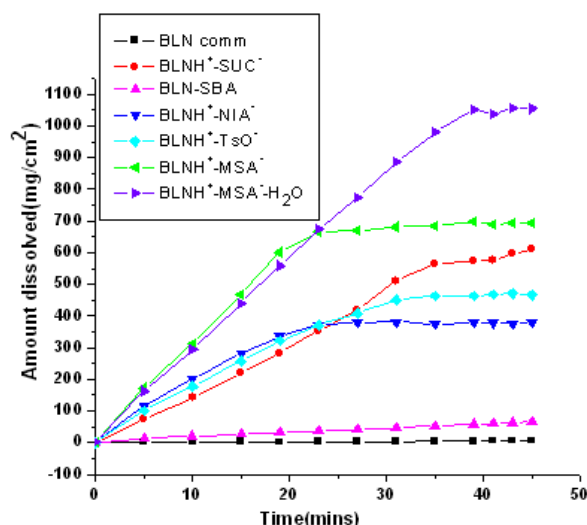
Figure 4 Intrinsic dissolution curves of BLN solid forms.

We also tested the solid forms for stability in accelerated WHO/ICH conditions (40 °C, 75% RH). They were stable in the test period of 2 months, except $BLN^+–MSA^-$ anhydrous salt which converted to its monohydrate after one month (by PXRD overlay) and $BLNH^+–SUC^-$ salt was stable for 2 months (no polymorphic change by PXRD).The salt hydrate exhibited the best dissolution rate as well as good form stability in solubility and humidity conditions. Thus, $BLNH^+–MSA^-–H_2O$ salt hydrate is a potential lead in drug formulation of Blonanserin as a stable, soluble salt. Moreover, the salt former MSA is completely safe for e.g. imatinib mesylate is a marketed drug, and several hydrates are marketed as drugs for e.g. Cephradine dihydrate. Our objective to improve the solubility of BLN without compromising solid form stability was achieved at the end of this study in this chapter.

CHAPTER FIVE

Polymorphism in Anti-hyperammonemic agent N-Carbmoyl-L-Glutamic acid

Carglumic acid is an orphan drug used for the treatment of hyperammonaemia in patients with N-acetylglutamate synthase (NAGS) deficiency. NAGS deficiency is one of the most severe and rarest of the hereditary urea cycle disorders (UCDs). This rare genetic disorder results in elevated blood levels of ammonia, which can eventually cross the blood–brain barrier and cause neurologic problems, cerebral edema, coma, and eventually death. CGA is a structural analogue of N-acetylglutamate, the naturally occurring activator of carbamoyl phosphate synthetase (CPS) and helps to break down ammonia, which results in reduction of blood levels and toxic effects. CGA is a acidic drug molecule in the form of white crystalline powder having aqueous solubility of 19.1 mg/mL and practically insoluble in organic solvents may be due to dicarboxylic nature. Even though the condition hyperammonemia is rare and it is particularly toxic to the central nervous system (CNS). The studies on the disease are limited due to the rarity of the disease. The crystal structures of the structural analog N-acetylglutamate has been reported in CSD (Refcode: TERRUD and TERRUD01 multiple determinations of same structure), but no attempts were made to explore the structural landscape of CGA so far to study physicochemical properties of the drug through crystal engineering approach. Hence we have screened for polymorphs of the drug because different polymorphs shown to exhibit different physicochemical properties such as solubility, stability, dissolution rate, melting point, bioavailability, etc., by various techniques like LAG, slurring, rotavap, freez dry, spray dry and solution crystallization. We obtained two polymorphs named Form-I, and Form-II and a degraded form Hydantoin-5-propionic acid (5-HPA), and report their complete characterization, phase transformations and stability studies in this chapter. The molecular structure of CGA and various synthons observed in this study are presented in scheme 3.

L-Carglumic acid, CGA

acid-acid catemer

acid-acid dimer

acid-amide

amide-amide
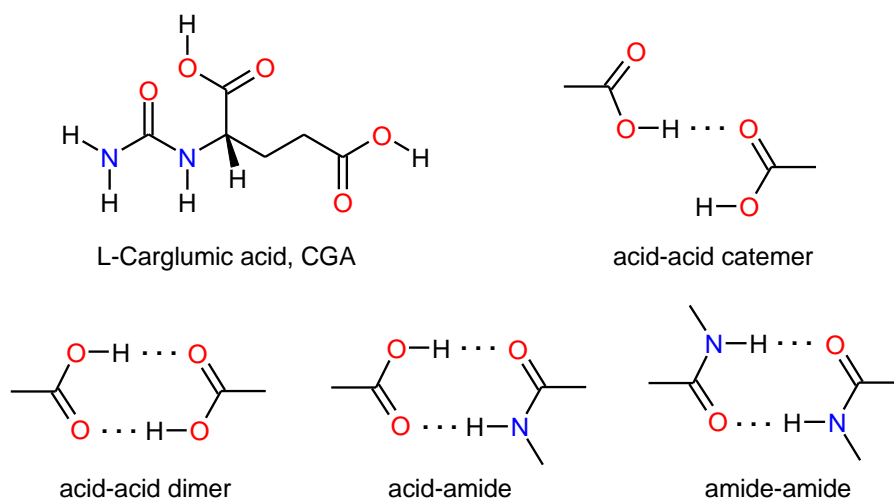
Scheme 3 Molecular structure and various hydrogen bonded synthons observed in our study.

The crystal structure of two novel polymorphs (Form-I in $P2_12_12_1$ and Form-II in $P2_1$ space groups) and a degraded form hydantoin-5-propionic acid (5-HPA) were characterized by X-ray diffraction. From the structural analysis of Form-I acid-acid and acid-amide synthons were observed where as in Form-II only acid-amide synthons were found, and in addition to these expected synthons $N–H\cdots O=C_{acid}$ and $N–H\cdots O=C_{carbamoyl}$ H bonds were present in both the forms (Figure 5a and 5b). Both the polymorphs showed significant conformational difference and hence they can be classified into conformational and synthon polymorphs. Crystal structure of a degraded form 5-HPA sustained by acid-acid and amide-amide synthons is also reporting in this study.

(a)

(b)

(c)
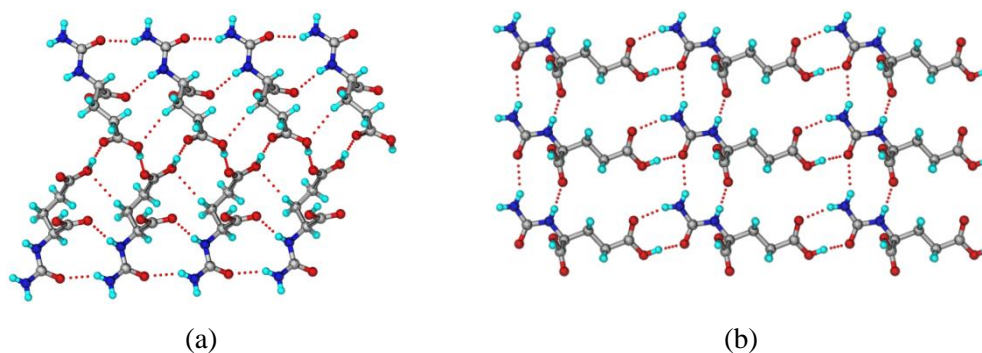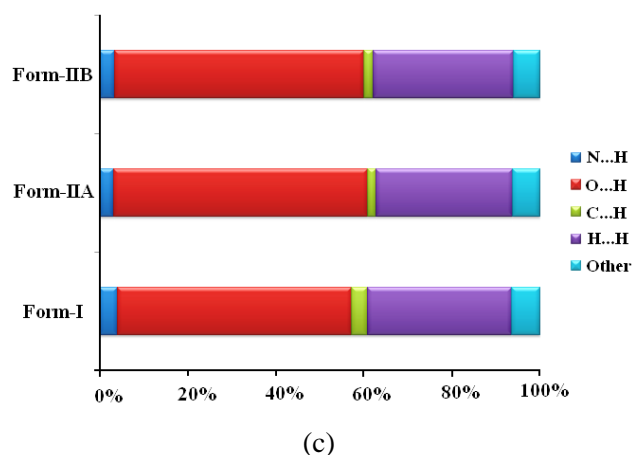
Figure5 (a) 1D tape formed through acid-acid $C(4)$ catemer and supporting C–H⋯O and N–H⋯O interactions. (b) 2D sheet structure formed through acid-amide synthon and N–H⋯O H bonds. (c) Major interactions percentage contributions to the Hirshfeld surface.

The polymorphs of CGA were compared by Hirshfeld surface analysis (d_{norm}) (Figure 5c) and, the bulk phases were distinguished by FT-IR and Raman, ^{13}C ss-NMR, DSC and powder X-ray diffraction line patterns. High melting polymorph (Form-I) has a higher enthalpy of fusion (48.4 kJ/mol) while the lower melting polymorph (Form-II) has lower enthalpy of fusion (36.5 kJ/mol) hence they were monotropically related. Interestingly, we observed that N-carbmoyl-L-glutamic was found to degrade into Hydantoin-5-propionic acid in acidic medium. Both the forms were stable at ambient conditions for more than 6 months and showed excellent stability in accelerated conditions for the test period of 2 months. Relative stability of the forms were established by solid-state grinding and slurry experiments and found that Form-I was thermodynamic and Form-II metastable. In this chapter we found Form-I was found to be the most stable form for formulation purpose.

CHAPTER SIX

Solubility and Stability of Blonanserin Salt Polymorphs

Blonanserin (BLN) is a new antipsychotic agent having dopamine D2 and serotonin 5-HT2 receptor antagonist properties. It was invented by Dainippon Sumitomo Pharma and launched in 2008 under the brand name Lonasen in Japan and Korea for the treatment of schizophrenia. BLN is effective towards positive symptoms of schizophrenia (such as

hallucinations and delusions) and negative symptoms of schizophrenia (such as flat affect and hypobulia). The crystal structure of blonanserin was reported by Suzuki et al. This compound is structurally unrelated to existing antipsychotics such as haloperidol, chlorpromazine and risperidone. Compared to many other antipsychotics, blonanserin has improved tolerability profile, lacking side effects such as extrapyramidal symptoms, excessive sedation and hypotension. A usual maintenance dose of Lonasen is 8–16 mg per day, and the highest dose is 24 mg per day. Generally salt forms of drugs are preferred due to higher solubility, improved stability, and ease of filtration. After the study of various salts of BLN in chapter 4 we found that few salts found to exhibit polymorphic behaviour. The salts with hydrochloric acid (HCl), succinic acid (SUC), and methane sulfonic acid (MSA) were found to be dimorphs (scheme 4). Our main intension of the work was to understand the behaviour of BLN salt polymorphs towards solubility, dissolution, stability and also to explore phase transformations behaviour.
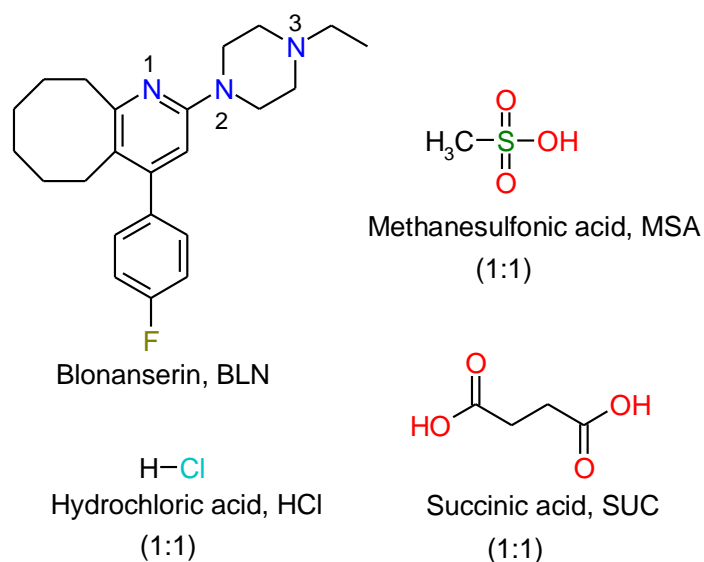
Scheme 4 Chemical structures of Blonanserin and saltformers which resulted salt polymorphs. The stoichiometry of API:coformer ratio is mentioned in brackets.

A proton is transferred to the piperazine N_3 position of BLN in all the salt structures. The $BLNH^+$–Cl^- salt was found to exhibit two polymorphs $BLNH^+$–Cl^-–Form-I and $BLNH^+$–Cl^-–Form-II. The $BLNH^+$–Cl^-–Form-I showed the endothermic phase transition at 200 °C and transformed to $BLNH^+$–Cl^-–Form-II and it is solid-to-solid transformation event by HSM and VT PXRD. Thus, the two polymorphs (Form-I and II) are enantiotropically

related. Similarly, salts with SUC and MSA found to exhibit polymorphic behavior. In DSC, $BLNH^+–MSA^-$–Form-II showed exothermic transition and converted into Form-I upon further heating hence both forms were monotropically related. Whereas in case of $BLNH^+–SUC^-$ salt forms I and II it was difficult define this behavior as an enantiotropic or a monotropic, because Form-II showed endothermic transition immediately followed by recrystallization to other polymorph.
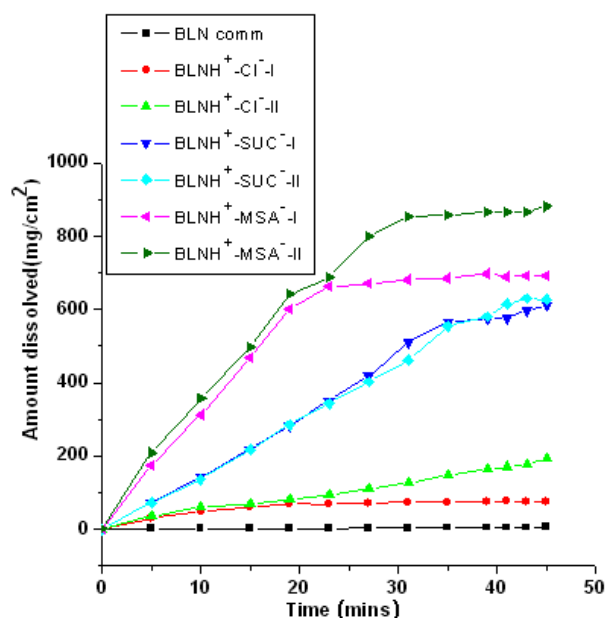
Figure 6 IDR curves of BLN salt polymorphs.

The relative stability $BLNH^+–Cl^-$ –Form-I , II and $BLNH^+–Cl^-$ salt monohydrate were established by grinding and slurry experiments and found that stability order as $BLNH^+–Cl^-$ monohydrate > $BLNH^+–Cl^-$–Form-I > $BLNH^+–Cl^-$–Form-II. With the similar experiments the stability order for $BLNH^+–MSA^-$ salt forms were found to be $BLNH^+–MSA^-$–Form-I > $BLNH^+–MSA^-$–Form-II and that of $BLNH^+–SUC^-$ salt forms in the order $BLNH^+–SUC^-$–Form-II > $BLNH^+–SUC^-$ –Form-I. For all the three salt polymorphic systems we have studied solubility and dissolution studies and found that they show improved solubility and dissolution than the parent drug (Figure 6). The calculated IDR values of the solid forms followed the order $BLNH^+–MSA^-$–Form-II > $BLNH^+–MSA^-$–Form-I > $BLNH^+–SUC^-$–Form-I $\approx$ $BLNH^+–SUC^-$–Form-II > $BLNH^+–Cl^-$–Form-II > $BLNH^+–Cl^-$–Form-I > BLN. Stability at accelerated conditions (40 °C, 75% RH) showed that salt forms of $BLNH^+–MSA^-$ were found convert into hydrated

form as expected, where as salt forms of BLNH$^+$–Cl$^-$ and BLNH$^+$–SUC$^-$ were found to be stable for 3 months and no polymorphic transformation or hydrate formation observed. In this chapter we have spotlighted screening of polymorphs for salts and found that BLNH$^+$–SUC$^-$–Form-II found to be promising candidate for formulation purpose with high solubility and excellent stability.

CHAPTER SEVEN

Conclusions and Future Prospects

The design of diverse pharmaceutical solid forms of the APIs relies on crystal engineering principles. The study of the nature and properties of different pharmaceutical solids and an understanding the phenomenon which govern their physicochemical behavior will lead to superior drug forms. In this thesis, extensive studies of different solid forms such as polymorphs, salts and their polymorphs, cocrystals, solvates/hydrates of different APIs were carried out to understand and to address the issues associated with the drugs for pharmaceutical applications. In chapter 2, we have highlighted that cocrystals represent a viable alternative for an ionizable API to improve solubility wherein salt formation is not an option. This is because sodium salt of the carboxylic acid functionality of Febuxostat will lead to the precipitation of uric acid as sodium urate crystals, and such crystals cause acute pain at the joints, thus justifying the need to study cocrystals as a potential alternative to salts. Generally any API can result polymorphs if time and money spent on it, and each polymorph will show different physicochemical properties. A thorough understanding of the relationship between a particular solid form and its properties are critical for selecting the most suitable form for formulation. In this context, in Chapter 3 exhaustive polymorphic screening was carried out and four polymorphs of trimethoprim were identified and their phase transformations and stability relationships were established.

In chapter 4 we have highlighted the importance of solid form screening for the low soluble antipsychotic drug Blonanserin. We have prepared pharmaceutical salts and cocrystals of this drug with various GRAS molecules to address the solubility issue. These novel solid phases also showed good stability under accelerated humidity conditions (75% RH, 40 °C) which is an important factor during tabletting and storage of the drug at a bulk scale. Salts and cocrystals can overcome the serious drawbacks found

in metastable polymorphs and amorphous forms of drugs, whose usage as solid formulations for solubility enhancement is sometimes limited due to potential/accidental phase transformations. In chapter 5, we have prepared two novel polymorphs of the anti-hyperammonemic agent N-carbmoyl glutamic acid and particular emphasis on stability relationship between single component polymorphs was highlighted. API is a multifunctional molecule and it is worth to know the self condensation/degradation/phase transformation at different conditions because it has to sustain various steps involved ranging from production to consumption. In this chapter we found Form I was found to be the most stable form for formulation, and in addition to that N-carbmoyl glutamic was found to degrade into Hydantoin-5-propionic acid in acidic medium. Salt formation represents the traditional methodology for solid form development with diverse applications in pharmaceutical industry as discussed in the chapter 4. Salt forms can affect the solubility, permeability, hygroscopicity, and processability of an ionizable drug candidate; thereby providing an effective means to balance the requirements of bioavailability, stability, manufacturability, and patient compliance. In spite of its vast applications and an estimated 50% of drug molecules used in medicinal therapy are administered as salts, polymorphism studies on salts were smaller as compared to single compound ones. However, it is important to know the behaviour of the salt polymorphs because each form can show different physicochemical properties. In this context in chapter 6 the intension was to understand the behaviour of Blonanserin salt polymorphs and solubility, dissolution, stability and phase transformations studies on the polymorphs were discussed. Thus this chapter highlights the proper selection of suitable polymorphic form of a salt as one of the most important activities that critically affect the successful development of a drug candidate.

CONTENTS

xxx

Chapter Five

Polymorphism in Anti-hyperammonemic agent N-Carbmoyl-L-Glutamic acid 161-192

Chapter Six

Solubility and Stability of Blonanserin Salt Polymorphs 193-226

Chapter Seven

Conclusions and Future Prospects   **227-231**

CHAPTER ONE

CRYSTAL ENGINEERING AND
PHARMACEUTICAL SOLIDS

Schematic representation of various solid forms (polymorphs, hydrates/solvates, cocrystals, salts, amorphous solids, solid solution and eutectic composition) as single and multicomponent systems possible for an Active Pharmaceutical Ingredient (API).

1.1 Crystal Engineering

The desire to understand the intermolecular interactions that exist in the molecular solids with the intention to apply them for the design of solid-state assemblies with tailor-made properties have given birth to the subject of crystal engineering. Crystal engineering is a continuously developing subject in solid state chemistry for the design of new crystal structures with the same or different molecules as building blocks. The quest of crystal engineering to answer the fundamental question: "*Given the molecular structure of a compound, what is its crystal structure?*" has significantly advanced in recent years towards predicting crystal structures of compounds from their molecular structures. The evolution of crystal engineering into a subject may be classified into two phases. This began with Bragg's observation[1] very early in 1921, who noted that the unit cell parameters of naphthalene and anthracene were related. Two axial lengths were nearly same while the third was 8.66 Å in naphthalene and 11.16 Å in anthracene. He concluded that the long axis of the molecules coincided with this third axis and further that the fused benzene ring dimension is approximately 2.50 Å. This is perhaps the earliest correlation between a crystal property and molecular property. Subsequently, significant contributions to the first phase were given by J. M. Robertson[2], one of the most illustrious students of W. H. Bragg. He investigated a large number of polynuclear aromatic hydrocarbons and classified them into two categories in 1951, based on molecular thickness and area. The first category in which molecular thickness is comparable to molecular area, hydrogen rich molecules like naphthalene and anthracene come under this group. In the second category, exemplified by coronene and ovalene, the molecular thickness is smaller than molecular area. In essence, Robertson performed the first systematic experiment in crystal engineering. He crystallized aromatic hydrocarbons, solved their crystal structures and established a correlation between molecular structure to crystal structure. In 1955, Pepinsky[3] introduced the term "Crystal Engineering" for the first time, and the subject was elaborated by Schmidt and coworkers[4] during 1950 to 1970 to address the issue of crystal packing in the context of organic solid state photochemical reactions of cinnamic acids and amides. They systematically established a link between molecular structure and reactivity through studies on the 2+2 cycloaddition reactions of trans-cinnamic acids to cyclobutanes. Based on their observations on dichloro substituted aromatic molecules where the crystal structure has a tendency to adopt a short axis of 4 Å, they synthesized alkenes (trans-

cinnamic acids) that would undergo photodimerization to cyclobutanes. They have crystallized α, β and γ forms of trans-cinnamic acids and irradiated them in the solid state. They found that α and β forms where the intermolecular distance is about 4 Å had undergone cycloaddition reaction whereas the γ form was photo stable (Scheme 1.1).
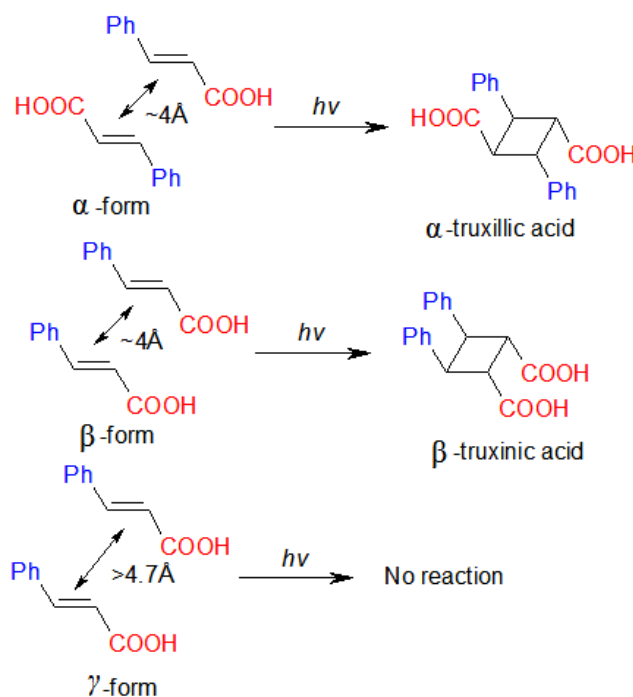
Scheme 1.1 Photo irradiation of α, β forms of trans-cinnamic acid with intermolecular distance of 4 Å has photodimerized to α truxillic and β truxinic acids respectively, whereas γ form with intermolecular distance of >4.7 Å was photo stable (adapted from ref. 4)

In late 1980s and early 1990s the next phase of crystal engineering began and we can call it as the modern crystal engineering phase. In this phase one of the major contributions include the first analysis of an interpenetrated organic solid by Ermer.[5a] He interpreted the crystal structure of adamantane-1,3,5,7-tetracarboxylic acid in terms of interpenetrated networks which could be defined as a pioneering work for describing crystals using topological approach. In addition to his major contributions, Desiraju (1989) provided the general meaning of the term crystal engineering[5b] as "*the understanding of intermolecular interactions in the context of crystal packing and the utilization of such understanding in the design of new solids with desired physical and chemical properties*". Subsequently, in 1990 Robson[6] studied some coordination compounds based on the theme of interpenetration which paved the way to the

investigations on coordination polymers and metal-organic framework structures (MOFs). In brief, the initial interest of crystal engineering was to understand and design organic solids but today, it is a mainstream interdisciplinary field with diverse applications.[7] Some of the key research areas within the realm of crystal engineering are catalysis, optical materials, conducting and magnetic materials, nanotechnology, electronic materials and sensors, nano and microporous materials, supramolecular devices, protein-receptor binding, molecular modeling, drug design and improving properties of existing APIs. Currently, crystal engineering is popular among academic and industrial chemists for its ability to design novel pharmaceutical solid forms for improved drug development.

1.2 Intermolecular Interactions and Supramolecular Synthons

A molecular crystal, is an assembly of millions of molecules held together in a periodic arrangement at an amazing level of precision by intermolecular interactions, guided by molecular recognition and organized self assembly. It is defined by Dunitz as '*a supermolecule par excellence*'[8a] while Lehn termed it as '*a very large supermolecule indeed*'.[8b] The nuts-and-bolts of entire exercise of (i) understanding intermolecular interactions in the context of crystal packing, (ii) developing a strategic plan by which these interactions can lead to a certain desired packing, and (iii) fine-tuning of crystal properties to achieve a pre-determined goal lies in full knowledge of intermolecular interactions. Intermolecular interactions include ion-ion, ion-dipole, dipole-dipole interactions, hydrogen bonding, London forces, etc. These intermolecular interactions are broadly classified as two types, (i) isotropic or non-directional (C···C, C···H, H···H interactions) that defines the shape, size and close packing and (ii) anisotropic or directional as hydrogen bonds, halogen interactions, and heteroatom interactions (e.g. O–H···O, N–H···O, C–H···O, C–H···N, O–H···π, halogen···halogen, nitrogen···halogen, sulfur···halogen, etc.). The importance of isotropic interactions is highlighted by Kitaigorodskii[9] who postulated the atom-atom potential method to describe intermolecular interactions in molecular crystals. This model describes crystals as being derived by the most efficient utilization of space or closest packing, hence it is also popularly known as the '*principle of close packing*'.

Among all intermolecular interactions hydrogen bonding is the most important of all the anisotropic interactions and it has a fundamental role in crystal engineering.[5b, 10] It is the anisotropic character of interactions in a crystal structure that allows one to suggest design strategies for crystals of related molecules. Typical hydrogen bond can be represented as an interaction between a donor X–H and an acceptor Y–Z, represented as X–H ⋯ Y–Z. In the early days of the subject, it was assumed that the elements X and Y are highly electronegative non-metals like F, O or N. It was believed that only in such case X–H could become sufficiently polarised so that it would be attracted electrostatically to the electronegative atom Y, represented as $X^{(\delta-)}$–H $^{(\delta+)}$ ⋯ $Y^{(\delta-)}$–Z. In 1939, Linus Pauling[11a] defined hydrogen bond that "*under certain conditions an atom of hydrogen is attracted by rather strong forces to two toms instead of only one, so that it may be considered to be acting as bond between them*". He pointed out that instead of being attracted only by X, the hydrogen atom is attracted to both X and Y with the assumption of strong forces. Recently (2010), hydrogen bond was redefined[11b] and accepted by IUPAC which states that "*The hydrogen bond is an attractive interaction between a hydrogen atom from a molecule or a molecular fragment X-H in which X is more electronegative than H, and an atom or a group of atoms in the same or a different molecule, in which there is evidence of bond formation*". For practical purpose, hydrogen bonds are classified into three categories[11c] based on their strength as very strong, strong and weak hydrogen bonds (Table 1.1)

Table 1.1 Some properties of very strong, strong and weak hydrogen bonds.

	Very strong	Strong	Weak
Bond Energy (Kcal/mol)	15-40	4-15	< 4
Examples	[F–H⋯F⁻]	O–H⋯O=C	C–H⋯O
IR *vs* relative shift	>25%	5-25%	< 5%
Bond lengths	H–A ≈ X–H	H⋯A > X–H	H⋯A >> X–H
Lengthening of X-H (Å)	0.05–0.2	0.01–0.05	≤ 0.01
D (X⋯A) range (Å)	2.2–2.5	2.5–3.2	3.0–4.0
d (H⋯A) range (Å)	1.2–1.5	1.5–2.2	2.0–3.0
Bonds shorter than vDW	100%	Almost 100%	30-80%
θ (X–H⋯A) range (°)	175–180	130–180	90–180
kT (at room temp.)	>25	7-25	<7

Effect on crystal packing	Strong	Distinctive	Variable
Covalency	Pronounced	Weak	Vanishing
Electrostatics	Significant	dominant	moderate

Adapted from ref. 11c.

In 1967, E. J. Corey[12a, b] coined the term 'Synthon' and defined as "*Structural units within molecules which can be formed and/or assembled by known or conceivable synthetic operations*". Using these synthon strategies in constructing a complex molecule with due consideration to its stereochemical preferences is popularly known as "Retrosynthesis". With the aim to simplify the complex supramolecular architectures which is a result of the compromise between isotropic and anisotropic interactions, Desiraju revived and introduced the term 'Supramolecular synthon'.[12c] Desiraju defined it as "*supramolecular synthons are structural units within supermolecules which can be formed and/or assembled by known or conceivable synthetic operations involving intermolecular interactions*." There is a direct analogy between the *supramolecular synthon* and the *molecular synthon*[12a, b] which was originally proposed by Corey. Subsequently, Zaworotko sub-classified synthons as homosynthons and heterosynthons based on the interacting functional groups. If supramolecular synthon forms between the same functional group it is a homosynthon, if it forms between two different functional groups it is called as heterosynthon.[12d]

As the operating intermolecular interactions are weak in nature, designing a crystal structure effectively becomes a synthon design[7c, 12c, d] which is possible through a vast knowledge of intermolecular interactions in various crystal structures. This can be quickly realised with the access of Cambridge Structural Database (CSD).[13] CSD, is a huge storehouse of crystal structures which has structural information on over 750,000 structures up to now, which represents the excellent contributions of the scientists from various fields as compared to very small entries about 2000 at the time of establishment CSD in 1965. CSD is an excellent tool for accessing and plays a pivotal role in establishing the synthon robustness between two different functional groups based on the number of crystal structures that are deposited with synthon formation between these functional moieties. Some of the well known homosynthons are $COOH \cdots COOH$, $CONH_2 \cdots CONH_2$, $OH \cdots OH$, $NH_2 \cdots NH_2$, halogen$\cdots$halogen, etc. which are between similar functional groups and $COOH \cdots pyridine$, $CONH_2 \cdots pyridine$, $COOH \cdots CONH_2$,

OH···NH$_2$, CONH$_2$···*N*-oxide, halogen bonds, etc. are heterosynthons (Scheme 1.2).[14] The advantage of using the synthon approach is that it offers a simplification in the understanding of crystal structures, and this concept is widely used to design novel solid forms which are important from scientific and commercial viewpoints.

Homosynthons   **Heterosynthons**

acid-acid, 33 %   acid-pyridine, 91 %   amide-pyridine, 4%

amide-amide, 35%   amide-acid, 47 %   amide-N-oxide, 70 %
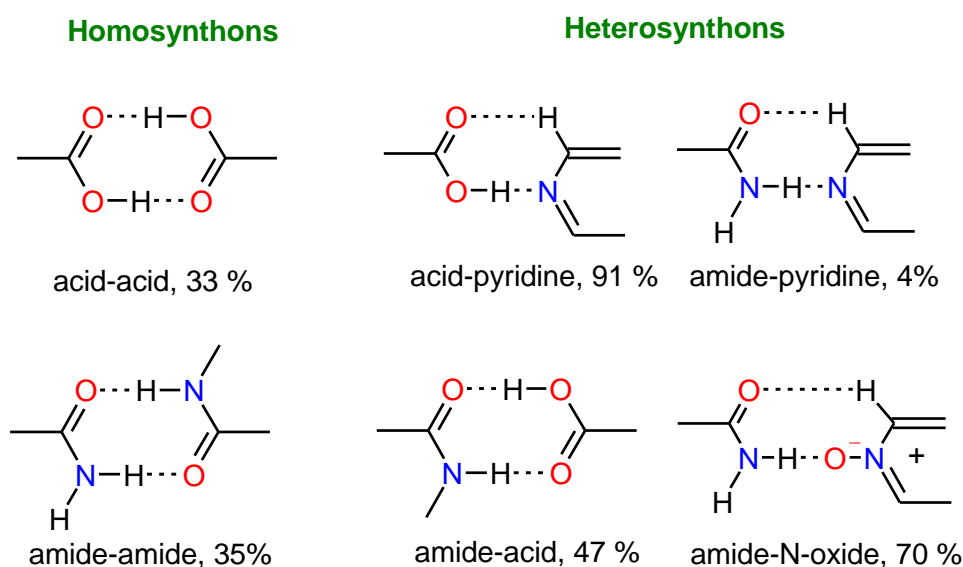
Scheme 1.2 Supramolecular synthons with their probabilities calculated from CSD statistical study (adapted from ref. 14)

1.3 Pharmaceutical Solids

Of the several states of matter (solid, liquid and gas) in which a substance can exist, solid state is most commonly encountered for drug substances therefore it is most important and relevant state for pharmaceutical development. Most of the pharmaceutical products in the market (about 80%) are solid dosage forms.[15a] The alarming increase in the number of drugs with poor physicochemical properties by the usage of high-throughput technology and combinatorial chemistry[15b] has increased the challenges for developing various solid forms of the drug molecules. Hence, understanding of various solid forms that may occur, as well as the rational selection of solid forms, is critical to the facile development of a particular active pharmaceutical ingredient (API). Several strategies and techniques are well pursued in the area of solid state chemistry of drugs which include polymorphism and amorphous state of the drugs, multi-component systems such as hydrates/solvates, salts, eutectics and, more recently, cocrystals.[14, 16] Each of these

solid forms, by virtue of their uniqueness, exhibit different physico-chemical properties (solubility, dissolution, stability, melting point, hygroscopicity, bioavailability, etc.) and thus are important for the optimization and development of a suitable solid drug formulation.[17] Generally various techniques are being carried out to screen the targeted new solid form, such as solution crystallization, grinding, milling, sublimation, freeze drying, spray drying, melt crystallisation, rotoevaporation and heating experiments.[18] The following sections give a brief introduction to various solid forms (Scheme 1.3), and this thesis deals with novel solid forms such as polymorphs, hydrates, cocrystals, salts and salt polymorphs of APIs in detail.
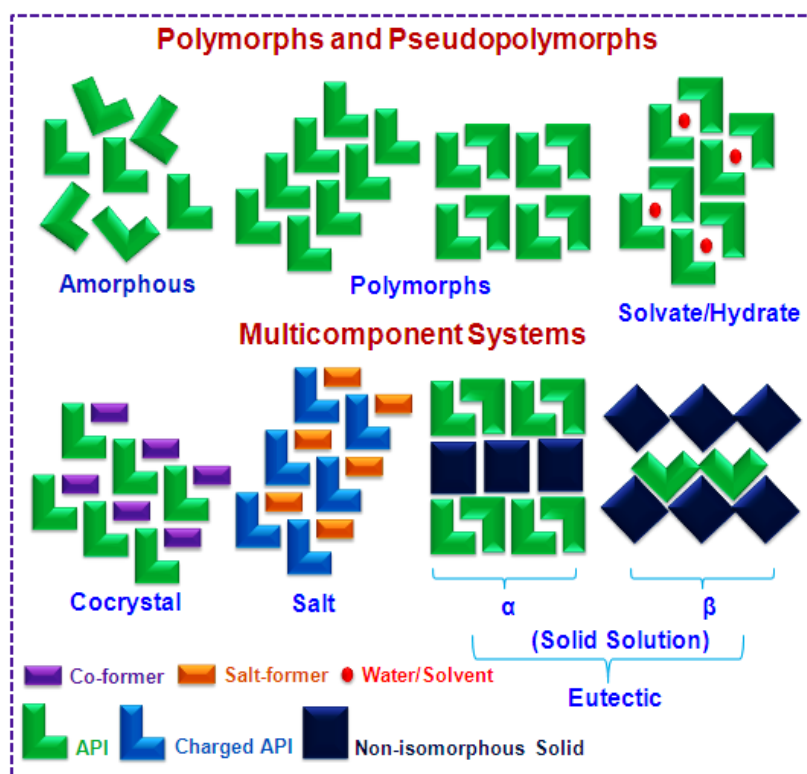
Scheme 1.3 Schematic representation of various solid forms possible for a solid when combined with the same solid or different phase.

1.3.1 Amorphous Solids

Amorphous solid forms posses the lack of long-range order. An amorphous solid is characterized by its glass transition temperature (T_g). It is the temperature at which a glassy material (plastic) is converted to rubbery phase retaining some properties of the liquid.[19a] Amorphous forms have higher free energy, enthalpy, and entropy than the

crystalline counterpart, thus finds application in improving solubility, dissolution and bioavailability for BCS class II or IV compounds.[19b] For example, antibiotic Novobiocin is poorly absorbed as its crystalline form and hence therapeutically ineffective. But, its amorphous form, which is 70 times more soluble than the crystalline form, is readily absorbed and thus is effective.[20] Amorphous forms can be produced by several techniques such as quench cooling, freeze drying, milling, spray drying, wet granulation and recently, grinding was shown to result in amorphous salts. On the other hand, though amorphous forms impart solubility/dissolution improvement in a drug formulation for a poorly soluble API, they tend to be unstable because of their high energy and can convert to the low energy crystalline form at any point of time.[19b, 21] Hence, they are generally not preferred in drug development and formulation unless there are clear-cut advantages over the crystalline forms. In reality, there are only a handful of pharmaceutical products containing amorphous API that have been successfully marketed, despite several decades efforts in research and development. Very few drug products like Itraconazole, Cefuroxime axetil, Griseofulvin, Lopinavir, etc., are marketed either as purely amorphous phases or in combination with other solid forms.[22a, b] As pointed out by Serajuddin,[22c] the limited commercial success reflected challenges from manufacturing difficulties to stability problems. Several excipients such as methyl cellulose, alginic acid, polyvinyl pyrrolidone (PVP), polyethylene glycol (PEG) etc.[19a] have been developed to stabilize the amorphous forms. Recently, 'Co-amorphous[23a, b]' strategy in which amorphization of two or more neutral compounds in stoichiometric ratio is becoming popular for their ability to enhance parent drug property. For example, Nangia et al.[23c] showed that curcumin–artemisinin coamorphous solid (CUR-ART, 1 : 1) exhibited improved solubility and pharmacokinetic profile of curcumin (Figure 1.1).
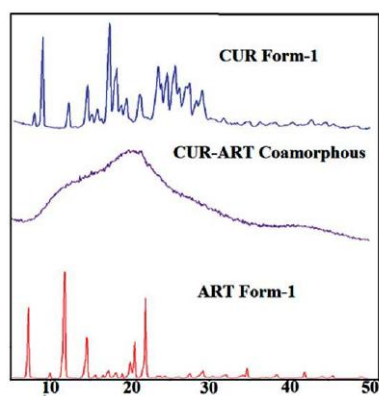
(a)
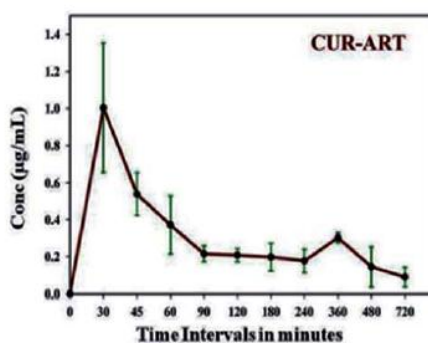
(b)

Figure 1.1 (a) Comparison of coamorphous CUR–ART (1:1) with starting materials CUR and ART form 1. The coamorphous product is lacking the sharp diffraction lines characteristic of the crystalline starting materials. (b) Mean Plasma concentration of curcumin vs. time profile of CUR–ART coamorphous in Sprague Dawley (SD) rats. No curcumin concentration could be detected with pure CUR (adapted from ref. 23c).

1.3.2 Polymorphism: Definition and Background

The word '*Polymorphism*' derived from the Greek literature (*poly* = many, *morph* = form). Although the concept of existence of different crystal forms was realized as early as the nineteenth century, its importance in the field in pharmaceuticals was brought to light by McCrone[24a] who also gave the widely accepted definition that "*a polymorph is a solid crystalline phase of a given compound resulting from the possibility of at least two different arrangements of the molecules of that compound in the solid state*". It can be broadly said that the 'existence of the same chemical compound in different crystalline environments' and 'different crystal forms of the compound are called 'polymorphs'. In modern science, polymorphism is relevant to the fields of pharmaceuticals, agrochemicals, pigments, dyestuffs, foods, and explosives.[7b, 24b, c] Mitscherlich, in 1822, was the first to document polymorphism in the context of crystallography.[25a] He noticed that arsenates and phosphates can exist as different crystal forms. Berzelius first described the existence of different crystal structures for the same element as allotrope.[25b] Allotropes and polymorphs are closely related. Polymorphism is used in general to refer to structural diversity of molecular compounds whereas allotropy is the structural diversity of elements. The first observation of polymorphism in organic materials is attributed to Friedrich Wöhler and Justus von Liebig[25c] in 1832, they found that a boiling solution of benzamide upon cooling initially crystallised as silky needles, but when standing these were slowly replaced by rhombic crystals. In 1844, Amici invented polarizing microscope which is responsible for the development of chemical crystallography and especially polymorphism.[25d] In 1876, Mallard reported that crystals to be built up by different packing arrangements of minute elementary crystallites giving rise to different crystal forms.[25e] In 1891 Lehman characterized polymorphism depending on their reversible or irreversible phase changes as enantiotropic and monotropic respectively.[25f] A major development in polymorphism came with the work of Ostwald in 1897, who found that unstable polymorphic forms have a greater solubility than the

more stable forms in a particular solvent.[25g] He developed the famous 'Rule of Steps' on relative stability of polymorphs. Generally, polymorphism occurs because the chance of differences in packing of molecules in the crystal lattice, conformational flexibilities, and supramolecular synthon competitions. Any number of polymorphs can be obtained if we spent time and money which was stated by McCrone[26a] long ago (1965), and this was recently realised in case of flufenamic acid which exhibited nine polymorphs (Figure 1.2). [26b] As per the structure-property relationship, different polymorphs exhibit different properties just as different compounds.[24a] In effect, polymorphs of an API by virtue of their difference in structures can display differences in physico-chemical properties, such as melting point, compressibility, stability, solubility, dissolution rate and bioavailability, which form important criterion for the selection of optimal solid form for formulation and usage.[27]
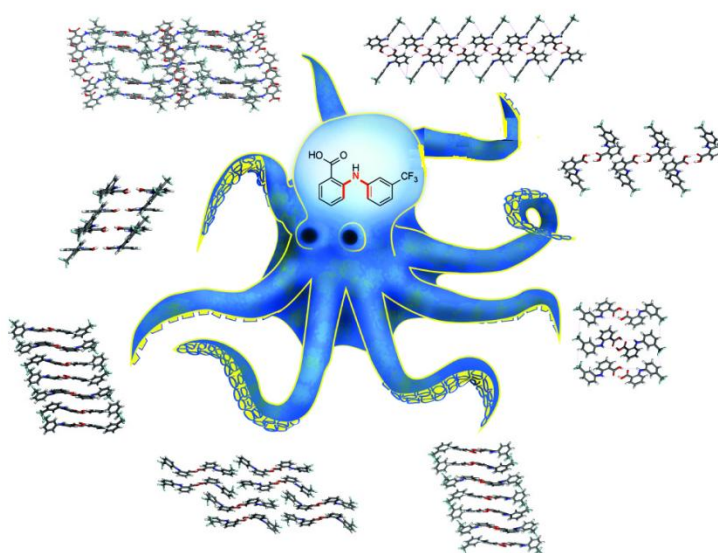
Figure 1.2 Nonamorphism in Flufenamic acid (FFA) and a new world record for a polymorphic compound with solved structures (adapted from ref. 26b).

1.3.3 Classification and Terminologies

In general, polymorphs (single or multicomponent) are synonymously called as 'forms', 'modifications' or 'phases' and represented as numerals (Arabic: 1, 2, 3 etc. and Roman: I, II, III etc) or alphabets (Greek: α, β, γ etc. and English: A, B, C etc) in the literature.[27a] In terms of structural aspect polymorphism can be classified mainly as three categories (i) conformational polymorphism, (ii) synthon polymorphism and (iii) packing

polymorphism.[28] Scheme 1.4 depicts the different types of polymorphism. When the differences in molecular conformations lead to different crystal structures, it is called 'conformational polymorphism'.[29a] For instance, two polymorphs are conformational polymorphs only when their conformations are related by changes in torsion angles of those two crystal structures. From the structural analysis, two polymorphs are said to be conformational polymorphs if the difference in torsion angle maximum change is $(\Delta\theta) \geq$ 95° between the conformers, otherwise it is a conformational adjustment.[29b] For example, chlorpropamide which is used for Type 2 diabetes exhibits the richest conformational polymorphic behaviour (Figure 1.3a)[29b], and other example include the Form-I and II of anti HIV drug Ritonavir (Figure 1.3b).[29c] When polymorphism arises, only because of different packing arrangement of molecules (conformationally flexible or rigid) with the presence of same synthon and similar conformation, then it represents a case of packing polymorphism.[30a] For example, synthon and conformation is same where as packing arrangement is different in four polymorphs of model compound 1-(3-Methylsulfanylphenyl)-3-pyridin-2-ylurea (Figure 1.4).[30b] When the supramolecular synthon or non-covalent interactions are different in different crystal structures, it is called 'synthon polymorphism'[31a, b] for example acid catemer and acid dimer in the dimorphs of Oxalic acid (Figure 1.5).[31c] These classifications are subjective because of overlap possible in polymorphic systems and more than one can coexist in a given system. For example, synthon and packing polymorphism coexist in the tetramorphs of anti-tubercular drug Pyrazinamide (Figure 1.6),[31d] and other example includes Form 1 and Form 2 of trimethoprim (discussed in chapter 3). Form-I and Form-II of the anti-hyperammonemic drug comes under the category of conformational and synthon polymorphs (discussed in chapter 5).
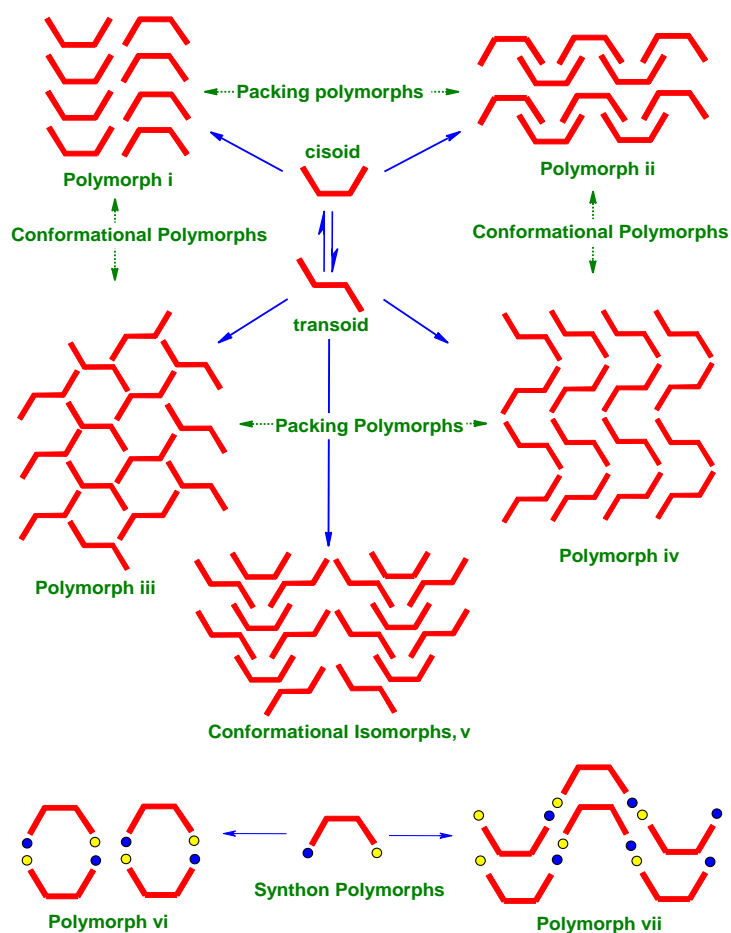
Scheme 1.4 Schematic representation of different kinds of polymorphs (adapted from ref. 29a).

Chlorpropamide

(a)

Ritonavir   Form I   Form II

(b)
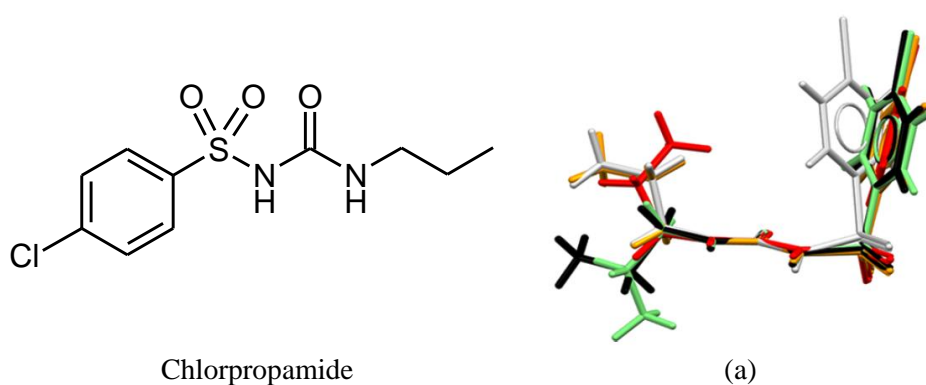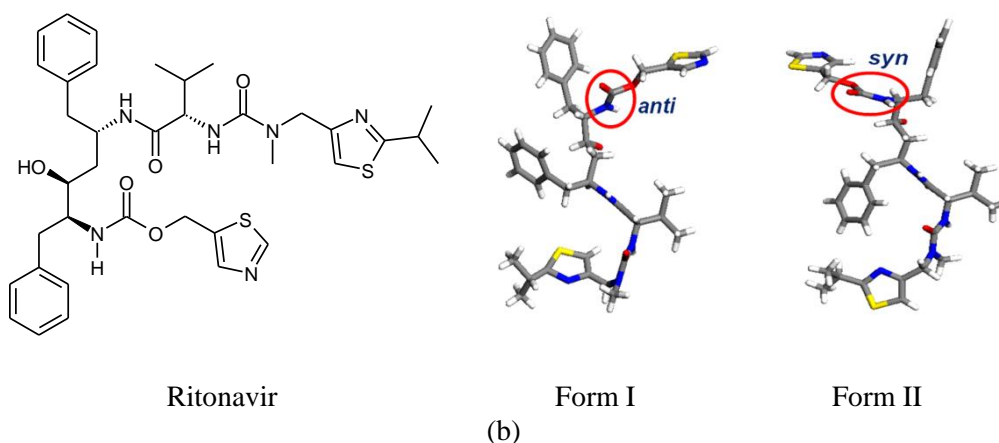
Figure 1.3 (a) Overlay of five different conformers in chlorpropamide polymorphs. (b) Conformational polymorphs of anti HIV drug Ritonavir (adapted from ref. 29b and c).

1-(3-Methylsulfanylphenyl) -3-pyridin-2-ylurea   Form-I   Form-II

Form-III   Form-IV
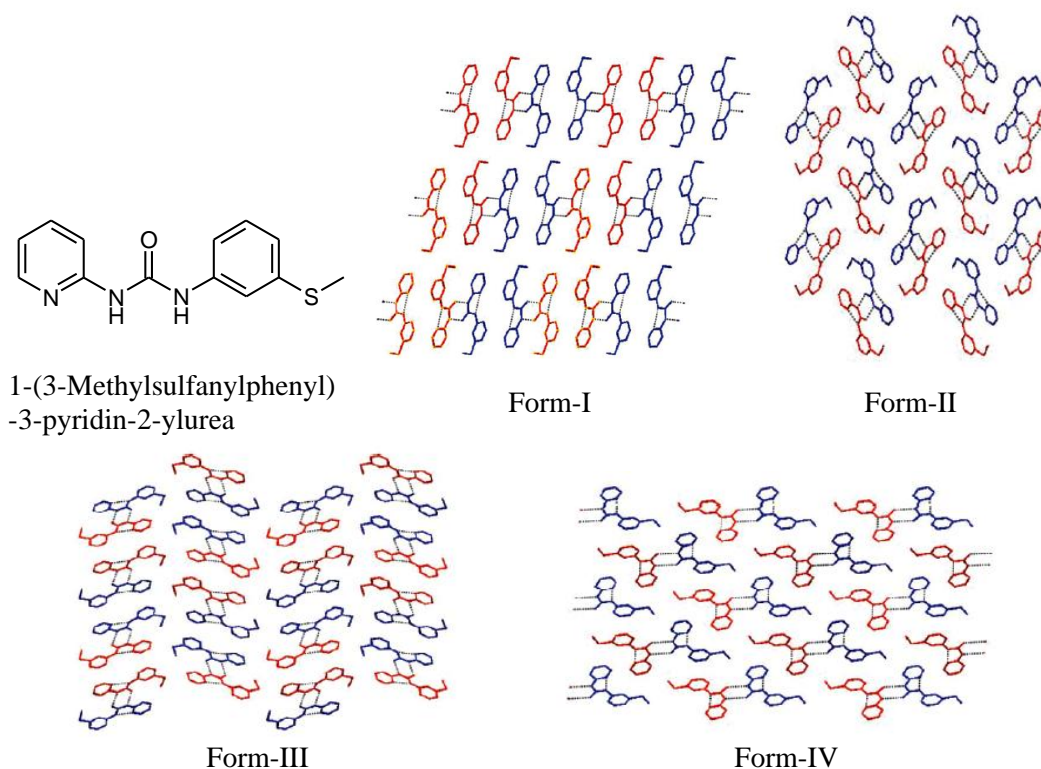
Figure 1.4 Shows four packing polymorphs of diaryl urea derivative, note that in all four crystal structures, dimers (R_2^2 (8)) formed through N–H···O and N–H···N intramolecular $S(6)$ hydrogen bonds are same (adapted from ref. 30b).

<center>(a)   (b)</center>
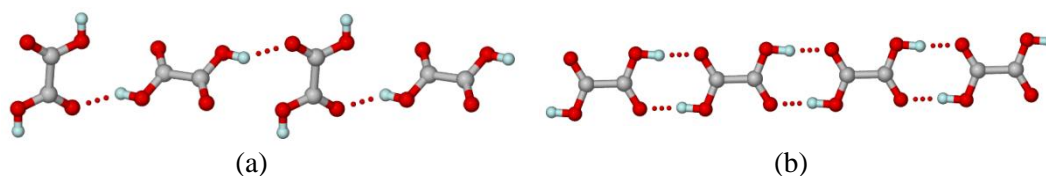
Figure 1.5 Synthon polymorphs of Oxalic acid. (a) α-form has acid catemer and (b) β-form has acid dimer in their crystal structures (adapted from ref. 31c).

<center>Pyrazinamide</center>

<center>α   β   γ   δ</center>
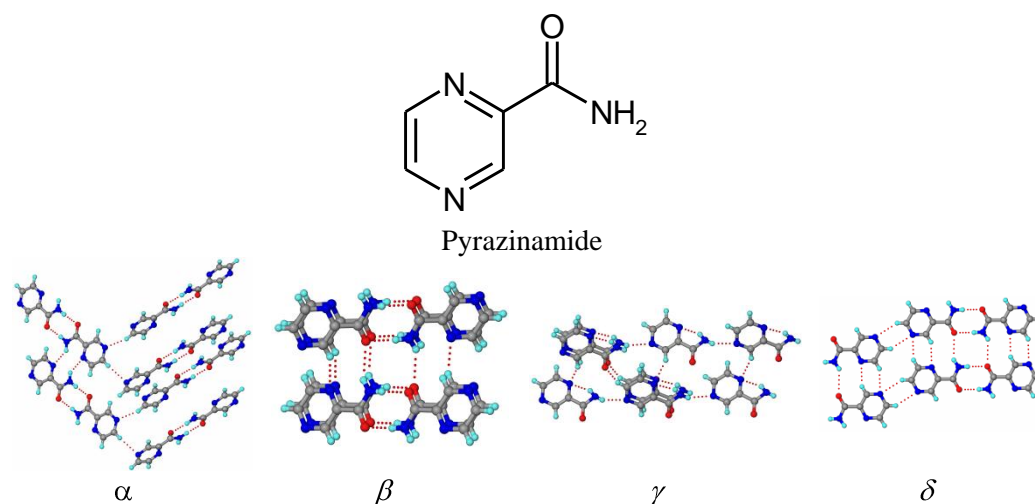
Figure 1.6 Synthon and packing polymorphism in Pyrazinamide. In α polymorph, zigzag tapes formed by $R_2^2(8)$ N–H⋯O and $R_2^2(10)$ N–H⋯N hydrogen bonds are connected orthogonally to 2_1 screw related tapes through C−H⋯N interactions in a 3D arrangement. The β polymorph has non-planar $R_2^2(8)$ N–H⋯O dimers that make a helix along the *b*-axis through anti N–H⋯O and C–H⋯N interactions. In γ polymorph, 1D tapes assembled via N–H⋯N hydrogen bonds of *C*(6) notation are connected through C–H⋯O and C–H⋯N interactions. In δ polymorph, carboxamide tapes formed by $R_2^2(8)$ dimer and *C*(4) catemer N–H⋯O synthons and $R_2^2(6)$ C–H⋯N synthons make 2D sheets (adapted from ref. 31d).

When polymorphs crystallize simultaneously in the same flask under identical crystal growth conditions from the same solvent, they are termed as concomitant polymorphs.[32a] This phenomenon occurs when the crystallizing polymorphs have almost similar energies. Concomitant polymorphism is exemplified by benzamide which incidentally is also the first example of a polymorphic organic substance.[32a] When the tautomers of a compound rapidly interconvert in solution or in melt but crystallize as polymorphs in their solid state then the phenomenon is known as tautomeric polymorphism,[32b] example, Omeprazole.[32c] Other terminology frequently used is 'Disappearing polymorphism[33a]' in

which polymorphs are crystal forms that fail to reappear after their initial isolation. They are kinetic forms whose subsequent appearance becomes elusive because of the isolation of the more stable polymorph. Examples for disappearing polymorphs include steroid progesterone[33b] and melatonin agonist (LY156735).[33c] Isotopomeric polymorphism is a term recently coined to describe a situation where a change in crystal structure is due to the changing the isotopic identity of one or more of the atoms in a molecule.[34a] The existence of a neutral polymorph in one crystal structure and zwitterionic polymorph in another crystal structure for the same molecule is known as neutral and zwitterionic and polymorphism.[34b, c] Very few drug examples in the literature are reported as neutral and zwitterionic polymorphs including the amphoteric drugs ciprofloxacin, norfloxacin, torsemide, etc.[34d, e] Another commonly encountered term 'color polymorphs'. It is not often that different polymorphs have different colours but when such an event occurs, the detection and separation of polymorphs becomes quite easy. A dramatic and well known example is the 5-Methyl-2-[(2-nitrophenyl)amino]-3-thiophene-carbonitrile, which has been crystallized in heptamorphs and it is popularly known as ROY[35] for its red, orange, and yellow crystal colors (Figure 1.7). Another commonly used term is 'pseudopolymorphism' which is discussed in the later section.
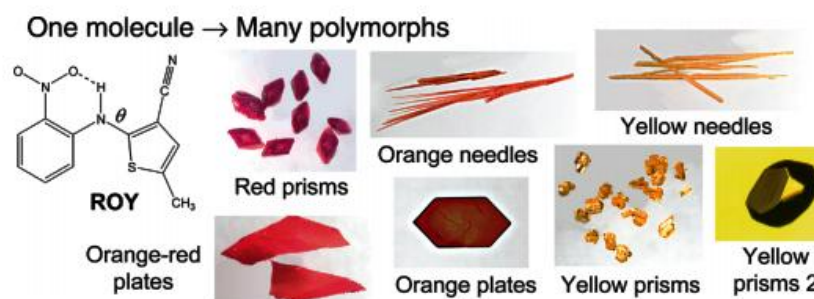
Figure 1.7 Polymorphs of ROY with different colors (adapted from ref. 35a)

1.3.4 Polymorphism in pharmaceutical industry

Polymorphism is of unusual importance in pharmaceutical context, and received particular attention in the recent literature because of its importance in drug substances and pharmaceutical formulation.[36a] Solubility and dissolution rate are important physico-chemical properties that have a direct influence on the physiological performance of the drug. Dissolution rate in particular is often the rate determining step which directly

affects the drug bioavailability.[27] There are many examples where the bioavailability of polymorphs varies significantly for example, Phenobarbital,[36b] Indomethacin,[36c] Mercaptopurine,[36d] etc. Hence, polymorph having higher solubility and dissolution rate which directly affect bioavailability may be considered for formulation. Sometimes high solubility is not preferred because of adverse effects. One such example is the antihelmentic drug Mebendazole,[37a] in which solubility of the forms in physiological media is Form B> Form C> Form A. Based on these differences Form C is pharmaceutically preferred since its solubility is sufficient enough to ensure optimal bioavailability without the possible toxicity of the more soluble Form B. A metastable polymorph of a drug is sometimes desirable because of special properties such as higher bioavailability, behaviour during grinding and compression or lower hygroscopicity. However a metastable form has a thermodynamic tendency to reduce its free energy by transforming into the stable form. Such polymorphic transformation is often detrimental to the efficacy of the formulation, examples include the case of chloramphenicol palmitate and ritonavir.[7b, 37b]

Difference in structures and properties make polymorphs patentable.[37c] If a generic pharmaceutical company discovers a novel polymorph of an already marketed drug, it will gain an early access into the market place; therefore, the innovator companies must find out all possible polymorphs of the drug and patent them in order to extend their monopoly in pharmaceutical industry and to protect their product. A well-known example is the case of anti-ulcer drug Ranitidine hydrochloride polymorphs.[7b, 27] Glaxo obtained the patent on the two polymorphs Form I (in 1977) followed by Form II (in 1985) of Ranitidine hydrochloride. Glaxo marketed ranitidine hydrochloride under the brand name of Zantac. Sales of Zantac reached $3.5 billion by 1991, and this single drug was practically the linchpin of the entire Glaxo group. In 1995, as the patent on the Form I was approaching expiration, several generic companies began preparing to market Form I. But the generic manufacturers were not able to crystallize Form I exclusively as it was always crystallizing as a mixture of Form I and II. This kept the generic companies products off the market, and during that period ultimately Novopharm could find a method to prepare Form I exclusively with non-detectable amounts of Form II (≤1 %), and won the legal battle. This is the first example of major legal event that brought the scientific field of polymorphism into the glare of commercial and industrial activities. Since then generic entry was made into the market and also pharmaceutical

companies came to know the importance of crystal engineering. Cefadroxil, terazosin hydrochloride and aspartame are other well known examples of patent issues surrounding polymorphism.[27]

1.3.5 Thermodynamics versus Kinetics of Polymorphs

When a compound exists in various solid state forms or polymorphs mainly two major issues need to be addressed (i) the relative stabilities and the transformations that can occur between the forms, and (ii) the time needed for the transformations to reach equilibrium. Thermodynamics provides information about the first aspect (how far), and kinetics about the second aspect (how fast). Generally, polymorphism results from the interplay of thermodynamic functions (free energy, enthalpy and entropy) and kinetic factors (activation energy, temperature, supersaturation, rate of evaporation etc.) that govern the crystallization process.[7b, 27] Consider the crystallisation process in terms of molecular events, initially molecules arrange themselves into energetically suitable aggregates or packing patterns under the action of non-covalent forces, notably hydrogen bonds and other directional interactions. The balance between the kinetic and thermodynamic can be illustrated by free energy coordinate (Figure 1.8a).[38a] Outcome of crystallization greatly depends on temperature, solvent, rates of heating and cooling, impurities, shock, and other experimental variables. A particular crystal form may not be the global minimum in free energy but it may be obtained repeatedly because it is kinetically locked in under the conditions employed. The appearance of these local minimum structures during crystallization is one of the main reasons for polymorphism. The kinetic product may dominate or even be formed exclusively in chemical reactions and this was reported by Curtin and Hammett.[38b] Curtin-Hammett principle[38b] states that the *distribution of products in a reaction that has many pathways need bear no relation to the relative stabilities of these products*. This definition is equally applicable to crystallization process where kinetically favoured crystal is obtained faster because the activation energy required to achieve this state is lower, whereas the thermodynamic polymorph is obtained later due to higher activation energy requirement. The behaviour of polymorphs appearing in the order of increasing stability is referred to as Ostwald's rule of stages (Figure 1.8b).[25g] This rule states that *when leaving an unstable state, a system does not seek out the most stable state, but rather the nearest metastable state which can be reached with least loss of free energy.* The role of nucleation governed by

the Ostwald's law of stages is vital in predicting the nature of polymorphic outcome of a molecule.

|(a)|(b)|
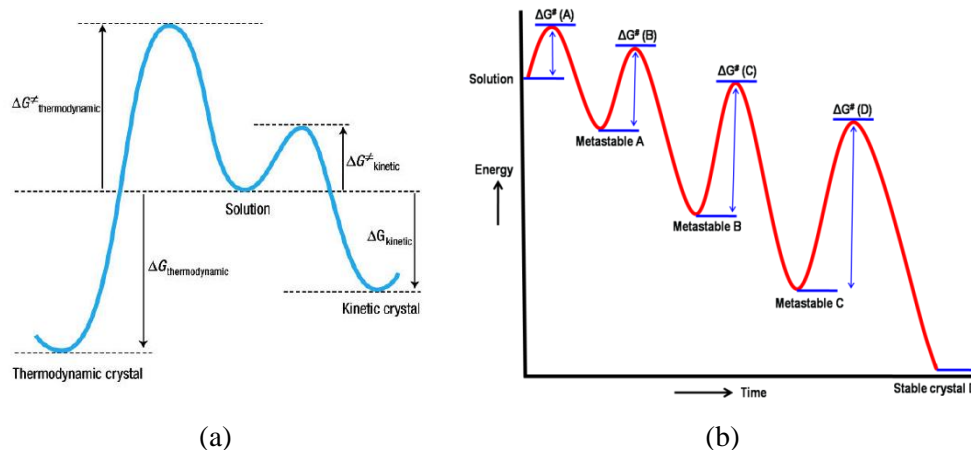
Figure 1.8 (a) Kinetic and thermodynamic outcome of crystallization reaction. (b) Ostwald's Rule of Stages. Initial high-energy state (metastable A) through minimal changes in free energy crystallizes first and is the one which has the lowest energy barrier. Metastable A form will then transform to the next lower energy polymorph (metastable B) and so on (metastable C) until thermodynamically stable crystal D. This is culled from ref. 38a.

Nevertheless, the polymorph obtained at the end is the most stable since its thermodynamic state is lowest in energy. If the same crystal structure is kinetically and thermodynamically favoured, then polymorphism is less likely.[38a] At a molecular level, close packing and intermolecular interactions are the competing factors that determine the polymorphic outcome. Thermodynamic polymorph is favoured when close packing dominate the intermolecular interactions. Similarly, kinetic polymorph is favoured when the crystal nucleus is stabilized by intermolecular interactions. It is highly unlikely to observe polymorphism in crystal systems where the best interactions are accompanied by the best packing. From thermodynamic consideration polymorphic pairs can be divided as monotropic and enantiotropic systems.[38c] Monotropic systems are defined as systems where a single form is more stable regardless of temperature. Enantiotropic systems are defined as systems where the relative stabilities of the two forms invert at some transition temperature. In other words, if the free energy curves of two forms cross below the melting point of the lower melting polymorph, they are said to be

enantiotropically related and if the free energy curves do not cross below the lower melting polymorph, they are said to be monotropically related.

1.4 Solvates and Hydrates – Pseudopolymorphism

McCrone introduced the term 'pseudopolymorphism'.[26a] It is defined as the phenomenon wherein a "*Compound is obtained in crystalline forms that differ in the nature or stoichiometry of included solvent molecules*" and the resulting solid forms are known as pseudopolymorphs.[39a] Pseudopolymorphs also termed as solvates or hydrates or solvatomorphs, and this class of compounds exhibit different solubility, dissolution rate, mechanical behavior, stability and bioavailability from their unsolvated counterparts.[39b] The propensity of a compound to form pseudopolymorphs is deemed to be relevant to molecular structures, hydrogen bonding ability and crystal packing.[39c] Generally, during crystallization process, strong solute-solvent interactions result in the nucleation of solvated crystals. In particular water molecule, because of its small size, and ability to act as both a hydrogen bond donor and acceptor found to be more capable of linking to drug molecules to form new crystal structures than any other solvent. It is found that approximately one third of active pharmaceutical ingredients (APIs) can form crystalline hydrates.[39d] Sometimes, solid can incorporate different ratios of the same solvent for example, antibiotic drug norfloxacin forms a dihydrate, 1.25 hydrate and 1.125 hydrate.[40a] On the other hand different solvents can incorporate in the crystal lattice for example, antibacterial drug nitrofurantoin forms solvates with water, DMF, DMSO, methanol etc.[40b] Sometimes polymorphs of solvates also observed example includes nitrofurantoin monohydrate polymorphs I and II (Figure 1.9).[40b] The choice between solvated or unsolvated forms of a drug will depend on its pharmaceutical properties like stability under different conditions, shelf life etc. Various drug molecules are currently marketed as solvates/hydrates, for example, indinavir sulfate is marketed as its ethanol solvate and paroxetine hydrochloride is marketed as its hemihydrate.[40c]
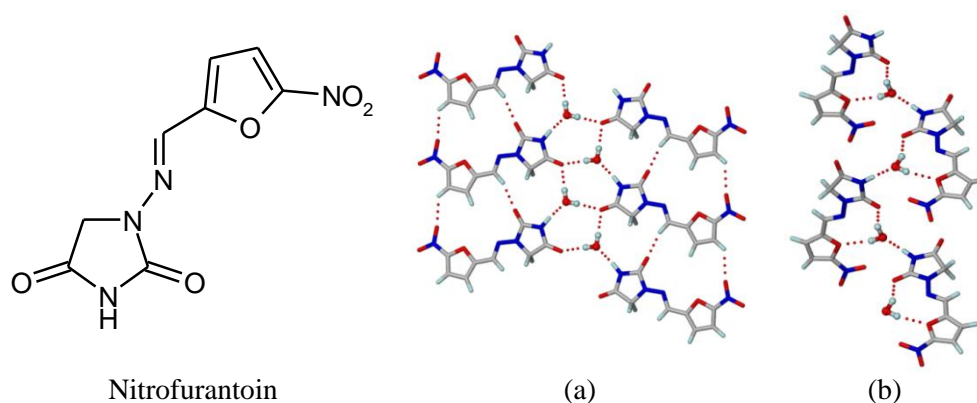
Nitrofurantoin   (a)   (b)

Figure 1.9 Pseudopolymorphs of nitrofurantoin monohydrate. (a) In form I, tapes of translation related nitrofurantoin molecules are connected by water molecules through O–H···O and N– H···O hydrogen bonds. (b) In form II, discrete nitrofurantoin molecules form a zigzag tape through water molecules (adapted from ref. 40b).

As a general rule, solvates are not favoured for pharmaceutical development, except for hydrates and occasionally ethanolates, because of the toxicity and undesirability of ingesting most of the solvents. Hence, solvents with low toxicity need to be used for pharmaceutical purpose, and these solvents are classified based on decreasing toxicity, from Class I (such as benzene, carbon tetrachloride etc., should be avoided) to Class II (such as acetonitrile, methanol, pyridine etc., should be limited) to Class 3 (such as ethanol, acetic acid, acetone etc., can be preferred).[41a] Some solvents although present in the crystal lattice of the parent solid (in channels/voids) have no or little role on the integrity of the crystal structure and hence can be readily desolvated and resolvated for practical purposes for instance, cephalosporin solvates.[42a] But, some solvents upon controlled desolvation can produce new polymorphs of the parent material example of caffeine Form II from its hydrate.[27c] Hence, purposive solvation and desolvation experiments are routine during polymorph screening of APIs and important for crystallization of a desired polymorph.[42b-d] In all, pseudopolymorphs are one of the important class of drug solid forms which have several applications in the pharmaceutical industry.

1.5 Pharmaceutical Salts

Salt formation is the first and one of the primary approaches to modify the physical properties of APIs, and it is estimated that over half of the drug molecules in the market

are administered as salts. Screening of salt is an indispensable step in preformulation characterization. In addition to solubility and dissolution rate, salt forms can affect other properties such as physical and chemical stability, melting point, hygroscopicity, crystallinity, toxicity, bioavailability, etc.[43] Because of its profound impact on biopharmaceutical and pharmaceutical properties; an appropriate choice of the most desirable salt form is a critical step in the development process. Generally, salt selection mainly depends on the p*Ka* difference. It is generally accepted that a minimum difference of 3 units between the p*Ka* value of the salt forming moiety of the drug and that of the salt counterion is required to form stable salts. Which is popularly known as 'rule of three[44]' and very useful guide to predict salt formation, Nangia[44b] and Childs[44c] independently tested experimentally and fine tuned the rule of three. However, recently Cruz-Cabeza revised[44d] and reported little broad range that for cocrystals pKa difference as < -1, salts > 4, and -1 to 4 for cocrystal-salt states. The orange book[44e] database is an excellent source of information on counterions which has list of various drugs products approved by the US-FDA, and the frequency of counterions used for salt formation over decades.

The interest in salt formation has grown greatly over the past half century, and in recent years, it has become the most commonly applied technique of increasing solubility and dissolution rate in drug product development.[43] Salt formation has diverse implications in pharmaceutical industry. Salts of their inherent strong ionic interactions tend to be stable and in general exhibit higher melting points than their parent APIs. Their ability to form electrostatic interactions and charge-assisted hydrogen bonds with water in the biological media confers higher solubility to the API salt formulation. For example, poor solubility and low melting point of well know drug ranitidine[45a, b] was overcome by forming hydrochloride salt of the drug which showed very high solubility (1g/mL) and improved melting point (136°C). The safety profile of the parent drug can also be altered by switching an ionic salt counter-ion, for example, the acute oral toxicity of propoxyphene was halved when prepared as the napsylate salt rather than the hydrochloride salt.[45c] The down side of salt formation is the hygroscopic nature of salts, by virtue of their inherent affinity to water/moisture, is a serious problem in several cases.[45c, d] For example, hygroscopicity of the anti-tuberculosis drug Ethambutol dihydrochloride salt was reported to cause instability of the anti-TB fixed dose combination (FDC) drug formulations, thus leading to poor quality medicines.[45e, f] In

pharmaceutical industry most of the time for low soluble APIs salt formation employed, since it increases solubility/dissolution by many fold higher than the free acid or base form of API. However, high solubility of salt forms also sometimes exhibit adverse effects for example; an irritant effect on the esophagus has been reported for highly soluble alprenplol hydrochloride, whereas less soluble alprenplol benzoate has no such irritant effect.[46a] In case salt formation is not feasible (for neutral compounds) or may be difficult to form salts, techniques like solid dispersions, nanoparticles, inclusion complexes and recently cocrystals seem to be very promising in addressing the poor physicochemical properties of drug molecules.[46b, c]

1.6 Pharmaceutical Cocrystals

Cocrystals were reported as far back as the 1840s[47a] and they were called by various terms such as addition compounds, organic molecular compounds, complexes and heteromolecular crystals. However, the term cocrystal as used today was not came into widespread usage until it was popularized by MC Etter[47b] in the 1980s, and the importance of 'pharmaceutical cocrystals' in the current context appreciated only around 2000s.[47c-f] The first cocrystal between quinine and hydroquinone was reported by Friedrich Wöhler in 1844.[47a] Recently, widely accepted definition of cocrystal was proposed in Indo-US Bilateral Meeting[48a] as the "*cocrystals are solids that are crystalline single phase materials composed of two or more different molecular and/or ionic compounds generally in a stoichiometric ratio."* Many definitions of cocrystals have been offered by various scientists and there is no hard and fast definition as of now,[7b, 48b-d] however a cocrystal is a stoichiometric multi-component system where the individual components are held together by heteromeric interactions like hydrogen bonds and are solids at room temperature. A pharmaceutical cocrystal follows the same definition of cocrystal except that the individual components are generally an active pharmaceutical ingredient (API) and a coformer from the generally regarded as safe (GRAS)[49] list.

Pharmaceutical cocrystals have generated enormous interest due to their potential for improving the physicochemical shortcomings of drug molecules, such as poor aqueous solubility. Poor aqueous solubility can compromise drug performance, and cocrystallization is an emerging strategy to design materials with desirable properties.

This approach is currently limited because cocrystal solution chemistry remains largely unexplored. Recently, Nangia et al.[19b] proposed a model to explain how a coformer can improve the solubility of cocrystals, based on 'spring and parachute' model of amorphous forms. According to the model, a cocrystal containing a high soluble coformer can facilitate faster dissolution of a low soluble component. They explained that fast release of high soluble coformer into aqueous medium (because of its higher affinity to the latter) results in the dissociation of cocrystal, thereby leaving behind the low soluble component in an amorphous/randomized state. This amorphous/randomized state understandably leads to an increase in the free energy of the system, ultimately leading to an improvement of solubility/dissolution of the low soluble component (Figure 1.10). This model comply with the 'coformer solubility rule'[50a] in that high solubility coformers will give rise to high solubility cocrystals and vice-versa. If the coformer has low water solubility, it does not dissociate from the lattice easily and in effect can control the solubility/dissolution of the drug.
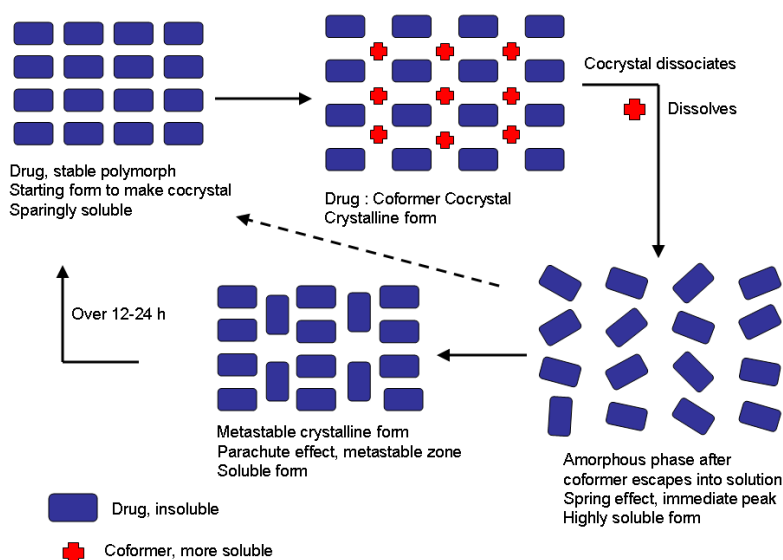
Figure 1.10 Nangia's model of solubility enhancement of a drug through a pharmaceutical cocrystal (adapted from ref.19b).

The main advantage of cocrystals is the ability to generate a variety of solid forms of a drug molecule that have physicochemical properties distinct from the cocrystal components. Various problems such as solubility, dissolution, bioavailability, hygroscopicity, hydrate/solvate formation, crystal morphology, fusion properties, chemical and thermal stability, and mechanical properties associated with drug

molecules are being addressed by cocrystallization technique.[50b, c] These properties can directly or indirectly affect the suitability of a particular API as a pharmaceutical product. Several studies have demonstrated independently by various scientific groups depending on the issues related to drug molecule for better formulation. For example, Remenar *et al.*[51a] showed that cocrystals of itraconazole (a poorly soluble antifungal agent) with four dicarboxylic acids (L-tartaric, L-malic, succinic, and fumaric acid) achieved dissolution rates 4 to 20 times higher than that of crystalline drug in 0.1 N HCl (Figure 1.11). The highest dissolution rate achieved with itraconazole-L-malic acid was comparable to the amorphous form of itraconazole. In the similar lines, cocrystals of fluoxetine hydrochloride with succinic acid,[51b] and baicalein with nicotinamide[51c] exhibit higher solubility/dissolution than the parent drugs. Cocrystallization can also be utilized as strategy for decreasing the solubility. For example, caffeine-gentisic acid (1:1 or 1:2) cocrystals are less soluble than pure caffeine.[52a] These complexes are used to formulate caffeine in dosage forms such as chewable tablets that are intended to linger in the mouth. Further, improved bioavailability with a cocrystal than with the parent API was carried out by Bak *et al.*,[52b] and showed that a 1:1 cocrystal of an Amgen compound AMG517 with sorbic acid exhibited 8 to 10-fold increase in Cmax and plasma AUC relative to an equivalent dose (500 mg/kg) of the crystalline drug in rats. Additional cocrystals that have demonstrated higher Cmax and plasma AUC relative to pure drug include a 1:1 cocrystal of indomethacin and saccharin in dogs.[52c]
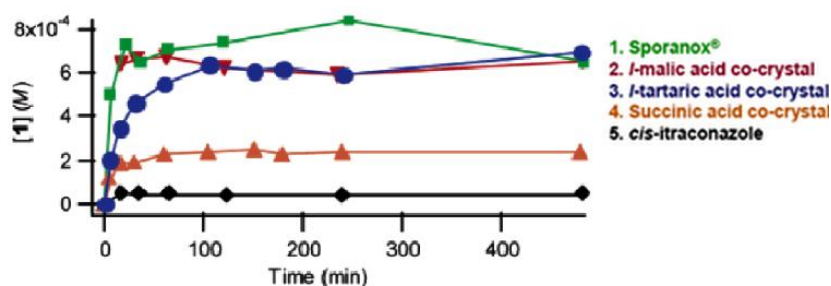
Figure 1.11 Dissolution curves of itraconazole cocrystals, and itraconazole –L-malic acid of cocrystal showed 20 times more solubility compared to parent drug, which is comparable with amorphous form "Sporanox" (adapted from ref.51a).

Sensitivity to water is an important consideration for any drug candidate, because of the risk of phase transformation from anhydrous solid into a hydrate.[50c] Cocrystals have been shown to prevent hydrate formation for example, the case of caffeine and

theophylline cocrystals with dicarboxylic acids.[50c, 53a] Cocrystals can protect against unwanted degradation processes in the solid state. For example, Carbamazepine undergoes photodegradation where as saccharin and nicotinamide cocrystals were found to be stable to the photodegradation.[53b] Similarly, Nangia *et al.*[53c] have reported that chemical stability of andrographolide without transformation to its inactive sulfate metabolite was achieved by forming a cocrystal with salicylic acid. Mechanical properties of molecular crystals are a function of intermolecular interactions and crystal packing. For example, widely used analgesic drug paracetamol Form-II (metastable form) has layered structure with superior compaction properties compared Form-I (thermodynamic form) which has corrugated structure. Hence Form-II is obviously preferred for tableting, but it is less stable than Form-I. This poor mechanical property of paracetamol was improved through the cocrystal strategy. Cocrystals of paracetamol with oxalic acid and theophylline were stable with improved tabletability property.[53d] The improved tabletability is due to the successful formation of layers in the rystal structure that are critical for elasticity and strength (Figure 1.12). In short, the most effective cocrystal research relies on both in depth understanding of structure-property relationship and efficient preparation of desired cocrystals for further pharmaceutical applications.
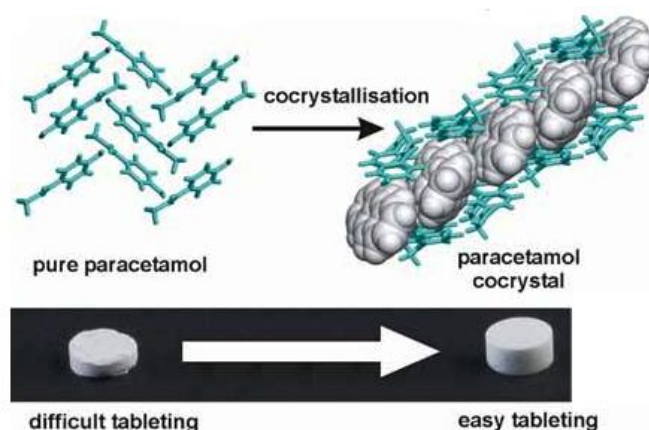
Figure 1.12 Improvement in tabletability of paracetamol by forming cocrystal with theophylline (adapted from ref.51a)

1.7 Eutectic Compositions

The above solid forms of APIs like salts, cocrystals, polymorphs, pseudopolymorphs and amorphous forms are conventionally employed to overcome problems associated with

drug molecules, however universal solution still proves elusive. Of late, eutectic compositions[54] with their excess thermodynamic functions[55] can act as alternate solid forms for solubility modulation. Eutectics are basically multi-component crystalline solids closely related to solid solutions.[54a, d] A solid solution possesses structural homogeneity throughout the structure (single phase) but a eutectic is a heterogeneous ensemble of individual components whose crystal structures are like discontinuous solid solutions (phase separated). Thus, a eutectic may be better defined as a '*conglomerate of solid solutions*'. To make it simpler, their crystalline arrangement is similar to the parent components but they are different with respect to the structural integrity. Recently, Nangia *et al.*[54a] revealed that the design principles for cocrystals can be extended to eutectics in an empirical way. They have concluded that when the adhesive interactions dominate, the result is a cocrystal; when the adhesive and cohesive interactions are balanced and there is size/shape match, the product is a solid solution; and when the cohesive interactions take over for size/shape mismatched components, the product is a eutectic.

In spite of long their long history, researchers dissuaded in exploring this strategy because the internal structural details of eutectic compositions are scarce. Of late, specific techniques like atomic pair distribution function (PDF) approach[56a, b] and extended X-ray absorption fine-structure spectroscopy (EXAFS)[56c, d] are used to analyze the local structure of materials. Eutectics have several applications in diverse fields of daily life such as traditional refrigeration and snow removal (sodium chloride–water eutectic), anti-freeze (ethylene glycol–water eutectic) in vehicles,[57a] energy storage devices,[57b, c] and in pharmaceutical formulations. For example, a eutectic composition of the local anesthetic drugs lidocaine and prilocaine (trade name EMLA®) is used to enhance the transdermal permeation of lidocaine.[57d] Like cocrystals, eutectics also confer higher solubility, dissolution and stability. For example, Chiou and colleagues[58a] have reported that a eutectic composition of antifungal drug Griseofulvin with succinic acid (55% w/w of Griseofulvin) have shown 6-7 times faster dissolution rate compared to pure Griseofulvin (Figure 1.13a). Recently, Nangia *et al.* reported[54a] that the hygroscopicity of anti-tuberculosis drug ethambutol dihydrochloride (EDH) was addressed by forming the eutectics with fumaric acid (FA) and succinic acid (SA) (Figure 1.13b). Further, eutectic mixtures have also been shown to improve the permeability of drug molecules.[58]

(a)   (b)
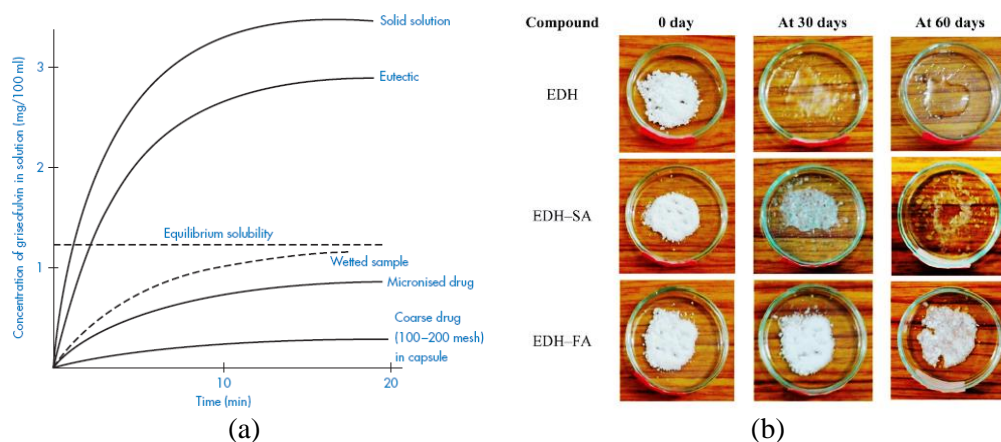
Figure 1.13 (a) Rate of dissolution of Griseofulvin- succinic acid solid solution, eutectic mixture and crystalline material. The dissolution rate of Griseofulvin was improved by 6-7 times on forming eutectic (adapted from ref. 58a). (b) The physical state of EDH compounds to show their hygroscopic behaviour at 40 °C and 75 RH as a function of time. Both the eutectics (EDH-SA and EDH-FA) exhibit greater hygroscopic stability than EDH (adapted from ref. 54a).

Solid dispersions[54] due to their amorphous nature are likely to undergo phase transformation under the pharmaceutical processing and storage conditions. Whereas eutectics are highly crystalline compounds hence they do not have any disadvantages associated with phase transformation. In short, eutectics can confer the dual advantages of solubility (because of high thermodynamic functions) and stability (due to their crystalline nature) there by bioavailablilty of drug forms. Nevertheless, this poorly understood area is worth exploring since significant understanding of its internal arrangement would not only widen the horizons of solid form screening strategies but would also be important in 'Intellectual property management'.[20b]

1.8 Characterization of Solid Forms

The characterization of solid material is the first step after screening all possible solid forms of a compound. First hand and quick information can be obtained through spectroscopic investigations which deliver chemical and physical information combined high throughput analysis and the non-invasive measurements with high selectivity and sensitivity. Various spectroscopic techniques such as FT-IR,[59a] FT-Raman,[59b] near IR[59c] and more recently solid state NMR[59d] are used regularly to characterize various solid

forms. Further, thermal analysis[60a, b] has been an extremely important analytical tool in the pharmaceutical industry for analysing various solid forms. Thermal analysis includes differential scanning calorimetry (DSC), thermogravimetric analysis (TGA) and hot stage microscopy (HSM). DSC measures the rate of heat flow and is used to measure the events such as the heat of transition and heat of fusion. As all the transitions in materials involve heat flow (uptake endothermic; give out exothermic), DSC became the universal technique for measuring the wide variety of temperature induced transitions in solid materials. TGA measures physical changes solid materials and provides quantitative measurement of mass change in materials associated with transition and thermal degradation. HSM[60c-e] is widely used to study various properties of solid forms such as homogeneity or diversity of crystalline samples, variations in size, shape or color, melting point, phase transformation, detection of discontinuous changes in polarization colours during the heating, sublimation behaviour.

Further, morphology and surface properties can be studied by various techniques such as scanning electron microscopy (SEM), atomic force microscopy (AFM) and scanning tunneling microscopy (STM). SEM provides greater magnification than optical microscopy, and AFM and STM are even higher and these techniques provide useful information about the physical properties of the solid forms.[61a, b] Different solid forms possess different X-ray powder patterns in most cases and hence it is a primary tool for characterization. Powder X-ray diffraction (PXRD)[61c, d] technique is one of the most definitive methods in identification and characterization of solid forms. The PXRD pattern of a solid is a plot of the diffraction intensity as a function of 2θ values and can be considered as a fingerprint of that solid. Finally, single crystal X-ray diffraction technique is the ultimate and employed to determine details of the structure and bonding interactions in the crystalline solid. However, it is not always possible to get diffraction quality single crystals for most of the compounds because of the complexity involved in getting the crystals, in which case other techniques play crucial role in characterising the solid forms.

1.9 Solubility and Dissolution

Solubility is a thermodynamic property while dissolution is a kinetic phenomenon.[62a-d] The equilibrium solubility of a compound is defined as *the maximum quantity of that*

substance which can be completely dissolved at a given temperature and pressure in a given amount of solvent, and is thermodynamically valid as long as a solid phase exists which is in equilibrium with the solution phase.[62e, f] The US Pharmacopeia and National Formulary describe solubility as the number of milliliters of solvent required to dissolve 1 gram of the solute. Equilibrium solubility of a solute will depend on its relative affinities towards solvent molecules and fellow solute molecules. Thus, the strength of molecular interactions, both inter and intra, affect solubility. The determination of solubility and the way to alter if necessary by amorhpisation, salt formation, cocrystallization, etc. are vital steps in pharmaceutical development programs. The bioavailability of an orally administered drug depends on its solubility in the gastrointestinal tract and its permeability across the cell membrane. This solubility and permeability are the basis for the Biopharmaceutics Classification System of the drugs.[63] Amidon *et al*.[63a] divided all drugs into four categories depending on the solubility and permeability (Figure 1.14).

Class I **High solubility, High permeability**	Class II **Low solubility, High permeability**
Phenobarbital, Chloroquine, Fluconazole, Zidovudine, Theophylline, Diazepam.	Carbamazepine, Griseofulvin Blonanserin, Nitrofurantoin, Nifedipine, Ketoconazole.
Class III **High solubility, Low permeability**	Class IV **Low solubility, Low permeability**
Cimetidine, Acyclovir, Ranitidine, Neomycin, Captopril, Enalprilate.	Itraconazole, Chlorothiazine, Furosemide, Tobramycin, Cefuroxime, Cyclosporin

Figure 1.14 The Biopharmaceutical Classification System.

Tablets or capsules taken orally remain one of the most effective means of treatment available. Orally administered solid dosage forms generally undergo disintegration, dissolution, and absorption to enter the blood stream and reach the site of action. For drugs with low solubility, dissolution is often the rate limiting step, and directly affects the rate and extent of drug absorption.[64a] Drug release in the human body can be measured *in-vivo* by measuring the plasma or urine concentrations in the subject concerned. However, there are certain obvious impracticalities involved in employing

such techniques on a routine basis. These difficulties have led to the introduction of official *in-vitro* tests which are now rigorously and comprehensively defined in the respective Pharmacopoeia. This is where the importance of the dissolution comes into play. Dissolution process generally involves two sequential steps (i) interaction between solid and solvent molecules to form solvated molecules (solvation), which takes place at the solid–liquid interface and (ii) mass transport of solvated molecules from the solid–liquid interface to the bulk solution. These two steps govern the rate and extent of solid dissolution. Solubility, a basic property for solids, controls the first step. Transport, on the other hand, usually controls the second step, which is generally slower than the first step. Overall, dissolution is governed by solubility and transport processes. To describe the dissolution phenomenon various models such as dissolution by pure diffusion, diffusion layer model, and convective diffusion model were proposed. Solubility is "how much" of drug dissolves and dissolution is "how fast" it reaches that concentration value.

1.9.1 Dissolution by Pure Diffusion

In dissolution processes, convection generally accompanies diffusion in transporting dissolved molecules. Dissolution through pure diffusion without any contribution from some form of convection is rare. Even without mixing, density gradients caused by concentration differences or thermal effects due to the heat of solvation can lead to natural convection. When a particle dissolves by pure diffusion, the concentration at every point away from the solid-liquid interface increases. But, the concentration gradient at any distance from the particle decreases with time. The overall dissolution rate of the particle keeps decreasing. In this case the concentration gradient may be constantly changing, so we will not be able to see the formation of a pseudo-steady state in this dissolution process.

1.9.2 Diffusion Layer Model

Noyes and Whitney proposed[64b] the basic transport-controlled model for solid dissolution. They suggested that when surface area is constant, the dissolution rate is proportional to the difference between solubility and the bulk solution concentration.

$$\text{Dissolution rate} = \frac{dQ}{dt} = K(Cs - Cb)$$

Where, K is a mass transfer coefficient.

Further, Nernst[64c] and Brunner[64d] suggested that rapid equilibrium (saturation) is achieved at the solid-liquid interface during dissolution, and then diffusion occurs across a thin layer of stagnant solution, called the diffusion layer, into the bulk solution. Diffusion across this diffusion layer is rate-controlling in most cases, which effectively converts the heterogeneous dissolution process into a homogeneous process of liquid-phase diffusion (Figure 1.15).

$$\text{Dissolution rate} = \frac{dQ}{dt} = \frac{DA}{h}(Cs - Cb)$$

Where,

D is the diffusion coefficient (cm^2/sec)

A is the surface area of the drug (cm^2)

h is the diffusion layer thickness (cm)

Cs is the saturation solubility of the drug

Cb is the bulk solution concentration
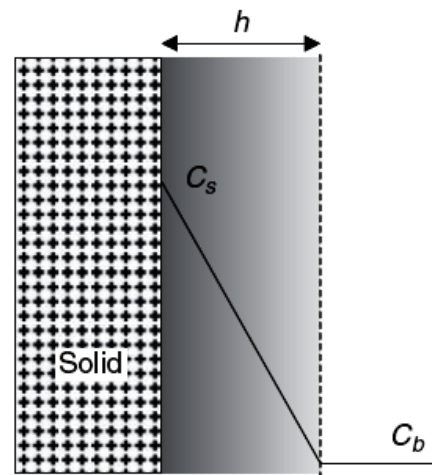
Figure 1.15 Diffusion layer model.

Adapted from ref. 64a.

Nernst and Brunner's concept of a diffusion layer being a stagnant or unstirred layer of liquid adhering to the solid surface is hydrodynamically unrealistic. Limitation to the model is that the notion of a stagnant liquid layer near the solid surface is not supported by fluid dynamics. Another limitation of the diffusion layer model is that it does not give a means to calculate independently a diffusion layer thickness based on hydrodynamics.

1.9.3 Convective Diffusion Model

The limitations of the diffusion layer model led to develop an improved model such as convective diffusion model.[65a-c] There are two mechanisms for the transport of solute molecules from a solid in a moving liquid, (i) there is molecular diffusion as a result of a concentration gradient and (ii) solute molecules are carried along by the moving solvent (convection). The general equation for convective diffusion is given.

$$\partial C/\partial t = D(\partial^2 C/\partial x^2 + \partial^2 C/\partial y^2 + \partial^2 C/\partial z^2) - v_x \partial C/\partial x - v_y \partial C/\partial y - v_z \partial C/\partial z$$

Where, v_x, v_y, and v_z are liquid velocities in the *x, y,* and *z* directions in Cartesian coordinates.

This equation is an extension of Ficks's second law of diffusion with a convection term. It is different from the Nernst's model by having a velocity gradient of the diffusion layer, mass transport by convection and diffusion both across and along the diffusion layer, and no definite boundary of the diffusion layer.

1.10 Types of Dissolution

There are two different types of dissolution methods (i) Planar surface dissolution and (ii) Particulate dissolution method.

1.10.1 Planar Surface Dissolution

Experimentally, planar surface dissolution is easier than particulate dissolution because of simpler mathematics. In order to calculate dissolution rate both Noyes-Whitney equation and convective methods can be used. Generally for pharmaceutical solids measuring dissolution rate from a well defined surface is a popular way, for that intrinsic dissolution rate (IDR) determination is one example.

Intrinsic dissolution rate: Parameters such as agitation intensity and surface area are fixed, dissolution rate can be considered as a property of the solid. This loosely defined property is called the "intrinsic" dissolution rate. Due to the close relationship between the IDR and solubility, measuring the IDR becomes an alternative method for solubility estimation when equilibrium solubility cannot easily be obtained experimentally. Since dissolution rate always affected by agitation intensity, surface area, and container configuration, these parameters should be kept constant to calculate IDR and to obtain good reproducibility. The compressed disk is put into the holder so that only one flat surface is in contact with the solvent. The disk is then rotated at a constant speed, and the dissolution rate is measured. The rotating disk apparatus for measuring IDR and the liquid flow[65d] are shown in the Figure 1.16.
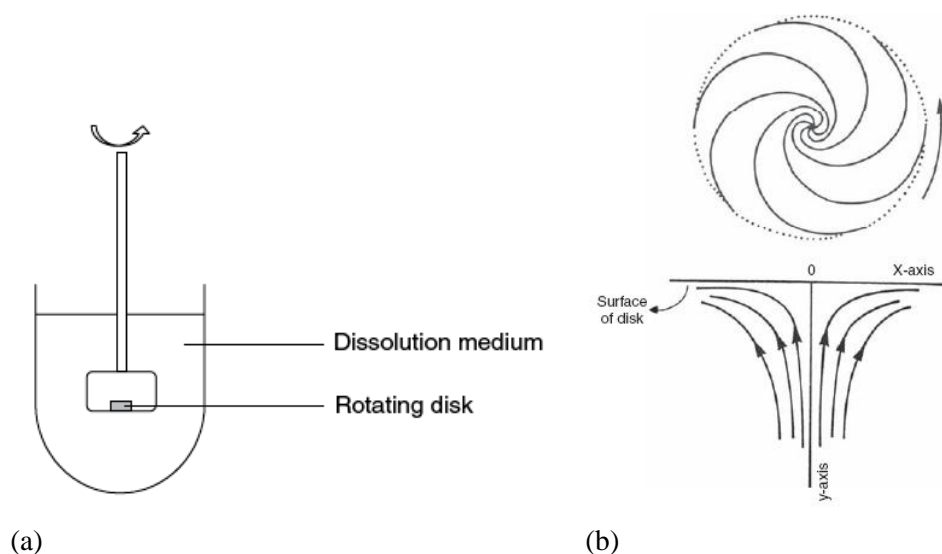
Figure 1.16 Rotating disk apparatus for measuring IDR, and (b) liquid flow pattern around the rotating disk apparatus (adapted from ref. 64a).

1.10.2 Particulate Dissolution

For practical purpose planar surface dissolution is important to understand dissolution mechanisms. However, dissolution of solid dosage forms usually involves solid particles. Oral dosage forms first disintegrate into small particles, which then dissolve for the drug to be bioavailable. The same dissolution theories that apply to planar surface dissolution are also applicable to particle dissolution.[65e] However, the dissolution of solid particles is more complicated, because total surface area changes during dissolution. Particles shape and size are the crucial parameters in this dissolution process.

1.11 Conclusions

In this thesis, we have explored the intermolecular interactions and supramolecular synthons and highlighted the importance of isotropic and anisotropic interactions in making complex crystalline architectures. We have briefly explored the origin and evolution of crystal engineering, and discussed the design of diverse pharmaceutical solid forms of the APIs which relies on crystal engineering principles. The study and understanding the nature and properties of the solid forms is important both from fundamental and application points of view. Such an understanding will be useful in the rational design of novel pharmaceutical solids and therefore to achieve the ultimate goal

of modulating the properties of APIs in a desired way. Upon solid form screening of API, we can end up with multitude of crystal forms such as polymorphs, hydrates/solvates, cocrystals, salts, eutectics, etc. These solid forms, by virtue of their uniqueness result in varied physicochemical properties which is important for optimal solid form selection and development. In the following chapters, chapter 2 deals with the improvement in solubility of poorly soluble febuxostat through cocrystals, chapter 3 describes the identification, characterization and stability relationships of tetramorphs of trimethoprim, chapter 4 explores the solubility enhancement of low soluble blonanserin drug through salts, chapter 5 explores polymorphism in N-carbmoyl-L-glutamic acid, and chapter 6 discusses the solubility, dissolution and stability aspects of blonanserin salt polymorphs. In short, this thesis deals with extensive studies of different solid state forms APIs and their relevance in addressing the various issues associated with drug molecules for pharmaceutical applications.

1.12 References

1. W. H. Bragg, *Proc. Phys. Soc.*1921, **34**, 33.

2. (a) J. M. Robertson, *Proc. R. Soc.* 1951, **207**, 101. (b) J. M. Robertson, *Organic Crystals and Molecules*, Cornell University Press, 1953.

3. R. Pepinsky, *Phys. Rev.,* 1955, **100**, 52.

4. (a) M. D. Cohen, G. M. J. Schmidt, F. I. Sonntag, *J. Chem. Soc.* 1964, 2000. (b) G. J. M. Schmidt, *Pure Appl. Chem.,* 1971, **27**, 647-678.

5. (a) O. Ermer, *J. Am. Chem. Soc.,* 1988, **110**, 3747. (b) G. R. Desiraju, *Crystal Engineering: The Design of Organic Solids*, Elsevier, Amsterdam, 1989.

6. (a) B. F. Hoskins, R. Robson, *J. Am. Chem. Soc.*, 1990, **112**, 1546. (b) B. F. Hoskins, R. Robson, *J. Am. Chem. Soc.*, 1989, **111**, 5962.

7. (a) E. R. T. Tiekink, J. J. Vittal, M. J. Zaworotko, *Organic Crystal Engineering: Frontiers in Crystal Engineering*, John Wiley & Sons, Ltd., West Sussex, 2010. (b) G. R. Desiraju, J. J. Vittal, A. Ramanan, *Crystal Engineering. A Textbook,* World Scientific Publishing, Singapore, 2011. (c) G. R. Desiraju (Ed.), *Crystal Design: Structure and Function, Perspectives in Supramolecular Chemistry*, Vol **7**. Wiley and Sons, 2003. (d) E. Weber (Ed.), *Design of Organic Solids*, Springer-Verlag, Berlin, 1998. (e) M. D. Hollingsworth, *Science,* 2002, **295**,

2410. (f) L. Brammer, *Chem. Soc. Rev.,* 2004, **33**, 476. (g) B. Moulton, M. J. Zaworotko, *Chem. Rev.*, 2001, **101**, 1629.

8. (a) J. D. Dunitz, *Pure Appl. Chem*. 1991, **63**, 177. (b) J.-M. Lehn, *Supramolecular Chemistry: Concepts and Perspectives*, VCH: Weinheim, 1995.

9. (a) A. I. Kitaigorodskii, *Molecular crystals and molecules*, Academic Press, New York, 1973. (b) A. J. Pertsin, A. I. Kitaigorodskii, *The Atom-Atom Potential Method*, Springer-Verlag, 1987.

10. (a) T. Steiner, *Angew. Chem. Int. Ed.,* 2002, **41**, 48-76. (b) G. R. Desiraju, *Acc. Chem. Res.,* 1991, **24**, 290-296. (c) G. A. Jeffrey, W. Saenger, *Hydrogen Bonding in Biological Structures*, Springer-Verlag, Berlin, 1991.

11. (a) L. Pauling, *The Nature of Chemical Bond*, Cornell University Press, Ithaca, New York, 1939. (b) E. Arunan, G. R. Desiraju, R. A. Klein, J. Sadlej, S. Scheiner, I. Alkorta, D. C. Clary, R. H. Crabtree, J. J. Dannenberg, P. Hobza, H. G. Kjaergaard, A. C. Legon, B. Mennucci, D. J. Nesbitt, *Pure Appl. Chem*., 2011, **83**, 1619. (c) G. R. Desiraju and T. Steiner, *The Weak Hydrogen Bond: In Structural Chemistry and Biology*, Oxford University Press, New York, 1999.

12. (a) E. J. Corey, *Pure Appl. Chem.* 1967, **14**, 19. (b) E. J. Corey, X. -M. Cheng, *The Logic of Chemical Synthesis*, 1989, Wiley, New York. (c) G. R. Desiraju, *Angew. Chem. Int. Ed. Engl.* 1995, **34**, 2311. (d) R. D. B. Walsh, M. W. Bradner, S. Fleishman, L. A. Morales, B. Moulton, N. Rodríguez-Hornedo, M. J. Zaworotko, *Chem Commun*, 2003, 186.

13. Cambridge Structural Database, ver. 5.36. ConQuest 1.17, November 2014 release, November 2014 update, CCDC, www.ccdc.cam.ac.uk.

14. (a) B. R. Bhogala, S. Basavoju, A. Nangia, *Cryst. Growth Des.*, 2005, **5**, 1683. (b) P. Vishweshwar, A. Nangia, V. M. Lynch, *CrystEngComm,* 2003, **5**, 164. (c) V. R. Vangala, R. Mondal, C. K. Broder, J. A. K. Howard, G. R. Desiraju, *Cryst. Growth Des.,* 2005, **5**, 99. (d) L. S. Reddy, P. M. Bhatt, R. Banerjee, A. Nangia and G. J. Kruger, *Chem. Asian J.* 2007, **2**, 505. (e) J. A. Bis and M. J. Zaworotko, *Cryst. Growth Des.* 2005, **5**, 1169. (f) L. S. Reddy, N. J. Babu, A. Nangia, *Chem Commun,* 2006, 1369.

15. (a) A. M. Thayer, *Chem Eng News*, 2010, **88**, 13. (b) C. G. Smith, J. J. O'Donnell, *The Process of New Drug Discovery and Development*, Informa, New York, 2006.

16. (a) S. Domingos, V. André, S. Quaresma, I. C. Martins, M. F. Minas da Piedade, M. T. Duarte, *J. Pharm. Pharmacol.* 2015, doi: 10.1111/jphp.12384. (b) R. Banerjee, P. M. Bhatt, G. R. Desiraju, *Cryst. Growth Des.* 2006, **6**, 1468. (c) P. Sanphui, N. Goud, U. Khandavilli, S. Bhanoth, A. Nangia, *Chem. Commun.*2011, **47**, 5013.

17. (a) P. Sanphui, M. K. Mishra, U. Ramamurty, G. R. Desiraju, *Mol. Pharmaceutics*, 2015, **12**, 889.(b) S. Bhandaru, N. Malothu, R. R. Akkinepally, *Cryst. Growth Des.* 2015, **15**, 1173. (c) A. A. Thorat, S. V. Dalvi, *Cryst. Growth Des.*2015, doi: 10.1021/cg501814q. (d) Ö. Almarsson, M. J. Zaworotko, *Chem. Commun.,* 2004, 1889.

18. (a) N. Shan, F. Toda, W. Jones, *Chem. Commun.* 2002, 2372. (b) A. V. Trask, W. Jones, *Top. Curr. Chem.* 2005, **254**, 41. (c) A. Dilori, T. Friščić, W. Jones, *CrystEngComm* 2012, **14**, 2350. (d) P. P. Bag, M. Patni, C. M. Reddy, *CrystEngComm* 2011, **13**, 5650.

19. (a) L. Yu, *Adv. Drug Deliv. Rev*., 2001, **48**, 27. (b) N. J. Babu, A. Nangia, *Cryst. Growth Des.* 2011, **11**, 2662.

20. (a) J. D. Mullins, T. J. Macek, *J. Pharm. Sci*., 1960, **49**, 245. (b) S. R. Byrn, R. R. Pfeiffer and J. G. Stowell, *Solid-State Chemistry of Drugs*; SSCI, West Lafayette, IN, 1999.

21. (a) S. L. Morrisette, Ö. Almarsson, M. L. Peterson, J. F. Remenar, M. J. Read, A. V. Lemmo, S. Ellis, M. J. Cima, C. R. Gardner, *Adv. Drug Deliv. Rev*., 2004, **56**, 275. (b) J. Lu and S. Rohani, *Curr. Med. Chem*., 2009, **16**, 884. (c) G. G. Z. Zhang, D. Law, E. A. Schmitt, Y. Qiu, *Adv. Drug Delivery Rev.*, 2004, **56**, 371.

22. (a) A. Nangia, *Acc. Chem. Res*., 2008, **41**, 595. (b) N. K. Nath, S. Nilapwar and A. Nangia, *Cryst. Growth Des.* 2012, **12**, 1613-1625. (c) A. T. M. Serajuddin, *J. Pharm. Sci.* 1999, **88**, 1058.

23. (a) Q. Wang, S. Li, X. Che, X. Fan, C. Li, *Asian J. Pharm. Sci.,* 2010, **5**, 188. (b) D. Bahl, R. H. Bogner, *Pharm. Res*., 2006, **23**, 2317.(c) K. Suresh, M. K. C. Mannava, A. Nangia, *RSC Adv*., 2014, **4**, 58357.

24. (a) J. Haleblian, W. McCrone, *J. Pharm. Sci*., 1969, **58**, 911. (b) P. Soni, C. Sarkar, R. Tewari, T. D. Sharma, *J. Energ. Mater.* 2011, **29**, 261.

25. (a) E. Mitscherlich, *Abhl. Akad. Berlin*, 1822, 43. (b) J. Berzelius, *Jahresbericht*, 1844, **23**, 44. (c) F. Wöhler, J. Liebig, *Annal. Pharm.*, 1832, **3**, 249. (d) G. B. Amici, *Ann. Chim. Phys., Ser.* 1844, **12**, 114. (e) E. Mallard, *Annales Mines*,

1876, **10**, 60. (f) O. Lehmann, *Die Krystallanalyse oder die chemische Analyse durch Beobachtung der Krystallbildung mit Hülfe des Mikroskps*, Wilhelm Engelmann, Liepzig, 1891. (g) W. F. Ostwald, *Z. Phys. Chem.*, 1897, **22**, 289.

26. (a) W. C. McCrone, in *Physics and Chemistry of the Organic Solid State*, Vol. *2*, eds. D. Fox, M. M. Labes and A. Weissberger, Wiley Interscience, New York, 1965, 725. (b) V. López-Mejías, J. Kampf, A. Matzger, *J. Am. Chem. Soc* 2012, **134**, 9872.

27. (a) J. Bernstein, *Polymorphism in Molecular Crystals*; Clarendon, Oxford, U. K., 2002. (c) H. G. Brittain, Polymorphism in Pharmaceutical Solids, Informa Health Care, New York, 2009. (a) R. Hilfiker, Ed., *Polymorphism in the Pharmaceutical Industry*; Wiley-VCH, Weinheim, Germany, 2006.

28. (a) N. J. Babu, S. Cherukuvada, R. Thakuria, A. Nangia, *Cryst. Growth Des*., 2010, **10**, 1979. (b) D. E. Braun, T. Gelbrich, V. Kahlenberg, G. Laus, J. Wieser, U. J. Griesser, *New J Chem.,* 2008, **32**, 1677.

29. (a) A. Nangia, *Acc. Chem. Res*., 2008, **41**, 595. (b) A. J. Cruz-Cabeza, J. Bernstein *Chem. Rev.* 2014, **114**, 2170.(c) J. Bauer, S. Spanton, R. Henry, J. Quick, W. Dziki, W. Porter, J. Morris, *Pharm. Res.* 2001, **18**, 859.

30. (a) S. R. Vippagunta, H. G. Brittain, D. J. W. Grant, *Adv. Drug Delivery Rev.* 2001, **48**, 3. (b) K. Fucke, N. Qureshi, D. S. Yufit, J. A. Howard, J. W. Steed, *Cryst. Growth Des*., 2009, **10**, 880.

31. (a) R. K. Jetti, R. Boese, J. A. R. P. Sarma, L. S. Reddy, P. Vishweshwar, G. R. Desiraju, *Angew. Chem., Int. Ed.*, 2003, **42**, 1963. (b) B. R. Sreekanth, P. Vishweshwar, K. Vyas, *Chem. Commun.*, 2007, 2375. (c) J. L. Derissen and P. H. Smit, *Acta Crystallogr.*, 1974, **B30**, 2240. (d) S. Cherukuvada, R. Thakuria and A. Nangia, *Cryst. Growth Des.,* 2010, **10**, 3931-3941.

32. (a) F. Wöhler, J. Liebig, *Annal. Pharm.*, 1832, **3**, 249. (b) J. Elguero, *Cryst. Growth Des.,* 2011, **11**, 4731. (c) P. M. Bhatt and G. R. Desiraju, *Chem. Commun,* 2007, 2057.

33. (a) J. D. Dunitz, J. Bernstein, *Acc. Chem. Res.* 1995, **28**, 193. (b) R. W. Lancaster, L. D. Harris, D. Pearson, *CrystEngComm*, 2011, **13**, 1775. (c) G. A. Stephenson, J. Kendrick, C. Wolfangel, F. J. Leusen, *Cryst. Growth Des*., 2012, **12**, 3964.

34. (a) J. Zhou, Y.-S. Kye and G. S. Harbison, *J. Am. Chem. Soc.*, 2004, **126**, 8392. (b) A. Trask, N. Shan, W.D. S. Motherwell, W. Jones, S. Feng, R. Tan, K.

Carpenter, *Chem. Commun*. 2005, 880. (c) N. K. Nath, S. S. Kumar, A. Nangia, *Cryst. Growth Des.* 2011, **11**, 4594. (d) R. Barbas, R. Prohens, C. Puigjaner, *J. Therm. Anal. Cal.* 2007, **89**, 687. (e) S. S. Kumar, A. Nangia, *Cryst. Growth Des.* 2014, **14**, 1865.

35. (a) L. Yu. *Acc. Chem. Res*., 2010, **43**, 1257. (b) L. Yu, G. A. Stephenson, C. A. Mitchell, C. A. Bunnell, S. V. Snorek, J. J. Bowyer, T. B. Borchardt, J. G. Stowell, S. R. Byrn, *J. Am. Chem. Soc.* 2000, **122**, 585. (c) C. A. Mitchell, L. Yu, M. D. Ward, *J. Am. Chem. Soc.* 2001, **123**, 10830. (d) S. Chen, I. A. Guzei, L. Yu, *J. Am. Chem. Soc.* 2005, **127**, 9881. (e) S. Chen, H. Xi, L. Yu, *J. Am. Chem. Soc.,* 2005, **127**, 17439.

36. (a)) S. R. Byrn, R. R. Pfeiffer and J. G. Stowell, *Solid-State Chemistry of Drugs*; SSCI, West Lafayette, IN, 1999. (b) M. Draguet-Brughmans, R. Bouche, J. P. Flandre, A. van den Bulcke, *Pharm. Acta helv*., 1979, **54**, 140. (c) T. Yokoyama, T. Umeda, K. Kuroda, T. Nagafuku, T. Yamamoto and S. Asada, *J. Pharm. Soc. Jpn*., 1979, **99**, 837. (d) T. Yokoyama, T. Umeda, K. Kuroda, T. Kuroda, S. Asada, *Chem. Pharm. Bull*., 1980, **29**, 194.

37. (a) J. Bauer, S. Spanton, R. Henry, J. Quick, W. Dziki, W. Porter and J. Morris, *Pharm. Res*., 18, **2001**, 859. (b) A. J. Aguiar, J. Krc, A. W. Kinkel, J. C. Samyn, *J. Pharm. Sci.* 1967, **56**, 847. (c) A. Nangia, G. R. Desiraju, *Chem Commun.,* 1999, 605.

38. (a) G. R. Desiraju, *Nature Materials*, 2002, **1**, 77. (b) J. I. Seeman, *J. Chem. Ed.* 1986, **63**, 42. (c) A. Burger, R. Ramberger, *Mikrochim. Acta II* 1979, 259.

39. (a) A. Nangia, G. R. Desiraju, *Chem Commun.,* 1999, 605. (b) B. Bechtloff, S. Nordhoff, J. Ulrich, *Cryst. Res. Technol*., 2001, **36**, 1315. (c) A. L. Bingham, D. S. Hughes, M. B. Hursthouse, R. W. Lancaster, S. Tavener, T. L. Threlfall Chem. Commun., 2001, 603. (d) D. Giron, C. Goldbronn, M. Mutz, S. Pfeffer, P. Piechon, P. Schwab, *J. Thermal Anal. Cal.* 2002, **68**, 453.

40. (a) S. Roy, N. R. Goud, N. J. Babu, J. Iqbal, A. K. Kruthiventi, A. Nangia, *Cryst. Growth. Des*. 2008, **8**, 4343. (b) M. R. Caira, E. W. Pienaar, A. P. Lötter, *Mol. Cryst. Liq. Cryst*., 1996, **279**, 241. (c) J. Lin, D. Ostovic, J. Vacca, *Pharm. Biotechnol.,* 1998, **11**, 233.

41. http://www.ich.org/products/guidelines/quality/article/quality-guidelines.html.

42. (a) R. R. Pfeiffer, K. S. Yang, M. A. Tukker, *J. Pharm. Sci*. 1970, **59**, 1809. (b) D. Martins, M. Sanselme, O. Houssin, V. Dupray, M. N. Petit, D. Pasquier, C.

Diolez, G. Coquerel, *CrystEngComm*, 2012, **14**, 2507. (c) B. Samas, C. Seadeek, A. M. Campeta, B. P. Chekal, *J. Pharm. Sci.*, 2011, **100**, 186. (d) B. Nicolaï, P. Espeau, R. Céolin, M. -A. Perrin, L. Zaske, J. Giovannini, F. Leveiller, *J. Ther. Anal. Cal.*, 2007, **90**, 337.

43. (a) A. T. M. Serajuddin, *Adv. Drug Delivery Rev.* 2007, **59**, 603. (b) R. Thakuria, A. Nangia, *CrystEngComm* 2011, **13**, 1759. (c) P. L. Gould, *Int. J. Pharm.*, 1986, **33**, 201.(d) D. Maddileti, B. Swapna, A. Nangia, *Cryst. Growth Des.* 2014, **14**, 2557.(e) S. M. Berge, L. D. Bighley, D. C. Monkhouse, *J. Pharm. Sci.* 1977, **66**, 1.

44. (a) S. L. Childs, G. P. Stahly, A. Park, *Mol. Pharmaceutics* 2007, **4**, 323. (b) B. Sarma, N. K. Nath, B. R. Bhogala, A. Nangia, *Cryst. Growth Des.* 2009, **9**, 1546. (c) S. L. Childs, G. P. Stahly, A. Park, *Mol. Pharmaceutics,* 2007, **4**, 323. (d) A. J. Cruz-Cabeza, *CrystEngComm* 2012, **14**, 6362. (e) G. S. Paulekuhn, J. B. Dressman and C. Saal, *J. Med. Chem.* 2007, **50**, 6665.

45. (a) M. Mirmehrabi, S. Rohani, K. S. K. Murthy, B. Radatus, *Int. J. Pharm.*, 2004, **282**, 73. (b) N. A. Kasim, M. Whitehouse, C. Ramachandran, M. Bermejo, H. Lennernäs, H. E. Junginger, S. A. Stavchansky, K. K. Midha, V. P. Shah and G. L. Amidon, *Mol. Pharm.*, 2004, **1**, 85. (c) P. L. Gould, *Int. J. Pharm.,* 1986, **33**, 201.(d) R. J. Bastin, M. J. Bowkerm, B. J. Slater, *Org. Pro. Res. Dev.*, 2000, **4**, 427. (e) H. Bhutani, S. Singh, K. C. Jindal, A. K. Charkraborti, *J. Pharm. Biomed. Anal.*, 2005, **39**, 892. (f) S. Singh, B. Mohan, *Int. J. Tuberc. Lung Dis.*, 2003, **7**, 298.

46. (a) S. G. Olovson, N. Havu, C. G. Regårdh, A. Sandberg, *Acta Pharmacologica et Toxicologica*, 1986, **58**, 55. (b) V. J. Stella, K. W. Nti-Addae, *Adv. Drug Deliv. Rev.* 2007, **59**, 677. (c) H. Matsumoto, T. Hamawaki, H. Ota, T. Kimura, T. Goto, K. Sano, Y. Hayashi, Y. Kiso, *Bioorg. Med. Chem. Let.*, 2000, **10**, 1227.

47. (a) F. Wöhler, *Justus Liebigs Ann. Chem.* 1844, **51**, 153. (b) M. C. Etter, *J. Phys. Chem.* 1991, **95**, 4601. (c) A. V. Trask, W. D. S. Motherwell, W. Jones, *Cryst. Growth Des.*, 2009, **5**, 1013. (d) P. Vishweshwar, J. A. McMahon, J. A. Bis, M. J. Zaworotko, *J. Pharm. Sci.* 2006, **95**, 499. (e) C. B. Aakeröy, S. Forbes, J. Desper, *J. Am. Chem. Soc.*, 2009, **132**, 17048. (f) A. Alhalaweh, S. P. Velaga, *Cryst. Growth Des.*, 2010, **10**, 3302. (g) M. K. Stanton, R. C. Kelly, A. Colletti,

Y.-H. Kiang, M. Langley, E. J. Munson, M. L. Peterson, J. Roberts, M. Wells, *J. Pharm. Sci.*, 2010, **99**, 3769.

48. (a) S. Aitipamula, et al. *Cryst. Growth Des.* 2012, **12**, 2147. (b) W. Jones, W. D. Motherwell, A. V. Trask, *MRS bulletin*, 2006, **31**, 875. (c) N. Schultheiss, A. Newman, *Cryst. Growth Des.* 2009, **9**, 2950. (d) C. B. Aakeröy, M. Fasulo, J. Desper, *Mol. Pharmaceutics,* 2007, **4**, 317.

49. US-FDA GRAS chemical list, http://www.fda.gov/Food/IngredientsPackagingLabeling/FoodAdditivesIngredients/ucm091048.htm (accessed on March 8, 2015).

50. (a) D. J. Good, N. Rodríguez-Hornedo, *Cryst. Growth Des.* 2009, **9**, 2252. (b) S. L. Childs, L. J. Chyall, J. T. Dunlap, V. N. Smolenskaya, B. C. Stahly, G. P. *J. Am. Chem. Soc.* 2004, **126**, 13335.(c) V. Trask, W. S. Motherwell, W. Jones, *Cryst. Growth Des.* 2005, **5**, 1013.

51. (a) J. F. Remenar, S. L. Morissette, M. L. Peterson, B. Moulton, J. M. MacPhee, H. R. Guzman, O. Almarsson, *J. Am. Chem. Soc.* 2003, **125**, 8456. (b) S. L. Childs, L. J. Chyal, J. T. Dunlap, V. N. Smolenskaya, B. C. Stahly, G. Stahly, *J. Am. Chem. Soc.* 2004, 126, 13335. (c) Y. Huang, B. Zhang, Y. Gao, J. Zhang, L. Shi, *J. Pharm. Sci.* 2014, **103**, 2330.

52. (a) T. Higuchi, I. H. Pitman, *J. Pharm. Sci.* 1973, **62**, 55. (b) Bak, A. Gore, E. Yanez, M. Stanton, S. Tufekcic, R. Syed, A. Akrami, M. Rose, S. Surapaneni, T. Bostic A. King, S. Neervannan, D. Ostovic, A. Koparkar, *J. Pharm. Sci.* 2008, **97**, 3942. (c) M. S. Jung, J. S. Kim, M. S. Kim, A. Alhalaweh, W. Cho, S. J. Hwang, S. P. Velaga, S. P. *J. Pharm. Sci.* 2010, **62**, 1560.

53. (a) A. V. Trask, W. D. S. Motherwell, W. Jones, *Int. J. Pharm.* 2006, **320**, 114. (b) S. Basavoju, D. Boström, S. P. Velaga, *Pharm. Res.* 2008, **25**, 530. (c) K. Suresh, N. R. Goud, A. Nangia, *Chem. Asian J.*, 2013, **8**, 3032. (d) S. Karki, T. Friščić, L. Fábián, P. R. Laity, G. M. Day, W. Jones, *Adv. Mater.* 2009*,* **21**, 3905.

54. (a) S. Cherukuvada, A. Nangia, *Chem. Commun*. 2014, **50**, 906. (b) S, Cherukuvada, A. Nangia, *CrystEngComm*, 2012, **14**, 2579. (c) N. R. Goud, K. Suresh, P. Sanphui, A. Nangia, *Int. J. Pharm.,* 2012, **439**, 63. (d) D. R. Askeland, P. P. Fulay, *Essentials of Materials Science and Engineering*, 2nd ed., Cengage Learning, 2009. (e) D. M. Stefanescu, *Science and Engineering of Casting Solidification*, 2nd Ed., Springer, 2009.

55. (a) S. S. Das, N. P. Singh, T. Agrawal, P. Gupta, S. N. Tiwari, N. B. Singh, *Mol. Cryst. Liq. Cryst.*, 2009, **501**, 107. (b) N. B. Singh, S. S. Das, N. P. Singh, T. Agrawal, *J. Cryst. Growth*, 2008, **310**, 2878.

56. (a) T. Proffen, K. L. Page, S. E. McLain, B. Clausen, T. W. Darling, J. A. Tencate, S. Y. Lee, E. Ustundag, *Z. Kristallogr.* 2005, **220**, 1002. (b) V. Petkov, M. Gateshki, J. Choi, E. G. Gillan, Y. Ren, *J. Mater. Chem.,* 2005, **15**, 4654. (c) A. M. Beale, B. M. Weckhuysen, *Phys. Chem. Chem. Phys.*, 2010, **12**, 5562-5574. (d) S. Cammelli, D. L. Hecht, C. Degueldre, J. Bertsch, R. Frahm, *J. Phys. Conf. Ser.,* 2009, **190**, 12027.

57. (a) M. Prasad, Refrigeration and Air Conditioning, New Age International Publishers, 2nd edn, 2006. (b) A. Karaipekli, A. Sari, *J. Ind. Eng. Chem.* 2010, **16**, 767. (c) L. Shilei, Z. Neng, F. Guohui, Energy Build., 2006, **38**, 708. (d) B. F. J. Broberg, H. C. A. Evers, *US Pat*., 4529601, 1985.

58. (a) W. L. Chiou, F. Niazi, *J. Pharm. Sci.* 1976, **65**, 1212. (b) C. W. Park, H. M. Mansour, T. O. Oh, J. Y. Kim, J. M. Ha, B. J. Lee, S. C. Chi, Y. S. Rhee, E. S. Park, *Int. J. Pharm.*, 2012, **436**, 652.

59. (a) E. Suzuki, K. –I. Shirotani, Y. Tsuda, K. Sekiguchi, *Chem. Pharm. Bull.*, 1985, **33**, 5028. (b) X. J. Gu and W. Jiang, *J. Pharm. Sci.*, 1995, **84**, 1438. (c) A. M. Tudor, M. C. Davies, C. D. Melia, D. C. Lee, R. C. Mitchell, P. J. Hendra, S. J. Church, *Spectrochim. Acta Part A*, 1991, **47**, 1389. (d) D. C. Apperley, R. A. Fletton, R. K. Harris, R. W. Lancaster, S. Tavener, T. L. Threlfall, *J. Pharm. Sci.*, 1999, **88**, 1275.

60. (a) Threlfall, *The Analyst*, 1995, **120**, 2435. (b) S. R. Vippagunta, H. G. Brittain, D. J. W. Grant, *Advanced Drug Deliv. Sys*., 2001, **48**, 3.(c) F. W. McLafferty, *Acc. Chem.Res.*, 1990, **23**, 63. (d) W. H. Streng, *Drug Disc. Today*, 1997, **2**, 415. (e) J. Bernstein, J. –O. Henck, *Cryst. Eng.*, 1998, **1**, 119.

61. (a) G. Nichols and C. S. Frampton, *J. Pharm. Sci.*, 1998, **87**, 684. (b) G. T. R. Palmore, T. J. Luo, T. L. Martin, M. T. McBride-Wieser, N. T. Voong, *Trans. Am. Crystallogr. Assoc.*, 1998, **33**, 45. (c) L. V. Azaroff, M. J. Burger, *The powder method in x-ray crystallography*. McGraw-Hill Book Company, New York, U. S. A., 1958. (d) C. Giacovazzo, (ed.), *Fundamentals of crystallography*. International Union of Crystallography, Oxford, 1992.

62. (a) A. Serajuddin, *Adv. Drug Del. Rev.,* 2007, **59**, 603. (b) A. Llinàs, R. C. Glen, J. M. Goodman, *J. Chem. Inf. Model.* 2008, **48**, 1289. (c) J. Alsenz, M. Kansy

Adv. Drug Del. Rev. 2007, **59**, 546. (d) D. Giron, *Thermochim. Acta* 1995, **248**, 1. (e) A. Avdeef, *Solubility in Absorption and Drug Development: Solubility, Permeability, and Charge State*, 2nd Eds. John-Wiley, USA, 2012, 251. (f) C. Lipinski, F. Lombardo, B. Dominy, P. Feeney, *Adv. Drug Del. Rev.* 2001, **46**, 3.

63. G. L. Amidon, H. Lennernäs, V. P. Shah, J. R. Crison, *Pharm. Res.*, 1995, **12**, 413. (b) A. Dahan, J. M. Miller, G. L. Amidon, *The AAPS Journal*, 2009, **11**, 740. (c) N. A. Kasim, M. Whitehouse, C. Ramachandran, M. Bermejo, H. Lennernäs, A. S. Hussain, H. E. Junginger, S. A. Stavchansky, K. K. Midha, V. P. Shah, G. L. Amidon, *Mol. Pharm.*, 2004, **1**, 85.

64. (a) Y. Qiu, Y. Chen, G. G. Zhang, L. Liu, W. Porter, (Eds.), *Developing solid oral dosage forms: pharmaceutical theory and practice*, Academic press, 2009. (b) A. Noyes and W. R. Whitney, *J. Am. Chem. Soc.* 1897, **19**, 930. (c) W. Nernst, *Zeitschrift für Physikalische Chemie*, 1904, **47**, 52. (d) E. Bruner, *Zeitschrift für Physikalische Chemie*, 1904, **47**, 56.

65. (a) G. Levich, *Physicochemical Hydrodynamics*, 2nd Ed., Prentice-Hall, Englewood Cliffs, New Jersey, 1962, 57. (b) D. P. McNamara, G. L. Amidon, *J. Pharm. Sci.*, 1986,**75**, 858. (c) K. G. Nelson, A. C. Shah, *J. Pharm. Sci.*, 1987, **76**, 799. (d) V. G. Levich, *Physicochemical Hydrodynamics*, 2nd Ed., Prentice-Hall, Englewood Cliffs, New Jersey, 1962, 61. (e) P. J. Niebergall, G. Milosovich, J. E. Goyan, *J. Pharm. Sci.*, 1963, **52**, 236.

CHAPTER TWO

SOLUBLE COCRYSTALS OF XANTHINE OXIDASE INHIBITOR FEBUXOSTAT
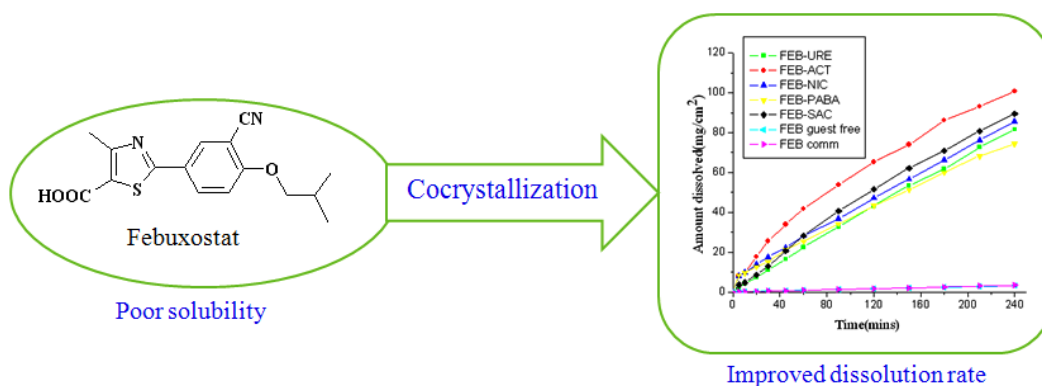
X-ray crystal structures of five novel cocrystals of the xanthine oxidase inhibitor Febuxostat (FEB) and its guest-free form are discussed. The crystal structure of FEB has COOH···N≡C hydrogen bond whereas the cocrystal structures are sustained by acid–amide (URE and NIC cocrystals) and acid–acid synthons (PABA cocrystal). All the cocrystals exhibited faster dissolution rate than the parent drug (35–50 times) and showed good stability at 40 °C, 75% RH.

2.1 Introduction

In recent decades both academic groups and pharmaceutical companies have shown considerable interest in the application of crystal engineering principles to the control and tuning of the physical and chemical properties of Active Pharmaceutical Ingredients (APIs). A majority of drug molecules (over 80%) fail at the late stage of drug formulation and pre-clinical studies due to the problems of low solubility and poor bioavailability.[1] Salt formation is the most common and well practiced approach to improve the physicochemical properties of drugs, e.g. solubility, stability, dissolution rate, melting point, filterability, etc.[2] However, salts are sometimes more likely to form hydrates and have an inherent tendency for hygroscopicity when compared to cocrystals.[3] Cocrystals are relatively new, in particular 'pharmaceutical cocrystals' which can be defined as crystalline molecular complexes of a fixed stoichiometry between an API with another pharmaceutically acceptable molecule or Generally Regarded As Safe (GRAS) chemical.[4,2e] Improving the aqueous solubility is a primary thrust in the development of novel solid-state forms such as amorphous, polymorphs, cocrystals, hydrates/solvates, and salts.[5] Among these options, advantage with cocrystallization is that the properties of the cocrystals can be tuned with pharmaceutically acceptable coformers without altering the chemical structure of the API. Cocrystals are more popular among the scientific community because of their diverse pharmaceutical applications and ability to address issues associated with drug molecules. Various groups all over the world have used cocrystallization technique to tackle various inherent problems associated with drug molecules. For instance, Trask et al.[6a] highlighted the importance of cocrystallization in addressing the hydration problems of caffeine. They have reported that caffeine-oxalic acid cocrystal did not transform to caffeine hydrate even under high relative humidity. Velaga et al.[6b] improved the dissolution rate of indomethacin by forming a cocrystal with saccharin. They showed that indomethacin-saccharin cocrystal had a greater than 50 times increase in dissolution rate in phosphate buffer (pH 7.4) compared to γ-indomethacin, the most stable polymorph.

Further, Nangia and coworkers[7a] have reported the remarkable improvement in inhibiting the chemical transformation of andrographolide to its inactive sulfate metabolite by cocrystal approach. They have highlighted the chemical stability and improved solubility (12-folds) of andrographolide by forming cocrystal with salicylic acid. Remenar and colleagues[7b] have reported that the Itraconazole-L-Malic acid cocrystal showed 20 fold higher dissolution rate compared to crystalline Itraconazole and comparable solubility to that of the marketed amorphous form. Florence et al.[7c] reported that liquid anesthetic propofol was cocrystallised with isonicotinamide and cocrystal exhibited melting point ∼50 °C higher than the native drug form, such that the liquid drug becomes a stable solid at room temperature. Since drug candidates are usually preferred in a solid dosage form, they have highlighted the potential of cocrystallization as a tool to raise API melting point and would have potential application for other drugs such as low melting and liquid drugs. The challenges of low aqueous solubility offer an ideal situation for the application of crystal engineering techniques to improve bioavailability, especially for the drugs which belong to Biopharmaceutics Classification System (BCS) Class II and Class IV. Similar to other solid forms of APIs, cocrystals also confer novel intellectual property and patent protection.[8] In this chapter we wish to highlight that cocrystals represent a viable alternative for an ionizable BCS Class II drug Febuxostat to improve solubility wherein salt formation is not an option.

2.2 Literature reports on Febuxostat

Febuxostat (chemical name: 2-(3-cyano-4-isobutyloxy)-phenyl-4-methyl-5-thiazolecarboxylic acid, abbreviated as FEB, Scheme 2.1) is a non-purine selective inhibitor of xanthine oxidase which is used for the management of hyperuricemia in patients with gout.[9] Gout is a disorder caused by the deposition of monosodium urate crystals in joints and tissues as a result of extracellular urate supersaturation. However, hyperuricemia is the most important risk factor for the development of gout and occurs as a result of increased uric acid production. Febuxostat is marketed under the brand name Uloric for the chronic management of hyperuricaemia in patients with gout. There are several patents on different crystalline forms of FEB wherein 14 forms named F1-F14 were disclosed in a US patent.[10] Forms A, B, C, D and G were reported in an EP patent,[11] and forms H, I and J in a WO

document.[12] Inorganic salts of FEB with Na, K, Li, Mg, Ca, Zn, Ba, Sr, choline, epolamine and derivatives of the ammonium salt were reported recently.[13] There are many solvates of FEB but we have not found any report in the literature on cocrystals to improve the solubility of this drug. FEB is a Biopharmaceutics Classification System (BCS) class II drug (low solubility, high permeability) having low aqueous solubility of 12.9 mg/L and $D_0 = 25$ (i.e. practically insoluble in water).[14] We prepared cocrystals of FEB with the objective to improve the solubility of FEB with a few GRAS[15] coformers: FEB cocrystals with urea (URE), acetamide (ACT), nicotinamide (NIC), p-aminobenzoic acid (PABA), and saccharin (SAC) (see Scheme 2.1) are discussed in this chapter.
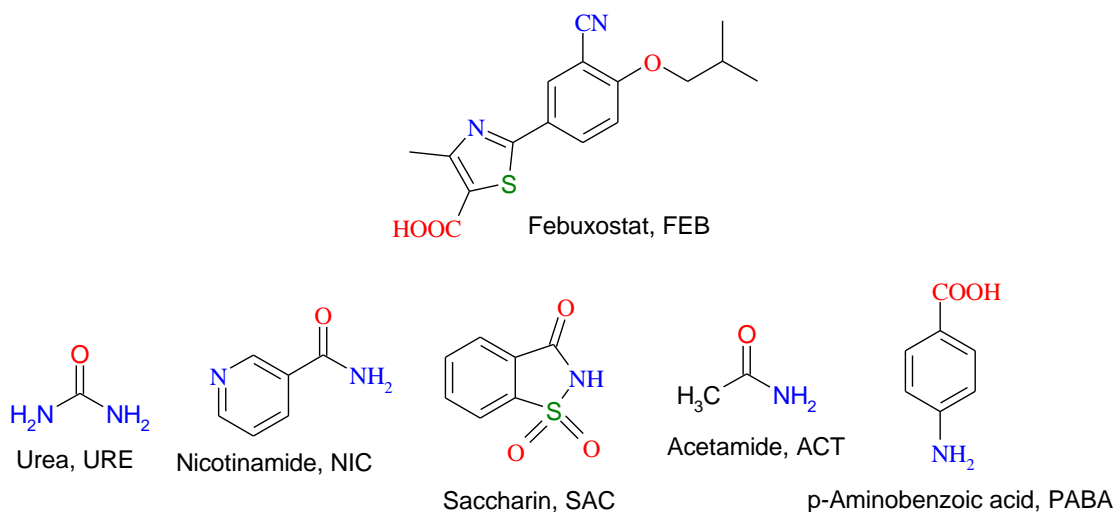
Scheme 2.1 Chemical structures of Febuxostat and Coformers.

2.3 Results and Discussion

FEB has a tendency to form solvates when crystallized from different solvents. Crystal structures of methanol, ethanol, and pyridine solvates were reported in the literature.[16] However, no crystal structure of the guest-free form of FEB was reported even though several crystalline polymorphs were disclosed in patents.[17, 10] Crystallization from CH_3CN afforded diffraction quality single crystals of a guest-free form. FEB cocrystals of equimolar stoichiometry were obtained upon solution crystallization of the ground materials (API: coformer in 1:1 stoichiometry) using mortar-pestle or by ball-mill grinding. All the

cocrystals were characterized by powder X-ray diffraction (PXRD), FT-IR, FT-Raman, ss-NMR, and DSC. Diffraction quality single crystals could be grown for all the cocrystals except FEB–SAC. Crystallographic parameters and hydrogen bonds for all the single crystal structures are listed in Table 2.1 and Table 2.2.

2.3.1 Crystal Structure Analysis

FEB guest-free form: The guest free form of FEB was crystallized from CH_3CN, which was solved and refined in the monoclinic space group $P2_1/c$ with one molecule of FEB in the asymmetric unit. An O–H⋯N hydrogen bond (1.83 Å, 161º) between the COOH donor and CN acceptor is the major interaction connecting FEB molecules in a 1D chain. The carboxylic carbonyl oxygen forms a weak C–H⋯O interaction (2.56 Å, 117º) to extend the structure as 2D sheets, which are connected by C–H⋯O interactions (2.34 Å, 166º) (Figure 2.1). The powder X-ray diffraction pattern of this crystal structure matches with form Q reported in a Chinese CN patent (discussed later).[18] This is the first report on the single crystal X-ray structure of a FEB polymorph.

(a)   (b)
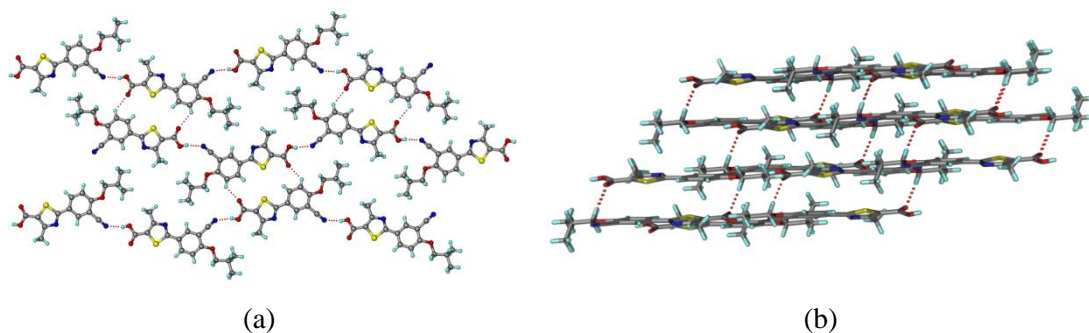
Figure 2.1 (a) A layered section of FEB structure to show the O–H⋯N hydrogen bond and C–H⋯O interactions. (b) C–H⋯O interactions in the inter-sheet region.

FEB–URE cocrystal (1:1): A 1:1 cocrystal of FEB and URE in $P\bar{1}$ space group was obtained upon crystallization from nitromethane. The same cocrystal was also obtained by liquid-assisted (CH_3CN solvent) grinding of the components (1:1 ratio) in a mortar-pestle. FEB and URE molecules were connected by robust R_2^2 (8) dimeric motif[19] through the

acid–amide synthon (O–H···O: 1.74 Å, 174º and N–H···O: 2.09 Å, 153º).[20] The other syn-NH of URE molecule forms N–H···N (2.21 Å, 168º) hydrogen bond with the thiazole ring of FEB to form a tape along the *b*-axis. Such tapes extend into 2D sheets through the URE anti-NHs (N–H···N: 2.47 Å, 149º; 2.28 Å, 158º) (Figure 2.2).
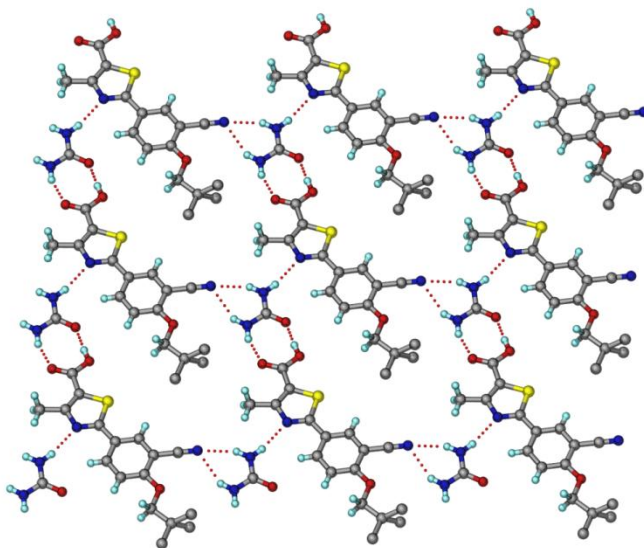
Figure 2.2 A sheet section of the 1:1 FEB-URE viewed along *a*-axis. H atoms of the disordered i-Pr group are removed for clarity. The i-Pr groups look like a t-Bu group due to rotation about the C–C bond.

FEB–ACT cocrystal (1:1): Crystallization of FEB and ACT from i-propylacetate : ethylmethylketone (1:1 v/v) solvent mixture gave a 1:1 cocrystal in $P2_1/c$ space group. Liquid-assisted (CH$_3$CN solvent) grinding resulted the same product which was confirmed by PXRD match. FEB and ACT molecules are connected through O–H···O (1.66 Å, 170º) hydrogen bond and the syn-NH of ACT forms N–H···N (2.12 Å, 166º) hydrogen bond with the thiazole moiety of FEB to form a molecular tape along the *a*-axis. Such tapes are connected by the anti-NH of ACT to the cyano group of FEB (N–H···N: 2.16 Å, 164º) in a corrugated sheet motif (Figure 2.3). The expected acid–amide synthon was not observed in this structure.
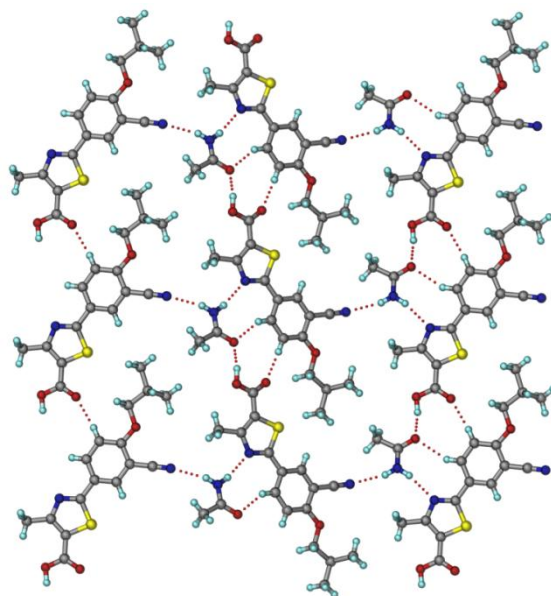
Figure 2.3 2D section of the FEB-ACT (1:1) cocrystal formed through O–H⋯O, N–H⋯N and C–H⋯O H-bonds.

FEB–NIC cocrystal (1:1): Upon dissolving the ground powder of FEB and NIC in EtOAc : cyclohexane (1:1 v/v), a 1:1 cocrystal was obtained whose structure was solved in $P\bar{1}$ space group. NIC molecules form a dimeric R_2^2 (8) motif, which were connected through the acid–pyridine O–H⋯N synthon[20] (1.65 Å, 171°) (Figure 2.4). Auxiliary C–H⋯O=C (acid) (2.48 Å, 137°) and C–H⋯O=C (amide) (2.59 Å, 133°) interactions make a sheet structure.

(a)   (b)
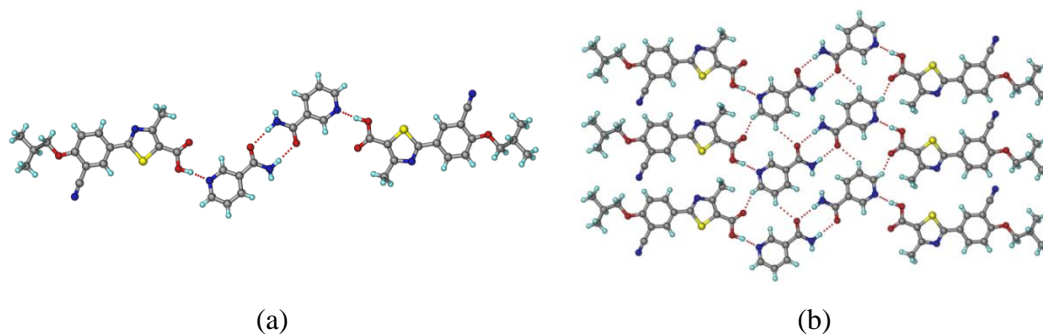
Figure 2.4 (a) Zigzag tapes of NIC and FEB molecules are assembled via amide dimer and acid–pyridine synthons. (b) Additional C–H⋯O interactions in the sheet structure.

FEB–PABA cocrystal (1:1): Upon dissolving the ground material of FEB and PABA in toluene: EtOAc (1:1 v/v), a 1:1 cocrystal was obtained in $P\bar{1}$ space group. The same product was isolated from slurry (in toluene) and liquid-assisted (CH_3CN) ball-mill grinding of the components. The carboxylic acid R_2^2 (8) dimer motifs of FEB and PABA are connected by N–H···N (2.06 Å, 175°; 2.29 Å, 157°) hydrogen bonds between the amine and cyano groups (Figure 2.5). The isopropyl (i-Pr) group of FEB is disordered in the crystal structure.

(a)

(b)
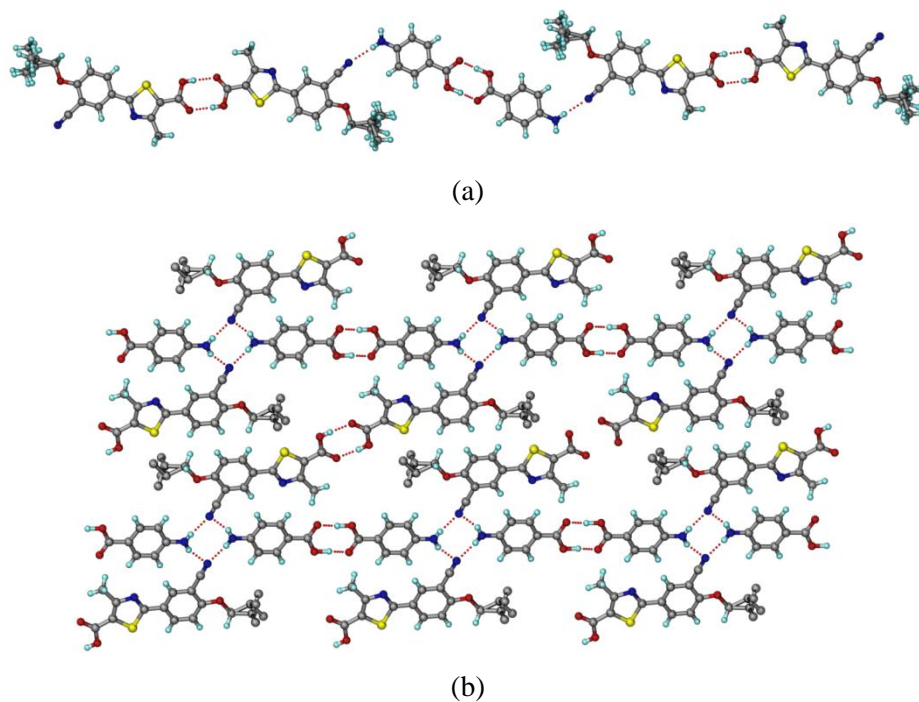
Figure 2.5 (a) Acid-acid homodimers of FEB and PABA are connected through N–H···N hydrogen bonds in infinite tapes. (b) A 2D hydrogen bonded sheet structure assembled through N–H···N interactions. H atoms of the disordered i-Pr group are removed for clarity.

Table 2.1 Crystallographic parameters of FEB and cocrystals.

	FEB guest free	FEB–URE	FEB–ACT	FEB–NIC	FEB– PABA
Emp form.	$C_{16} H_{16} N_2 O_3$ S	$C_{17} H_{20} N_4$ O_4 S	$C_{18} H_{21} N_3$ O_4 S	$C_{22} H_{22} N_4 O_4$ S	$C_{23} H_{23} N_3$ O_5 S
Form wt	316.37	376.43	375.44	438.50	453.50
Cryst syst	monoclinic	triclinic	monoclinic	triclinic	triclinic
Sp gr	$P2_1/c$	$P\bar{1}$	$P2_1/c$	$P\bar{1}$	$P\bar{1}$
T/K	298(2)	100(2)	298(2)	298(2)	100(2)
a/Å	4.6756(4)	7.6525(13)	10.8516(4)	6.9957(5)	8.4227(9)
b/Å	17.6317(15)	10.9684(18)	23.6670(9)	11.6356(11)	11.1544(12)
c/Å	19.4992(15)	12.261(2)	7.4362(4)	13.7925(11)	12.9327(14)
α/°	90	82.627(3)	90	102.644(7)	79.689(2)
β/°	94.523(8)	71.822(3)	95.290(4)	91.221(6)	81.524(2)
γ/°	90	69.866(3)	90	90.410(7)	68.220(2)
Z	4	2	4	2	2
V/Å^3	1602.5(2)	917.7(3)	1901.67(14)	1095.14(16)	1105.7(2)
D_{calc}/g cm^{-3}	1.311	1.362	1.311	1.330	1.362
μ/mm^{-1}	0.215	0.207	0.198	0.184	0.187
Rflns collect	6299	8831	6961	7011	10626
Unique rflns	2099	3222	2839	2838	3586
Obsd rflns	3268	2795	3339	3850	3873
R_1 [I>2σ(I)]	0.0549	0.0496	0.0400	0.0519	0.0443
wR_2 [all]	0.1043	0.1281	0.0974	0.1213	0.1134
GOF	0.982	1.069	1.046	1.025	1.040

Table 2.2 Hydrogen bond metrics in the crystal structures.

D–H⋯A	H⋯A (Å)	D⋯A (Å)	D–H⋯A (°)	symmetry code
		FEB guest-free		
O2–H2⋯N2	1.83	2.782(3)	161	–2+x, 1/2–y, –1/2 +z
C10–H10⋯O1	2.56	3.197(3)	117	–x, –y+1, –z+1
C13–H13A⋯O1	2.34	3.401(3)	166	1–x, 1–y, 1–z
		FEB–URE		
O2–H2⋯O4	1.74	2.559(2)	174	–1+x, 1+y, 1+z
N3–H3A⋯N1	2.21	3.062(3)	168	1+x, y, –1+z
N3–H3B⋯N2	2.28	3.097(3)	158	x, y, z
N4–H4A⋯O1	2.09	2.879(4)	153	1+x, –1+y, –1+z
N4–H4B⋯N2	2.47	3.241(4)	149	x, y, z

C5–H5A···N3	2.46	3.335(4)	151	−1+x, y, 1+z
C11–H11···O4	2.38	3.173(3)	143	−1+x, y, 1+z
FEB–ACT				
O2–H2···O4	1.66	2.639(2)	170	1+x, y, z
N3–H3B···N2	2.16	3.145(3)	164	1−x, 1/2 +y, 3/2−z
N3–H3A···N1	2.12	3.131(3)	166	x, y, z
C10–H10···O1	2.21	3.278(2)	168	−1+x, y, z
C11–H11···O4	2.43	3.409(2)	150	x, y, z
FEB–NIC				
O2–H2···N4	1.65	2.630(3)	171	−1+x, y, −1+z
N3–H3A···N2	2.21	3.194(3)	165	−x, 1−y, 1−z
N3–H3B···O4	1.93	2.920(3)	165	2−x, −y, 1−z
C20–H20···O4	2.59	3.425(2)	133	X−1, +y, +z
C21–H21···O1	2.48	3.351(3)	137	x, y, 1+z
FEB–PABA				
O2–H2···O1	1.69	2.669(18)	176	3−x, 1−y, −z
O5–H5···O4	1.60	2.581(18)	176	1−x, 2−y, 1−z
N3–H3A···N2	2.29	3.239(3)	157	-1+x, y, z
N3–H3B···N2	2.06	3.062(2)	175	1−x, 1−y, 2−z
C15A–H15C···O1	2.61	3.677(8)	167	2−x, 1−y, 1−z

2.3.2 Spectral Analysis

IR and Raman spectroscopy are quantitative tools for the characterization and identification of different solid-state forms.[21] These spectra are based on the vibrational modes of a compound and are extremely sensitive to the structure, hydrogen bonding, molecular conformations, and environment of the API. FEB has carboxylic acid and cyanide functional groups and a thiazole ring. The FT-IR stretching frequencies are at 1677.2 cm^{-1} (COOH C=O stretch), 2961.2 cm^{-1} (O–H stretch), 2231.6 cm^{-1} (C≡N stretch), and 1510.9 cm^{-1} (C=N thiazole ring). Based on the changes in these signature values, the formation of novel crystalline forms was concluded. The cocrystals exhibited FT-IR spectral shifts (Δν) in C=O stretching frequency of 5-20 cm^{-1}, O–H 2-15 cm^{-1}, and N–H 3-40 cm^{-1} (see Figure 2.6 and IR frequencies in Table 2.3). Similarly, the Raman shifts also indicated changes in peak positions, e.g. 1698.3 cm^{-1} for C=O, 3092.1 cm^{-1} of O–H, 2235.3 cm^{-1} for C≡N, and 1608.4 cm^{-1} of C=N thiazole ring (see Table 2.3). The solid-state ^{13}C NMR spectrum of the cocrystals showed all the peaks for FEB and the coformer, but the chemical shifts were moved upfield/downfield relative to the pure components. Since short range aggregation and

shielding/deshielding will be different in the starting components and the hydrogen-bonded product, there were small but distinct chemical shift differences in the ^{13}C ss-NMR spectra (Figure 2.7, see Table 2.4 for chemical shift values). The equimolar stoichiometry of FEB–SAC cocrystal (1:1), for which single crystal X-ray diffraction was not possible, was confirmed by NMR integration (see experimental section).
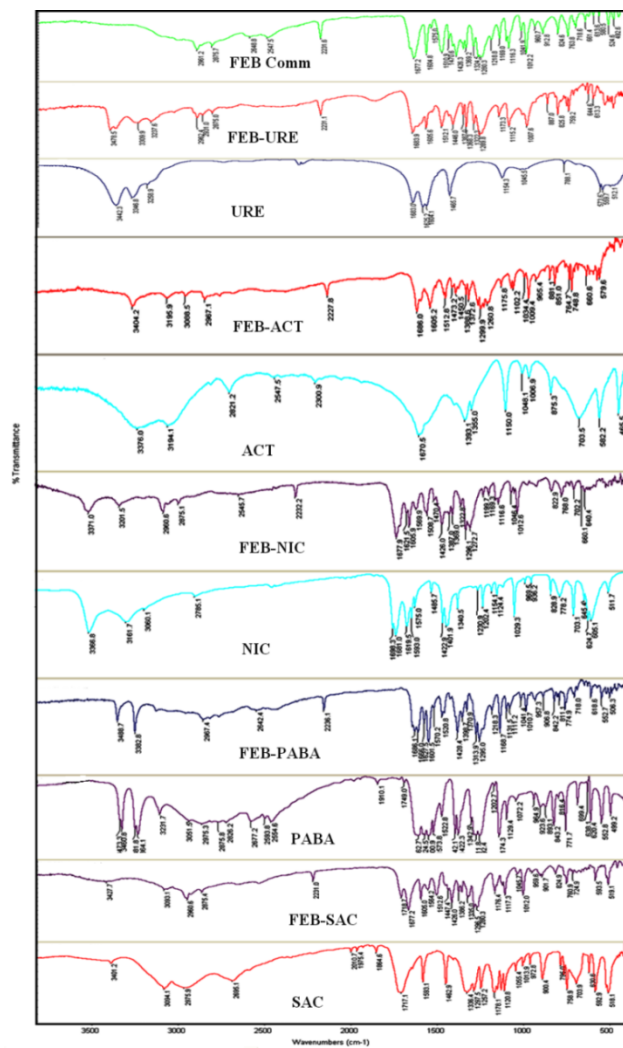
Figure 2.6 FT-IR spectral comparison of FEB cocrystals with its individual components.

Table 2.3 IR and Raman frequencies of FEB cocrystals and starting components (in cm^{-1}).

	INFRARED					
compound	C–H Stretch (cm^{-1})	C– F stretch (cm^{-1})	Carboxylic C=O stretch (cm^{-1})	–COO$^-$ asym stretch (cm^{-1})	–COO$^-$ sym stretch (cm^{-1})	S=O stretch (cm^{-1})
FEB	-	2231.6	1677.2	-	2961.2	1510.9
URE	1465.7	--	1683.0	3442.3, 3346.8	--	--
FEB–URE	1446.0	2231.1	1683.9	3478.5, 3309.9	2962.4	1512.1
ACT	1393.1	--	1670.5	3376.0, 3194.1	--	--
FEB–ACT	1473.2	2227.6	1686.0	3404.2, 3195.9	2967.1	1512.6
NIC	1422.9	--	1698.3	3366.8, 3167.7	--	--
FEB–NIC	1426.0	2232.2	1677.9	3371.0, 3201.5	2960.6	1508.7
PABA	1292.4	--	1662.7	3460.8, 3364.1	2975.3	
FEB–PABA	1295.0	2236.1	1686.1	3488.7, 3382.8	2967.4	1520.8
SAC	--	--	1717.1	3401.2	--	--
FEB– SAC	1426.0	2231.0	1718.7	3427.7	--	1512.6
	RAMAN					
FEB	--	2235.3	1698.3	--	3092.1	1608.4
URE	1388.9	--	1648.5	3426.5, 3360.7	--	--
FEB–URE	1386.8	2235.0	1699.8	3304.5	3105.4	1607.5
PABA	1311.7	--	1600.3	3365.1, 3257.2	3064.0	--
FEB–PABA	1319.8	2237.6	1693.9	3389.5, 3206.2	3075.9	1605.4
NIC	1390.8	--	1675.8	3095.4, 3060.6	--	--
FEB–NIC	1395.0	2232.0	1682.4	3399.3, 3114.1	3078.8	1611.1
ACT	1355.4	--	1657.1	3368.8, 3281.6	--	--
FEB–ACT	1376.8	2232.7	1692.2	3378.2, 3320.1	3083.1	1608.1
SAC	1335.9	--	1700.4	3092.7	--	--
FEB–SAC	1374.3	2240.2	1697.6	3091.0	3067.6	1605.4
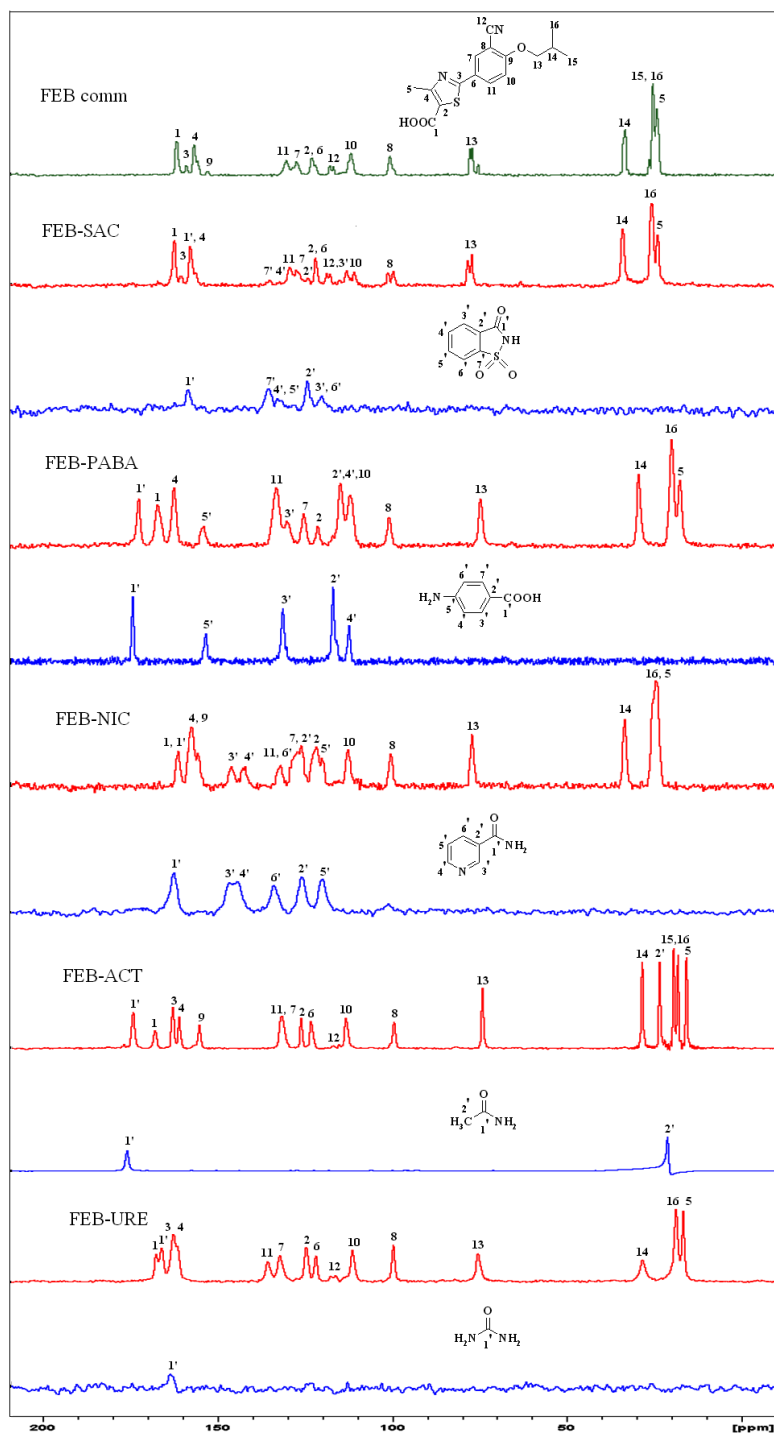
Figure 2.7 ^{13}C ss-NMR spectrum of FEB cocrystals compared with the API and the coformer.

Table 2.4 ^{13}C ss-NMR chemical shifts (δ, ppm) of FEB cocrystals.

Carbon No.	FEB	URE	FEB–URE	ACT	FEB–ACT	NIC	FEB–NIC	PABA	FEB–PABA	SAC	FEB–SAC
1	168.7		167.6		169.8		168.2		167.6		168.8
2	126.4		124.7		127.0		125.0		121.7		124.7
3	165.7		162.7		163.8		-		-		166.7
4	163.3		162.6		162.0		164.1		162.9		162.3
5	18.6		16.7		16.5		18.9		17.6		17.7
6	125.4		121.9		124.1		-		-		124.7
7	131.3		132.2		132.4		130.7		125.7		130.7
8	102.1		99.7		100.4		101.8		101.0		102.1
9	159.1		-		156.2		162.2		-		-
10	114.2		111.4		114.2		115.2		112.3		112.7
11	134.4		135.7		132.5		136.2		133.5		132.7
12	119.7		116.2		115.7		-		-		120.1
13	76.9		75.4		75.0		76.4		74.9		77.1
14	28.5		28.3		29.2		28.6		29.5		28.7
15	20.8		-		20.1		-		-		-
16	19.8		18.7		18.9		18.9		20.0		19.6
1'		163.6	166.1	176.9	175.2	169.6	168.2	174.5	173.0	164.0	163.8
2'				21.9	24.1	129.6	129.8	117.1	115.1	126.7	126.8
3'						152.2	151.7	131.6	130.4	122.2	114.9
4'						149.6	147.9	112.4	112.3	136.1	136.2
5'						123.1	123.3	153.7	154.3	136.1	136.2
6'						138.4	136.2	112.4		122.2	114.9
7'								131.6		138.8	139.2

2.3.3 Powder X-ray diffraction analysis

The PXRD pattern of FEB guest-free form was not identical with that of the commercial material (anhydrous form) as confirmed by overlaying the experimental pattern of the commercial form with the calculated pattern of the crystal structure (Figure 2.8). The powder diffraction lines of commercial FEB matched with the H polymorph in WO 2008/067773 A1 patent[12] and that of the guest-free form in this study matched with the line pattern for form Q given in patent CN 101648926A.[18] The absence of strong hydrogen bonding in the crystal structure (no carboxylic acid O–H···O dimer or catemer synthon) could be a possible reason that polycrystalline powders were obtained in a majority of the crystallization experiments. The cocrystals exhibited distinctive PXRD patterns compared to that of FEB and the coformers (Figure 2.8). All the cocrystals were prepared in bulk by liquid-assisted grinding (LAG) and found to match with the calculated diffraction line pattern of the X-ray crystal structure. At the time of submitting this paper, we became aware of a recent publication[21] of FEB−URE cocrystal with the same analytical data. However, the details of FEB−NIC reported by us are different from that in the WO patent application.[22]
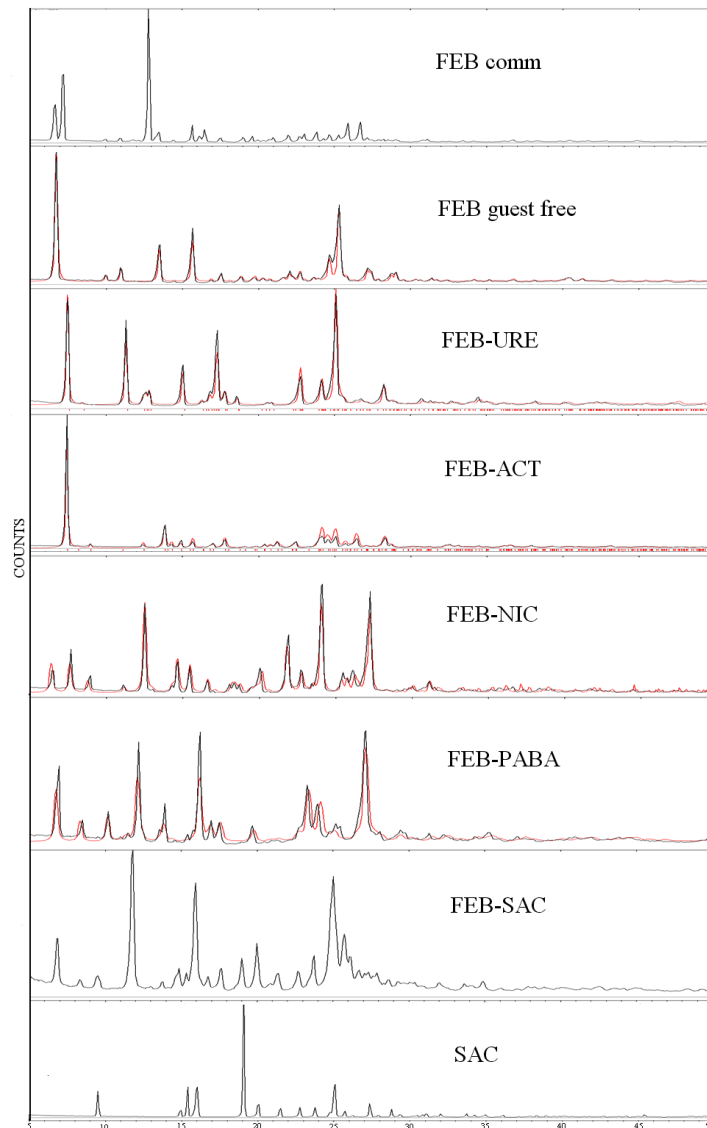
Figure 2.8 Overlay of experimental (black) PXRD of FEB cocrystals obtained from LAG. The calculated PXRD from the crystal structure (red) matches with that of the crystallized products FEB–URE, FEB–ACT, FEB–NIC, and FEB–PABA. FEB–SAC shows clear differences in powder lines compared to the starting materials.

2.3.4 Thermal Analysis

DSC of the FEB commercial material showed a single melting endotherm at 208.4 °C without any phase transition. URE melts at 133-135 °C, where as DSC of the ground material of FEB and URE showed melting endotherm at 172 °C, suggesting the formation of a cocrystal. All cocrystals were analysed by DSC (Figure 2.9). The melting endotherm of FEB–URE, FEB–ACT and FEB–NIC was at an intermediate temperature compared to that of the pure compounds, whereas FEB–PABA and FEB–SAC cocrystals melt at lower temperature of 171 °C and 187 °C respectively, and the respective coformers melt at higher temperature (187-189 °C and 226-229 °C, see Table 2.5). Generally, low melting cocrystals have higher solubility,[23] and this trend was observed for FEB cocrystals which exhibited higher IDRs compared to the drug (discussed later).
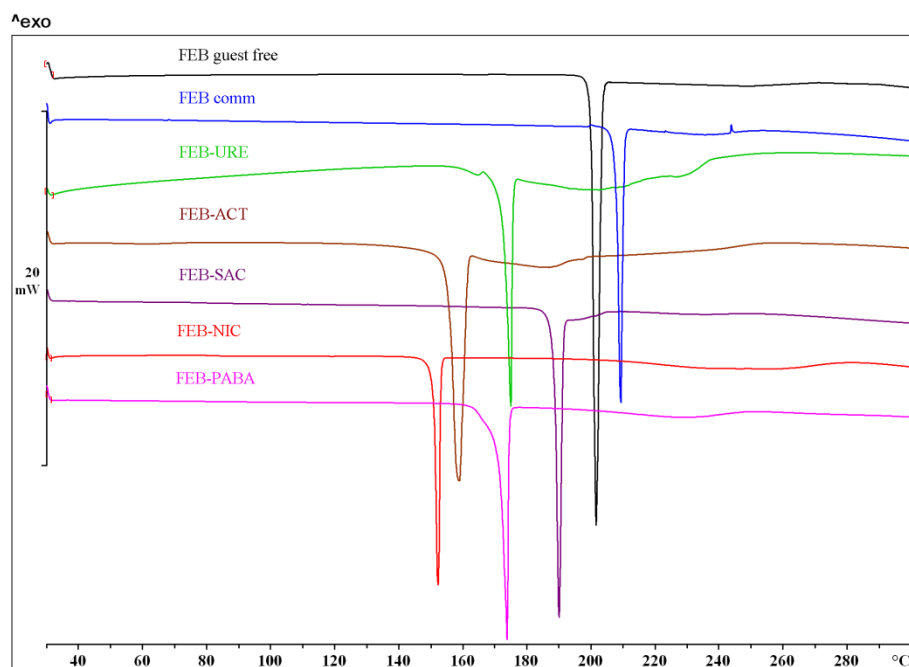
Figure 2.9 DSC thermogram of FEB and its cocrystals. Note that the guest free from obtained from CH$_3$CN crystallization has a different melting point than the commercial FEB.

Table 2.5 Melting point of FEB cocrystals.

Drug/ coformer	M.p. of Drug/coformer (°C)	Cocrystal	M.p. of cocrystal (°C)
FEB commercial	207–208	---	---
FEB guest free	199–203	---	---
URE	133–135	FEB-URE	172
ACT	78–80	FEB-ACT	155
NIC	128–131	FEB-NIC	151
PABA	187–189	FEB-PABA	171
SAC	226-229	FEB-SAC	187

2.3.5 Solubility, Stability and Dissolution

The current attention towards screening and development of cocrystals is because of the ability of cocrystals to tune solubility and dissolution properties of APIs. Hence, poorly water soluble APIs are targeted for cocrystal screening. Due to the poor solubility of FEB in aqueous medium, solubility and dissolution experiments were conducted in 60% EtOH–H_2O medium (v/v). Equilibrium solubility values of FEB cocrystals could not be determined because they were unstable in 60% EtOH medium for 24 h. It is well accepted that though a solid form is unstable in the equilibrium solubility conditions (long span, agitation, supersaturation etc.), it can confer dissolution advantage by releasing the desired amount of the drug within a shorter time frame (4-8 h). Therefore intrinsic dissolution rate (IDR) experiments were conducted on FEB and cocrystals (values are listed in Table 2.6), and their dissolution profiles are displayed in Figure 2.10. All the cocrystals showed an improved dissolution rate compared to FEB and followed the coformer solubility rule,[23] i.e. a high solubility coformer gave high solubility of the cocrystal; the only exception being FEB−URE. A possible reason for the lower dissolution rate of FEB-URE cocrystal could be its dense packing (1.362 g/cm^3) compared to the other cocrystals and also strong acid-amide H-bonds (O–H···O: 1.74 Å, 174º and N–H···O: 2.09 Å, 153º). FEB-PABA cocrystal shows faster dissolution rate than FEB-URE cocrystal. It shows higher dissolution rate than FEB-URE cocrystal (even though they have the same density, see Table 2.1) because the API and the coformer are bonded through homo-molecular acid–acid H-bonds, and there were no strong API···coformer H-bonds. Crystal structure analysis suggested that FEB−ACT

cocrystal should have the highest dissolution rate because the API and coformer are bound by a single hydrogen bond, compared to stronger acid–acid and acid–amide cyclic synthons. Indeed, FEB–ACT is the fastest dissolving cocrystal exhibiting an enhancement of 52 times faster than FEB. A recent report[24] on correlating crystal structure with dissolution behavior guided our rationalization. Solubility values of the coformers are listed in Table 2.6. The dissolution rates of cocrystals followed the order FEB–ACT > FEB–NIC > FEB–PABA > FEB–SAC > FEB–URE > FEB guest free > FEB commercial material. The melting points of the cocrystals are lower than that of FEB, and all the cocrystals followed the inverse melting point to solubility rule except FEB–SAC. The exceptionally fast dissolution rate of FEB-SAC (even though its m.p. is high) may be due to the lack of strong interactions between FEB and SAC, similar to the FEB-PABA case. PXRD analysis of the undissolved residue at the end of the IDR experiment (4 h) matched with the starting cocrystals, thus confirming the physical form stability of the cocrystal in the dissolution slurry medium of 60% ethanol–water for 4 h (Figure 2.11).

(a)   (b)
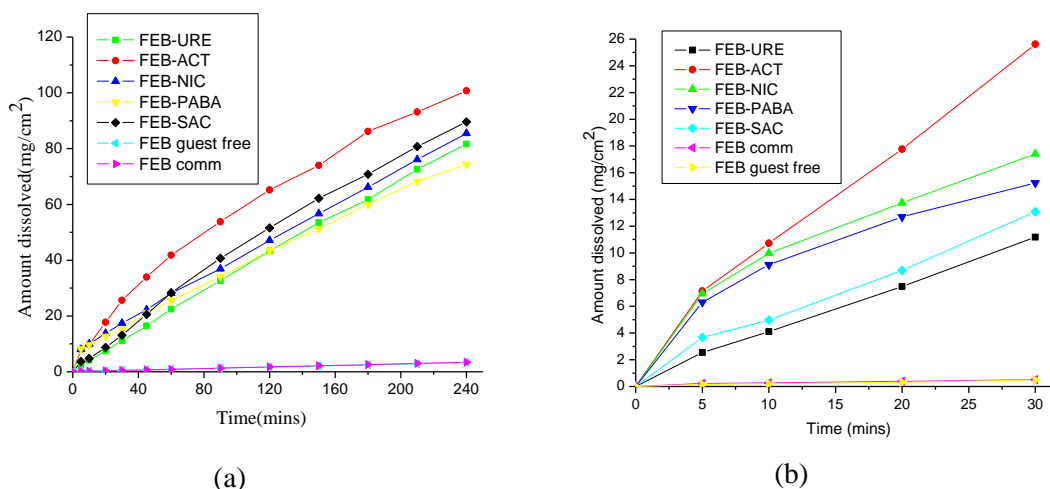
Figure 2.10 Dissolution curves of FEB cocrystals (a) for 4 h duration and (b) 30 min duration.

Table 2.6 Molar extinction coefficients, IDRs of FEB cocrystals in 60% ethanol−water and solubility of coformers in water.

Drug/cocrystal	ε (mL mg^{-1} cm^{-1})	IDR (mg cm^{-2} min^{-1})	Drug/coformer	Solubility g/mL (in water)
FEB commercial	72.86	0.015	FEB	1.2x10^{-5}
FEB guest-free	74.96	0.017 (x1.1)	---	---
FEB–URE	79.08	0.371 (x 24.1)	URE	1.1
FEB–ACT	64.09	0.806 (x 52.5)	ACT	2.0
FEB–NIC	52.58	0.562 (x 36.6)	NIC	1.0
FEB–PABA	56.43	0.523 (x 34.1)	PABA	0.006
FEB–SAC	48.05	0.452 (x 29.4)	SAC	0.003

(a)

(b)

(c)

(d)

(e)
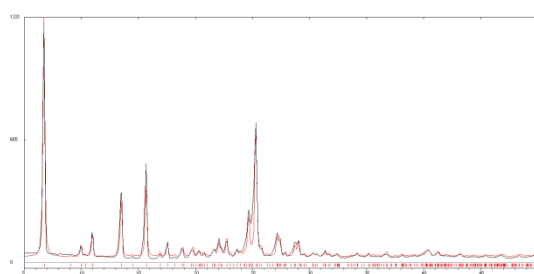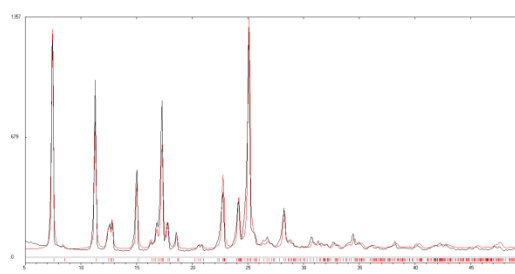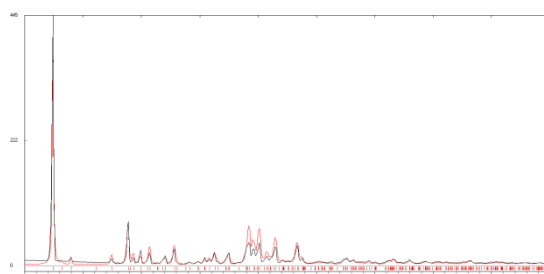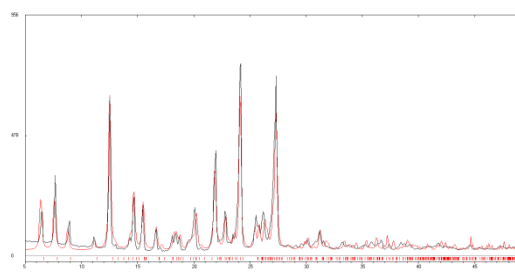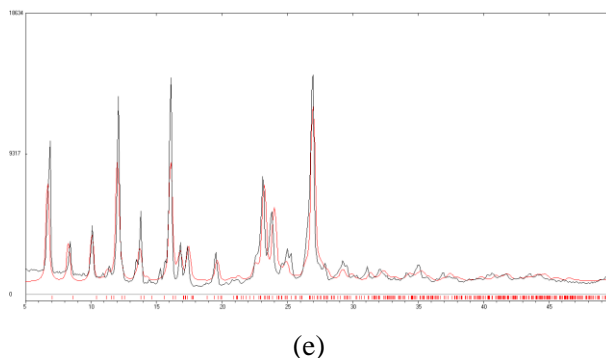
Figure 2.11 Overlay of experimental PXRD pattern (black) of (a) FEB guest-free form (b) FEB–URE (c) FEB–ACT (d) FEB–NIC (e) FEB–PABA cocrystals obtained after dissolution for 4 h with the calculated lines form the crystal structure (red) show complete match of diffraction peaks.

The improvement in the solubility of a drug must be accompanied with good physicochemical stability of the solid form. The physical form stability of FEB cocrystals was established under ICH conditions (accelerated) of 40 °C, 75% RH for 6 weeks (see summary in Table 2.7, and Figure 2.12a-2.12f). No hydrate formation or the dissociation of the cocrystals to the API and coformer was observed, except for FEB-ACT (Figure 2.12g). This last case dissociated to give FEB hydrate as suggested by a water loss endotherm in DSC at 80-90 °C and then melting of the drug at 200 °C (Figure 2.12h). The chemical stability of cocrystals was further tested by ^{1}H NMR and confirmed that there is no degradation of the FEB/coformer during the test periods. This result was a mild setback because FEB−ACT is the fastest dissolving cocrystal in this study.

Table 2.7 Stability of FEB cocrystals under ICH conditions of 40 °C and 75% RH. [a]

Compound	1W	2W	3W	4W	5W	6W
FEB	√	√	√	√	√	√
FEB guest free	√	√	√	√	√	√
FEB–URE	√	√	√	√	√	√
FEB–ACT	√	×	×	×	×	×
FEB–NIC	√	√	√	√	√	√
FEB–PABA	√	√	√	√	√	√
FEB–SAC	√	√	√	√	√	√

[a]W = week, √ = no hydrate formation, × = onset of hydrate formation

(a)

(b)

(c)

(d)

(e)

(f)

(g)   (h)
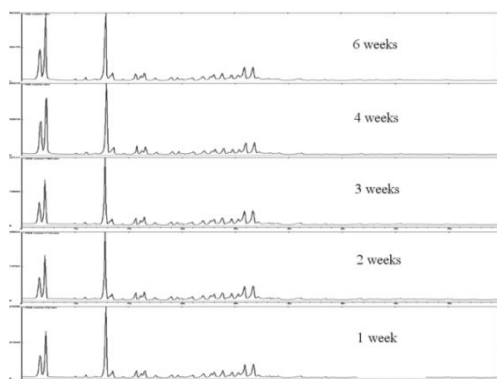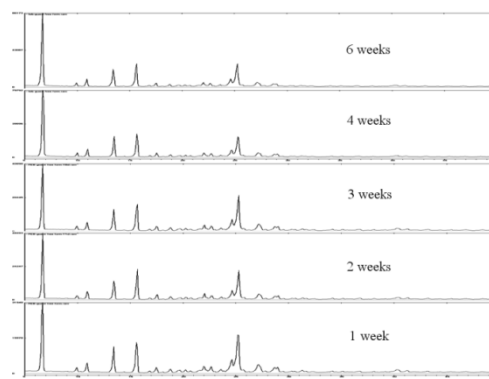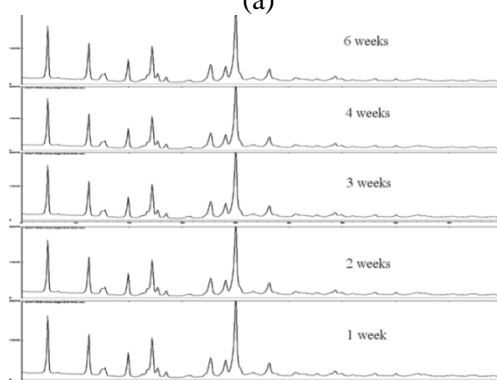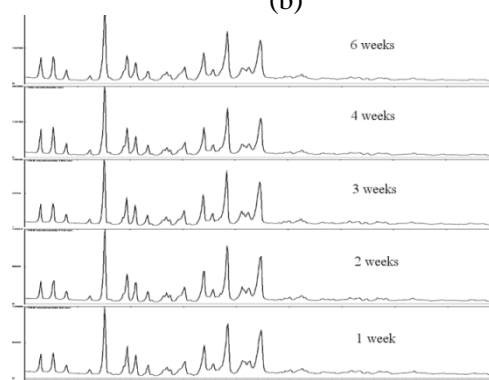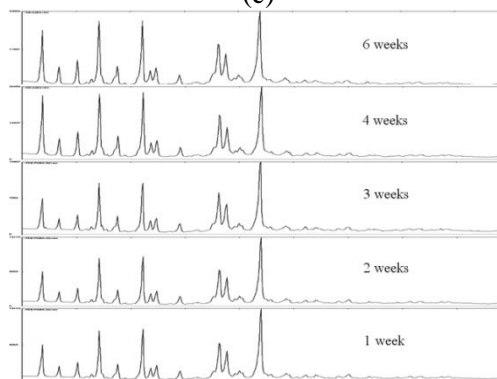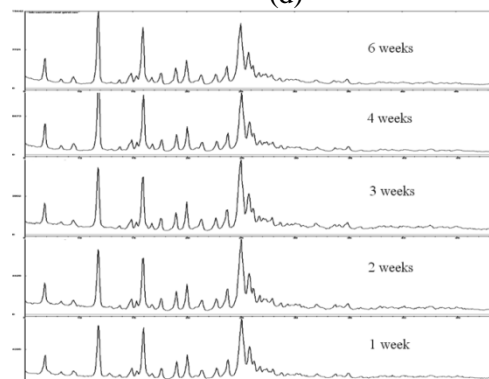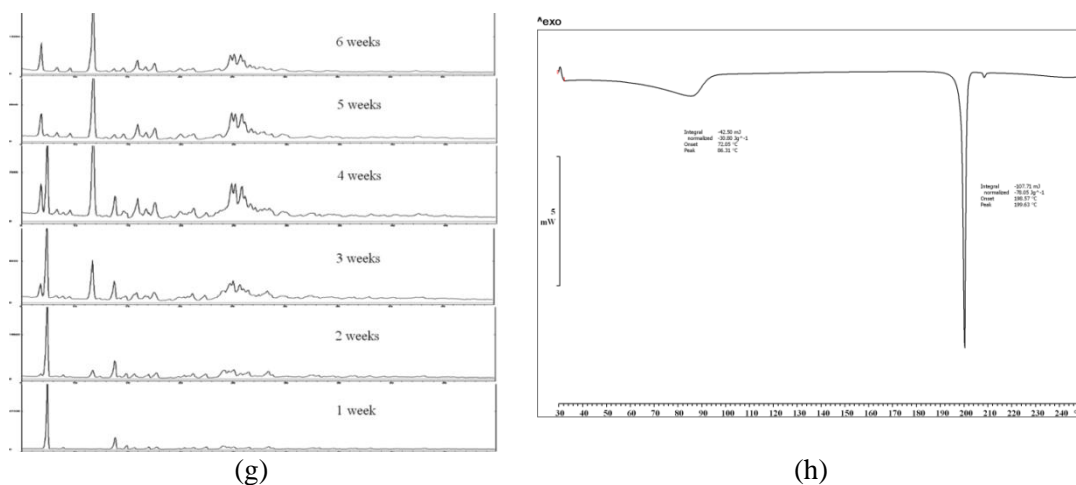
Figure 2.12 Stability study at 40 °C and 75% RH of (a) FEB commercial (b) FEB guest-free form (c) FEB–URE (d) FEB–NIC (e) FEB–PABA (f) FEB–SAC (g) FEB-ACT cocrystals and (h) DSC thermogram of FEB−ACT cocrystal in the stability chamber at 40 °C and 75% RH gave FEB hydrate, which shows an endotherm for water loss at 80-90 ℃ and then melting of FEB at 200 ℃.

Improving the solubility of BCS class II drug FEB in neutral state without recourse to the obvious sodium salt of the carboxylic acid is necessary here because the presence of Na^+ will lead to the precipitation of uric acid as sodium urate crystals (and thereafter Ca stones).[25] At physiological pH conditions uric acid (first pK_a of uric acid 5.5) converts to sodium urate crystals in the presence of excess Na^+, and such crystals cause acute pain at the joints. These crystals are stable at pH>6 which leads to gout. Hence even though FEB is carboxylic acid, the obvious route to make a sodium salt of FEB is not a practical solution. Thus, the alternative strategy of pharmaceutical cocrystals, which is usually a choice method for non-ionizable APIs, is the suitable method in such special cases where metal carboxylates cause side complications.

2.4 Conclusions

Our aim was to improve the aqueous solubility and bioavailability of Febuxostat in cocrystals with appropriate GRAS coformers to obtain novel solid-state forms of the API with good stability. Furthermore, the extensive polymorphism characteristic of this API

appears to be controlled in that no polymorphic cocrystals were observed in our preliminary study. In addition to the crystal structure of a guest-free form of FEB (which matches with Form Q), five new cocrystals are reported for the first time. All the new crystalline forms were characterized by spectroscopy, thermal analysis, and X-ray diffraction. We report here FEB–ACT as the fastest dissolving cocrystal (52.5 times compared to FEB) but it was not stable under ICH conditions of 75% RH at 40 °C. The second best candidate FEB–NIC cocrystal may be preferable because it is stable and has good dissolution rate (36.6 times faster than FEB). All cocrystals exhibited faster dissolution rates and good to moderate stability. These screening results suggest that cocrystals represent a viable alternative for an ionizable API wherein salt formation is not an option for other reasons, thereby offering new avenues for expanding the structural landscape in pharmaceutical formulation.

2.5 Experimental Section

Materials and Methods: Febuxostat was purchased from Beijing Mesochem Technology Co. Ltd., China and used without further purification. The coformers (purity >99.8%) were purchased from Sigma-Aldrich. All other chemicals were of analytical or chromatographic grade. Water purified from a deionizer-cum-mixed-bed purification system (AquaDM, Bhanu, Hyderabad, India) was used in the experiments.

Preparation of FEB cocrystals

FEB guest-free form: A guest-free form (non-solvated) crystal of FEB was obtained upon dissolving 30 mg of commercial material in 5 mL hot CH_3CN and left for slow evaporation at room temperature. Colorless needle-shape crystals suitable for X-ray diffraction were obtained after 3-4 days upon solvent evaporation.

FEB–URE cocrystal (1:1): FEB–URE was obtained upon grinding about 100 mg of a 1:1 stoichiometric ratio of FEB and URE for 30 min with CH_3CN liquid-assisted grinding. The formation of cocrystal was confirmed by FT-IR, FT-Raman, ss-NMR, PXRD and DSC. 30 mg of the ground material was dissolved in 6 mL of hot nitromethane and left for slow

evaporation at room temperature. Colorless needle crystals suitable for X-ray diffraction were obtained after 3-4 d upon solvent evaporation.

FEB–ACT cocrystal (1:1): FEB–ACT cocrystal was obtained upon grinding about 100 mg of a 1:1 stoichiometric ratio of FEB and ACT for 30 min with CH_3CN liquid-assisted grinding. The formation of cocrystal was confirmed by FT-IR, FT-Raman, ss-NMR, PXRD and DSC. 30 mg of the ground material was dissolved in 8 mL of hot isopropyl acetate: ethyl methyl ketone (1:1, v/v) and left for slow evaporation at room temperature. Colorless needle-shape crystals suitable for X-ray diffraction were obtained after 3-4 d upon solvent evaporation.

FEB–NIC cocrystal (1:1): FEB–NIC cocrystal was obtained upon grinding about 100 mg of a 1:1 stoichiometric ratio of FEB and NIC for 30 min by CH_3CN liquid-assisted grinding. The formation of cocrystal was confirmed by FT-IR, FT-Raman, ss-NMR, PXRD and DSC. 30 mg of the ground material was dissolved in 8 mL of hot ethyl acetate: cyclohexane (1:1, v/v) and left for slow evaporation at room temperature. Colorless needle-shape crystals suitable for X-ray diffraction were obtained after 3-4 d upon solvent evaporation.

FEB–PABA cocrystal (1:1): FEB–PABA cocrystal was obtained upon grinding about 100 mg of a 1:1 stoichiometric ratio of FEB and PABA for 30 min by CH_3CN liquid-assisted grinding. The formation of cocrystal was confirmed by FT-IR, FT-Raman, ss-NMR, PXRD and DSC. 30 mg of the ground material was dissolved in 6 mL hot toluene: ethyl acetate (1:1, v/v) and left for slow evaporation at room temperature. Colorless needle-shape crystals suitable for X-ray diffraction were obtained after 3-4 d upon solvent evaporation.

FEB–SAC cocrystal (1:1): FEB–SAC cocrystal was obtained upon grinding about 100 mg of a 1:1 stoichiometric ratio of FEB and SAC for 30 min by CH_3CN liquid-assisted grinding. The formation of cocrystal was confirmed by FT-IR, FT-Raman, ss-NMR, PXRD, DSC and ^{1}H NMR. Several attempts were made to get diffraction quality single crystals in different solvent systems such as ethanol, CH_3CN, THF, nitromethane, toluene, acetone, and also mixtures of solvents. We always end up with the polycrystalline powders but no diffraction quality single crystals were obtained.

^{1}H NMR (DMSO-d_6): 8.20 (1 H, s), 8.15 (1 H, d, *J* 8.8 Hz), 8.06 (1 H, d, *J* 7.5 Hz), 7.95 (1 H, d, *J* 7.3 Hz), 7.89 (2 H, t, *J* 7.1 Hz), 7.31 (1 H, d, *J* 9.0 Hz), 3.95 (2 H, d, *J* 6.4 Hz), 2.61 (3 H, s), 2.04 (1 H, m, *J* 6.6 Hz), 0.98 (6 H, d, *J* 6.7 Hz).

Vibrational spectroscopy: Thermo-Nicolet 6700 Fourier transform infrared spectrophotometer with NXR-Fourier transform Raman module (Thermo Scientific, Waltham, Massachusetts) was used to record IR and Raman spectra. IR spectra were recorded on samples dispersed in KBr pellets. Raman spectra were recorded on samples contained in standard NMR diameter tubes or on compressed samples contained in a gold-coated sample holder. Data was analyzed using the Omnic software (Thermo Scientific, Waltham, Massachusetts).

Solid-state NMR spectroscopy: Solid-state ^{13}C NMR (ss-NMR) spectroscopy provides structural information about differences in hydrogen bonding, molecular conformations, and molecular mobility in the solid state.[26] The solid-state ^{13}C NMR spectra were obtained on a Bruker Ultrashield 400 spectrometer (Bruker BioSpin, Karlsruhe, Germany) utilizing a ^{13}C resonant frequency of 100 MHz (magnetic field strength of 9.39 T). Approximately 100 mg of crystalline sample was packed into a zirconium rotor with a Kel-F cap. The crosspolarization, magic angle spinning (CP-MAS) pulse sequence was used for spectral acquisition. Each sample was spun at a frequency of 5.0 ± 0.01 kHz and the magic angle setting was calibrated by the KBr method. Each data set was subjected to a 5.0 Hz line broadening factor and subsequently Fourier transformed and phase corrected to produce a frequency domain spectrum. The chemical shifts were referenced to TMS using glycine (δglycine = 43.3 ppm) as an external secondary standard.

Differential Scanning Calorimetry (DSC): DSC was performed on a Mettler Toledo DSC 822e module. Samples were placed in crimped but vented aluminium sample pans. The typical sample size is 3-4 mg, and the temperature range is 30-300 °C @ 5 °C min^{-1}. Samples were purged by a stream of dry nitrogen flowing at 80 mL min^{-1}.

X-ray crystallography: X-ray reflections for the guest-free form and FEB–ACT and FEB–NIC were collected on Oxford Xcalibur Gemini Eos CCD diffractometer at 298 K using Mo-

Kα radiation (λ = 0.7107 Å). Data reduction was performed using CrysAlisPro (version 1.171.33.55)[27] and OLEX2-1.0[28] was to solve and refine the structures. X-ray reflections for FEB–URE and FEB–PABA were collected at 100 K on Bruker SMART-APEX CCD diffractometer equipped with a graphite monochromator and Mo-Kα fine-focus sealed tube (λ = 0.71073 Å). Data reduction was performed using Bruker SAINT Software.[29] Intensities were corrected for absorption using SADABS,[30] and the structure was solved and refined using SHELX-97.[31] The isopropyl group of FEB in FEB–URE and FEB–PABA structures was disordered and it was modeled using the FVAR command. All non-hydrogen atoms were refined anisotropically. Hydrogen atoms on heteroatoms were located from difference electron density maps and all C−H hydrogens were fixed geometrically. Hydrogen bond geometries were determined in Platon.[32] X-Seed[33] was used to prepare packing diagrams.

Powder X-ray diffraction: Powder X-ray diffraction of all the samples were recorded on Bruker D8 Advance diffractometer (Bruker-AXS, Karlsruhe, Germany) using Cu-Kα X-radiation (λ = 1.5406 Å) at 40 kV and 30 mA power. X-ray diffraction patterns were collected over the 2θ range 5-50° at a scan rate of 1° min^{-1}. Powder Cell 2.4[34] was used for Rietveld refinement of experimental PXRD and calculated lines from the X-ray crystal structure.

Dissolution and solubility measurements: Intrinsic dissolution rate (IDR) and solubility measurements were carried out on a USP certified Electrolab TDT-08 L Dissolution Tester (Electrolab, Mumbai, MH, India). A calibration curve was obtained for all the cocrystals including FEB by plotting absorbance vs. concentration UV-Vis spectra curves on a Thermo Scientific Evolution EV300 UV-Vis spectrometer (Waltham, MA, USA) for known concentration solutions in 60% EtOH−water medium. The slope of the plot from the standard curve gave the molar extinction coefficient (ε) by applying the Beer−Lambert's law. 125 mg of the solid (drug/cocrystal) was taken in the intrinsic attachment and compressed to a 0.5 cm^2 pellet using a hydraulic press at a pressure of 2.5 ton inch^{-2} for 4 min. The pellet was compressed to provide a flat surface on one side and the other side was sealed. Then the pellet was dipped into 500 mL of 60% EtOH−water medium at 37 °C with the paddle rotating at 150 rpm. At a regular interval of 5−10 min, 5 mL of the dissolution

medium was withdrawn and replaced by an equal volume of fresh medium to maintain a constant volume. Samples were filtered through 0.2 μm nylon filter and assayed for drug content spectrophotometrically at 315 nm on a Thermo-Nicolet EV300 UV−vis spectrometer. There was no interference to FEB UV-Vis maxima at 315 nm by coformers which absorb strongly at 220−280 nm. The amount of drug dissolved in each time interval was calculated using the calibration curve. The linear region of the dissolution profile was used to determine the intrinsic dissolution rate (IDR) of the compound (= slope of the curve, that is, the amount of drug dissolved divided by the surface area of the disk (0.5 cm^2) per minute). The dissolution rates for FEB and its cocrystals were computed from their IDR values.

2.6 References

1. A. M. Thayer, *Chem. Eng. News*, 2010, **13**, 88. (b) N. J. Babu, A. Nangia, *Cryst. Growth Des*. 2011, **11**, 2662.

2. (a) S. M. Berge, L. D. Bighley, D. C. Monkhouse, *J. Pharm. Sci*., 1977, **66**, 1. (b) A. T. M. Serajuddin, *Adv. Drug Delivery Rev.*, 2007, **59**, 603. (c) R. Banerjee, P. M. Bhatt, N. V. Ravindra, G. R. Desiraju, *Cryst. Growth Des*. 2005, **5**, 2299. (d) R. Thakuria, A. Nangia, *CrystEngComm*, 2011, **13**, 1759. (e) Ö. Almarsson, M. J. Zaworotko, *Chem. Commun.,* 2004, 1889.

3. (a) S. Cherukuvada, N. J. Babu, A. Nangia, *J. Pharm. Sci.*, 2011, **100**, 3233. (b) A. V. Trask, W. D. S. Motherwell, W. Jones, *Cryst. Growth Des.*, 2009, **5**, 1013.

4. P. Vishweshwar, J. A. McMahon, J. A. Bis, M. J. Zaworotko, *J. Pharm. Sci.*, 2006, **95**, 499.

5. (a) J. F. Remenar, S. L. Morissette, M. L. Peterson, B. Moulton, J. M. MacPhee, H. R. Guzmán, Ö. Almarsson, *J. Am. Chem. Soc.*, 2003, **125**, 8456. (b) P. Sanphui, N. R. Goud, U. B. R. Khandavilli, A. Nangia, *Cryst. Growth Des.*, 2011, **11**, 4135. (c) P. Sanphui, N. R. Goud, U. B. R. Khandavilli, S. Bhanoth, A. Nangia, *Chem. Commun*. 2011, **47**, 5013. (d) R. Banerjee, P. M. Bhatt, N. V. Ravindra, G. R. Desiraju, *Cryst. Growth Des.*, 2005, **5**, 2299. (e) D. J. Good. N. Rodríguez-Hornedo, *Cryst. Growth Des.*, 2009, **9**, 2252.

(f) D. P. McNamara, S. L. Childs, J. Giordano, A. Iarriccio, J. Cassidy, M. S. Shet, R. Mannion, A. Park, *Pharm. Res*. 2006, **23**, 1888. (g) S. Basavoju, D. Boström, S. P. Velaga, *Cryst. Growth Des*., 2006, **6**, 2699.

6.   (a) A. V. Trask, W. D. S. Motherwell, W. Jones, *Cryst. Growth Des*., 2005, **5**, 1013. (b) S. Basavoju, D. Boström, S. P. Velaga, *Pharm. Res.,* 2008, **25**, 530.

7.   (a) K. Suresh, N. R. Goud, A. Nangia, *Chem. Asian J*., 2013, **8**, 3032. (b) J. F. Remenar, S. L. Morissette, M. L. Peterson, B. Moulton, J. M. MacPhee, H. R. Guzmán, Ö. Almarsson, *J. Am. Chem. Soc.,* 2003, **125**, 8456. (c) S. C. McKellar, A. R. Kennedy, N. C. McCloy, E. McBride, A. J. Florence, *Cryst. Growth Des*., 2014, **14**, 2422.

8.   A. V. Trask, *Mol. Pharmaceutics*, 2007, **4**, 301.

9.   (a) K. H. Yu, *Recent Pat. Inflamm Allergy Drug Discov.*, 2007, **1**, 69. (b) T. Yamamoto, Y. Moriwaki, Y. Fujimura, S. Takahashi, Z. Tsutsumi, T. Tsutsui, K. Higashino, T. Hada, *Pharmacology*, 2000, **60**, 34. (c) K. Okamoto, B. T. Eger, T. Nishino, S. Kondo, E. F. Pai, T. Nishino, *J. Biol. Chem.* 2003, **278**, 1848.

10. M. Piran, L. Metsger, *US 2010/0317702 A1*.

11. M. Koichi, W. Kenzo, H. Toshiyuki, K. Mitsutaka, *EP 1020454 B1*.

12. X. Zhou, X. Tang, J. Deng, W. Ye, J. Luo, D. Zhang, B. Fan, *WO 2008/067773 A1*.

13. S. D. Dwivedi, A. Prasad, R. U. Roy, M. R. Patel, *WO 2011/101867 A2*.

14. R. Khosravan, B. Gabowski, J. T. Wu, N. Joseph-Ridge, L. Vernillet, *Br. J. Clin. Pharmacol*., 2007, **65**, 355.

15. US-FDA GRAS chemical list, http://www.fda.gov/Food/IngredientsPackagingLabeling/FoodAdditivesIngredients/ ucm091048.htm (accessed on April 8, 2013).

16. (a) X. Zhu, Y. Wang, T. Lu, *Acta Cryst*. 2009, **E65**, o2603. (b) Q.-Y. Jiang, J.-J. Qian, J.-M. Gu, G.-P. Tang, X.-R. Hu, *Acta Cryst*. 2011, **E67**, o1232.

17. (a) R. Thaimattam, P. K. Dash, R. Prasad, S. Dhar, *WO 2011/080651 A2*. (b) D. G. Tombari, C. P. Mangone, M. B. Garcia, A. Vecchioli, R. A. Labriola, *WO 2012/048861 A1.*

18. D. Zhang, W. Yan, R. Li, P. Dong, Y. Hu, *CN 101648926 A,* 2010.

19. M. C. Etter, *Acc. Chem. Res*., 1990, **23**, 120. (b) J. Bernstein, R. E. Davis, L. Shimoni, N. L. Chang, *Angew. Chem., Int. Ed. Engl*. 1995, **34**, 1555.

20. R. D. B. Walsh, M. W. Bradner, S. Fleischman, L. A. Morales, B. Moulton, N. Rodriguez-Hornedo, M. J. Zaworotko, *Chem. Commun*. 2003, **2**, 186. (b) G. R. Desiraju, *Angew. Chem., Int. Ed. Engl*. 1995, **34**, 2311. (c) F. H. Allen, W. D. S. Motherwell, P. R. Raithby, G. P. Shields, R. Taylor, *New J. Chem.* 1999, **23**, 25.

21. R. M. Silverstein, G.C. Bassler, T. C. Morrill, *Spectrometric Identification of Organic Compounds, 7th Ed.,* 2005. (b) E. Smith, G. Dent, *Modern Raman Spectroscopy, A Practical Approach*, John Wiley, New York, 2005.

22. P. Kaushik, R. Thaimattam, M. Prasad, *WO 2012/098501 A1*.

23. (a) N. Schultheiss, A. Newman, *Cryst. Growth Des.* 2009, **9**, 2950. (b) C. B. Aakeröy, S. Forbes, J. Desper, *J. Am. Chem. Soc*. 2009, **131**, 17048.

24. N.A. Tumanov, S.A. Myz, T.P. Shakhtshneider, E.V. Boldyreva, *CrystEngComm*, 2012, **14**, 305.

25. (a) C. Y. C. Pak, O. Walters, L. Arnold, K. Holt, C. Cox, D. *J*. Barilla, *Clin. Investigation*, 1977, **59**, 426. (b) A. So, *Arthiritis Research and Therapy,* 2008, **10**, 221.

26. A. W. Newman, S. L. Childs, B. A. Cowans, *Salt Cocrystal Form Selection, In Preclinical Development Handbook*; John-Wiley, Hoboken, 2008, pp. 455–481.

27. *CrysAlis CCD and CrysAlis RED*, Ver. 1.171.33.55; Oxford Diffraction Ltd: Yarnton, Oxfordshire, U.K., 2008.

28. O. V. Dolomanov, L. J. Bourhis, R. J. Gildea, J. A. K. Howard, H. Puschmann, OLEX2: A complete structure solution, refinement and analysis program. *J. Appl. Crystallogr*., 2009, **42**, 339.

29. *SAINT-Plus*, version 6.45; Bruker AXS Inc.: Madison, Wisconsin, U.S.A., 2003.

30. SADABS, *Program for Empirical Absorption Correction of Area Detector Data*; Sheldrick, G. M. University of Göttingen: Göttingen, Germany, 1997.

31. (a) *SMART*, version 5.625 and *SHELX-TL*, version 6.12, Bruker AXS Inc.: Madison, Wisconsin, USA, 2000. (b) Sheldrick, G. M. *SHELXS-97* and *SHELXL-97*, University of Göttingen: Göttingen, Germany, 1997.

32. A. L. Spek, *PLATON, A Multipurpose Crystallographic Tool*; Utrecht University: Utrecht, Netherlands, 2002.

33. L. J. Barbour, *X-Seed*, *Graphical Interface to SHELX-97 and POV-Ray*, *Program for Better Quality of Crystallographic Figures*; University of Missouri-Columbia, Missouri, U.S.A., 1999.

34. Powder Cell, A Program for Structure Visualization, Powder Pattern Calculation and Profile Fitting, http://www.ccp14.ac.uk/index.html (accessed on April 8, 2013).

CHAPTER THREE

TETRAMORPHS OF THE ANTIBIOTIC DRUG TRIMETHOPRIM:

CHARACTERIZATION AND STABILITY
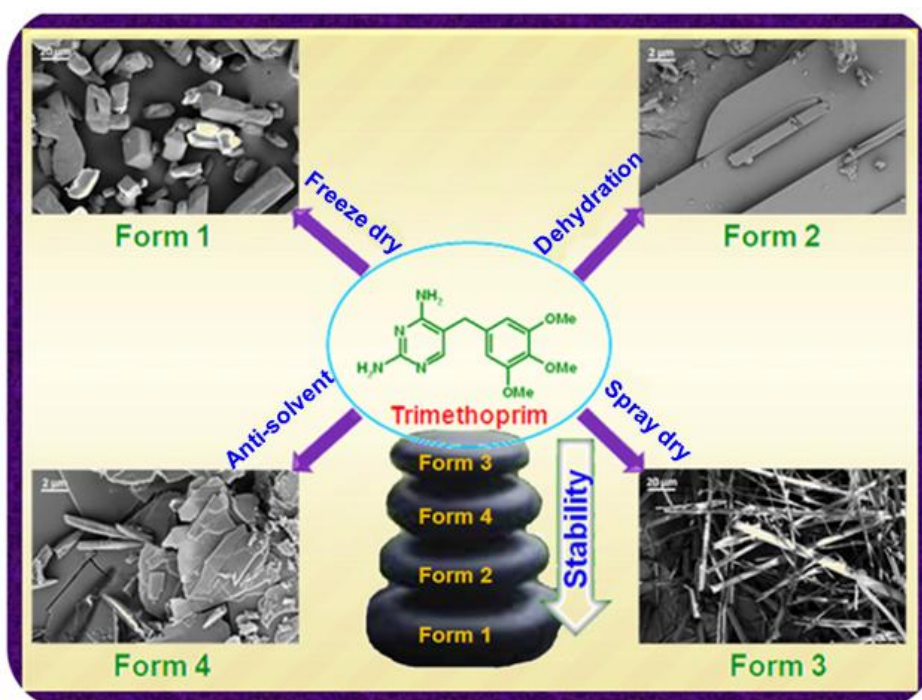
Four polymorphs (Forms 1, 2, 3 and 4) and a hemihydrate of the well known antifolate drug trimethoprim are reported. Thermodynamic relationship, phase transformations, slurry grinding stability, and ICH conditions of 40 °C, 75% RH were studied, together with DVS. The stability order of trimethoprim polymorphs is Form 3 (least stable) < Form 4 < Form 2 < Form 1 (thermodynamic).

3.1 Introduction

A thorough characterization of pharmaceutical solids for polymorphs, salts, hydrates, solvates, cocrystals, etc., is of fundamental importance and practical utility in pharmaceutical research and development (R&D) to develop the optimal solid form for oral dosage and a robust and reliable manufacturing process.[1] Polymorphism, the existence of more than one crystalline form of the same compound, is of current topical interest in Active Pharmaceutical Ingredients (APIs) for both physical property modification as well as intellectual property reasons.[2] Polymorphs can exhibit different physical and/or chemical properties such as melting point, density, stability, manufacturability, mechanical behavior, solubility and bioavailability, etc.[3] Different polymorphs of a drug can be patented, and the commercial interests of a company could be threatened by new polymorphs being discovered.[4] Solid form screening, the activity of generating and analyzing different solid forms and a study all possible polymorphic transformations of an API, has become an essential and important activity in pharmaceutical development. The sudden appearance of a more stable polymorphic form (which is less soluble) can lead to a serious setback for the marketed dosage form. McCrone[5] said almost 50 years ago, "that the number of polymorphs of a given compound is proportional to the time and money spent on research on the compound". In spite of rigorous polymorph screening methods and continuous efforts, the appearance of new polymorphs in late stages is still a surprise. For example, the recent discoveries of polymorphs of aspirin,[6] curcumin,[7] and ibuprofen,[8] compounds which are crystallized in ton quantities, mean that there is still opportunity for traditional methods of crystallization in polymorph hunting.

3.2 CSD analysis and literature reports on Trimethoprim

Trimethoprim (TMP) is a well-known antifolate drug used mainly in the treatment of urinary tract infections, which selectively inhibit the bacterial enzyme dihydrofolate reductase (DHFR).[9] It is a specific inhibitor of formylation and a competitive inhibitor of DHFR in the class of chemotherapeutic agents known as dihydrofolate reductase inhibitors.[9] It is one of the most widely used broad-spectrum antibiotics because of its high selectivity (>60,000 times) for bacterial rather than human DHFR.[10] TMP is on the World Health Organization's

List of Essential Medicines,[11] a list of the most important medications needed in a basic health system. TMP was first approved by the US-FDA in combination with sulfamethoxazole (SMZ) in 1973. The combination of both the drugs is known as co-trimoxazole. The synergy between TMP and SMZ was first described in a series of *in vitro* and *in vivo* experiments published in the late 1960s.[12] Its use has been declining due to reports of bone marrow toxicity by SMZ, resistance and lack of greater efficacy in treating common urine and chest infections,[13] and the side effects of antibacterial sulfonamides. As a consequence the use of co-trimoxazole was restricted in some countries in 1995,[14] following the availability of TMP alone. The usual oral adult dosage of TMP tablet is 100 mg for every 12 hours or 200 mg TMP tablet every 24 hours, for 10 days. It was previously marketed by GlaxoSmithKline the trade names. TMP is a Biopharmaceutics Classification System (BCS) class II drug with high permeability and low solubility (0.4 mg/mL) having dose number (D_0) of 2.[15] We found various salts of TMP in the literature, e.g. TMP formate,[16a] TMP nitrate,[16b] TMP perchlorate,[16c] TMP acetate,[16d] TMP monobenzoate,[16e] TMP glutarate,[16f] TMP trifluoroacetate,[16g] TMP maleate,[16h] and TMP o-nitrobenzoate,[16i] and the most well known TMP-SMZ.[16j] Furthermore, TMP salt hydrates/solvates such as TMP m-chlorobenzoate dihydrate,[17a] TMP salicylate monohydrate,[17b] TMP sulfate trihydrate,[17c] TMP salicylate methanol solvate,[17d] TMP sorbatedihydrate,[16i] etc. have been reported. Even as several research groups have reported multi-component crystals of TMP, only one guest-free form is reported in the CSD.[18] Bettinetti et. al. reported three forms of TMP (Form I, Form II, Form III) and TMP hydrate.[19] Despite its pharmaceutical significance for over five decades, there is no report on the systematic screen of TMP polymorphs, their characterization and stability relationships. A search of the CSD[20] for trimethoprim furnished 80 hits, out of which two hits (Refcode: AMXBPM10 and AMXBPM11) were found to be entries of the same guest-free form (multiple structure determinations of Form I in $P\bar{1}$ space group); the remaining entries belong to multi-component structures, i.e. salts and solvates. We describe four polymorphs and one hemihydrate form of TMP, of which Forms 1 and 2 are structurally confirmed by X-ray diffraction, and the remaining Forms 3 and 4 were characterized by spectroscopic (FT-IR, Raman, ^{15}N ss-NMR), field emission scanning electron microscopy (FESEM), differential scanning calorimetry (DSC), and powder X-ray

diffraction (PXRD) techniques. Further, phase transformations and stability relationships among the forms were established.

3.3 Results and Discussion

In spite of its pharmaceutical significance since 1960s, detailed structural information on trimethoprim polymorphs is scarce and fragmented. We initiated a systematic study to explore the structural landscape of TMP. The conformational flexibility of TMP molecule and the different donor–acceptor hydrogen bond pairing of pyrimidine moiety are favorable factors for new polymorphs. Even as single crystal X-ray diffraction is the most definitive proof of polymorphic solids, the need for good quality crystals and difficulties with growing single crystals mean that powder X-ray diffraction (PXRD) becomes the first choice method for most pharmaceuticals, and this is the case with Form 3 and 4. Four anhydrous TMP Forms 1, 2, 3, 4 and a TMP hemihydrate are characterized as part of this study. Among the reported TMP Forms I, II, and III and TMP-H_2O,[19] Forms I and II match with our Form 1 and Form 2 respectively, but reported Form III is different from our Form 3, and hence Form 3 and Form 4 of this study are novel TMP polymorphs. The bulk materials could be consistently prepared for all the polymorphs by optimizing different techniques such as dehydration, anti-solvent method, freeze drying and spray drying. The commercial material matches with Form 1, and the bulk material of Form 3 was obtained by spray drying of commercial TMP in MeOH solvent. Form 4 was isolated by anti-solvent methods and Form 2 by dehydration of TMP-H_2O in a programmable oven as well as by anti-solvent supersaturation. Freeze drying of commercial TMP in water and water-MeOH solvents resulted in Form 1. Conditions have been standardized to obtain the desired polymorph in bulk which is generally a challenge when multiple polymorphs crystallize for pharmaceuticals. The crystal structure of the TMP Form 1 has been reported previously.[18] Crystallographic parameters of Forms 1 and 2 and hydrogen bonds in their crystal structures are listed in Table 3.1 and Table 3.2. Molecular overlay of both the Forms 1 and 2 showed that there is not much of a conformational difference between the forms (Figure 3.1). A detailed structural analysis of Forms 1 and 2 shows three different synthon types (Type I, II and III motifs) sustained by N–H···N$_{arom}$ interactions of TMP molecules (Scheme 3.1).

Trimethoprim,TMP

Type I, N1 and N3 make H bond dimer

Type II, N2 and N4 make H bond dimer   Type III, N2 and N3 make H bond dimer
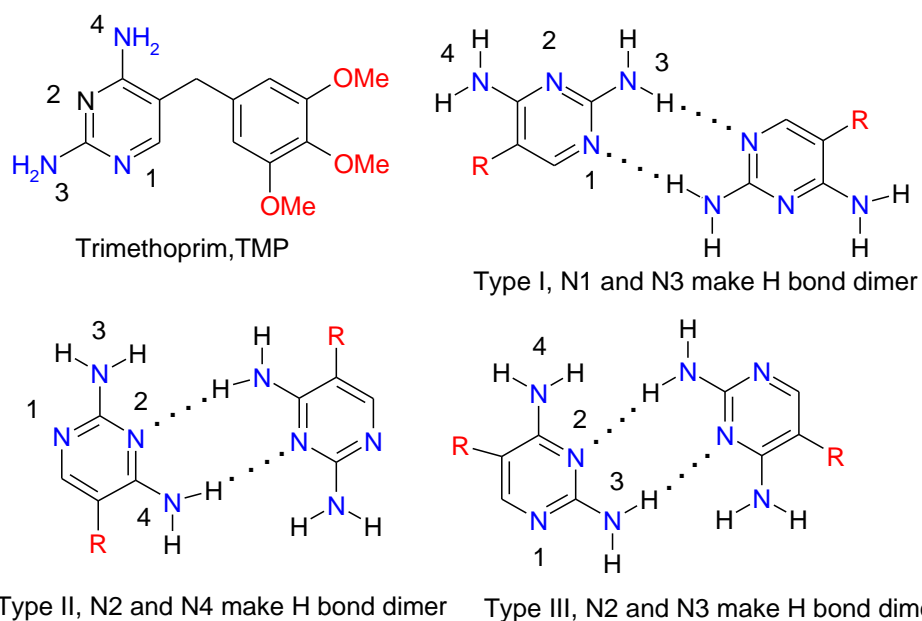
Scheme 3.1 Molecular structure of Trimethoprim and hydrogen bonded synthons Types I, II and III in polymorphs. Note that the N–H···N dimer is the same but the difference is in the orientation of NH_2 and R groups and which of the pyrimidine N / NH_2 engages in H bonding.
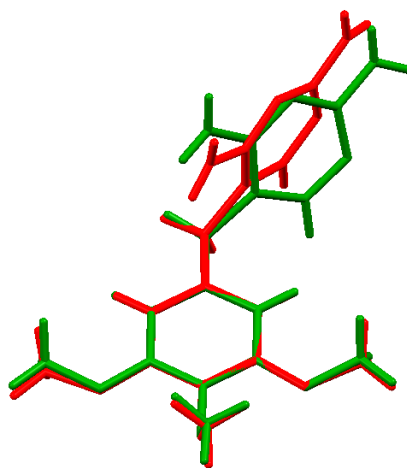
Figure 3.1 An overlay diagram of the TMP molecule in crystal structures. Green: TMP Form 1, Red: TMP Form 2.

3.3.1 Crystal Structure Analysis

TMP Form 1: Block morphology crystals of TMP Form 1 were crystallized from isopropanol solvent which solved and refined in the triclinic space group $P\bar{1}$ (Z' = 1). TMP molecules bonded by the amino-pyrimidine synthon[21a,b] (N−H···N$_{arom}$: 1.99 Å, 174º; 1.96 Å, 178º) result in a ribbon like pattern via two types of R_2^2 (8) motifs,[21c,d] named as type I and type II (Figure 3.2a). Trimethoxy phenyl ring of TMP connects the chains through N−H···O (2.29 Å, 128º; 2.55 Å, 129º) and C−H···O (2.54 Å, 163º) bonds resulting in a corrugated sheet like structure (Figure 3.2b).

(a)   (b)

(c)
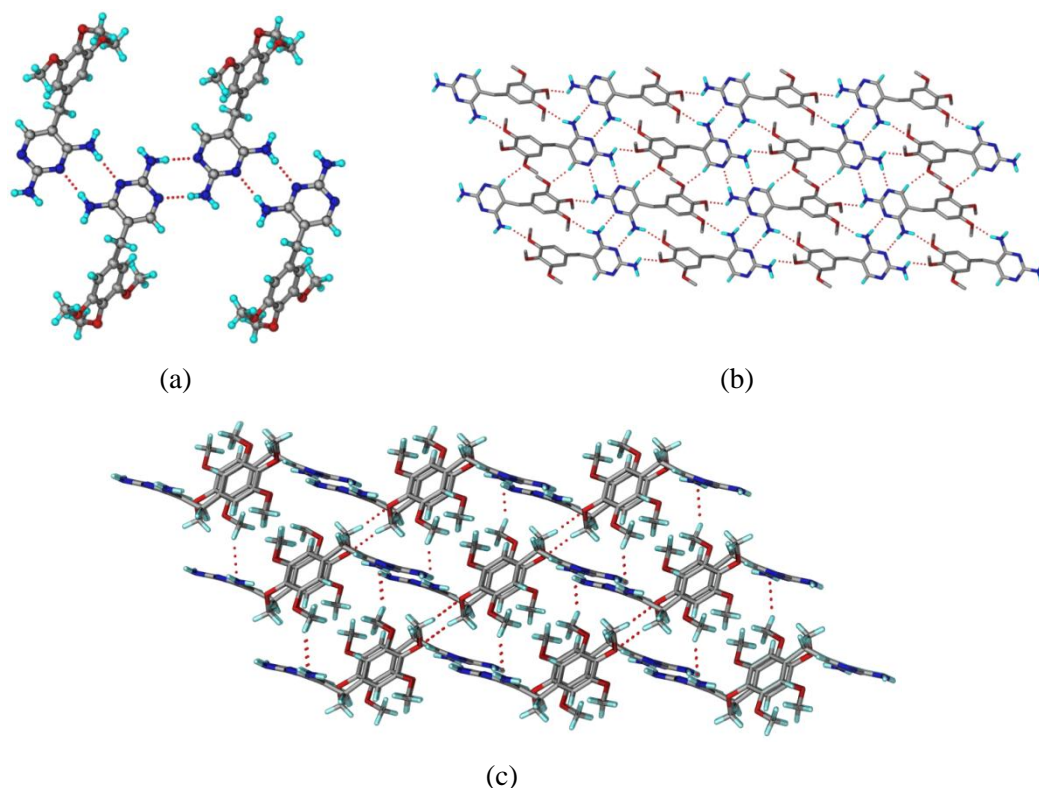
Figure 3.2 (a) The ribbon hydrogen bond network of Form 1 sustained by type I and type II N−H···N motifs. (b) Corrugated sheet formed by N−H···O and C−H···O bonds (H atoms not involved in hydrogen bonding are removed for clarity). (c) There are weak C−H···O and C−H···π interactions between the sheets.

TMP Form 2: Plate morphology crystals of TMP Form 2 were crystallized from methanol-chlorobenzene (1:1 v/v) (monoclinic space group $P2_1/c$, Z' = 1). TMP molecules are connected through type III R_2^2 (8) dimer motif [21c, d] (N−H⋯N_{arom}: 1.97 Å, 172º) (Figure 3.3a). Each dimer is connected to neighboring molecules through N−H⋯N_{arom} (2.16 Å, 163º; 2.15 Å, 143º) hydrogen bonds resulting in a R_3^2 (8) motif, whereas in Form 1 it is a R_2^2 (8) motif. Such TMP dimers between inversion related molecules propagate into a chain along [001] through anti N−H⋯N_{arom} interactions (R_3^2 (8) motif) (Figure 3.3b). Auxiliary C−H⋯O (2.58 Å, 120º) interactions between the adjacent chains complete the 3D packing.

(a)

(b)
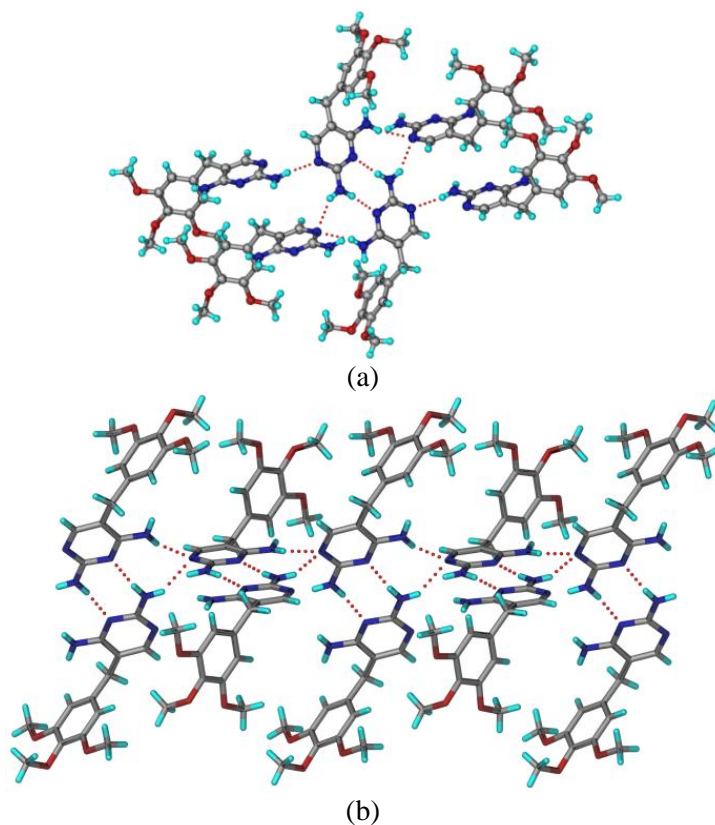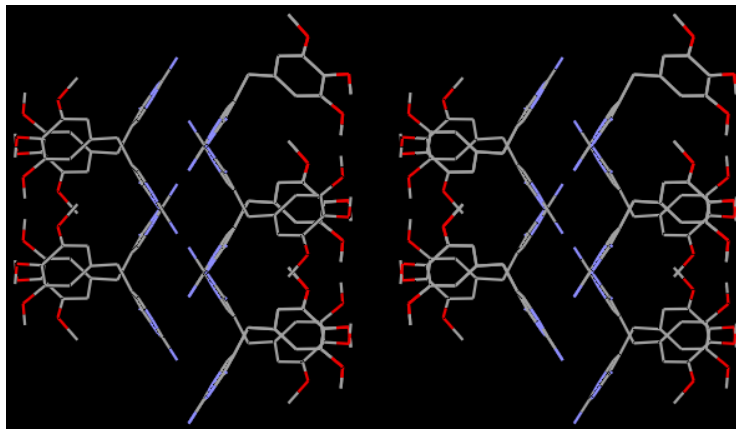
(c)

Figure 3.3 (a) Inversion related TMP molecules form N−H···N$_{arom}$ dimers of type III. (b) 1D chain formed through R$_3^2$ (8) motif. (c) Overall molecular packing in Form 2 (H atoms are omitted for clarity).

Table 3.1 Cystallographic parameters of TMP forms.

	TMP Form 1	TMP Form 2	TMP Form 1	TMP Form 1
Reference	This work	This work	AMXBPM10[a]	AMXBPM11[a]
Emp form.	C14 H18 N4 O3	C14 H18 N4 O3	C14 H18 N4 O3	C14 H18 N4 O3
Form wt	290.32	290.32	290.32	290.32
Cryst syst	Triclinic	Monoclinic	Triclinic	Triclinic
Sp gr	$P\bar{1}$	$P2_1/c$	$P\bar{1}$	$P\bar{1}$
T/K	100(2)	100(2)	283-303	173
a/Å	7.9202(8)	18.250(2)	10.523(4)	8.0211(11)
b/Å	10.4378(11)	5.9580(7)	11.222(4)	10.5296(12)
c/Å	10.5434(11)	12.7527(14)	8.068(3)	10.5957(11)
α/°	106.8710(10)	90	101.22(1)	107.002(9)
β/°	101.686(2)	93.969(2)	112.15(1)	101.320(10)
γ/°	111.8230(10)	90	112.65(1)	112.104(9)
Z	2	4	2	2
V/Å^3	725.51(13)	1383.4(3)	747.269	743.998
D_{calc}/g cm^{-3}	1.329	1.394	1.292	1.296
μ/mm^{-1}	0.096	0.101	-	-
Rflns collect	7521	13551	-	-
Unique rflns	2828	2720	-	-
Obsd rflns	2666	2361	-	-
R_1 [$I>2\sigma(I)$]	0.0374	0.0366	0.045	0.045
wR_2 [all]	0.1002	0.0939	-	-
GOF	1.102	1.045	-	-

[a]Ref 17

Table 3.2 Hydrogen bond metrics in the crystal structures.

D–H⋯A	H⋯A (Å)	D⋯A (Å)	D–H⋯A (°)	symmetry code
		TMP Form 1		
N3–H3A⋯N1	1.99	3.023(2)	174	-x,-y,-z
N3–H3B⋯O2	2.29	2.999(1)	128	x,-1+y,-1+z
N4–H4B⋯O3	2.55	3.303(1)	129	-x+1,-y+2,-z+1
N4–H4A⋯N2	1.96	2.989(2)	178	1-x,1-y,-z
C2–H2⋯O1	2.54	3.584(2)	163	-x,-y+1,-z+1
C13–H13A⋯O2	2.57	3.471(2)	141	-x+1,-y+2,-z+2
		TMP Form 2		
N3–H3A⋯N1	2.15	3.030(2)	143	-x,+y-1/2,-z+1/2+1
N3–H3B⋯N2	1.97	2.990(2)	172	-x,-y-1,-z+1
N4–H4A⋯N1	2.16	3.160(2)	163	x,-y-1/2,+z-1/2
C5–H5B⋯N2	2.45	3.314(2)	136	x,+y+1,+z
C12–H12A⋯O3	2.45	3.364(2)	142	x,-y+1/2,+z+1/2
C13–H13A⋯O2	2.58	3.250(1)	120	-x+1,+y-1/2,-z+1/2

3.3.2 Spectroscopic Characterization of Forms

Spectroscopic methods such as FT-IR and Raman are able to identify and distinguish between polymorphs, molecular conformations, and hydrogen bonding interactions by probing the vibrational frequencies of atoms.[22] The sensitivity of these techniques to subtle changes in the crystal structure have led to their application in a wide variety of investigations of polymorphic studies, and in confirming results obtained from PXRD analysis. The four polymorphs of TMP (Forms 1, 2, 3 and 4) and TMP-H_2O showed diagnostic differences in IR and Raman spectra. The very strong absorption bands of TMP Form 1 at 3471.0 cm^{-1} and 3319.5 cm^{-1} are the symmetric and asymmetric N-H stretching vibrations of the amino group. There are fairly strong bands in the region 3140 to 2830 cm^{-1} due to the C–H stretch of the pyrimidine ring, the benzyl aromatic and methyl groups. The peaks at 3136.8 and 3006.6 cm^{-1} are the most characteristic due to the C–H stretch of the pyrimidine ring and their intensity is approximately the same as that of the N–H bands. The stretching frequencies around the 1236.7 and 1045.4 cm^{-1} are due to C–O–C vibrations, and

1596.0 cm^{-1} is of pyrimidine ring C=N stretch. Similarly, the NH symmetric and asymmetric stretching frequency was observed at 3470.5, 3319.2 cm^{-1} in Form 2, 3499.1, 3326.5 cm^{-1} in Form 3, 3470.2, 3320.6 cm^{-1} in Form 4 (Figure 3.4a). An additional peak was observed for the NH stretch at 3407.9 cm^{-1} in Form 2, at 3408.1 cm^{-1} in Form 3, and 3409.3 cm^{-1} for Form 4, which are absent for Form 1. These differences in IR stretching bands are related to the different N–H⋯N hydrogen bonding motifs of the amine group, as discussed in the crystal structures of Form 1 and Form 2. TMP-hydrate was identified by O–H stretching frequency at 3627.2 cm^{-1} in addition to NH stretch at 3472.4, 3332.8 2 cm^{-1}. A list of stretching frequencies of complete spectra is provided in Table 3.3. Raman measurements are also recorded for characterization, with the added advantage that this technique does not require any sample preparation (such as KBr pellet) and hence unintended phase transitions are avoided.[22] Similar to IR, the N–H Raman shift for TMP molecule was observed at 3471.7 cm^{-1}, 3315.8 cm^{-1} in Form 1, and 3467.2 cm^{-1}, 3329.2 cm^{-1} in Form 2, and 3467.2 cm^{-1}, 3328.1 cm^{-1} in Form 3, and 3467.2 cm^{-1}, 3315.8 cm^{-1} in Form 4 (Figure 3.4b). Even the other stretching frequencies showed significant differences in Forms 1, 2, 3, and 4. The Raman spectrum of TMP-H$_2$O is readily distinguishable from the four other polymorphic forms. The detailed peak values of different functional groups and Raman spectra are given in Table 3.3.
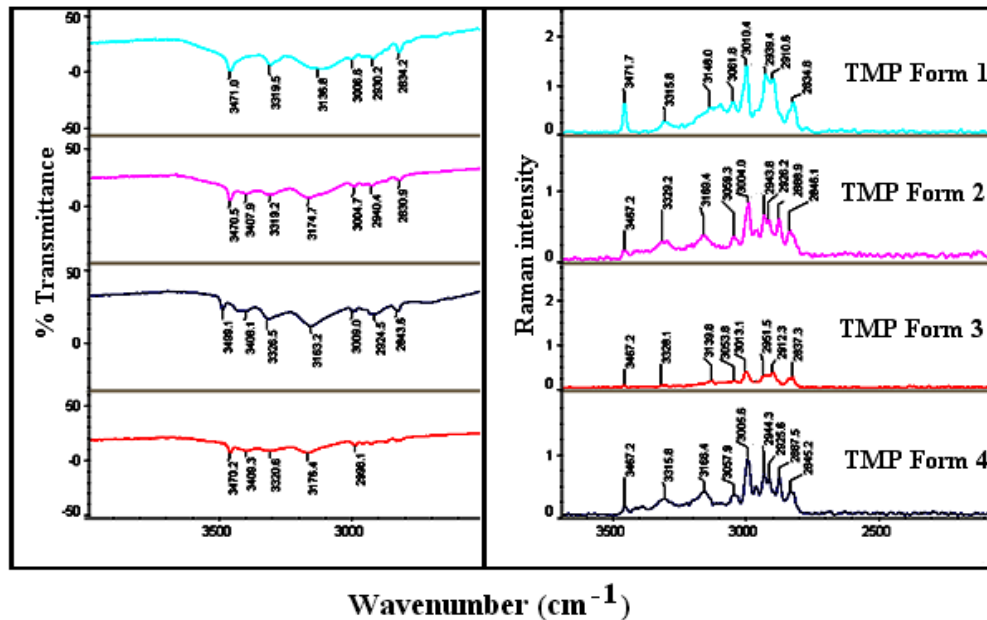
(a)   (b)

Figure 3.4 (a) FT-IR spectral comparison and (b) FT-Raman spectral comparison of TMP forms to show significant differences in bond frequencies among polymorphs.

Table 3.3 Summary of FT-IR and Raman stretching frequencies of TMP polymorphs (cm^{-1}).

compound	NH2 (stretch)	C–O–C (stretch)	Aromatic C–H (stretch)	C=N (stretch)	C–N (stretch)
INFRARED					
TMP Form 1	3471.0 3319.5	1236.7 1045.4	3006.6	1596.0	1458.3
TMP Form 2	3470.5 3407.9 3319.2	1235.6 1038.4	3004.7	1599.4	1460.0
TMP Form 3	3499.1 3408.1 3326.5	1241.4 1039.9	3009.0	1585.5	1453.7
TMP Form 4	3470.2 3409.3 3320.6	1234.8 1037.1	2998.1	1600.4	1458.6
TMP Hydrate	3472.4 3431.2 3332.8	1262.6 1040.8	3006.6	1591.4	1458.7
RAMAN					
TMP Form 1	3471.7	1269.1	3010.4	1603.0	1458.5

	3315.8	1048.1			
TMP Form 2	3467.2 3329.2	1265.0 1039.9	3004.0	1597.4	1458.7
TMP Form 3	3467.2 3328.1	1263.9 1042.8	3013.1	1599.3	1460.0
TMP Form 4	3467.2 3315.8	1269.1 1044.0	3005.6	1598.2	1461.5
TMP Hydrate	3471.3 3062.0	1268.1 1045.7	3010.4	1602.3	1462.1

In addition to vibrational modes, the local environment changes in the crystal lattice and molecular conformations may be gleaned by solid-state NMR.[23] The nitrogen rich molecule TMP is best studied by ^{15}N ss-NMR. We were able to see the N peaks in Forms 1, 2, and 4 after overnight run (Figure 3.5 and Table 3.4), but polymorph 3 did not show good intensity. The differences in packing modes are evident from the shift of up to 5 ppm in ^{15}N chemical shifts. There is an upfield shift of 2−3 ppm in ^{15}N of pyrimidine N in TMP Form 1 (−182.89 ppm) compared to Form 2 (−180.69 ppm) and Form 4 (−179.86 ppm). A shift of ~ 2−5 ppm was observed for amine N3 and N4 of Form 1 (−301.31, −303.93 ppm), indicating formation of a strong hydrogen bonds (two dimers type I, II in Form 1 and only type III in Form 2), compared to Form 2 (−296.39, −301.67 ppm) and Form 4 (−296.38, −301.66 ppm). The NMR spectrum of Form 3 could not be recorded because the hair-like fine crystals were very difficult to compress in the NMR rotor, and because this is a metastable form it converted to form 1 during the long measurement time.
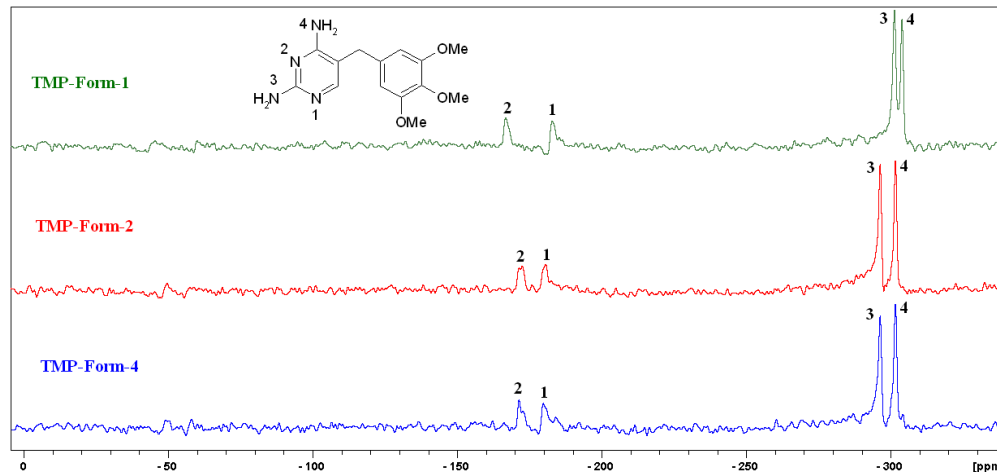
Figure 3.5 ^{15}N ss-NMR spectrum of TMP forms 1, 2 and 4 shows significant difference in the chemical shifts of forms.

Table 3.4 ^{15}N ss-NMR chemical shifts (δ, ppm) of TMP Polymorphs.

Polymorph	Pyrimidine N_1, N_2	1° amine N_3, N_4
TMP Form 1	-182.89, -166.81	-301.31, -303.93
TMP Form 2	-180.69, -172.58	-296.39, -301.67
TMP Form 4	-179.86, -171.46	-296.38, -301.66

3.3.3 Powder X-ray diffraction

Powder XRD is a quantitative tool for the analysis of polycrystalline materials and a first choice method for the characterization of polymorphs.[24] The experimental PXRD pattern of commercial TMP matches with the literature pattern and overlays on the calculated pattern of TMP Form 1 (Figure 3.6a). Bulk material of Forms 2 and 4 were prepared by the anti-solvent method (see Experimental section), and Form 3 was obtained by dehydration of TMP-H_2O. TMP-hydrate was crystallized from an aqueous alkaline solution (see Experimental section, PXRD of the hydrate is presented in Figure 3.6b. Forms 1, 2, 3, and 4 are readily distinguishable by their unique PXRD patterns, and can be identified by the diagnostic peaks for Form 1 at 2θ position 11.49, 14.65, 17.12, 21.78°, for Form 2 at 4.72,

14.49, 16.21, 20.29°, for Form 3 at 12.92, 14.67, 21.88, 27.15°, and for Form 4 at 4.96, 14.61, 19.47, 24.41, 29.35° (Figure 3.7). The PXRD characteristics reported by Bettinetti et al.[19] for their Form III are different from TMP Form 3 of this work. In a separate experiment, TMP-H_2O was kept in a programmable oven at 90 °C for 30 min and the PXRD of the resulting material matched with the TMP Form 2, and when kept at 140 °C for 30 min the hydrate gave Form 1. In another experiment, the hemihydrate was heated at 45 °C (and up to 80 °C) in a vacuum oven to give Form 2. However, we were able to obtain Form 3 by dehydration. Since TMP hemihydrate is easy to prepare in bulk quantity, a simple dehydration under specific conditions to give Form 1 or Form 2 is a practical method for making these polymorphs in bulk. When Form 2 or Form 4 was kept in an oven at 170 °C for 25-30 min, the PXRD of the product matched with Form 1. In another experiment, Form 3 was kept at 90 °C for 10 min and the PXRD of the product matched with Form 2, and at 140 °C for 35-40 min the product matched with Form 1. Furthermore, PXRD together with DSC establish that Form 3 and 4 of this study are novel polymorphs of TMP. Because there are very few diffraction lines in the PXRD pattern of Form 4, which is unusual for an organic compound, we confirmed the identity of this material by ^{1}H NMR and it matches with that of TMP form 1.

(a)   (b)
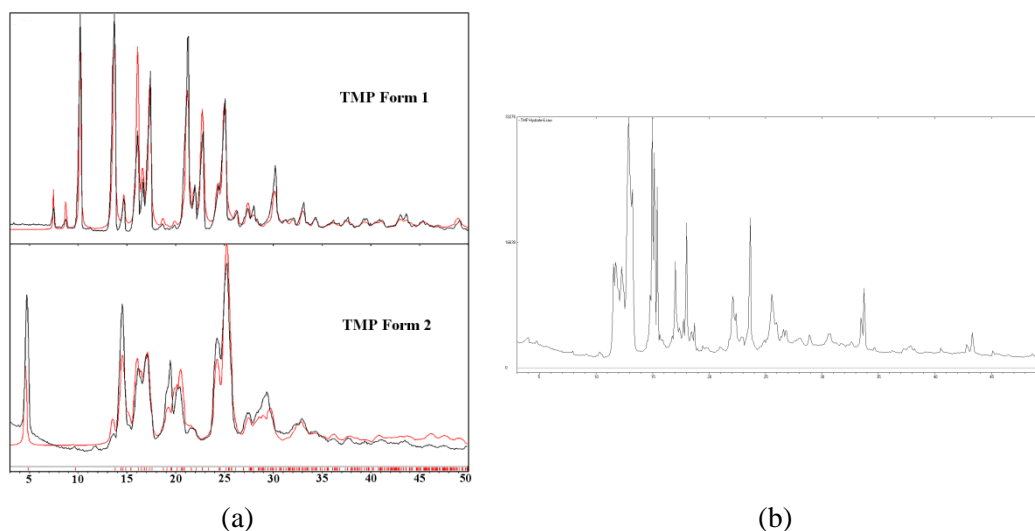
Figure 3.6 (a) Overlay of experimental PXRD patterns (black) of TMP forms 1 and 2 matches with their respective calculated powder lines from the crystal structures (red). (b) PXRD pattern of TMP hemihydrate obtained from aqueous alkaline solution.
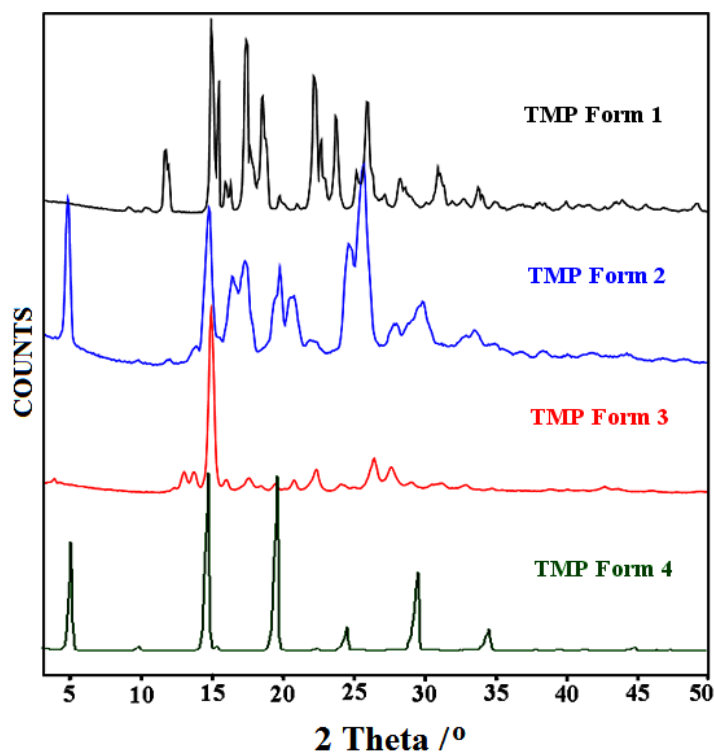
Figure 3.7 Overlay of experimental PXRD patterns of the TMP forms shows that each form exhibits unique powder lines.

3.3.4 Thermal Analysis

DSC provides direct information on thermodynamic parameters associated with polymorphic transitions.[25] Upon heating Form 1 in the DSC pan, a sharp endotherm peak was observed at 201.8 °C due to melting (ΔH_{fus} = −47.44 kJ/mol) and there was no indication of any phase transformation prior to melting (Figure 3.8). It was not possible to observe the pure fusion peaks and enthalpies of Forms 2, 3, and 4 because they undergo a crystal-to-crystal transformation upon heating to a high temperature stable polymorph, and it is the latter modification which melts. We recorded the enthalpy of the polymorphic transitions 2→1, 3→2→1, and 4→1 (Table 3.5). DSC of Form 2 showed an endothermic transition at 162.5 °C which was ascribed to phase transformation of Form 2 to 1, and the melting endotherm corresponds to the latter Form 1. In a separate experiment, Form 2 was kept at 170 °C for 10

min in a programmable oven and the resulting material exhibited no phase changes in DSC and its PXRD matched with that of Form 1. These phase transitions are shown in the expanded inset of 30-190 °C range (Figure 3.9). Based on the heat of transition rule, the transformation of Form 2 to Form 1 is enantiotropic the transition point being below the melting point at 162.5 °C. In order to visualize the conversion of Form 2 to1, HSM showed a plate like crystal of Form 2 undergoing a solid-to-solid phase transition at 158-160 °C to Form 1 and then melting of latter polymorph at 198-199 °C (Figure 3.10), consistent with the DSC. HSM on Form 1 did not show any phase transition of the block crystals before melting at 197-200 °C, as expected from its thermodynamic nature (Figure 3.11). DSC of Form 3 exhibited a small broad exothermic peak corresponding to a polymorphic transformation to Form 2 at 80.8 °C, and further heating gave an endothermic transition at 131 °C, and then Form 1 (Figure 3.9), which melted (Figure 3.8). The transition 3→2 is exothermic, which means that these two polymorphs are monotropically related. DSC thermogram of Form 3 in our study is different from the reported Form III,[26] for which the transition from Form III to II was endothermic. Hence Form 3 of this study is novel. DSC thermogram of Form 4 exhibits an endothermic transition to Form 1 at 165.8 °C (enantiotropic polymorphs) (Figure 3.9). Heating of Form 4 in an oven gave Form 1. Similar to the enantiotropic pair Form 1 and 2, Form 4 is stable below the transition temperature of 165.8 °C while Form 1 is stable at high temperature. DSC of TMP-hydrate exhibited a broad endotherm between 69–74 °C for water loss and converted to form 2, and then endothermic transition of form 2→1 at 129.2 °C, and finally melting of stable Form 1 at 201.9 °C (Figure 3.12a). TGA of TMP-hydrate exhibited water loss at 60–75 °C matching with hemihydrate stoichiometry (Figure 3.12b, calc. 3.01%, obs. 3.09%). The original paper on TMP hydrate[19] did not disclose the stoichiometry and now we know that it is a hemihydrate by TGA.
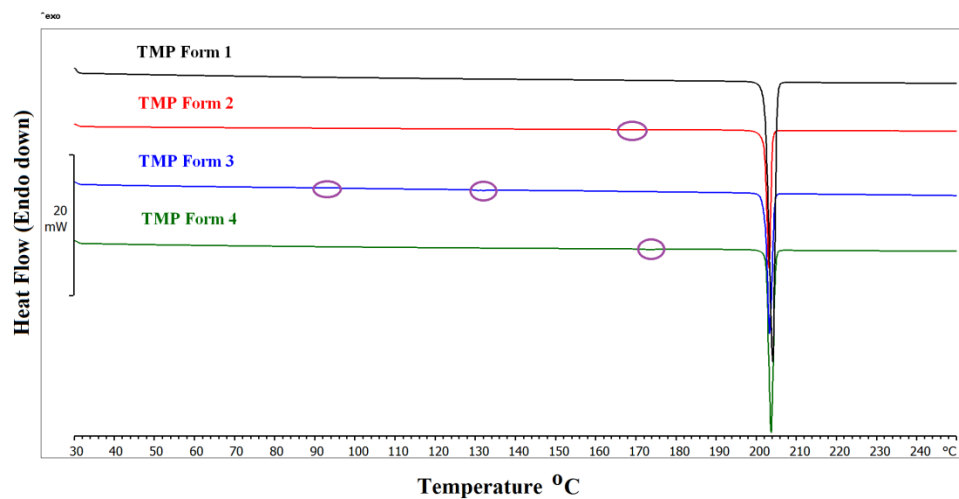
Figure 3.8 DSC thermograms of TMP polymorphs. Note that the circles (purple) represent the transition points and were clearly shown in Figure 3.9.
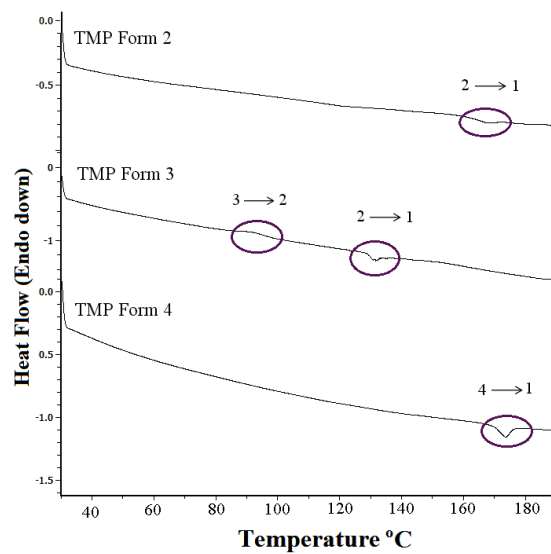
Figure 3.9 DSC thermograms of Forms (2, 3 and 4) to show the phase transition.
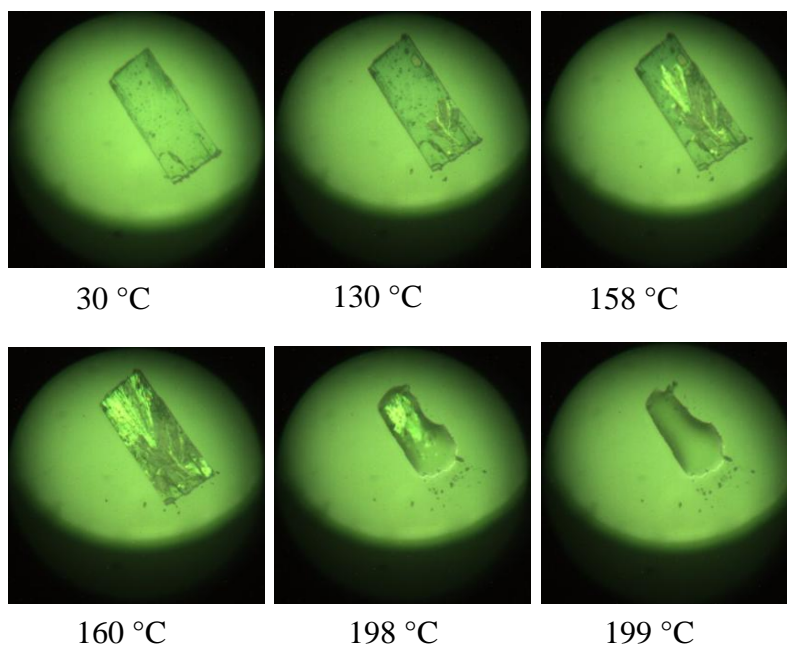
Figure 3.10 HSM snapshots of TMP-Form-2 shows significant morphological changes to TMP-Form-1 between 158-160°C and melting of later can be seen at 198-199 °C.
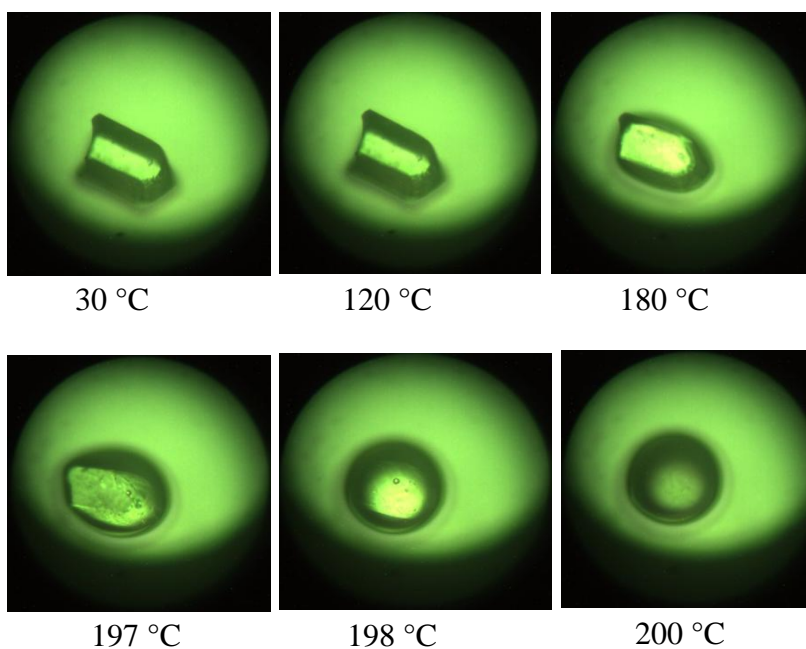
Figure 3.11 HSM snapshots of TMP-Form-1 showed no morphological changes instead direct melting was observed at 197-200 °C.

(a)   (b)
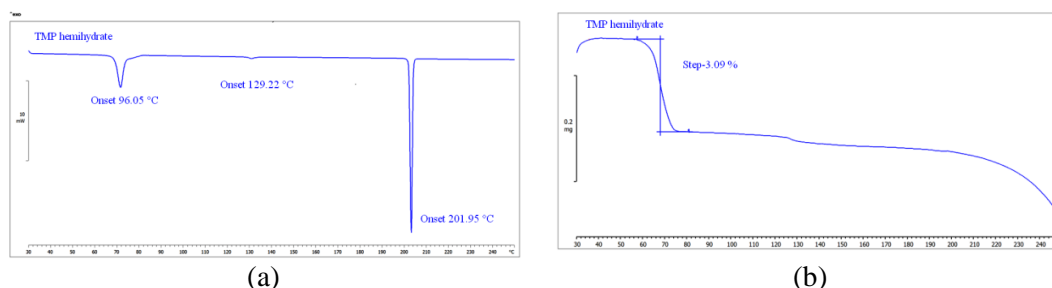
Figure 3.12 (a) DSC thermogram of TMP hydrate to show water loss around 69–74 °C and converted into Form 2, and endothermic transition of Form 2→1 was observed at 129.2 °C followed by melting of the latter form at 201.9 °C. (b) TGA plot of TMP hydrate to show water loss around 60–75 °C.

Table 3.5 Transition temperature and enthalpy values of TMP forms.

Drug Forms	T_{trs} (°C) T_{onset}/ T_{peak}	ΔH_{trs} kJ/mol, (trs)	M.p. (°C) T_{onset}/ T_{peak}	Stability relation
TMP Form 1	-	-	201.81/201.96	-
TMP Form 2	162.54/164.75	−0.171, (2→1)	-	enantiotropic
TMP Form 3	80.81/87.05	+0.476, (3→2)	-	monotropic
TMP Form 4	165.75/170.54	−0.224, (4→1)	-	enantiotropic

3.3.5 Hirshfeld surface and 2D fingerprint plot

The Hirshfeld surface[27] shows the molecular environment in the crystal structure thereby giving a clear and easy visual comparison of structures. Hirshfeld surfaces (with d_{norm} property) of both Forms 1 and 2 are shown to highlight the differences in the molecular environments (Figure 3.13). 2D fingerprint plots[27] (di vs. de, where di is the distance to the nearest atom center interior to the surface, and de exterior of the surface) represent the

intermolecular contacts in the structures (Figure 3.14). The sharp spikes in the fingerprint plots of both Form 1 and 2 near $d_e+d_i \approx 2.0$ Å are due to strong N···H interactions resulting from N−H···N$_{arom}$ H bonds, whereas contribution from these interactions to the total Hirshfeld surface is 17.0% in Form 1and 14.1% in Form 2. The moderate spikes near $d_e+d_i \approx$ 2.3 Å in Form 1 and at $d_e+d_i \approx 2.5$ Å in Form 2 are due to O···H interactions, the lower value in Form 1 (2.3 Å) represents the relatively strong H bonding compared to Form 2 and their respective contributions to Hirshfeld surface is 14.1% and 14.0%. There are fewer voids in the upper region of the fingerprint plot and higher contribution of H···H contacts (54.0%) in Form 2, and the H···H contacts are fewer (49.1%) in Form 1 (Figure 3.15). This indicates a more efficient packing of TMP molecules in Form 2, which is consistent with the difference in calculated densities and packing efficiencies from the crystal structures (Form 1, 1.329 g cm^{-3}, 68.6%; Form 2, 1.394 g cm^{-3}, 71.5%). However, the major interactions such as N···H and O···H comprise 31.1% of the total Hirshfeld surface in Form 1 and 28.1% in Form 2 explains the greater stability of Form 1 (Figure 3.15).

(a)   (b)
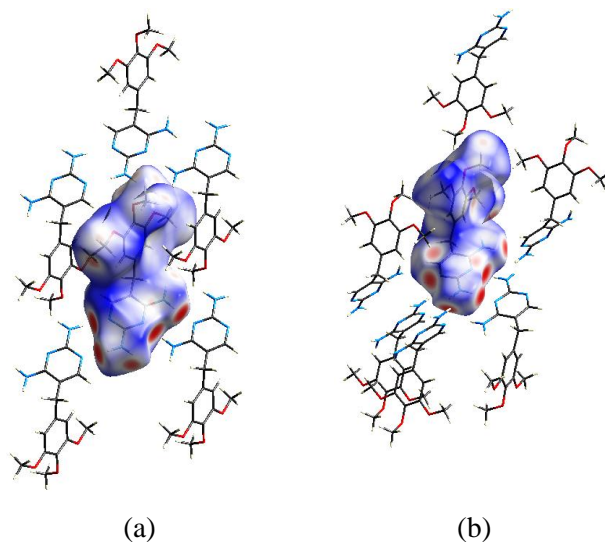
Figure 3.13 Hirshfeld surface maps of (a) form-1 and (b) Form-2 of TMP with the neighboring molecules to show the significant intermolecular hydrogen bonds. The surfaces are shown as transparent to allow visualization of the molecular moiety.

All interactions   N···H interactions   O···H interactions
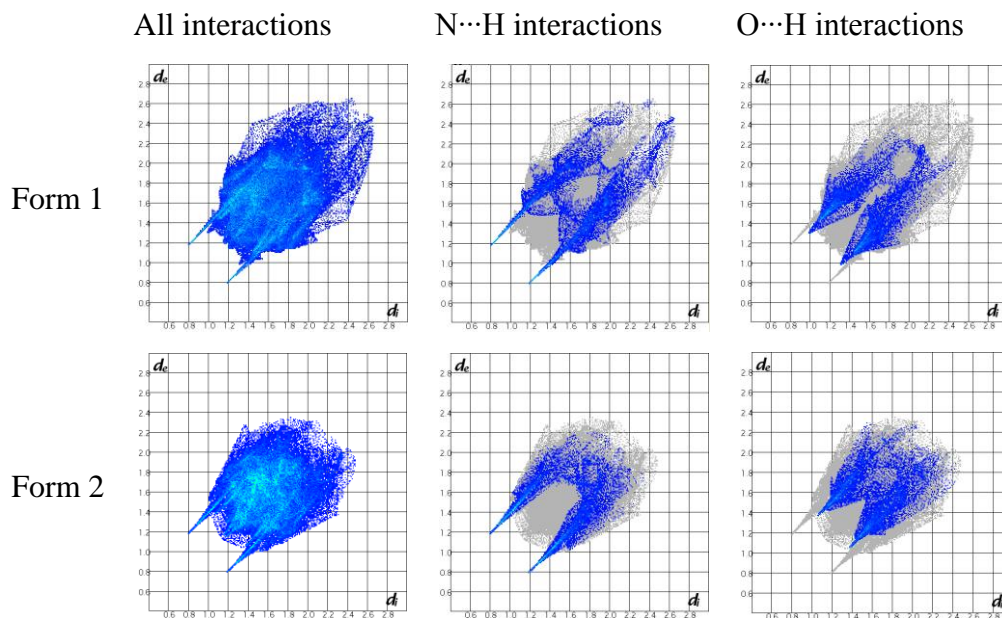
Form 1

Form 2

Figure 3.14 2D Hirshfeld fingerprint plots for Form 1 and Form 2.
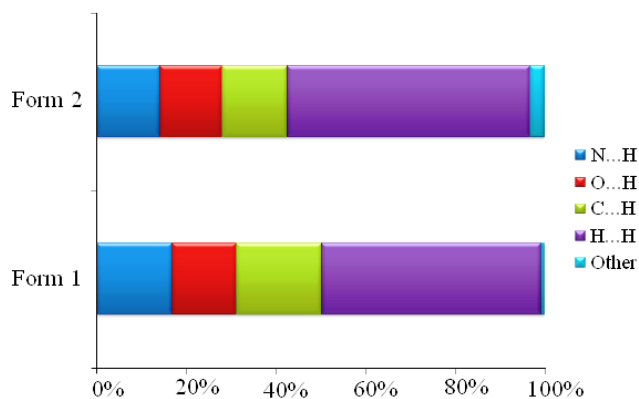
Figure 3.15 Percentage contributions to the Hirshfeld surface area for the major intermolecular interactions in Form 1 and Form 2 crystal structures.

3.3.6 Field Emission Scanning Electron Microscopy (FESEM)

Field emission scanning electron microscopy (FESEM) provides vital information about the morphology and particle size at the nm scale. FESEM is extremely informative for powdered pharmaceutical samples to understand the morphology and physico-chemical behavior. The FESEM images of the four forms (Form 1, 2, 3 and 4) were presented in Figure 3.16. Form 1

and 3 appeared as block and needle morphology respectively at 20 µm magnification scale and form 2 and 4 were found to be aggregated as flat plate-type morphology at 2 µm range. The morphologies of the Form 1 (block) and Form 2 (plate) in FESEM images are in excellent match with those of the single crystals mounted for X-ray diffraction (Figure 3.10 and Figure 3.11).

(a) (b)

(c) (d)
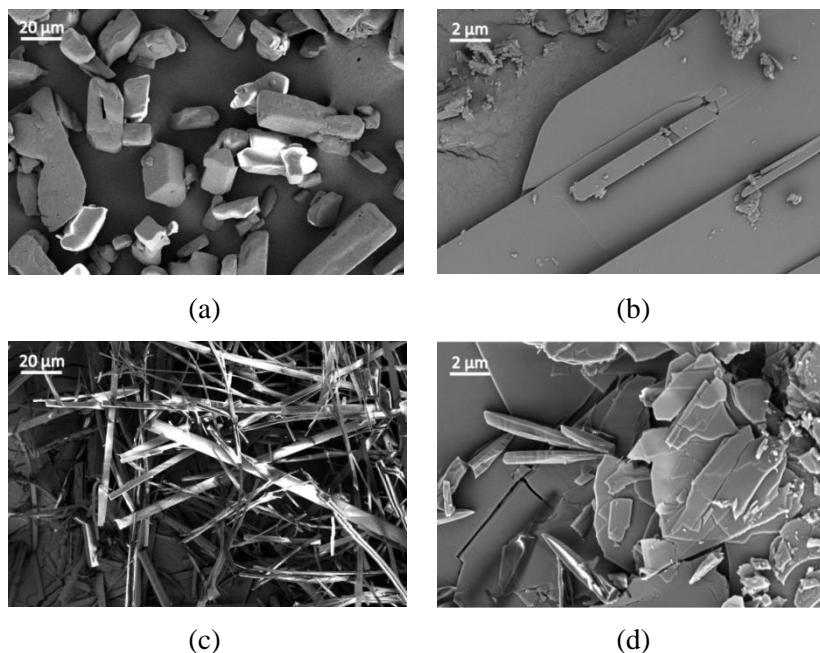
Figure 3.16 SEM images of TMP polymorphs (a) Form 1 (b) Form 2 (c) Form 3 and (d) Form 4 to show the differences in morphology and bulk particles.

3.3.7 Phase Transformations upon Grinding and Slurry

Slurry experiments were carried out on polymorphs to first know the solvent systems in which the drug is chemically stable. Slurry experiments were performed in water on all the forms 1, 2, 3 and 4, taken separately in pure form, as well as competitive slurry experiment in which any two forms were taken together in 1:1 stoichiometry. In slurry grinding experiments (see Experimental Section for details), pure Forms 2, 3 and 4 completely converted into stable Form 1 after 5-15 min, and competitive slurry experiments of polymorph mixtures resulted in Form 1 in less than 10 min, as confirmed by PXRD. Pure

Form 1 stable to the aqueous slurry conditions for up to 2 days no conversion to TMP-H_2O was observed. Thus Form 1 of TMP is established as the thermodynamically stable polymorph.

Metastable forms are known to transform to the more stable polymorph upon grinding, several pharmaceutical compounds undergo phase transformation upon grinding/milling, e.g. indomethacin,[28a] cimetidine,[28b] sulfamerazine.[28c] Phase transformations of TMP were studied under mechanochemical grinding conditions after slurry experiments. Neat grinding (NG)/ liquid assisted grinding (LAG) of pure Forms 3 and 4 showed complete conversion to Form 2 after 5 min, continued grinding for 20-25 min gave Form 1 (monitored by PXRD) (Figure 3.17a and 3.17b). Pure Form 2 converted to Form 1 after grinding for 25 min under similar conditions (Figure 3.18). Extended NG/LAG and also ball milling on Form 1 did not show any changes even after 3 h. This observation is in accordance with the Ostwald's law of stages,[29] metastable polymorphs appear first followed by more stable forms and finally the thormodynamic polymorph, which grow at the expense of metastable phases. Competitive NG/LAG experiments confirmed the above results (summarized in Figure 3.19). The stability of Form 1 compared to less stable Form 2 was rationalized by X-ray structures. Even though Form 2 has higher density and packing efficiency (1.394 g cm^{-3}, 71.5%) compared to Form 1 (1.329 g cm^{-3}, 68.6%), the stability of Form 1 was understood through Hirshfeld analysis[27] of crystal structures. The strong H bonding and higher contribution of the major H bonds (N−H···N_{arom}: 1.96 Å, 178º; 1.99 Å, 174º; O···H + N···H = 31.1%) in Form 1 compared to Form 2 (N−H···N_{arom}: 1.97 Å, 172º; 2.15 Å, 143º and 42.7%; O···H + N···H = 28.1%) is the reason for the stability for Form 1. These two forms of trimethoprim are an exception to the density rule,[30] but so are other polymorph pairs, e.g. ritonavir, paracetamol, resorcinol, etc.[31] Thus NG/ LAG, slurry grinding experiments and X-ray crystal structure analysis and thermal data suggest the stability order of TMP polymorphs as Form 3 (least stable) < Form 4 < Form 2 < Form 1 (thermodynamic).

(a) (b)
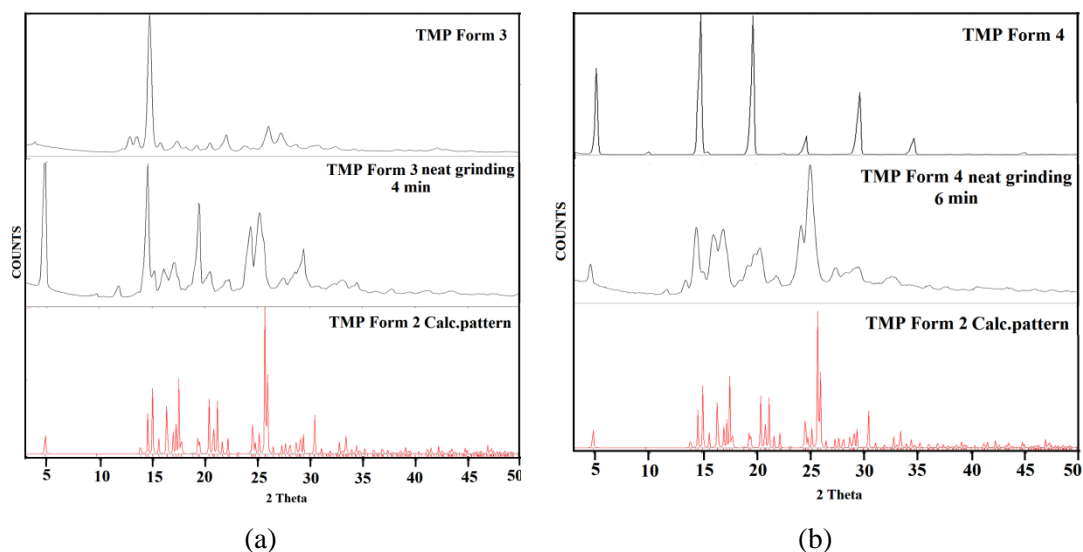
Figure 3.17 (a) Overlay of experimental PXRD pattern of TMP Form 3 (Top) with the experimental PXRD matching with Form 2 obtained after neat grinding of Form 3 for 4 min (middle). (b) Overlay of experimental PXRD pattern of TMP Form 4 (Top) with the experimental PXRD matching with Form 2 obtained after neat grinding of Form 4 for 6 min (middle). The calculated pattern of form 2 is shown for comparison (below).
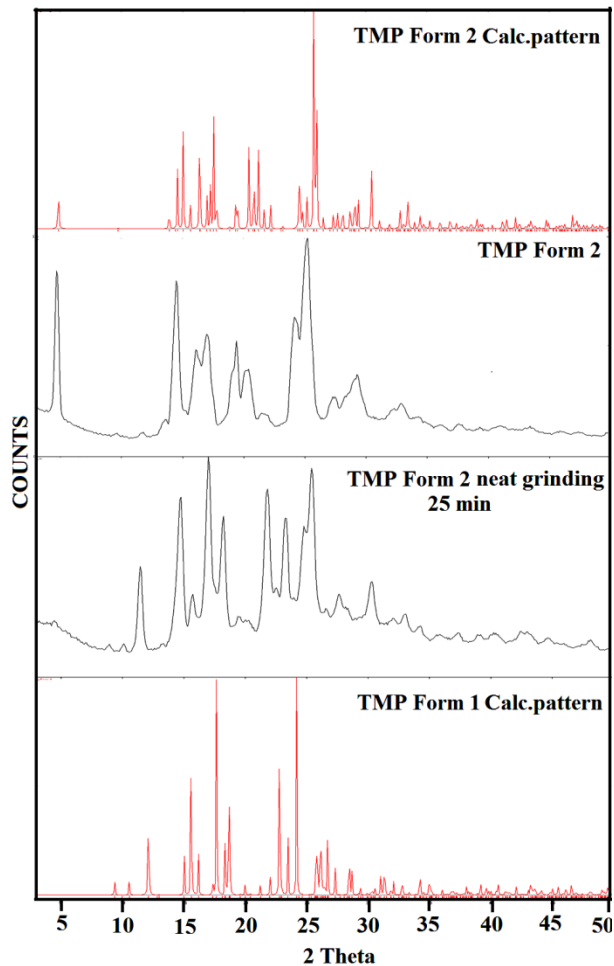
Figure 3.18 Overlay of calculated PXRD pattern of TMP Form 2 (top) with the experimental PXRD matching with Form 1 obtained after neat grinding of Form 2 for 25 min (3rd from top). The calculated patterns of Form 1 (bottom) and Form 2 (top) are shown for comparison.
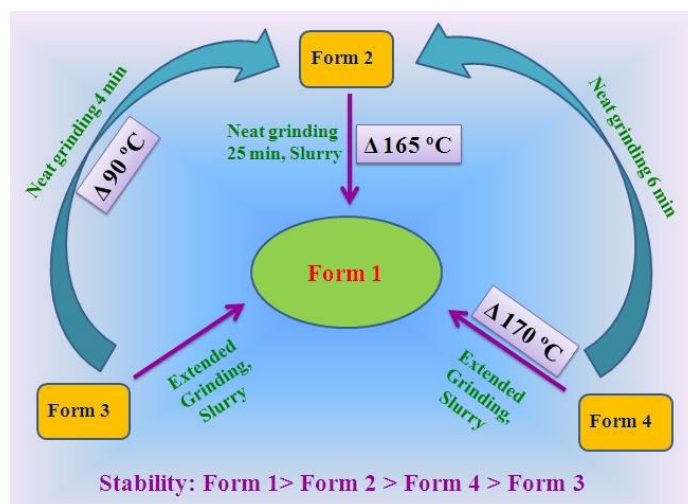
Figure 3.19 Schematic representations of TMP polymorphs to show the phase transformations.

3.3.8 Moisture Sorption Analysis and Form Stability

Water uptake by pharmaceutical samples as a function of change in humidity is measured by dynamic vapor sorption analysis. DVS is a gravimetric technique in which the sample is subjected to varying conditions of humidity and temperature, and measures how quickly and how much of water absorbed by the sample (and desorbed upon reducing humidity levels). DVS isotherms for all four polymorphs and TMP hemihydrate were studied at constant temperature (40 °C) and variable RH conditions (10-90-10% RH, Figure 3.20). TMP polymorphs and TMP hemihydrate are stable even at high RH conditions and there was no uptake of water (< 0.3 %) in the range from 10-90% RH adsorption cycle and reverse 90-10% RH in desorption cycle.

(a)

(b)

(c)

(d)

(e)
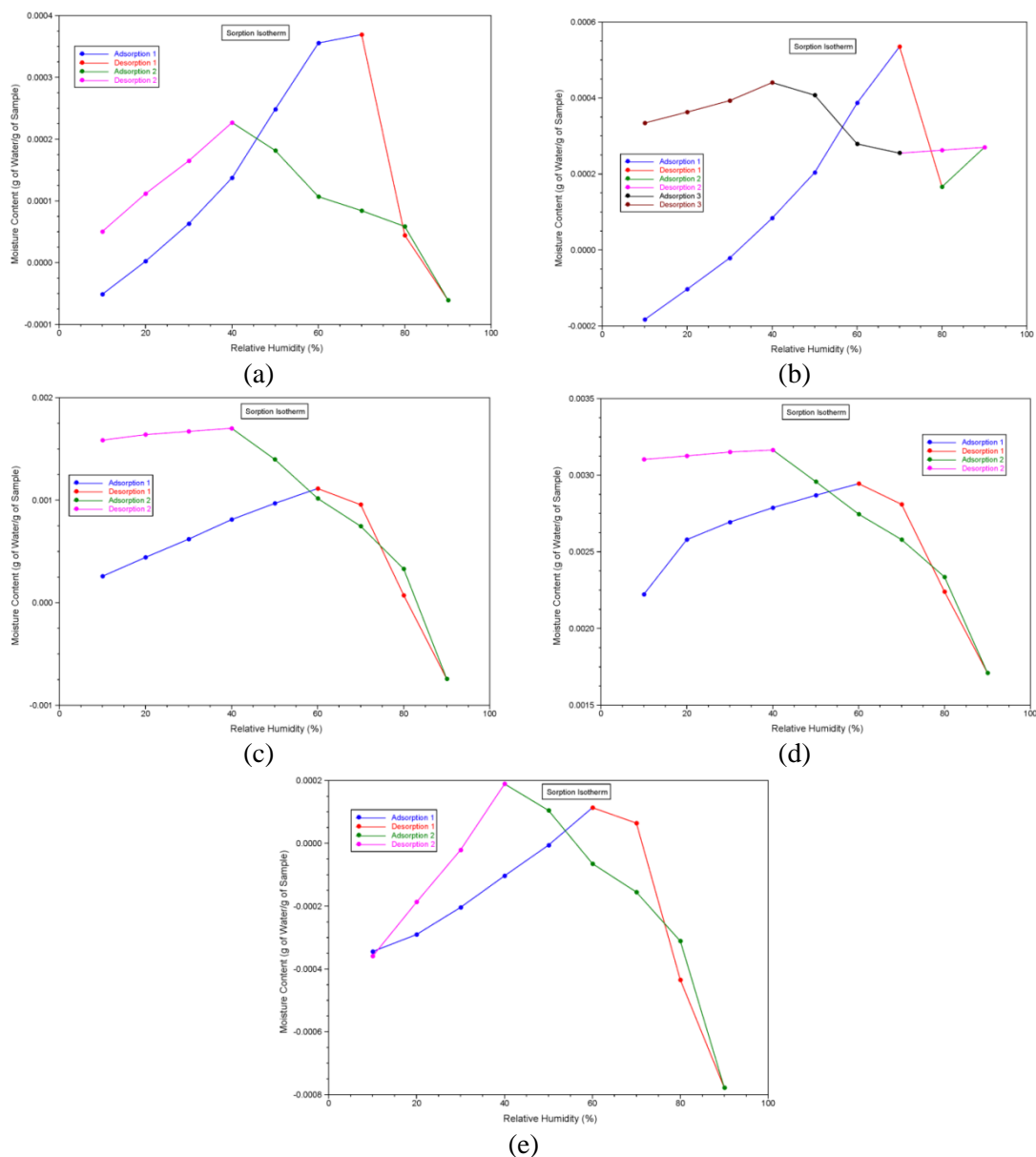
Figure 3.20 DVS isotherms of the TMP forms indicate stability towards moisture uptake and retention. (a) Form 1, (b) Form 2, (c) Form 3, (d) Form 4, (e) TMP hemihydrate.

All the forms of TMP were stable at ambient conditions of Hyderabad (35 °C, 40% RH) for more than six months except Form 3 which converted into Form 2 after one week. The stability of polymorphs is important study because phase transformations can change bioavailability and drug activity. For example, theophylline, phenobarbital, nitrofurantoin

and sulfathiazole polymorphs[32] are known to covert to their hydrate forms under high humidity conditions. At 40 °C and 75% RH ICH conditions,[33] polymorphs 1, 3 and 4 and TMP hydrate did not exhibit any form change or hydrate content changes in the test period of three months (see PXRD plots in Figures 3.21 to 3.24, and summary of results in Table 4).
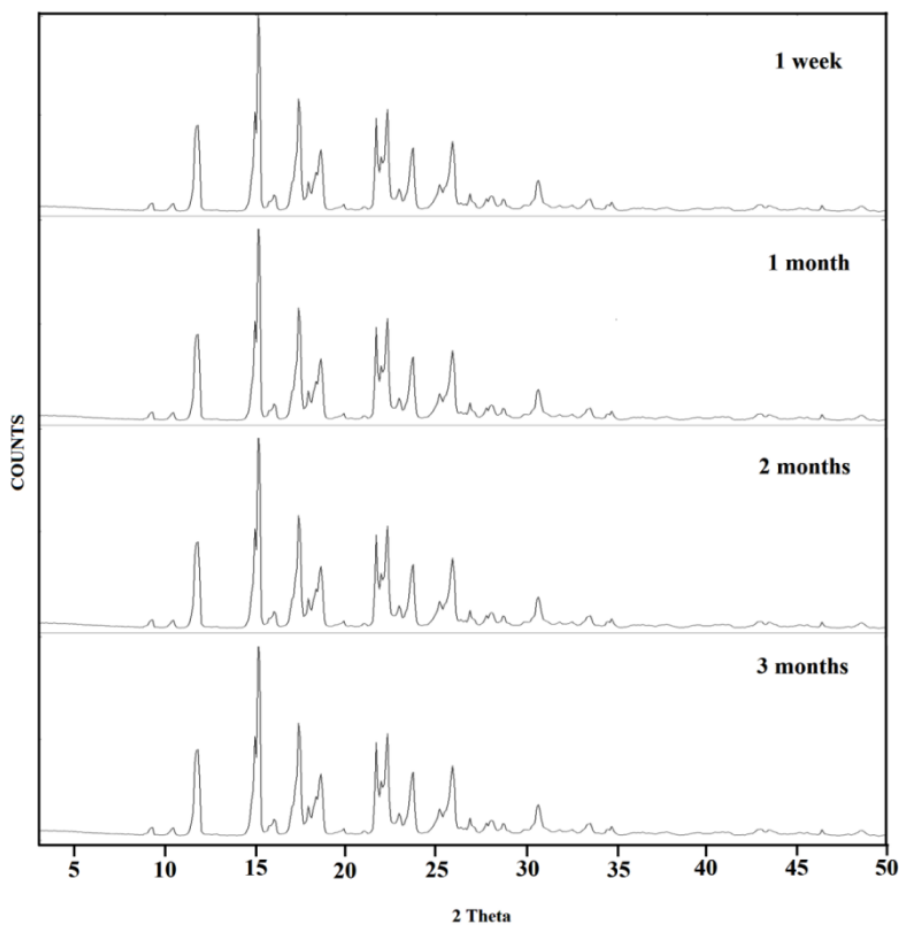
Figure 3.21 Overlay of PXRD patterns from the stability study of TMP Form 1 at 40 °C and 75% RH shows that no form change/hydrate formation up to 3 months.
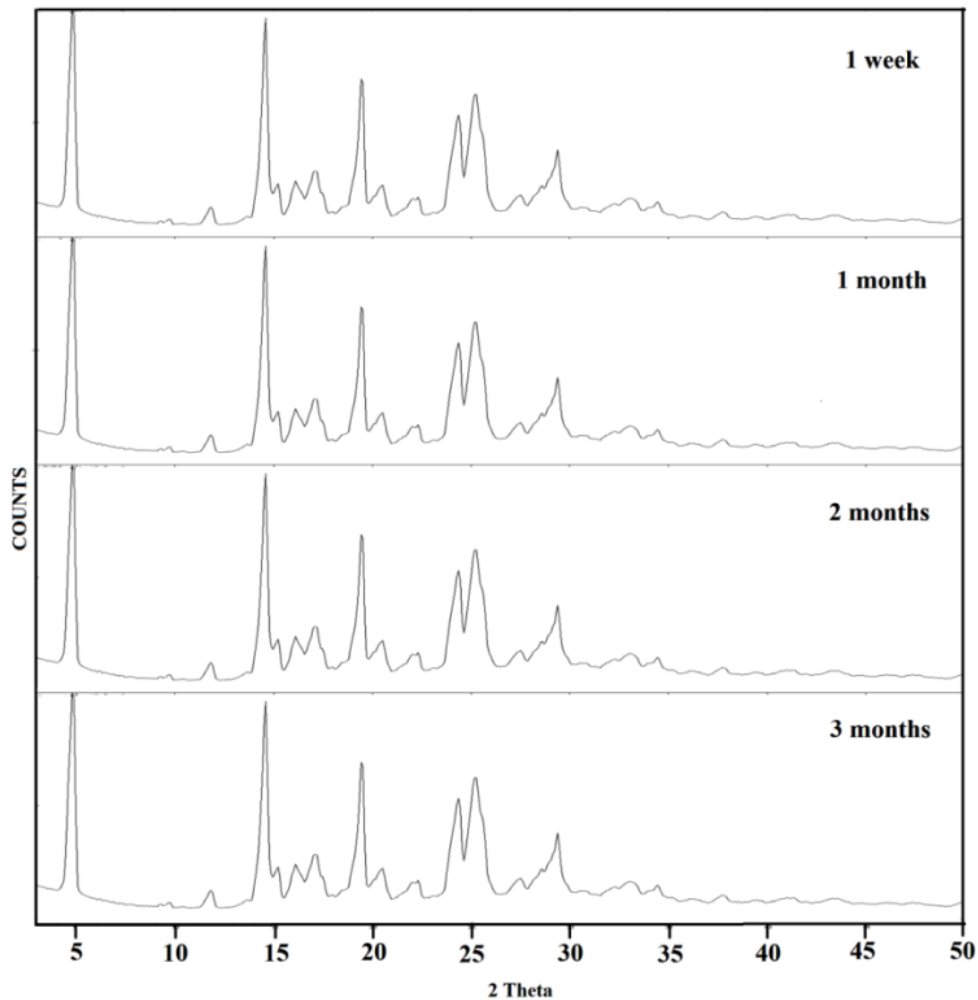
Figure 3.22 Overlay of PXRD patterns from the stability study of TMP Form 2 at 40 °C and 75% RH shows that no polymorphic transition/hydrate formation up to 3 months.
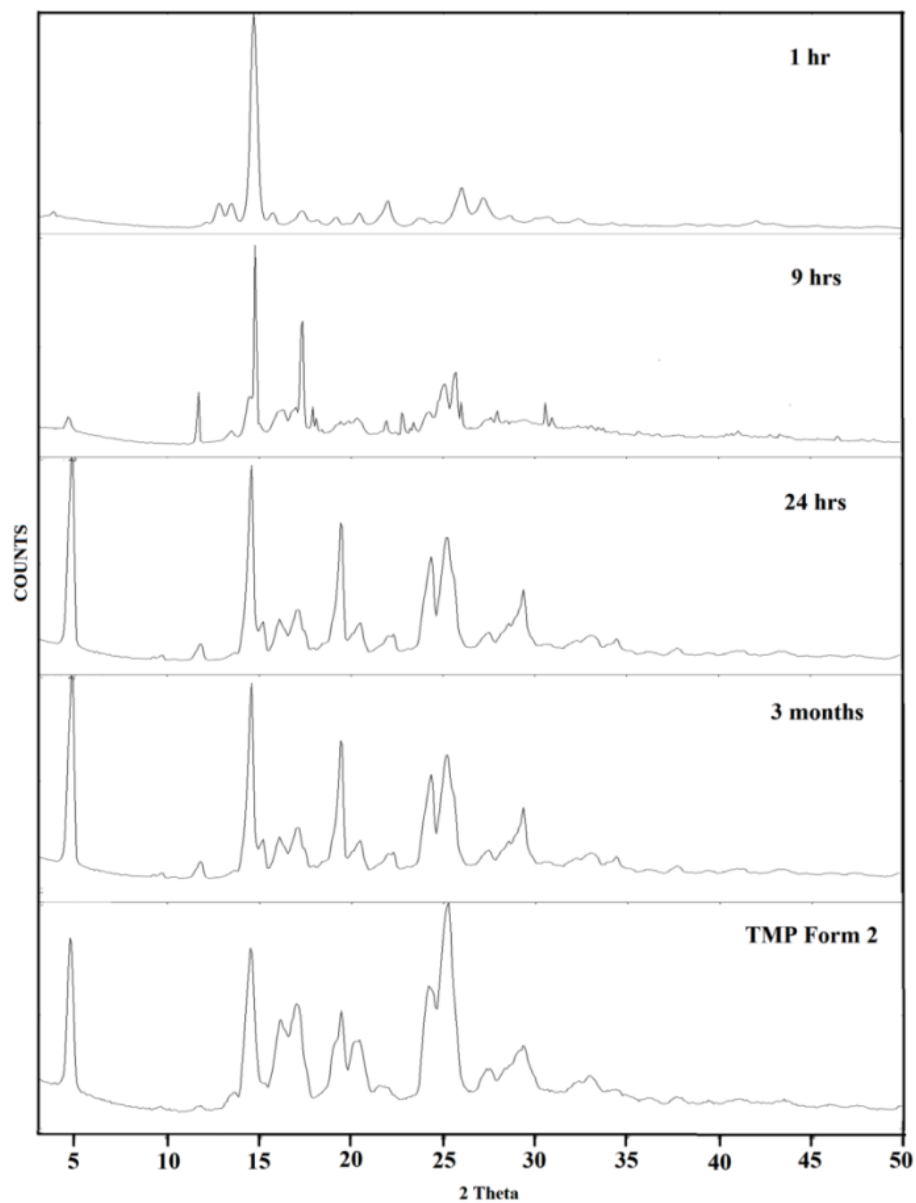
Figure 3.23 Overlay of PXRD pattern from the **s**tability study of TMP Form 3 at 40 °C and 75% RH shows that after 9 hrs Form 3 converted into Form 2.
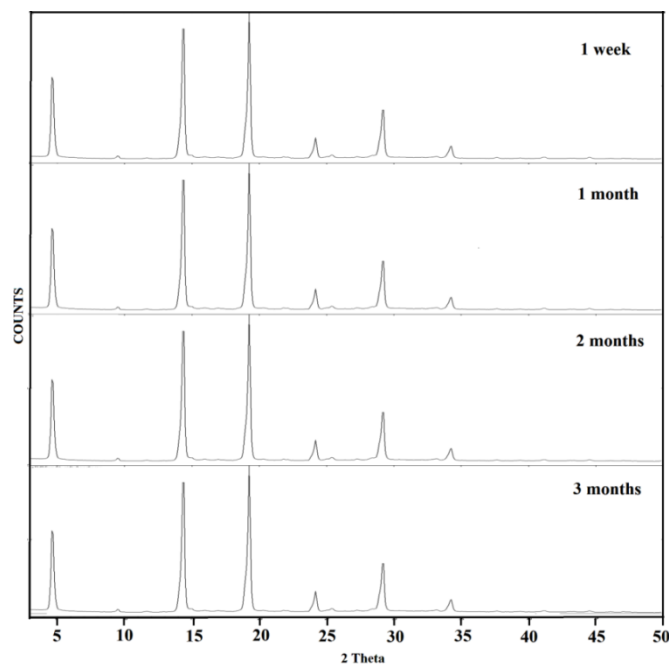
Figure 3.24 Overlay of PXRD patterns from the **s**tability study of TMP Form 4 at 40 °C and 75% RH shows that no form change/hydrate formation up to 3 months.

Table 3.6 Stability of TMP forms under ICH Conditions of 40 °C and 75% RH [a]

Compound	Time period			
TMP Form 1	√ 1W	√ 1M	√ 2M	√ 3M
TMP Form 2	√ 1W	√ 1M	√ 2M	√ 3M
TMP Form 3	√ 1H	× 9H	× 24 H	× 3M
TMP Form 4	√ 1W	√ 1M	√ 2M	√ 3M

[a] H= hour, W= week, M = month, √ = no phase change/no hydrate formation, × = phase change.

3.4 Conclusions

An exhaustive polymorphic screen of the well-known antibiotic drug Trimethoprim (TMP) resulted in four anhydrous polymorphs and a hemihydrate form. Conformational flexibility of TMP and strong hydrogen bonding ability of the amino-pyrimidine moiety of TMP promote different hydrogen bond synthons and result in polymorphs (Forms 1, 2, 3, and 4). All the polymorphic forms were reproduced by multiple crystallization methods, and spray

drying was useful to obtain the bulk material of Form 3 in pure state. The polymorphs were characterized by spectroscopic (FT-IR and Raman, ^{15}N ss-NMR), thermal (DSC, HSM), field emission scanning-electron microscopy (FESEM), and powder X-ray diffraction (PXRD). We were successful in getting difraction quality single X-ray crystal data for Form 1 and Form 2. Crystal structure analysis showed that both the structures are sustained by N–H⋯N$_{arom}$ hydrogen bonds and the main difference was R_2^2 (8) type I and type II motifs in Form 1, and R_2^2 (8) type III and R_3^2 (8) motifs in Form 2. Thus Form 1 and Form 2 may be classified as synthon and packing polymorphs. The major intermolecular interactions were quantified by Hirshfeld surface analysis the stability order was rationalized by the percentage of strong H bond contribution. Based on DSC thermogram, the relative thermodynamic relationships (enatiotropic or monotropic) of TMP polymorphic pairs were evaluated. DVS analysis revealed that all the TMP forms show negligible moisture uptake (< 0.3 %) even at high RH conditions. All the polymorphs were found to be stable for a test period of three months in accelerated ICH conditions of 40 ºC and 75% RH, except Form 3 which converted to Form 2. From slurry and grinding experiments Form 2, Form 3 and Form 4 found to be metastable and Form 1 is stable, and the stability order of the polymorphs follows the order Form 3 < Form 4 < Form 2 < Form 1 (most stable). Slurry, grinding, and thermal experiments confirm that TMP Form 1 is the most stable modification for drug formulation.

3.5 Experimental Section

Materials and Methods: TMP was purchased from Sigma-Aldrich and used without further purification. All other chemicals were of analytical or chromatographic grade. Water purified from a deionizer-cum-mixed-bed purification system (AquaDM, Bhanu, Hyderabad, India) was used in the experiments.

Preparation of TMP forms

TMP Form 1: The commercial material obtained from Sigma-Aldrich matches to Form 1 which was confirmed by PXRD and DSC. Upon freeze drying the commercial material in

Water, Water-MeOH solvents the resulting material matched to Form 1 by PXRD. Colorless single crystals suitable for X-ray diffraction were obtained upon dissolving 30 mg of TMP in 8 mL hot iso-propanol solvent and left for slow evaporation at ambient conditions. Colorless block crystals suitable for X-ray diffraction were obtained after 3-4 d upon solvent evaporation.

TMP Form 2: Form 2 was obtained in bulk upon dissolving 100 mg of TMP Form 1 in 50 ml of ethyl acetate and heated until the volume reduced to half to obtain saturated solution. To this saturated solution, 30 ml of heptane was added suddenly in hot condition there by precipitating out Form 2 in the solution. The precipitate was filtered and the formation of Form 2 was confirmed by FT-IR, FT-Raman, ss-NMR, PXRD and DSC. The bulk material of Form 2 can also be obtained by dehydration of TMP-hydrate in programmable oven at 90 °C for 30 min. Colorless single crystals were obtained upon dissolving 30 mg of TMP in 10 mL hot MeOH: Chlorobenzene (1:1 v/v) solvent mixture and left for slow evaporation at ambient conditions. Colorless plate crystals suitable for X-ray diffraction were obtained after 3-4 d upon solvent evaporation.

TMP Form 3

Procedure 1: Spray Dryer Model LU-222 advanced Spray Dryer (Lab Ultima, Mumbai, India) was used to obtain TMP Form 3. The experimental conditions and parameters used to deposit the fine Powder of Form 3 from MeOH solvent is listed in Table 3.7.

Table 3.7 Parameters used in the Spray drying experiment for MeOH solvent.

Parameters			
Inlet temperature	80 °C	Cycle time	120 min
Outlet temperature	120 °C	% of O2	5%
Inlet high temperature	140 °C	Log interval	60 Sec
Outlet high temperature	160 °C	Atomization pressure	0.82 Kg/cm^2
Cool temperature	60 °C	D.Bloc. On	1 Sec
Aspirator flow rate	65 Nm^3/hr	D.Bloc. On	60 Sec
Feed pump flow rate	2 mL/min		

Procedure 2: Form 3 was obtained in bulk upon dehydrating the TMP-hydrate over P_2O_5 under vacuum (0.1 mm), after six hours dehydration was complete and found that Form 3 was formed. This bulk material was confirmed as by FT-IR, FT-Raman, PXRD and DSC. Single crystals suitable for X-ray diffraction were not obtained even after number of crystallization experiments.

TMP Form 4: Form 4 was obtained in bulk upon dissolving 100 mg of TMP Form 1 in 50 mL of ethyl acetate and heated until the volume reduced to half to obtain saturated solution. To this saturated solution, 20 mL of heptane was added suddenly in hot condition there by precipitating out Form 4 in the solution. The precipitate was filtered and the formation of Form 4 was confirmed by FT-IR, FT-Raman, ss-NMR, PXRD and DSC. Even after number of crystallization experiments we were unsuccessful to obtain single crystals suitable for X-ray diffraction.

TMP hemihydrate: TMP hemihydrate was prepared by dissolving the 100 mg of the TMP in 10 mL of aqueous alkaline (NaOH) solution of pH 8.0-9.0 and heated until the clear solution was observed. The resultant solution was filtered through whatman filter paper in hot condition and immediately kept the solution in refrigerator (at 4-5 °C). After 20 min TMP hemihydrates was aggregated as white hair-like crystalline material in the solution which was filtered and dried at ambient conditions, and characterized by FT-IR, Raman, PXRD, DSC.

Vibrational spectroscopy: Thermo-Nicolet 6700 Fourier transform infrared spectrophotometer with NXR-Fourier transform Raman module (Thermo Scientific, Waltham, Massachusetts) was used to record IR and Raman spectra. IR spectra were recorded on samples dispersed in KBr pellets. Raman spectra were recorded on samples contained in standard NMR diameter tubes or on compressed samples contained in a gold-coated sample holder. Data was analyzed using the Omnic software (Thermo Scientific, Waltham, Massachusetts).

Solid-state NMR spectroscopy: Solution and solid state NMR spectra were recorded on a BrukerUltrashield 400 MHz spectrometer (BrukerBioSpin, Karlsruhe, Germany).

Approximately 100 mg of crystalline sample was packed into a zirconium rotor with a Kel-F cap. The crosspolarization, magic angle spinning (CP-MAS) pulse sequence was used for spectral acquisition. Solid-state ^{15}N cross-polarisation magic angle spinning (CP-MAS) spectra were recorded on a Bruker 4 mm double resonance CP-MAS probe in zirconia rotors at a frequency of 5.0 ± 0.01 kHz with a cross-polarization contact time of 2.5 ms and a recycle delay of 8 s. The ^{15}N CP-MAS spectra were calibrated relative to nitromethane using glycine ($\delta_{glycine} = -347.6$ ppm) as an external standard. Additionally the integrity of the forms were established through solution ^{1}H NMR.

Differential Scanning Calorimetry (DSC): DSC was performed on a Mettler Toledo DSC 822e module. Samples were placed in crimped but vented aluminium sample pans. The typical sample size is 3-5 mg, and the temperature range is 30-250 °C @ 5 °C min^{-1}. Samples were purged by a stream of dry nitrogen flowing at 80 mL min^{-1}.

Hot-Stage microscopy (HSM): HSM was performed on a Wagner & Munz PolythermA Hot Stage and Heiztisch microscope. A Moticam 1000 (1.3 MP) camera supported by software Motic Image Plus 2.0ML is used to record images.

Field Emission Scanning Electron Microscope (FESEM): The shape and morphology of the TMP forms were examined on a Carl Zeiss model Merlin Compact 6027 FESEM with a beam voltage of 3.0 kV. The sample was spread on a carbon-coated copper grid. Prior to FESEM imaging, an ultrathin layer of gold was coated in order to enhance the conductivity of the sample.

Dynamic Vapor Sorption (DVS): Dynamic vapor sorption (DVS) was used to obtain sorption–desorption kinetic data of TMP Forms. DVS measurements were performed using a Q5000SA vapor sorption analyzer (TA Instruments, Delaware, USA) at 40°C. About 4-10 mg of the sample was placed in a metalized quartz sample pan and subjected to relative humidity flux from 10% RH to 90% RH and back to 10% RH with a step size of 10% change in humidity. A dwell time of 60 min was set for a weight change of >0.1% in the adsorption/desorption phase at a particular RH (5 min dwell time for a weight change of <0.1%). Thus, if the weight loss/gain is >0.1% at a particular RH, the instrument maintains

the same RH for 60 min and then automatically sets at the next higher/lower value. If the weight gain/loss is <0.1%, the DVS cycle (10%−90%−10%) will be completed within 2 hours, otherwise it will take a longer duration.

X-ray crystallography: X-ray reflections for TMP-Form-I and TMP-form-II were collected at 100 K on Bruker SMART-APEX CCD diffractometer equipped with a graphite monochromator and Mo-Kα fine-focus sealed tube (λ = 0.71073 Å). Data reduction was performed using Bruker SAINT Software.[34] Intensities were corrected for absorption using SADABS,[35] and the structure was solved and refined using SHELX-97.[36] All non-hydrogen atoms were refined anisotropically. Hydrogen atoms on heteroatoms were located from difference electron density maps and all C−H hydrogens were fixed geometrically. Hydrogen bond geometries were determined in Platon.[37] X-Seed[38] was used to prepare packing diagrams.

Powder X-ray diffraction: Powder X-ray diffraction of all the samples were recorded on Bruker D8 Advance diffractometer (Bruker-AXS, Karlsruhe, Germany) using Cu-Kα X-radiation (λ= 1.5406 Å) at 40 kV and 30 mA power. X-ray diffraction patterns were collected over the 2θrange 5-50° at a scan rate of 1º min^{-1}. Powder Cell 2.4[39] (Federal Institute of Materials Research and Testing, Berlin, Germany) was used for Rietveld refinement of experimental PXRD and calculated lines from the X-ray crystal structure.

3.6 References

1. (a) S. L. Morissette, Ö. Almarsson, M. L. Peterson, J. F. Remenar, M. J. Read, A. V. Lemmo, S. Ellis, M. J. Cima, C. R. Gardner, *Adv. Drug Delivery Rev.* 2002, **56**, 275. (b) M. Müller, U. Meier, D. Wieckhusen, R. Beck, S. Pfeffer-Hennig, R. Schneeberger, *Cryst. Growth Des.* 2006, **6**, 946. (c) S. M. Reutzel-Edens, *Curr. Opin. Drug Discov. Dev.* 2006, **9**, 806. (d) N. J. Babu, A. Nangia, *Cryst. Growth Des.* 2011, **11**, 2662.

2. (a) J. Bernstein, *Polymorphism in Molecular Crystals*, Clarendon: Oxford, 2002. (b) S. L. Morissette, S. Soukasene, D. Levinson, M. J. Cima, Ö. Almarsson, *Proc. Natl. Acad. Sci. U. S. A.* 2003, **100**, 2180. (c) S. Byrn, R. Pfeiffer, M. Ganey, C. Hoiberg,

G. Poochikian, *Pharm. Res*. 1995, **12**, 945. (d) A. V. Trask, *Mol. Pharmaceutics* 2007, **4**, 301.

3. (a) L. F. Huang, W. Q. T. Tong, *Adv. Drug Delivery Rev.* 2004, **56**, 321. (b) T. L. Threlfall, *Analyst* 1995, **120**, 2435.

4. (a) J. Bernstein *Polymorphism in Molecular Crystals*, New York: Oxford University Press, 2008. (b) S. Datta, D. J. W. Grant, *Nat. Rev. Drug Discov.* 2004, 3, 42. (c) J. Bauer, S. Spanton, R. Henry, J. Quick, W. Dziki, W. Porter, K. Morris, *Pharm. Res*. 2001, **18**, 859.

5. (a) W. C. McCrone, in *Physics and Chemistry of the Organic Solid State*, Vol. *2*, eds. D. Fox, M. M. Labes and A. Weissberger, Wiley Interscience, New York, 1965, 725.

6. (a) P. Vishweshwar, J. A. McMahon, M. Oliveira, M. L. Peterson, M. J. Zaworotko, *J. Am. Chem. Soc.* 2005, 127, 16802. (b) C. Ouvrard, S. L. Price, *Cryst. Growth Des.* 2004, **4**, 1119.

7. P. Sanphui, N. R. Goud, U. B. R. Khandavilli, S. Bhanoth, A. Nangia, *Chem. Commun*. 2011, **47**, 5013.

8. (a) E. Dudognon, F. Danède, M. Descamps, N. T. Correia, *Pharm. Res.* 2008, **25**, 2853. (b) P. A. Williams, C. E. Hughes, K. D. M. Harris, *Cryst. Growth Des.* 2012**, 12**, 5839.

9. (a) G. H. Hitching, L. F. Kuyper, D. P. Baccananari, *Design of Enzyme Inhibitors as Drugs*, M. Sandler, and H. J. Smith, Eds.; New York: Oxford University Press, 1988. (b) J. Feeney, *Angew. Chem. Int. Ed.* 2000*,* **39***,* 291. (c) G. H. Hitchings, S. L. Smith, *Advances in Enzyme Regulation*, 1980, **18**, 347. (d) G. H. Hitchings, *Postgraduate Medical Journal* 1969, **45,** 7.

10. (a) R. N. Brogden, A. A. Carmine, R. C. Heel, T. M. Speight, G. S. Avery, *Drugs* 1982, **23**, 405. (b) B. Roth, C. C. Cheng, *Prog. Med. Chem.* 1982, **19***,* 269.

11. WHO *Model List of Essential Medicines*, October 2013. http://www.who.int/medicines/publications/essentialmedicines/en/

12. (a) S. R. M. Bushby, G. H. Hitchings, *Br. J. Pharmacol.* 1968, **33**, 72. (b) P. Huovinen, L. Sundström, G. Swedberg, O. Sköld, *Antimicrob. Agents*

Chemother. 1995, **39**, 279. (c) P. B. Ward, M. Carson, J. S. Dodd, E. R. *J.* Pavillard, *Clin. Microbiol.* 1984, **19**, 899.

13. (a) D. C. Bean, D. M. Livermore, I. Papa, L. M. Hall, *J. Antimicrob. Chemother.* 2005, **56**, 962. (b) D. Felmingham, R. R. Reinert, Y. Hirakata, A. Rodloff, *J. Antimicrob. Chemother.* 2002, **50**, 25. (c) J. R. Johnson, A. R. Manges, T. T. O'Bryan, L. W. Riley, *The Lancet* 2002, **359**, 2249. (d) R. A. Lawrenson, J. W. Logie, *J. Antimicrob. Chemother.* 2001, **48**, 895.

14. Anonymous, *Drug Ther. Bull.* 1995, **33**, 92.

15. (a) R. Dahlan, C. McDonald, V.B. Sunderland, *J. Pharm. Pharmacol.* 1978, **39**, 246. (b) M. Lindenberg, S. Kopp, J. B. Dressman, *Eur. J. Pharm. Biopharm.* 2004, **58**, 265–278.

16. (a) B. Umadevi, P. Prabakaran, P. T. Muthiah, *Acta Crystallogr.* 2002, **C58**, o510. (b) S. Murugesan, P. T. Muthiah, *Acta Crystallogr.* 1997, **C53**, 763. (c) P. T. Muthiah, B. Umadevi, N. Stanley, G. Bocelli, A. Cantoni, *Acta Crystallogr.* 2002, **E58**, o59. (d) R. F. Bryan, R. C. Haltiwanger, M. K. Woode, *Acta Crystallogr.* 1987, **C43**, 2412. (e) G. Giuseppetti, C. Tadini, G. P. Bettinetti, F. Giordano, A. La Manna, *Acta Crystallogr.* 1984, **C40**, 650. (f) J. J. Robert, S. Baskar Raj, P. T. Muthiah, *Acta Crystallogr.* 2001, **E57**, o1206. (g) S. Francis, P. T. Muthiah, G. Bocelli, L. Righi, *Acta Crystallogr.* 2002, **E58**, o717. (h) P. Prabakaran, J. J. Robert, P. T. Muthiah, G. Bocelli, L. Righi, *Acta Crystallogr.* 2001, **C57**, 459. (i) S. B. Raj, N. Stanley, P. T. Muthiah, G. Bocelli, R. Olla, A. Cantoni, *Cryst. Growth Des.* 2003, **3**, 567. (j) H. Nakai, M. Takasuka, M. Shiro, *J. Chem. Soc., Perkin Trans. II* 1984, **9**, 1459.

17. (a) S. B. Raj, P. T. Muthiah, U. Rychlewska, B. Warzajtis, *CrystEngComm*, 2003, **5**, 48. (b) S. Murugesan, P. T. Muthiah, *Academy Discussion Meeting on Frontiers in Structural Chemistry*, IIT Madras, Chennai, India, Abstract No. 3.4, 1996. (c) P. T. Muthiah, B. Umadevi, N. Stanley, X. Shui, D. S. Eggleston, *Acta Crystallogr.* 2001, **E57**, o1179. (d) P. Panneerselvam, N. Stanley, P. T. Muthiah, *Acta Crystallogr.* 2002, **E58**, o180.

18. (a) T. F. Koetzle, G. J. B. Williams, *J. Am. Chem. Soc.* 1976, **98**, 2074. (b) Rauf, K.; Bolte, M. *Private Communication* 2006.

19. G. P. Bettinetti, F. Giordano, A. La Manna, G. Giuseppetti, *Boll. Chim. Farm.* 1978, **117**, 522.

20. Cambridge Structural Database, ver. 5.35. ConQuest 1.16, November 2013 release, May 2014 update, CCDC, www.ccdc.cam.ac.uk.

21. (a) R. D. B. Walsh, M. W. Bradner, S. Fleischman, L. A. Morales, B. Moulton, N. Rodriguez-Hornedo, M. J. Zaworotko, *Chem. Commun.* 2003, **2**, 186. (b) G. R. Desiraju, *Angew. Chem., Int. Ed. Engl.* 1995, **34**, 2311. (c) M. C. Etter, *Acc. Chem. Res.* 1990, **23**, 120. (d) J. Bernstein, R. E. Davis, L. Shimoni, N. L. Chang, *Angew. Chem., Int. Ed. Engl.* 1995, **34**, 1555.

22. (a) R. M. Silverstein*Spectrometric Identification of Organic Compounds*, 6th Ed.; John Wiley & Sons, Inc.: New York, 2002. (b) E. Smith, G. Dent, *Modern Raman Spectroscopy, A Practical Approach*, John Wiley: New York, 2005. (c) D. E. Bugay, H. G. Brittain, *Raman Spectroscopy, in Spectroscopy of Pharmaceutical Solids*, New York: Taylor and Francis, 2006, 271.

23. (a) R. K. Harris, *J. Pharm. Pharmacol.* 2007, **59**, 225. (b) F. G. Vogt, J. S.VClawson, M. Strohmeier, A. J. Edwards, T. N. Pham, S. A. Watson, *Cryst. Growth Des.* 2008, **9**, 921. (c) A. E. Aliev, K. D. Harris, *Supramolecular Assembly via Hydrogen Bonds I,* 2004, 1, (d) A. W Newman, S. L. Childs, B. A. Cowans, Salt Cocrystal Form Selection, In *Preclinical Development Handbook*, John-Wiley, Hoboken, 2008, 455.

24. (a) H. B. Brittain, *Am. Pharm. Rev.* 2002, **5**, 74. (b) G. P. Stahly, *Cryst. Growth Des.* 2007, **7**, 1007.

25. (a) J. L. Ford, P. Timmins, *Pharmaceutical Thermal Analysis*, Techniques and Applications. New York: Horwood, E.; Chichester, 1989. (b) H. G. Brittain, *Polymorphism in Pharmaceutical Solids*, Marcel Dekker, New York, 1999.

26. G. P. Bettinetti, F. Giordano, P. Ferloni, *Farmaco Ed. Sc.* 1980, **35**, 706.

27. (a) M. A. Spackman, D. Jayatilaka, *CrystEngComm* 2009, **11**, 19. (b) J. J. McKinnon, D. Jayatilaka, M. A. Spackman, *Chem. Commun.* 2007, 3814. (c) J. Bernstein, *Cryst. Growth Des.* 2011, **11**, 632. (d) F. P. A. Fabbiani, L. T. Byrne, J. J. McKinnon, M. A. Spackman, *CrystEngComm* 2007, **9**, 728.

28. (a) M. Otsuka, K. Otsuka, N. Kaneniwa, *Drug Dev. Ind. Pharm*. 1994, **20**, 1649. (b) A. Bauer-Brandl, *Int. J. Pharm.* 1996, **140**, 195. (c) G. G. Zhang, C. Gu, M. T. Zell, R. T. Burkhardt, E. J. Munson, D. J. Grant, *J. Pharm. Sci.* 2002, **91**, 1089.

29. W. Ostwald, *Z. Phys. Chem.* 1987, **22**, 289.

30. A. Burger, R. Ramberger, *Microchim. Acta II* 1979, 273.

31. J. Bauer, S. Spanten, R. Henry, J. Quick, W. Dziki, W. Porter, J. Morris, *Pharm. Res*. 2001, **18**, 859. (b) J. M. Robertson, A. R. Ubbelohde, *Proc. Royal Soc. London* 1938, **A167**, 122. (c) Y. V. Nelyubina, I. V. Glukhov, M. Y. Antipin, K. A. Lyssenko, *Chem. Commun.* 2010, **46**, 3469.

32. (a) N. V. Phadnis, R. Suryanarayanan, *J. Pharm. Sci*. 1997, **86**, 1256. (b) M. Otsuka, R. Teraoka, Y. Matsuda, *Pharm. Res.* 1991, **8**, 1066. (c) Y. Hu, A. Erxleben, B. K. Hodnett, B. Li, P. McArdle, Å. C. Rasmuson, A. G. Ryder, *Cryst. Growth Des.* 2013, **13**, 3404. (d) M. Otsuka, M. Onoe, Y. Matsuda, *Pharm. Res.* 1993*, **10**, 577.

33. http://www.ich.org/fileadmin/Public_Web_Site/ICH_Products/Guidelines/Quality/Q 1F/Stability_Guideline_WHO.pdf (accessed 31 July, 2014).

34. *SAINT-Plus*, version 6.45, Bruker AXS Inc.: Madison, Wisconsin, U.S.A., 2003.

35. SADABS, *Program for Empirical Absorption Correction of Area Detector Data,* Sheldrick, G. M. University of Göttingen, Göttingen, Germany, 1997.

36. (a) *SMART*, version 5.625 and *SHELX-TL*, version 6.12; Bruker AXS Inc.: Madison, Wisconsin, USA, 2000. (b) G. M. Sheldrick, *SHELXS-97* and *SHELXL-97*, University of Göttingen, Göttingen, Germany, 1997.

37. A. L. Spek, *PLATON, A Multipurpose Crystallographic Tool*, Utrecht University: Utrecht, Netherlands, 2002.

38. L. J. Barbour, *X-Seed*, *Graphical Interface to SHELX-97 and POV-Ray*, *Program for Better Quality of Crystallographic Figures*; University of Missouri-Columbia, Missouri, U.S.A., 1999.

39. Powder Cell, A Program for Structure Visualization, Powder Pattern Calculation and Profile Fitting, http://www.ccp14.ac.uk/index.html, 2013.

CHAPTER FOUR

HIGH SOLUBILITY CRYSTALLINE PHARMACEUTICAL FORMS OF BLONANSERIN
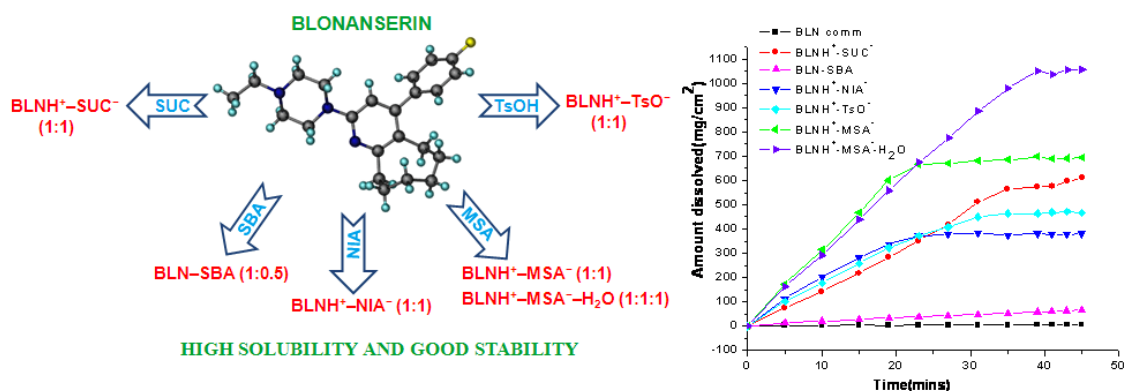
Novel crystalline forms of the antipsychotic drug Blonanserin (BLN) were prepared with GRAS coformers. The crystal structures of the salts were stabilized by N^+–$H\cdots O^-$ ionic H-bond. $BLNH^+$–MSA^-–H_2O salt hydrate exhibited the highest solubility (464 times) and dissolution rate (126 times) in 60% EtOH−water medium compared to the reference drug and showed stability for 2 months at 40 °C, 75% RH.

4.1 Introduction

Active pharmaceutical ingredients (APIs) are generally administered in solid oral dosage formulations (e.g., tablets, capsules, etc.) for drug product convenience and patient compliance. Understanding and controlling the solid-state properties of APIs as pure drug substances and in formulated products is therefore an important goal in drug development. There is an increased interest in different solid-state forms of APIs, such as polymorphs,[1] hydrates/solvates,[2] salts,[3] cocrystals,[4] solid dispersions,[5] etc. notably in the last two decades. Drug molecules with limited aqueous solubility are becoming increasingly prevalent in the research and development portfolios. This may be due to recent introduction of combinatorial chemistry and high-throughput screening in identifying new chemical entities (NCE)[6] the solubility of new drug molecules has decreased sharply.[7] While a value of less than 20 μg/mL for the solubility of a NCE were practically unheard until 1980s, the situation has been changed so much that in the present day drug candidates with solubilities less than 1 μg/mL are very common.[8] This kind of molecules provide number of challenges in pharmaceutical development and may potentially lead to slow dissolution in biological fluids, insufficient and inconsistent systemic exposure and consequent sub-optimal efficacy in patients, particularly when delivered via the oral route of administration. Advances in the pharmaceutical sciences have led to the establishment of a number of approaches for addressing the issues of low aqueous solubility. The strategies for improving solubility include micronisation,[9a] nanosizing,[9b] solubilisation of drugs in co-solvents,[9c] micellar solutions,[9d] complexation with cyclodextrins[9e] and salt formation,[3] etc. Out of all, salt formation was found to be simplest, most cost effective strategy to address poor aqueous solubility and enhance bioavailability for ionizable drugs. Over 50% of APIs are marketed as salts. It is generally accepted that the reaction of an acid with a base will form a salt when $\Delta pK_a > 3$ ($\Delta pK_a = pK_a$ (conjugate acid of base) $- pK_a$ (acid)) and a cocrystal if $\Delta pK_a < 0$.[10a] The region of ΔpK_a 0–3 is a salt–cocrystal continuum zone for APIs.[10b]

The drugs with poor aqueous solubility especially those of BCS Class II cause biopharmaceutical and pharmacokinetic hurdles in developing successful oral drug delivery of these drugs.[11] Recently, it has been reported that approximately 45% of the top 200

marketed oral drug products running in the US, Britain, Spain and Japan are poorly water soluble.[12] This emphasizes the requirement of new water soluble and stable APIs and better formulation strategies for existing drug molecules. Improvement in solubility/dissolution rate of weakly acidic or basic drugs which are poorly soluble is one of the primary reasons for preparation of salts because, salts can improve solubility about 100-1000 fold or even 2000 fold. For example, recently Stephenson et al. reported[13] that the increment in solubility of anti-HIV drug delavirdine by forming delveridine mesylate was about 2000 fold (solubility of free base 143 μg/ml vs salt 320 mg/ml). Salt formation technique is not only used to improve solubility but also sometimes used to slow-release oral dosage forms for certain pharmaceutical uses, such as inhalation products, parenteral depot systems, etc. For instance, Jashnani et al. reported[14] that albuterol stearate salt found to be dissolved much more slowly than the free base and other salt forms, with potential application in extending the duration of drug in lungs following aerosol delivery. Tableting properties also can be improved by salts for example, Sun et al. has reported[15] the superior compaction properties of Acetaminophen by making a hydrochloride salt hydrate (A.HCl) for acetaminophen which has extremely poor tableting properties. Other applications include such as photochemical stability for instance hydrochloride salt of the GG818 showed much improved light stability compared to the free base.[16] The crystal lattice of the hydrochloride salt may either be less accessible to light compared to that of the free base or have different ''microenvironments'' in the crystal lattice and hence, have differing photochemical stability. Looking forward into the future, salt formation will remain the primary approach to improve solubility and dissolution rate of poorly water-soluble acidic and basic drugs. However, as the potential drug candidates are becoming extremely water-insoluble, it might not be possible in many cases to form optimal salts. Hence, solid form discovery and selection of the best oral dosage form is a topical theme in crystal engineering and pharmaceutical development.[17]

4.2 Literature reports on Blonanserin

Blonanserin (BLN) is a novel antipsychotic agent, having dopamine D2 and serotonin 5-HT2A receptor antagonist properties.[18] It belongs to the series of 4-phenyl-2-(1-piperazinyl) pyridines, a second-generation antipsychotic agent similar to risperidone and olanzapine. Schizophrenia is a heterogeneous devastating psychiatric disorder characterized by positive, negative, affective, and cognitive symptoms. It generally occurs in late adolescence or early adulthood and is associated with an increased risk of mortality and social or occupational dysfunction.[19] The development of effective pharmacotherapy began with the development of chlorpromazine in 1952,[20] which revolutionized the treatment of schizophrenia. Older agents such as haloperidol and chlorpromazine (first-generation antipsychotics; FGAs) are quite effective for managing the positive symptoms of schizophrenia but generally display relatively poor long-term efficacy for negative symptoms, mood disturbances, and cognitive deficits. BLN overcomes this drawback in the treatment of both positive and negative symptoms of schizophrenia without extra-pyramidal symptoms.[21] It is marketed under the brand name Lonasen® in Japan and Korea, and is currently under clinical investigation in Phase III trials in China.[22] BLN is a basic drug molecule in Biopharmaceutics Classification System (BCS) under the category II (low solubility, high permeability) with aqueous solubility of 0.033 mg/L.[23] BLN form B was reported in CN101747272 (A)[24] and a few organic and inorganic salts were mentioned in a US patent.[25] Our literature survey suggested an opportunity to improve the solubility and dissolution of BLN by making salts and cocrystals of the drug.

4.3 Design and Preparation of Blonanserin Solid Forms

From the above back ground we planned a systematic crystal engineering of BLN to improve its solubility for better drug formulation. Solubility enhancement of certain drug molecules through amorphous and metastable crystalline forms[26] were documented, however uncertainty about accidental phase transformation to the stable crystalline modification during dissolution or upon storage makes this strategy less attractive for formulation development. Hence, we aimed to address the poor solubility of BLN through salts/cocrystals. Cocrystals are relatively new and currently popular supramolecular

approach to tune the solubility and pharmacokinetic properties of drug substances, and salt formation, a well know strategy for solubility enhancement. The major functional groups of BLN are piperazine moiety and pyridine N, hence our idea was to use these functional groups to result novel solid forms with various salt formers/coformers, resulting in enhancement of solubility of the parent drug molecule without compromising the stability. The drug was subjected to various solid form screening techniques with several generally regarded as safe (GRAS) molecules for salt and cocrystal forms. In this process we synthesized novel salts of BLN with succinic acid (SUC), nicotinic acid (NIA), methanesulfonic acid (MSA), toluenesulfonic acid (TsOH), and a salt hydrate with methanesulfonic acid (MSA), and cocrystal with suberic acid (SBA) (Scheme 4.1). These solid forms were characterized by X-ray diffraction, spectroscopic, and thermal techniques, and all the forms exhibited good stability in accelerated ICH conditions of 75% RH at 40 °C, except $BLN^+–MSA^-$ anhydrate. All the solid forms exhibited higher solubility and dissolution rate compared to the parent drug.
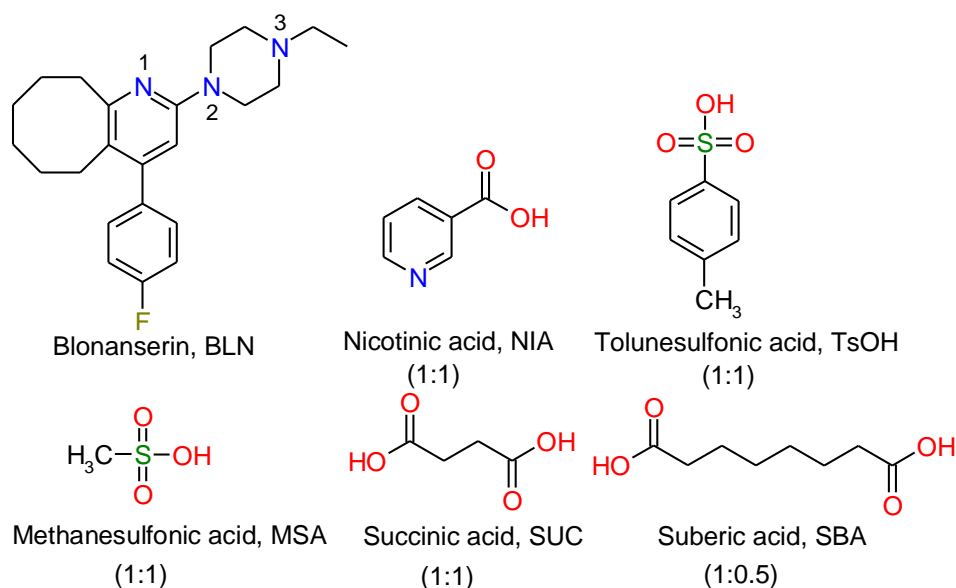
Scheme 4.1 Chemical structures of Blonanserin and coformers used in this study. The stoichiometry of API:coformer ratio is mentioned in brackets.

4.4 Results and Discussion

Salts and cocrystals of BLN (molecular structures are shown in Scheme 1) were prepared by different methods, such as reaction of BLN base with stoichiometric amounts of an acid in a suitable solvent, cogrinding,[27] rotavaporization,[28] solution crystallization, etc. (see Experimental Section for details). BLN is a weak base (pK_a 7–8) and so salt formation was expected only with strong acids.[10a] The calculated ΔpK_a values (in Marvin pK_a calculator)[29] between the piperazine basic moiety of BLN and the carboxylic/sulfonic acid coformer (pK_a1) suggested salt formation. All the crystalline forms are consistent with the ΔpK_a rule[10a] except for BLN–SBA which formed a cocrystal, perhaps due to the "fatty acid" lipophilic nature of the acid (Table 4.1). The ionic state in the salt structures was confirmed by single crystal X-ray diffraction and that of BLN–SBA as a neutral cocrystal. The exception of BLN–SBA to the "rule of 3" (ΔpK_a 3.82) is within the limits recently revised for cocrystals as < -1, salts > 4, and -1 to 4 for cocrystal−salt states.[10b, 30] The products were characterized as salts for succinic acid ($BLNH^+–SUC^-$), nicotinic acid ($BLNH^+–NIA^-$), toluenesulfonic acid ($BLNH^+–TsO^-$), and methanesulfonic acid ($BLNH^+–MSA^-$ and $BLNH^+–MSA^-–H_2O$ salt hydrate), and a cocrystal with suberic acid (BLN–SBA). All the new solid forms were fully characterized by spectroscopic (FT-IR, FT-Raman, ss-NMR), thermal (DSC), and X-ray diffraction techniques, and their solubility was measured in 60% EtOH−water medium, and stability was assessed in accelerated conditions.

Table 4.1 pK_a values of coformers resulting in salts/ cocrystal of BLN.[a]

	pK_a/ pK_b	ΔpK_a	Cocrystal/salt
BLN	7.97	--	--
SUC	3.55	4.42	1:1 salt
SBA	4.15	3.82	1:0.5 cocrystal
NIA	2.79	5.18	1:1 salt
TsOH	−2.14	10.11	1:1 salt
MSA	−1.61	9.58	1:1 salt
MSA	−1.61	9.58	1:1:1 salt hydrate

[a] pK_a's were calculated using Marvin 5.10.1, 2012, ChemAxon (http://www.chemaxon.com).

Upon CSD search on C-COOH and N(tertiary amine) fragments with 3D coordinates determined, no disorder, and organic structures only gave 1898 hits, out of which the below mentioned 40 Refcodes contain a neutral COOH⋯N$_{(tertiary\ amine)}$ synthon (Table 4.2). Crystallographic data on the new X-ray crystal structures and hydrogen bonding are listed in Table 4.3 and Table 4.4.

Table 4.2 List of Refcodes in which COOH⋯N$_{(tertiary\ amine)}$ synthon is present (ver. 5.36, November 2014 update).

AYUCED	HEPXOP	IPEVOP	MIPVIQ	UNEFUO
CELVEV	ICOQIB	IPEVUV	NAZWIV	UNEGAV
CUWZAW	IDUTUX	IPEWEG	PECDIM	UNEGEZ
DOTFEX	IJETOG	IPEWIK	RASYEP	VIJTIR
EGUVAE	IJETOG02	IZAXIQ	SEGHUI	WEGTAF
EKECOM	IJOYAI	KAQGAM	SOBPUV	WOCRIP
FEQXIJ	IPEVEF	LEDYUQ	TACDEI	YAGPUT
GOTSOX	IPEVIJ	LOKRAE	UNEFEY	YEJKON

4.4.1 Crystal Structure Description

BLNH$^+$–SUC$^−$ salt (1:1): Single crystals of 1:1 Blonanserinium succinate salt were obtained from EtOAc−ethyl methyl ketone. The X-ray crystal structure was solved and refined in space group $P2_12_12_1$ with a proton being transferred from one of the carboxylic acid groups of SUC to the piperazine N$_3$ position of BLN as observed in BLN HCl salt.[31a] SUC$^−$ anions connect through O–H⋯O$^−$ (1.60 Å, 174º) hydrogen bonds forming a channel along the [010] axis, and BLNH$^+$ cations were arranged in an alternate fashion on both sides of this channel through N$^+$–H⋯O$^−$ (1.71 Å, 171º) hydrogen bonds. CH donors adjacent to the protonated ammonium cation form auxiliary C–H⋯O (2.46 Å, 136º; 2.65 Å, 109º) interactions with COO$^−$ and COOH groups of SUC$^−$ anions in R_2^2 (7) and R_3^2 (9) ring motifs.[31b-c] Adjacent channels were connected by auxiliary C–H⋯O (2.48 Å, 172º) and bifurcated C–H⋯F (2.51 Å, 158º; 2.54 Å, 150º) interactions (Figure 4.1).
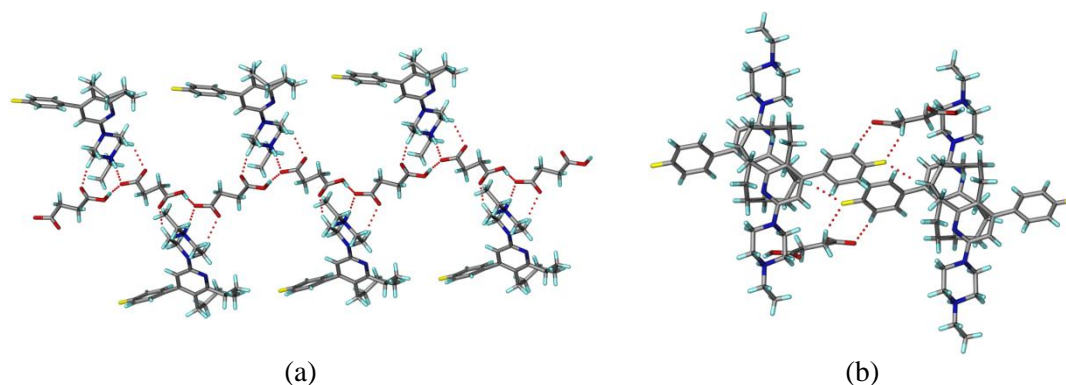
Figure 4.1 (a) SUC⁻ anions form a channel along the *b*-axis and BLNH⁺ cations are flanked through N⁺–H···O⁻ and C–H···O interactions. (b) Adjacent channels are connected by auxiliary C–H···O and C–H···F interactions.

BLN−SBA cocrystal (1:0.5): Dissolution of the ground starting materials BLN and SBA in CH_3NO_2:MeOH (1:1 v/v) resulted in a 1:0.5 cocrystal which solved and refined in the monoclinic space group $P2_1/n$ with one molecule of BLN and half molecule of SBA in the asymmetric unit. The same cocrystal was also obtained in bulk upon liquid-assisted grinding[32] (EtOH solvent) of the components using a mortar-pestle in 1:0.5 stoichiometric ratio. Unlike BLNH⁺−SUC⁻ salt, the proton resides on the acid group of SBA making a cocrystal adduct. The structure shows a rare COOH···N (tertiary amine) synthon (see CSD search results in Table 4.2). Two BLN molecules are connected by SBA through COOH···N (1.62 Å, 169º) and auxiliary C–H···O (2.46 Å, 131º) interactions in a R_2^2 (8) motif.[31b-c] BLN molecules extend the chain to give a layer structure through weak C–H···π interactions (Figure 4.2).

(a)   (b)

(c)
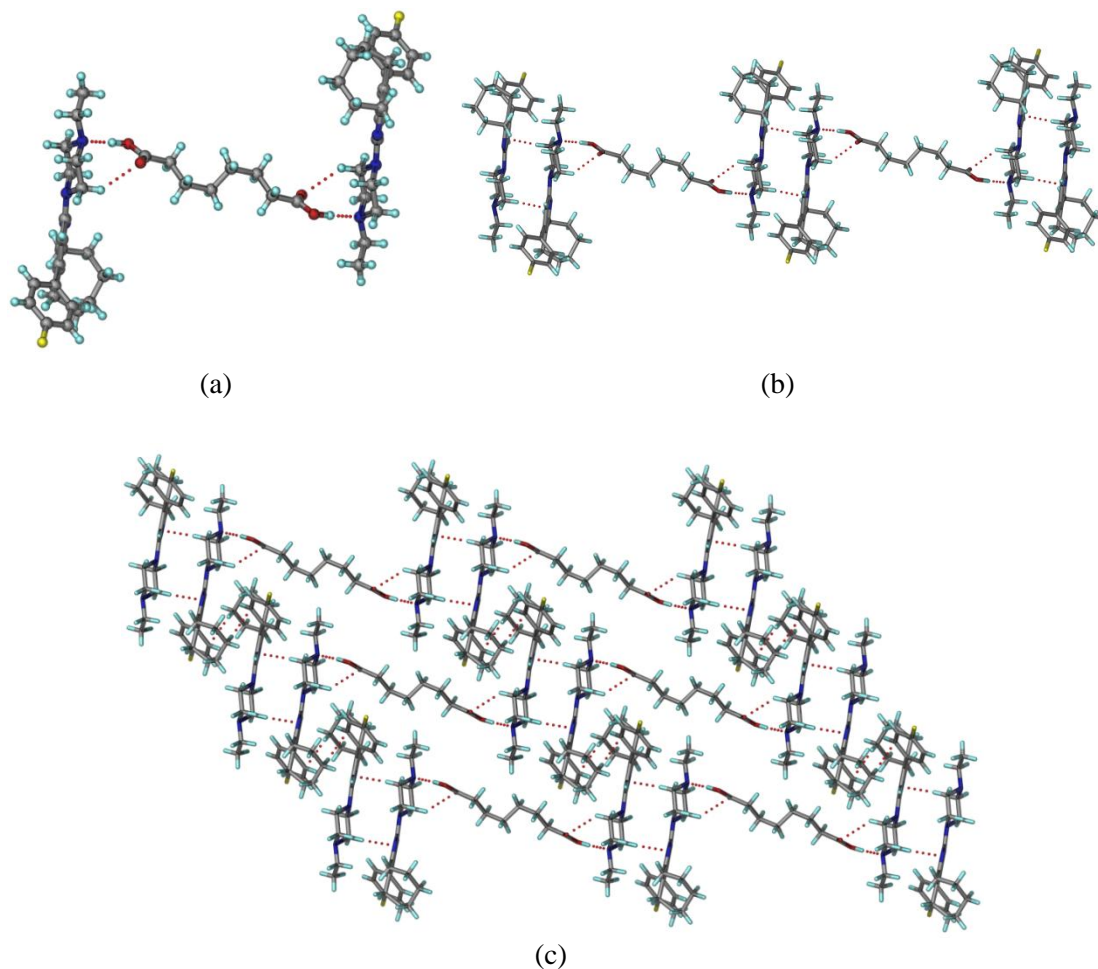
Figure 4.2 (a) A finite unit of the BLN–SBA cocrystal sustained by acid–amine O–H···N and C–H···O H-bonds. (b) Such acid–amine units are assembled via C–H···π interactions along the *a*-axis. (c) The 2D sheet structure.

BLNH$^+$−NIA$^-$ salt (1:1): Crystallization of powdered BLN and NIA from CH_3NO_2 afforded single crystals of the salt BLNH$^+$–NIA$^-$ in the monoclinic space group *P*2$_1$/*n*. The same salt was also obtained in bulk upon liquid-assisted grinding (EtOH solvent) of the components using a mortar-pestle in stoichiometric ratio. A proton is transferred from NIA to N-ethyl piperazine N$_3$ of BLN base to give the salt structure (N$^+$–H···O$^-$ 1.56 Å, 171°) and the carboxylate C=O of NIA$^-$ forms auxiliary C–H···O (2.47 Å, 135°) interactions in a R_2^2 (8) motif. BLNH$^+$ cations form a dimeric motif by C–H···π interactions, which are further

connected to adjacent BLNH$^+$ cations through C–H$\cdots$F (2.34 Å, 158º; 2.43 Å, 142º) interactions (one activated CH donor adjacent to ammonium cation and the other is a phenyl ring CH donor). Each dimeric motif is connected to six neighboring BLNH$^+$ cations through C–H$\cdots$F (2.34 Å, 158º; 2.43 Å, 142º) interactions (Figure 4.3).

(a)   (b)

(c)
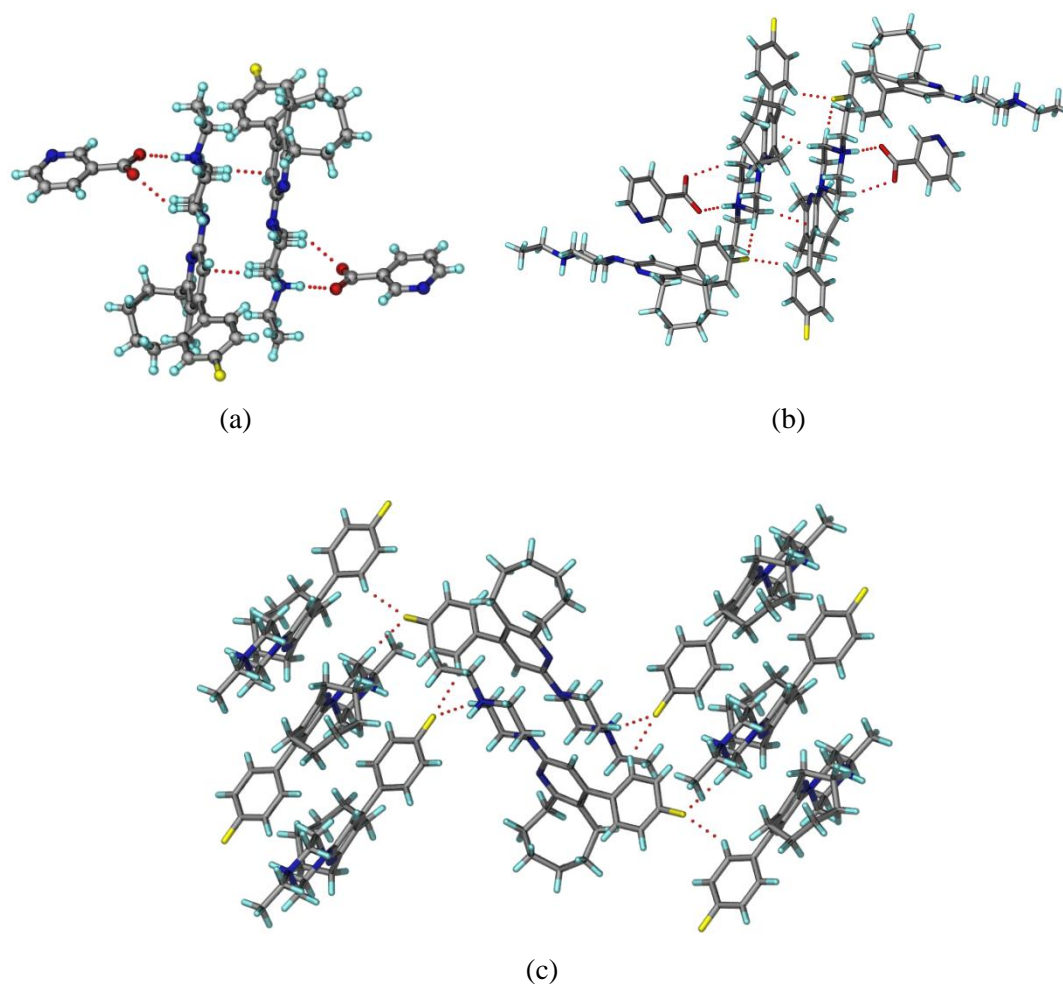
Figure 4.3 (a) Ionic N$^+$–H$\cdots$O$^-$ and auxiliary C–H$\cdots$O interactions in BLNH$^+$–NIC$^-$ salt form a R_2^2 (8) motif. (b) Centrosymmetrically related BLNH$^+$ cations form a dimeric motif through C–H$\cdots\pi$ interactions. (c) Each dimeric motif is connected to adjacent BLNH$^+$ cations through C–H$\cdots$F interactions.

BLNH⁺–TsO⁻ salt (1:1): Crystallization of ground BLN and TsOH from ethyl methyl ketone afforded needle morphology crystals of the salt which solved and refined in monoclinic space group $P2_1/n$ with one BLNH⁺ cation and TsO⁻ anion in the asymmetric unit. The same salt was also obtained in bulk upon liquid-assisted grinding (EtOH solvent) of the components using a mortar-pestle in stoichiometric ratio. Similar to the above salts, a proton is transferred from TsOH to N-ethyl piperazine N_3 of BLN base resulting in the salt structure (N⁺–H···O⁻ 1.69 Å, 167°). Activated CH donors (adjacent to protonated ammonium cation) are connected to TsO⁻ through auxiliary C–H···O (2.34 Å, 151 Å; 2.49 Å, 163º; 2.49 Å, 167º; 2.57 Å, 140º) interactions resulting in a zigzag 1D tape (Figure 4.4).

(a)   (b)
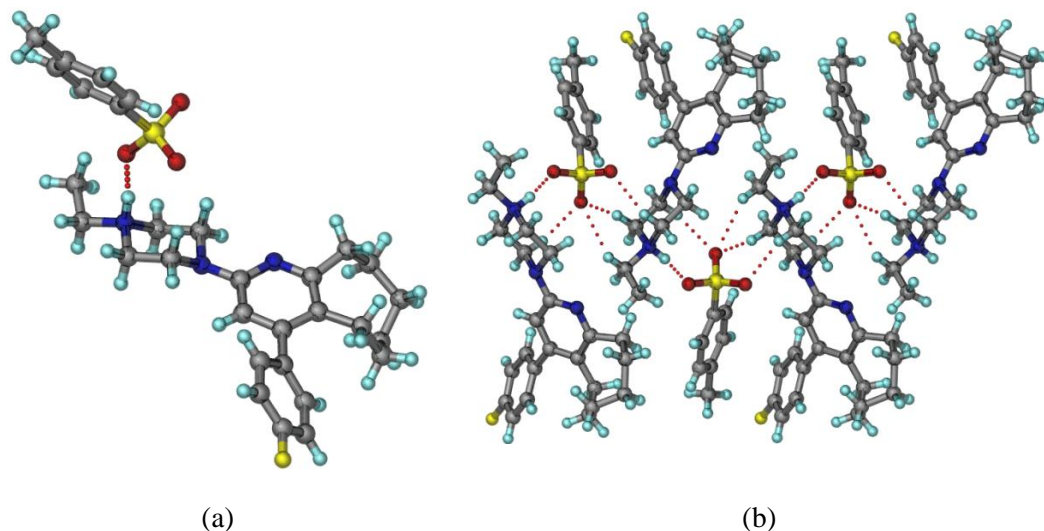
Figure 4.4 (a) BLNH⁺–TsO⁻ salt structure with N⁺–H···O⁻ ionic hydrogen bond at N_3 position of the drug. (b) Auxiliary C–H···O interactions with the sulfonate anion.

BLN⁺−MSA⁻ salt (1:1): This salt was obtained in bulk when a stoichiometric ratio of the components was ground in a mortar-pestle with a few drops of EtOH solvent. Single crystals of the salt were obtained when the ground material was crystallized from toluene−EtOAc (1:1, v/v), and the crystal structure of BLNH⁺−MSA⁻ (2 symmetry-independent ions of each component) was solved in $P\bar{1}$ space group. The flexible cyclooctane ring C atoms (C33A, C33B; C34A, C34B) are disordered in one of the BLNH⁺ cations (shown in ball and stick). Protonation occured at the piperazine N_3 of BLNH⁺, similar to other salts (N⁺−H···O⁻ 1.66 Å,

169º; 1.66 Å, 169º). BLNH$^+$ cations are connected through C–H···π interactions to form a dimeric motif. Symmetry-independent BLNH$^+$ cations are connected by MSA$^-$ anions in a 1D tape via N$^+$−H···O$^-$ (1.66 Å, 169º; 1.66 Å, 169º) and C−H···O (2.41 Å, 132º; 2.39 Å, 151º; 2.61 Å, 115º) H-bonds (Figure 4.5).

(a)   (b)

Figure 4.5 (a) BLNH$^+$ cations form a dimeric motif through C−H···π interactions. Hydrogen atoms which are not involved in H-bonding are removed for clarity. (b) N$^+$−H···O$^-$ and C−H···O H-bonds in BLNH$^+$−MSA$^-$ anhydrous salt. Crystallographic independent ions are shown in ball-stick and capped-stick representation.

BLNH$^+$–MSA$^-$–H$_2$O (1:1:1): This salt hydrate was obtained in bulk when a stoichiometric ratio of the components was ground in a mortar-pestle with a few drops of water added. Single crystals of the salt hydrate (1:1:1) were obtained upon crystallizing the ground material from i-PrOH. The structure solved in the monoclinic space group $P2_1/n$. Water and mesylate anions are connected through O−H···O (1.90 Å, 173º; 1.96 Å, 168º) hydrogen bonds along the [100] axis and BLNH$^+$ cations flank on one side of this chain through N$^+$−H···O$^-$ (1.77 Å, 168º) hydrogen bonds (Figure 4.6).

(a)   (b)
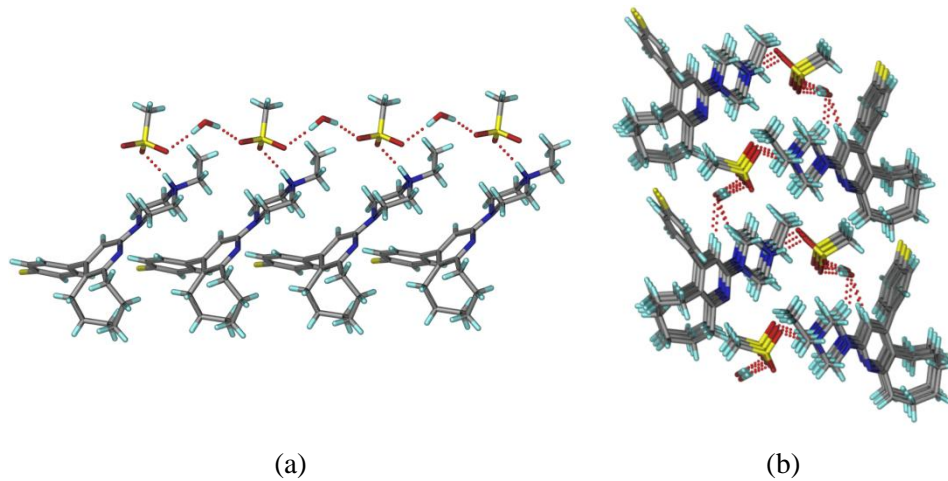
Figure 4.6 (a) BLNH⁺ cations are hydrogen bonded to water and mesylate anions through N⁺−H···O⁻ H-bonds. (b) The tapes were connected through C−H···O interactions.

Table 4.3 Cystallographic parameters of BLN salts.

	BLNH$^+$–SUC$^-$	BLN–SBA	BLNH$^+$–NIA$^-$	BLNH$^+$–MSA$^-$	BLNH$^+$–MSA$^-$–H$_2$O	BLNH$^+$–TsO$^-$
Emp form.	C27 H36 F N3 O4	C27 H37 F N3 O2	C29 H35 F N4 O2	C24 H34 F N3 O3 S	C24 H36 F N3 O4 S	C30 H38 F N3 O3 S
Form wt	485.59	454.60	490.61	463.60	481.62	539.69
Cryst syst	Orthorhombic	Monoclinic	Monoclinic	Triclinic	Monoclinic	Monoclinic
Sp gr	$P2_12_12_1$	$P2_1/n$	$P2_1/n$	$P\bar{1}$	$P2_1/n$	$P2_1/n$
T/K	100(2)	100(2)	298(2)	100(2)	100(2)	100(2)
a/Å	8.9999(9)	13.655(12)	12.2184(12)	12.6945(9)	6.7308(8)	6.3176(9)
b/Å	13.0762(13)	11.540(10)	11.6715(9)	13.7444(9)	10.5808(13)	36.767(5)
c/Å	21.704(2)	15.669(14)	18.5188(17)	14.4954(10)	34.376(4)	11.6580(17)
α/°	90	90	90	98.5020(10)	90	90
β/°	90	103.515(13)	94.867(8)	98.8410(10)	91.931(2)	99.549(2)
γ/°	90	90	90	105.9490(10)	90	90
Z	4	4	4	4	4	4
V/Å^3	2554.2(4)	2401(4)	2631.4(4)	2354.3(3)	2446.8(5)	2670.4(7)
D_{calc}/g cm^{-3}	1.263	1.258	1.238	1.308	1.307	1.342
μ/mm^{-1}	0.090	0.085	0.084	0.176	0.175	0.166
Rflns collect	26650	22172	10214	24415	24476	25043
Unique rflns	5015	4787	5384	9148	4816	4714
Obsd rflns	4715	3499	2247	8046	4068	4409
R_1 [$I>2\sigma(I)$]	0.0339	0.0430	0.0623	0.0464	0.0423	0.0600
wR_2 [all]	0.0762	0.0960	0.1008	0.1121	0.0970	0.1345
GOF	1.032	0.988	0.872	1.041	1.044	1.158

Table 4.4 Hydrogen bond metrics in the crystal structures.

D–H···A	H···A (Å)	D···A (Å)	D–H···A (°)	symmetry code
		BLNH$^+$–SUC$^-$		
O1–H1···O4	1.60	2.5460(16)	174	–x, –1/2+y,1/2–z
N3–H3···O3	2.49	3.1894(17)	128	1–x, –1/2+y,1/2–z
N3–H3···O4	1.71	2.6676(17)	171	1–x, –1/2+y,1/2–z
C2–H2···O3	2.52	3.3369(19)	144	1–x, –1/2+y,1/2–z
C10–H10···F1	2.54	3.516(2)	150	x,+y+1, z
C16–H16···O4	2.48	3.556(2)	172	–x+1/2+1, –y,+z+1/2
C19–H19B···O3	2.65	3.176(2)	109	x+1,+y,+z
C20–H20B···O2	2.46	3.246(2)	136	1+x,y,z
C21–H21A···O3	2.59	3.2322(19)	122	1+x,y,z
C26–H26B···F1	2.51	3.530(2)	158	–x+1/2+1, –y,+z–1/2
		BLN–SBA		
O1–H1···N3	1.62	2.570(3)	169	x, y, z
C6–H6B···O2	2.60	3.671(3)	171	x+1/2, –y+1/2,+z–1/2
C18–H18B···O2	2.46	3.297(3)	131	x, y, z
C14–H14···N1	2.58	3.657(3)	176	x–1/2, –y+1/2,+z–1/2
		BLNH$^+$–NIA$^-$		
N3–H3···O2	1.56	2.586(3)	171	x, y, z
C13–H13···F1	2.43	3.349(3)	142	–x–1/2,+y–1/2, –z–1/2
C19–H19A···F1	2.34	3.368(3)	158	x+1/2, –y+1/2,+z+1/2
C19–H19B···N1	2.74	3.678(3)	161	–x, –y, –z
C21–H21A···O1	2.47	3.319(3)	135	x, y, z
		BLNH$^+$–MSA$^-$		
N3–H3···O3	1.66	2.675(2)	169	–x+2, –y+1, –z+1
N6–H6···O6	1.66	2.677(2)	169	x, y, z
C6–H6B···O1	2.45	3.413(2)	170	1–x,1–y,1–z
C10–H10B···O6	2.57	3.538(2)	174	x, –1+y,z
C14–H14···F2	2.54	3.118(3)	120	1+x,1+y, –1+z
C18–H18A···O2	2.52	3.406(3)	152	–1+x,y,z
C21–H21B···O5	2.41	3.226(2)	132	x, y, z
C23–H23A···O3	2.57	3.419(3)	135	x, y, z
C31–H31B···O5	2.53	3.475(3)	166	–x,1–y,1–z
C43–H43B···O4	2.57	3.399(2)	144	1–x,1–y,1–z
C45–H45A···O1	2.61	3.211(2)	115	–x+1, –y, –z+1
C46–H46A···O2	2.39	3.374(2)	151	1–x, –y,1–z
C48–H48B···O6	2.49	3.369(3)	138	–x+1, –y, –z+1
		BLNH$^+$–MSA$^-$–H$_2$O		
N3–H3···O1	1.77	2.783(19)	168	x, y, z
N3–H3···O2	2.48	3.117(2)	126	1/2–x, –1/2+y,1/2–z
O4–H4A···O3	1.96	2.886(2)	168	–x+1/2, y–1/2, –z+1/2

O4–H4B···O2	1.90	2.833(2)	173	−x+1/2, y−1/2, −z+1/2
C2–H2···O4	2.24	3.309(2)	168	x, y, z
C20–H20B···O2	2.53	3.245(2)	130	−1+x, −1+y,z
C20–H20B···O3	2.58	3.445(2)	148	−1+x, −1+y,z
C21–H21A···O4	2.63	3.499(2)	137	x, y, z
C23–H23B···O1	2.52	3.443(2)	161	−1/2−x, −1/2+y,1/2−z
		BLNH$^+$–TsO$^-$		
N3–H3···O2	1.69	2.711(3)	167	−1/2+x,1/2−y,1/2+z
C19–H19A···O3	2.49	3.544(3)	163	x, y, z
C19–H19B···O1	2.43	3.344(3)	153	1/2+x,1/2−y,1/2+z
C20–H20A···O1	2.34	3.323(3)	151	x, y, z
C21–H21A···O1	2.49	3.560(3)	167	−1/2+x,1/2−y,1/2+z
C21–H21B···O3	2.33	3.261(3)	157	−1+x, y, z
C22–H22B···O1	2.57	3.471(3)	140	x, y, z

4.4.2 Spectral Analysis

A wave number shift in the IR frequency[33] of the product with respect to the starting materials indicates formation of cocrystal/salt. BLN free base has no H-bonding functional groups (OH/NH) except C–F, tertiary amine N, and pyridine N. So the only changes in stretching frequencies observed were with respect to salt/cocrystal formers. Generally peak shifts of 10–15 cm^{-1} are indicative of changes in hydrogen bonding for salt/ cocrystal. A neutral carboxylic acid (COOH) absorbs strongly at 1700 cm^{-1} for the C=O stretching band and a weaker C–O stretch around 1200 cm^{-1}, whereas the carboxylate group (COO$^-$) exhibits two characteristic coupled carbonyl absorption bands at 1600 cm^{-1} (asymmetric) and 1400 cm^{-1} (symmetric). The fingerprint stretching frequency at 1700 cm^{-1} in BLN–SBA ground material indicates unionized carboxylic group for the cocrystal, as confirmed by X-ray diffraction. The stretching frequencies for the carboxylic group in BLNH$^+$–SUC$^-$ at 1709 cm^{-1} and for the carboxylate at 1605 cm^{-1} (asymmetric) and 1413 cm^{-1}(symmetric) mean a salt structure with one free and one ionized COOH. The carboxylate stretch in BLNH$^+$–NIA$^-$ at 1641 cm^{-1} (asymmetric) and 1400 cm^{-1} (symmetric) are clear indication of a salt. Generally S=O exhibits stretching frequency in the range of 1060-1020 cm^{-1}. The shift in the stretching frequency of S=O (1048 cm^{-1}) in MSA to the 1037 cm^{-1} in BLN$^+$–MSA$^-$ indicate a salt of SO$_3^-$ group. The IR resonances in BLN$^+$–TsO$^-$ salt and BLN$^+$–MSA$^-$ H$_2$O salt hydrate are similar at 1167 cm^{-1} and 1046.1 cm^{-1}, with the latter showing an additional O–H

peak at 3482 cm^{-1}. FT-IR frequencies are summarized in Table 4.5 and spectra are displayed in Figure 4.7. Similarly, the salts/cocrystal were identified by FT-Raman spectroscopy (Figure 4.8 and Table 4.5).
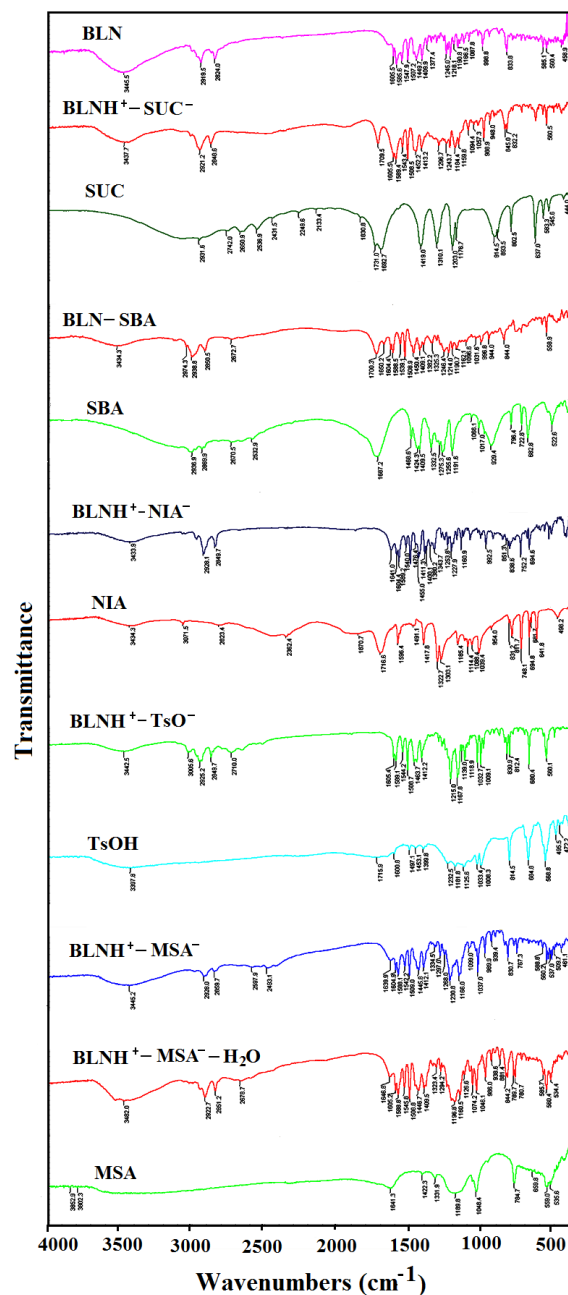
Figure 4.7 FT-IR spectral comparison of BLN solid forms obtained from LAG with its individual components.
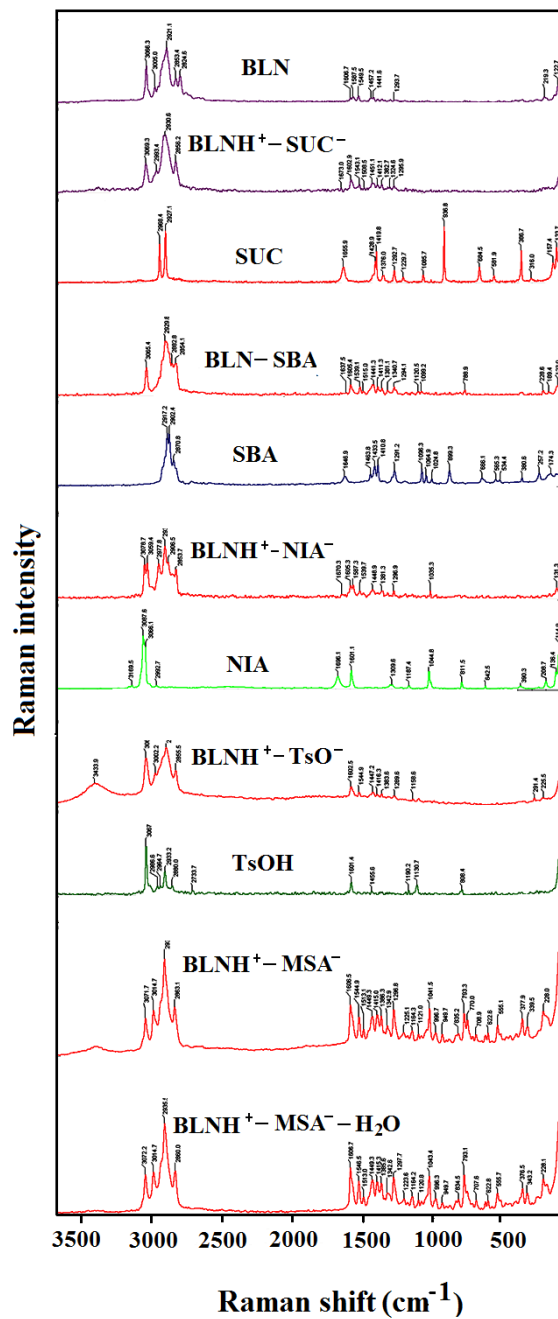

Figure 4.8 FT-Raman spectral comparison of BLN solid forms obtained from LAG with its individual components.

Table 4.5 IR and Raman frequencies of BLN solid forms and starting components (in cm^{-1}).

compound	C–H Stretch	C–F stretch	Carboxylic C=O stretch	–COO⁻ asym stretch	–COO⁻ sym stretch	S=O stretch
INFRARED						
BLN	2919.5	1245.0	-	-	-	-
NIA	-	-	1716.6	-	-	-
BLN⁺–NIA⁻	2928.1	1253.8	-	1641.0	1400.1	-
SBA	-	-	1687.2	-	-	-
BLN–SBA	2938.8	1246.4	1700.3	-	-	-
TsOH	-	-	-	-	-	1181.8
BLN⁺–TsO⁻	2925.2	1215.0	-	-	-	1167.8
SUC	-	-	1731.0	-	-	-
BLN⁺–SUC⁻	2921.2	1243.7	-	1709.5	1413.2	-
MSA	-	-	-	-	-	1048.4
BLN⁺–MSA⁻	2928.0	1230.8	-	-	-	1037.0
BLN⁺–MSA⁻–H₂O	2922.7	1196.8	-	-	-	1046.1
RAMAN						
BLN	2921.1	1293.7	-	-	-	-
NIA	-	-	1696.1	-	-	-
BLN⁺–NIA⁻	2932.2	1296.9	-	1670.3	1448.9	-
SBA	-	-	1646.9	-	-	-
BLN–SBA	2929.8	-	1637.5	-	-	-
TsOH	2933.2	-	-	-	-	1190.2
BLN⁺–TsO⁻	2924.6	1289.6	-	-	-	1158.6
SUC	2927.1	-	1655.9	-	-	-
BLN⁺–SUC⁻	2930.6	1295.9	-	1673.0	1412.1	-
MSA	2936.8	1296.8	-	-	-	1041.5
BLN⁺–MSA⁻	2935.5	1297.7	-	-	-	1043.4
BLN⁺–MSA⁻–H₂O	2921.1	1293.7	-	-	-	-

Solid-state NMR spectroscopy can provide information about differences in hydrogen bonding, molecular environment, and short range order in crystalline and amorphous solids.[34] ^{13}C ss-NMR analysis of the novel solid forms of BLN showed clear differences in the product phases when compared with the starting components. Based on the extent of proton transfer and the position of the COOH carbon in salt/ cocrystal, the δ values are different in ^{13}C ss-NMR spectra of the products (Figure 4.8 and Table 4.6).
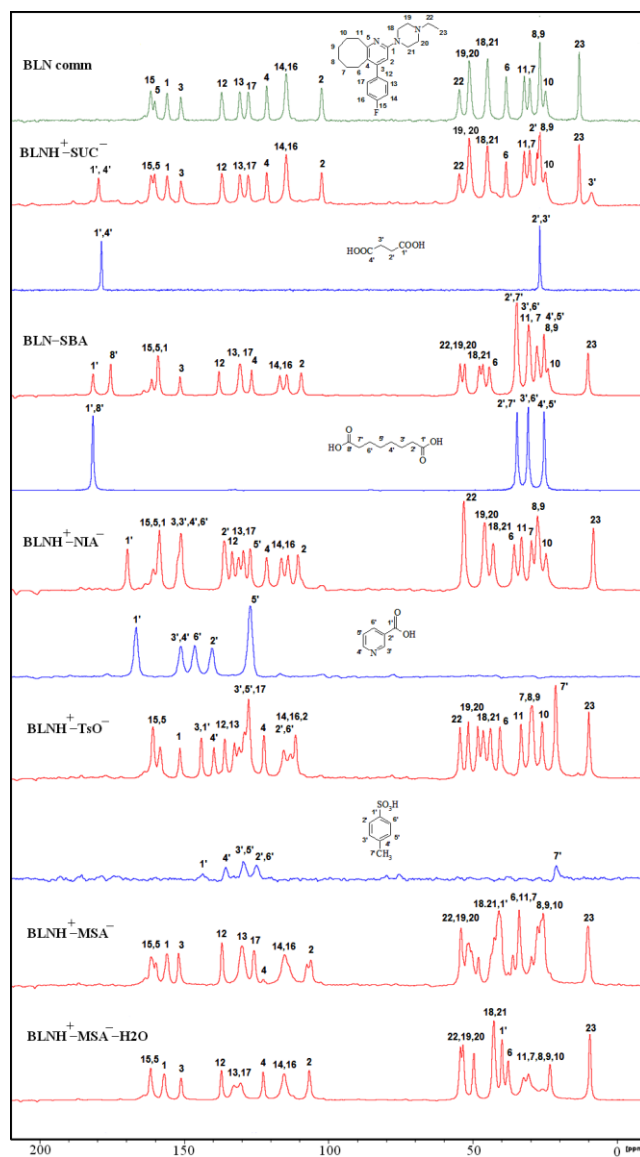
Figure 4.8 ^{13}C ss-NMR spectra of BLN crystalline forms.

Table 4.6 ^{13}C ss-NMR chemical shifts (δ, ppm) of BLN solid forms.

Carbon No.	BLN	SUC	BLN$^+$–SUC$^-$	SBA	BLN–SBA	NIA	BLN$^+$–NIA$^-$	TsOH	BLN$^+$–TsO$^-$	BLN$^+$–MSA$^-$	BLN$^+$–MSA$^-$–H$_2$O
1	155.9		155.9		158.9		158.4		151.3	155.8	156.8
2	102.4		102.3		109.3		110.5		111.3	106.0	106.5
3	151.2		151.2		151.3		151.0		143.9	151.8	150.9
4	121.4		121.4		126.5		121.3		122.2	120.4	122.5
5	160.2		160.3		161.1		160.6		158.2	159.7	161.5
6	38.4		38.4		44.2		35.6		40.5	36.1	37.7
7	30.2		30.3		30.6		29.6		29.4	33.9	30.6
8	26.8		26.8		27.7		27.5		29.4	29.7	25.8
9	26.8		26.8		27.7		27.5		29.4	27.5	23.1
10	24.8		24.8		23.9		24.5		25.9	25.6	23.1
11	32.1		32.2		30.6		33.0		33.2	33.9	32.3
12	137.0		137.0		137.8		133.2		135.8	136.8	137.0
13	130.7		130.7		130.6		131.0		132.5	129.9	132.6
14	114.6		114.6		116.7		116.2		113.0	115.2	115.2
15	161.6		161.5		164.1		160.6		160.7	161.4	161.5
16	114.6		114.6		114.3		113.9		113.0	115.2	115.2
17	127.8		127.8		130.6		129.3		127.6	125.7	130.3
18	44.9		44.9		47.6		42.8		46.3	42.5	42.6
19	51.2		51.3		52.7		45.8		51.5	51.4	53.3
20	51.2		51.3		52.7		45.8		48.2	48.0	49.5
21	44.9		44.9		46.4		42.8		43.8	41.0	42.6
22	54.6		54.7		54.3		53.0		54.3	54.1	54.2
23	13.1		13.1		10.0		8.1		9.7	10.2	9.3
1'		180.2	179.7	181.5	181.4	166.5	169.5	144.1	143.9	37.7	39.8
2'		28.2	27.8	34.6	34.7	140.2	136.0	114.8	115.4		
3'		28.2	8.9	30.7	30.6	151.0	151.0	130.1	130.8		
4'		180.2	179.7	25.2	25.2	151.0	151.0	137.3	139.6		
5'				25.2	25.2	127.0	127.0	130.1	129.0		
6'				30.7	30.6	146.2	151.0	114.8	115.4		
8'				181.5	175.3						

4.4.3 Thermal Analysis

DSC of BLN commercial material showed a single melting endotherm at 123.9 °C. All new solid phases were prepared by liquid-assisted grinding (LAG) and the resulting bulk material was used for DSC measurements. A single melting endotherm confirmed purity and homogeneity of the bulk phases, and their melting points were different from the starting materials (Table 4.7). $BLNH^+–SUC^-$ and $BLNH^+–NIA^-$ salts showed characteristic melting points at 148.9 °C, 136.5 °C, values that are intermediate compared to the starting materials. DSC on the residue of $BLNH^+–SUC^-$ salt after the equilibrium solubility experiment exhibited an endothermic transition immediately followed by recrystallization to a new polymorph, which melted upon further heating (discussed in chapter 6). It is difficult to define this behavior as an enantiotropic or a monotropic[35] system. Similarly, the ground material of BLN and SBA (BLN–SBA cocrystal as confirmed by single crystal XRD) showed a unique melting endotherm at 122.1 °C, which is lower than that of the coformer (141-144 °C) and comparable to that of the free API. $BLNH^+–TsO^-$ and $BLNH^+–MSA^-$ salts showed higher melting endotherms at 206.3 °C and 210.3 °C compared to the respective salt formers. A monohydrate of $BLNH^+–MSA^-$ salt was obtained upon cogrinding of salt formers with a small amount of H_2O added. $BLNH^+–MSA^-$ salt hydrate loses water at 94-106 °C and melts at 211.7 °C. The onset endotherms of $BLNH^+–MSA^-$ anhydrous salt (210.3 °C) and $BLN^+–MSA^-–H_2O$ salt hydrate (211.7 °C) are very close, suggesting formation of the anhydrous salt upon dehydration. However the PXRD of the dehydrated material is different from that of $BLNH^+–MSA^-$ salt. When $BLNH^+–MSA^-–H_2O$ salt hydrate was kept in an oven at 100 °C for 30 min, the PXRD and DSC of the dehydrated product did not match with $BLN^+–MSA^-$ single crystal phase. Hence dehydration of $BLNH^+–MSA^-–H_2O$ salt hydrate gives what appears to be a novel polymorph (discussed in chapter 6). The DSC heating curves of salts are shown in Figure 4.9.
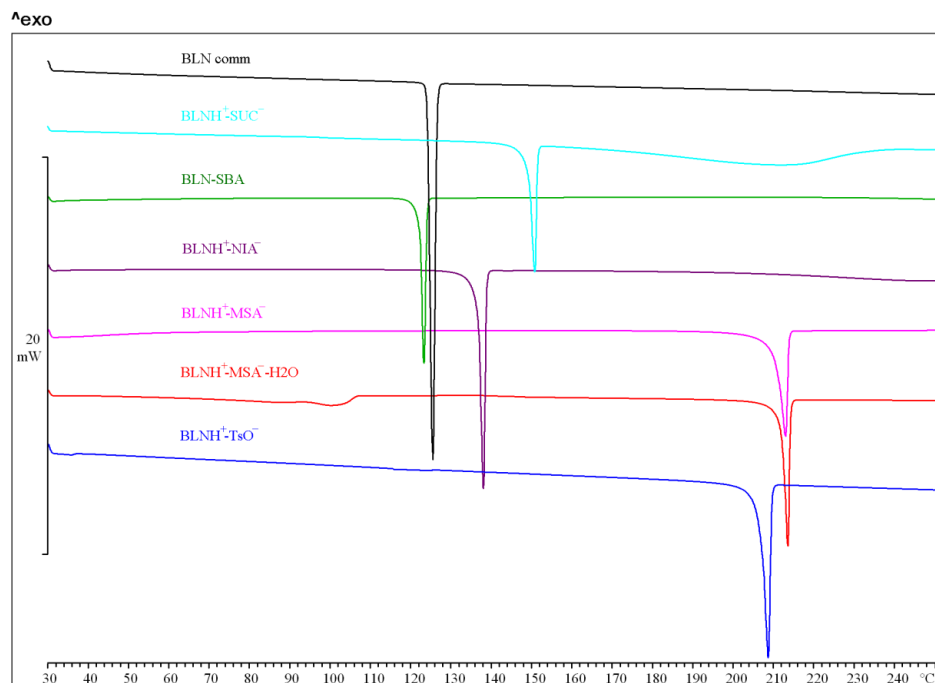
Figure 4.9 DSC heating curves of BLN salts exhibit a unique and sharp melting endotherm.

Table 4.7 Melting points of BLN and its solid forms, compared with those of the drug and salt/cocrystal formers used.

Drug/ coformer	M.p. of Drug/coformer (°C)	Salt/salt hydrate/ cocrystal	M.p. of adduct (°C) T_{onset}/ T_{peak}
BLN	123-124	---	---
SUC	185-187	$BLNH^+–SUC^-$	148.9/ 150.4
SBA	141-144	BLN H–SBA	122.1/ 122.9
NIA	234-238	BLN $H^+–NIA^-$	136.5/ 137.5
TsOH	103-106	BLN $H^+–TsO^-$	206.3/ 208.0
MSA	---	BLN $H^+–MSA^-$	210.3/ 212.6
MSA	---	BLN $H^+–MSA^-–H_2O$	211.7/ 213.1

4.4.4 Powder X-ray diffraction

Powder X-ray diffraction is a reliable characterization tool to establish the formation of novel crystalline forms,[36] and to distinguish the resulting products from the starting materials

in the solid-state. The powder diffraction lines of BLN commercial material matched with those of form A reported in patent CN101747274 (A).[37] Similarly, all the novel solid forms prepared by liquid-assisted grinding (LAG) exhibited unique powder diffraction line pattern matching with the X-ray crystal structure (Figure 4.10a and Figure 4.10b). The slight variation in the overlay of lines for BLNH$^+$–SUC$^-$ salt could be due to temperature effects, because the X-ray crystal structure reflections were collected at 100 K and the experimental PXRD was recorded at room temperature (Figure 4.10b). Various methods such as liquid-assisted grinding, neat (dry) grinding, slurry crystallization methods, rotavaporization, and even single crystals obtained from solution crystallization gave repeatedly the same PXRD line pattern for BLNH$^+$–SUC$^-$ salt, and moreover we did not observe any exothermic/endothermic transition or solvent loss in DSC, thereby confirming purity of the salt. The residue at the end of the equilibrium solubility experiment gave a different PXRD pattern for BLNH$^+$–SUC$^-$ salt (Figure 4.11a). When this material was kept at 125 °C in a temperature-controlled oven for 30 min, the product matched with the calculated powder XRD lines for the crystal structure of BLNH$^+$−SUC$^-$ salt. Hence BLNH$^+$−SUC$^-$ salt has two crystalline forms based on this preliminary study, which was supported by DSC. Similarly, BLNH$^+$–MSA$^-$ anhydrous salt also exists in two different crystalline forms, because the experimental PXRD of dehydrated BLNH$^+$–MSA$^-$ salt obtained from BLN H$^+$–MSA$^-$–H$_2$O salt hydrate by dehydration (as discussed above) did not match with the calculated X-ray lines from the crystal structure of BLNH$^+$–MSA$^-$ anhydrous form (Figure 4.11b). Thus BLNH$^+$−SUC$^-$ and BLNH$^+$–MSA$^-$ salts exhibit polymorphic modifications (which are being fully discussed in chapter 6).

(a)   (b)
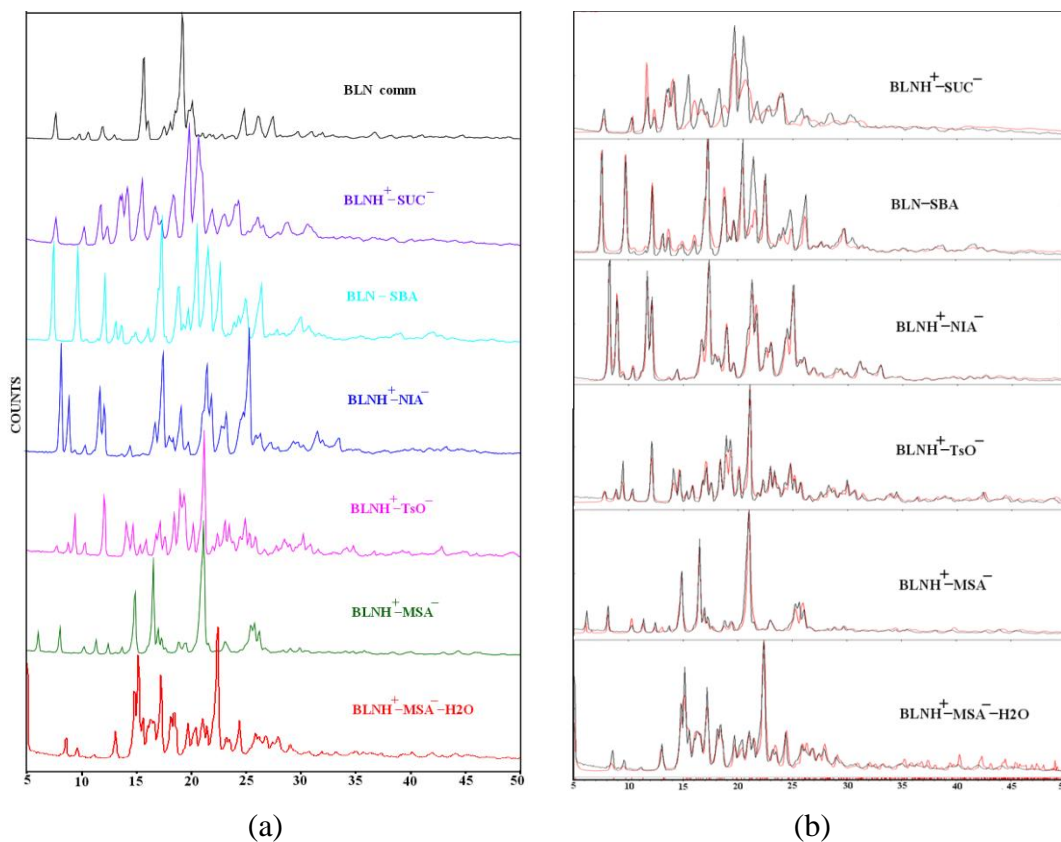
Figure 4.10 (a) Experimental PXRD patterns of BLN commercial and salts. (b) Overlay of experimental PXRD (black) pattern of BLN solid forms obtained from liquid assisted grinding (LAG) matches with their respective calculated powder lines from the crystal structure (red).

(a)   (b)

Figure 4.11 (a) Experimental PXRD pattern (black) obtained from slurry (60% EtOH solvent) was found to be different from the calculated powder lines from the crystal structure of BLNH$^+$–SUC$^-$ salt (red). (b) PXRD pattern of dehydrated BLNH$^+$–MSA$^-$ salt

form (black) was found to be different from the calculated powder lines from the crystal structure of $BLNH^+–MSA^-$ anhydrous salt (red).

4.4.5 Form Stability and Conformational Flexibility

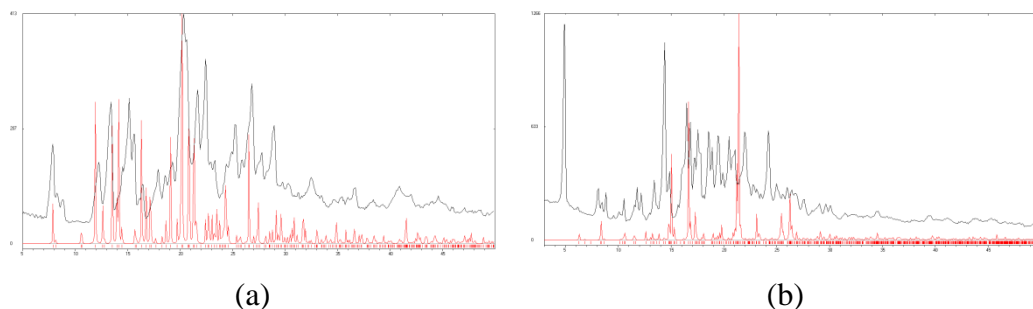The advantage of high solubility/dissolution rate for a drug solid form should also be accompanied with good physicochemical form stability. The solid forms were found to be stable in ambient conditions of Hyderabad (about 35 °C and 40% RH) for more than 6 months. In this context, slurry experiments performed on the novel solid forms indicated stability in the slurry medium, except $BLN^+–SUC^-$ and $BLN^+–MSA^-$ (discussed above). We also tested the solid forms for stability in accelerated WHO/ICH conditions[38] (40 °C, 75% RH). They were stable in the test period of 2 months, except $BLN^+–MSA^-$ anhydrous salt which converted to its monohydrate after one month (by PXRD overlay) and $BLN^+–SUC^-$ salt was stable for 2 months (no polymorphic change by PXRD) (Figure 4.12-4.14).
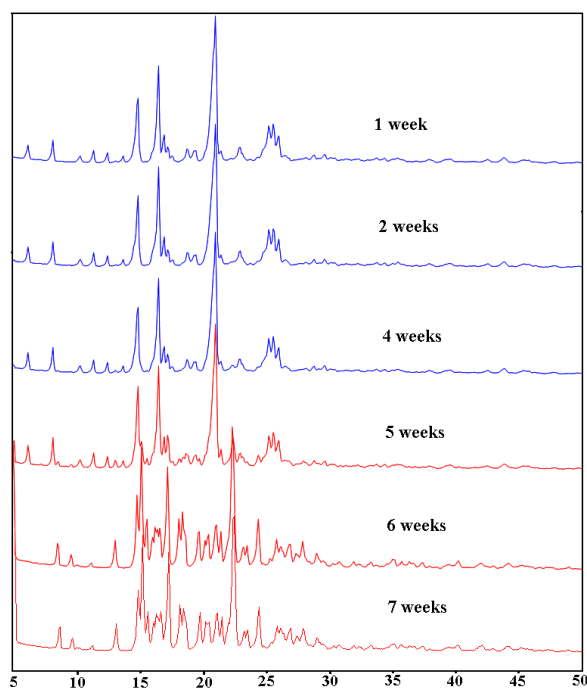
Figure 4.12 PXRD pattern from the stability study of $BLN^+–MSA^-$ anhydrous salt at 40 °C and 75% RH shows that after one month anhydrous salt converted to monohydrate form.
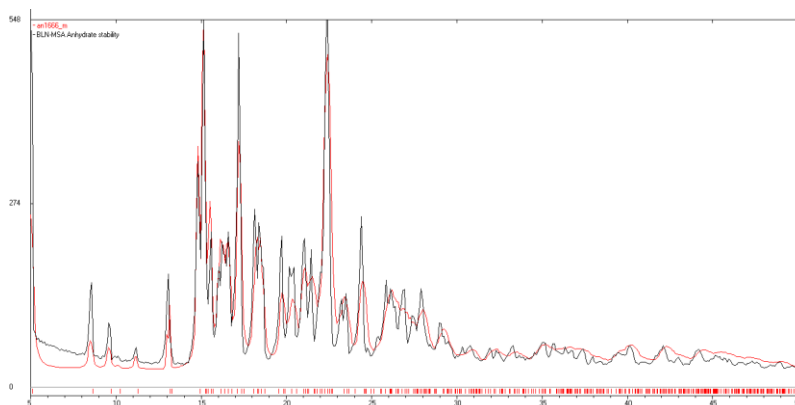
Figure 4.13 Formation of BLN$^+$–MSA$^-$–H$_2$O salt hydrate after keeping at 40 °C and 75% RH from anhydrous BLN$^+$–MSA$^-$ salt was confirmed by matching with calculated powder lines of BLN$^+$–MSA$^-$–H$_2$O salt hydrate.
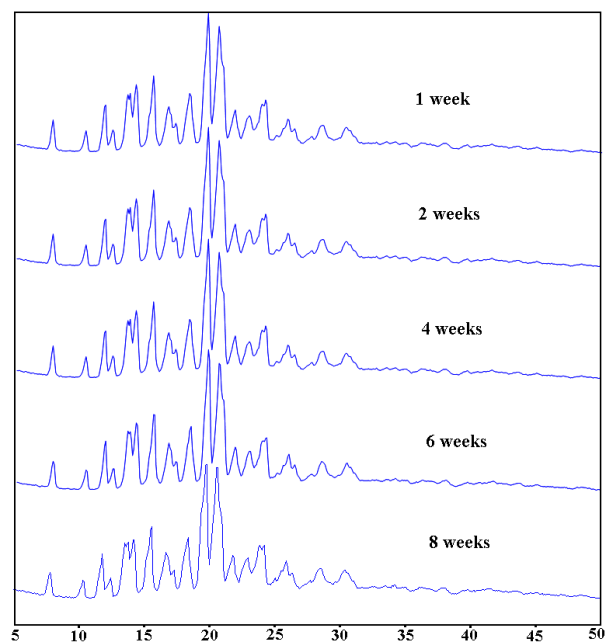
Figure 4.14 PXRD pattern of BLN$^+$–SUC$^-$ salt shows that it is stable up to 2 months at 40 °C and 75% RH conditions (did not show any polymorphic change).

The molecular structure of BLN has conformational flexibility about the C_{Pyr}–C_{Ph} and C_{Pyr}–N_{Pip} single bonds as well as cyclooctane ring bonds (Figure 4.15). Further attempts to correlate the solid-state conformation with structural properties and stability were not pursued in the present study.
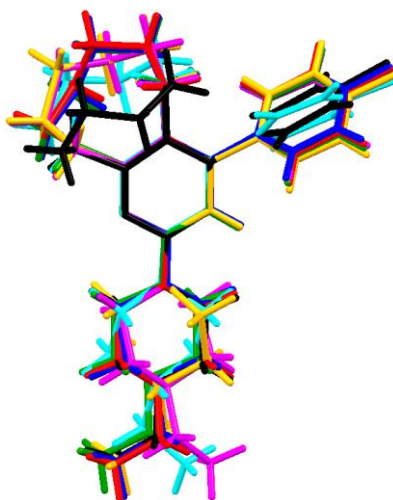
Figure 4.15 An overlay diagram of the BLN molecule extracted from the guest free form and salt/salt hydrate/cocrystal. Color codes: Black–BLN, Magenta– $BLNH^+$–$SUC^-$, Blue–BLN–SBA, Green– $BLNH^+$–NIA^-, Yellow–$BLNH^+$–TsO^-, Red–$BLNH^+$–MSA^- and Cyan–$BLNH^+$–MSA^-–H_2O.

4.4.6 Solubility and Dissolution

An important goal in drug development is to improve physicochemical parameters for enhanced drug efficacy. Solubility and permeability of a drug molecule determine its mode of administration into the body. Solubility remains a major complication for BCS class II drugs (low solubility, high permeability) since bioavailability is limited by poor dissolution.[11] BLN is a BCS class II drug having aqueous solubility of 0.033 mg/L, and solubility of 1.6 mg/mL in 60% EtOH−water. Thus BLN salts of high solubility and good stability are desirable in drug formulation. Solubility and dissolution studies on BLN solid forms were conducted in 60% EtOH−water medium because the solubility of pure BLN in water is very low. Solubility is a thermodynamic quantity and usually taken as the

concentration of the solute in equilibrium with the solvent at 24 or 48 h. The solubility of the new solid forms in this study (measured at 24 h) was superior to that of the reference drug BLN. BLNH$^+$–MSA$^-$–H$_2$O exhibited the highest solubility (742.9 mg/mL, 464 times higher) and the second highest is BLNH$^+$–NIA$^-$ (408.2 mg/mL, 255 times higher). Equilibrium solubility of BLNH$^+$–SUC$^-$ and BLNH$^+$–MSA$^-$ salts could not be determined because the former converted to a different form and the latter to its monohydrate (previous discussion) at 24 h. The other salts were stable at the end of the solubility experiment as confirmed by PXRD of the residue at 24 h (Figure 4.16). There was no apparent correlation between the solubility of the coformer to the solubility of the salt/cocrystal.
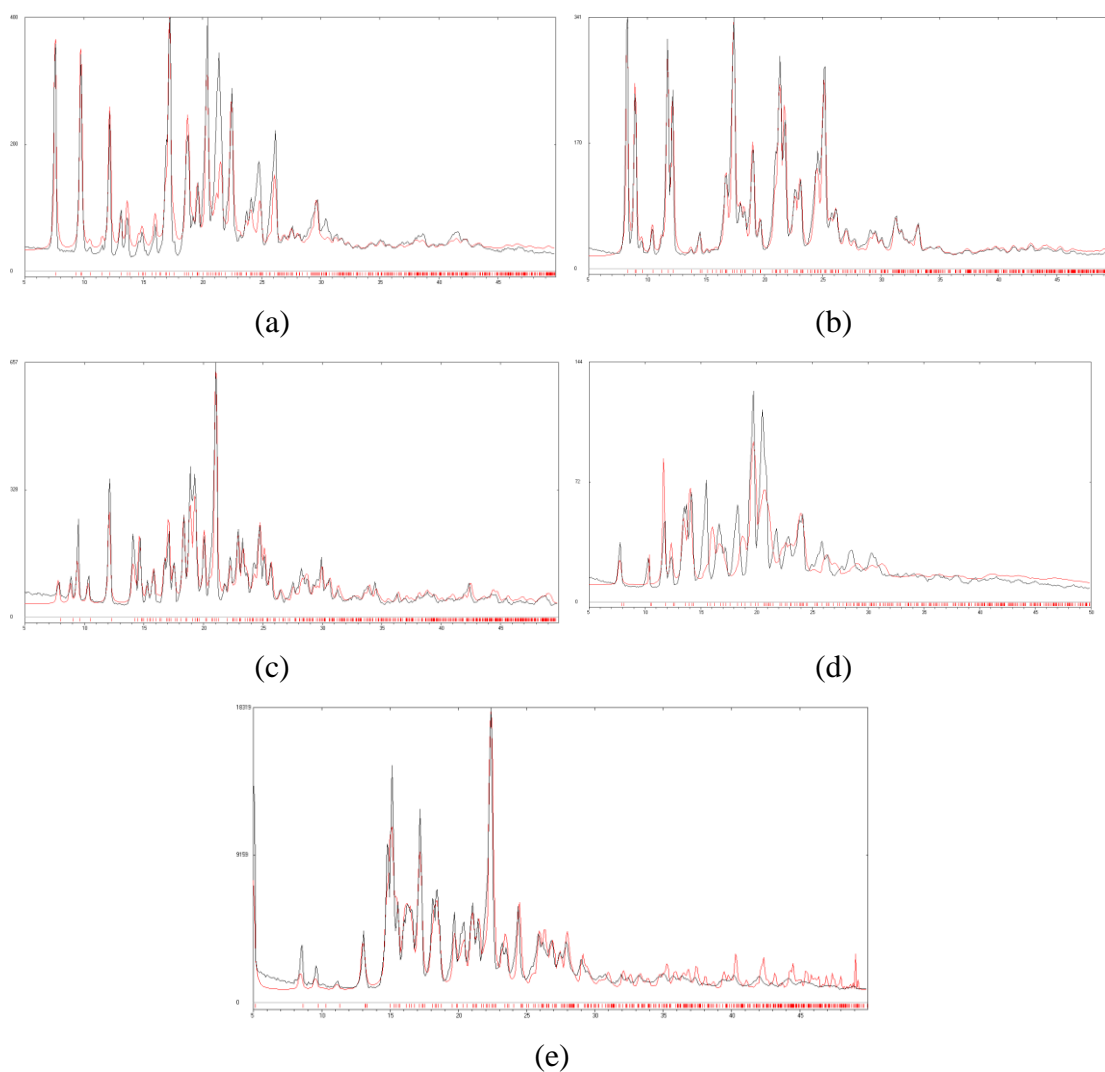

(a)

(b)

(c)

(d)

(e)

Figure 4.16 Overlay of experimental PXRD (black) of (a) BLN-SBA cocrystal (b) BLN$^+$–NIA$^-$ salt (c) BLN$^+$–TsO$^-$ salt (d) BLN$^+$–SUC$^-$ salt (e) BLN$^+$–MSA$^-$–H$_2$O obtained after solubility/dissolution experiments with the calculated lines from the crystal structure (red) show complete match of diffraction peaks.

Dissolution rate is a time dependant phenomenon and this method is preferable for those drugs which undergo phase transformation during the equilibrium solubility experiment. Intrinsic dissolution rate (IDR) gives an idea of the peak concentration and the amount of drug dissolved in a short time period (30 min to 2 h), preferably before it undergoes any phase transformation/ dissociation.[39] IDR experiments on BLN salts were performed in 60% EtOH−water for 45 min by the rotating disk intrinsic dissolution rate (DIDR) method[40] at 37 °C. The intrinsic dissolution experiment could not be run beyond 45 min because of the large difference in solubility between the parent drug BLN and the highly soluble salts; after 45 min the pellet of the salt was completely dissolved and a hole was observed in the center of the pellet. All the solid forms exhibited improved dissolution rate compared to the parent drug and were stable until the end of the IDR experimental conditions as confirmed by PXRD of the residue at 45-60 min (Figure 4.16). BLNH$^+$–MSA$^-$ salt was converted to its monohydrate form as expected. We did not observe any trend between the melting point of the salt and its dissolution rate, i.e. lower melting point meaning higher IDR, similar to the trend observed for certain cocrystals.[41] The extent of solid form dissolved over 30 min was BLNH$^+$–MSA$^-$–H$_2$O 74%, BLNH$^+$–MSA$^-$ 68%, BLNH$^+$–TsO$^-$ 65%, BLNH$^+$–SUC$^-$ 51%, BLNH$^+$–NIA$^-$ 38%, BLN–SBA 6%, BLN 0.5% (Figure 4.17). BLNH$^+$–MSA$^-$ salt exhibited faster dissolution for the first 23 min but dropped below BLNH$^+$–MSA$^-$–H$_2$O salt hydrate between 23-45 min (Figure 4.17), perhaps due to conversion of anhydrous BLNH$^+$–MSA$^-$ salt to the monohydrate salt. All the salts are faster dissolving compared to BLN–SBA cocrystal. The calculated IDR values of the solid forms followed the order BLNH$^+$–MSA$^-$ > BLNH$^+$–MSA$^-$–H$_2$O > BLNH$^+$–NIA$^-$ > BLNH$^+$–TsO$^-$ > BLNH$^+$–SUC$^-$ > BLN–SBA > BLN. The salt hydrate exhibited the best dissolution rate as well as good form stability in solubility and humidity conditions. Thus, blonanserin mesylate monohydrate (BLN$^+$–MSA$^-$–H$_2$O) appears to be a soluble, stable BLN oral formulation. Moreover, the salt former MSA is completely safe (e.g. imatinib mesylate is a marketed drug, Gleevec) and several hydrates

are marketed as drugs (e.g. Paroxetine HCl hemihydrates, Paxil; Cephradine dihydrate, Velosef, and Atorvastatin calcium trihydrate, Lipitor). The solubility at 24 h and dissolution rate in the linear region of the IDR curve are summarized in Table 4.8.
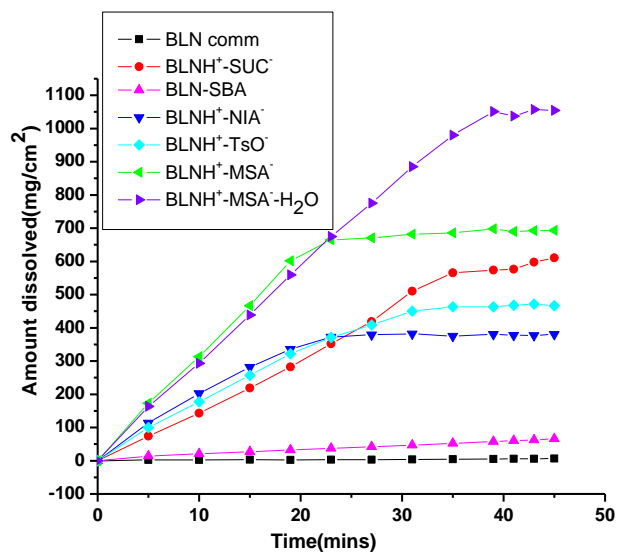
Figure 4.17 IDR curves of BLN salts.

Table 4.8 Solubility and IDR values of the BLN and its solid forms in 60% ethanol−water.

Drug/ Coformer	Solubility of coformer in water (mg/mL)	Salt/salt hydrate/ cocrystal	Solubility in 60% EtOH−water (mg/mL)	ε (mL mg^{-1} cm^{-1})	IDR in 60% EtOH−water (mg cm^{-2} min^{-1})
BLN	3.3×10^{-5}	---	1.6	9.92536	0.20
SUC	83.5	BLNH$^+$−SUC$^-$	---	9.48963	12.32 (x61.9)
SBA	11.9	BLN−SBA	39.67 (x24.7)	8.80969	1.67 (x8.4)
NIA	18.0	BLNH$^+$−NIA$^-$	408.16 (x255.1)	9.73148	15.93 (x80.0)
TsOH	620	BLNH$^+$−TsO$^-$	46.60 (x29.1)	9.11932	14.66 (x73.9)
MSA	1000.0	BLNH$^+$−MSA$^-$	---	10.44853	26.28 (x132.0)
MSA	1000.0	BLNH$^+$−MSA$^-$−H$_2$O	742.86 (x464.1)	9.92536	24.99 (x125.6)

4.5 Conclusions

Blonanserin is an antipsychotic drug of BCS class II having poor aqueous solubility. Novel crystalline salts of BLN were prepared using screening techniques. Liquid-assisted grinding and solvent evaporative crystallization with GRAS coformers resulted in four salts (BLNH$^+$–SUC$^-$, BLNH$^+$–NIA$^-$, BLNH$^+$–TsO$^-$ and BLNH$^+$–MSA$^-$), one salt hydrate (BLNH$^+$–MSA$^-$–H$_2$O), and one cocrystal (BLN–SBA) of higher solubility and dissolution rate. All the novel solid forms were characterized by thermal, spectroscopic and X-ray diffraction techniques. In all the crystal structures proton transferred to the piperazine N$_3$ atom of BLN is sustained by N$^+$–H···O$^-$ ionic H-bond, except in BLN–SBA which has neutral COOH···N(tertiary amine) H-bond. All the solid forms were stable in the laboratory storage conditions of ambient temperature and humidity over six months. These solid forms were tested in accelerated stability ICH conditions at 40 ºC and 75% RH. They were stable except BLNH$^+$–MSA$^-$ which converted to its monohydrate BLNH$^+$–MSA$^-$–H$_2$O after one month. BLNH$^+$–MSA$^-$–H$_2$O salt hydrate exhibited the highest solubility (742.9 mg/mL, 464 times) and dissolution rate (126 times) in 60% EtOH−water. Stability experiments confirmed that BLNH$^+$–MSA$^-$–H$_2$O salt hydrate is a potential lead in drug formulation of Blonanserin as a stable, soluble salt. Our objective to improve the solubility of BLN without compromising solid form stability was achieved at the end of this study.

4.6 Experimental Section

Materials and Methods: Blonanserin was purchased from Beijing Mesochem Technology Co. Ltd., China and used without further purification. The coformers (purity >99.8%) were purchased from Sigma-Aldrich, Hyderabad, India. All other chemicals were of analytical or chromatographic grade. Water purified from a deionizer-cum-mixed-bed purification system (AquaDM, Bhanu, Hyderabad, India) was used in the experiments.

Preparation of BLN solid forms

BLN$^+$–SUC$^-$ salt (1:1): BLN$^+$–SUC$^-$ salt was obtained by co-grinding BLN (100 mg, 0.272 mmol) and SUC (32.1 mg, 0.272 mmol) in stoichiometric ratio for 30 min by adding catalytic amount (two or three drops) of EtOH solvent. The formation of salt was confirmed by FT-IR, FT-Raman, ss-NMR, PXRD and DSC. Colorless single crystals suitable for X-ray diffraction were obtained upon dissolving 30 mg of ground material in 8 mL hot EtOAc−ethyl methyl ketone (1:1 v/v) solvent mixture and left for slow evaporation.

BLN–SBA cocrystal (1:0.5): This cocrystal was obtained in bulk upon co-grinding BLN (100 mg, 0.272 mmol) and SBA (23.7 mg, 0.136 mmol) in a mortar-pestle for 30 min by adding catalytic amount (two or three drops) of EtOH solvent. The product was confirmed as cocrystal by FT-IR, FT-Raman, ss-NMR, PXRD and DSC. Colorless single crystals suitable for X-ray diffraction were obtained upon crystallizing 30 mg of ground material in 8 mL hot CH_3NO_2:MeOH (1:1 v/v) solvent mixture and left for slow evaporation.

BLN$^+$–NIA$^-$ salt (1:1): This salt was obtained upon grinding about 150 mg of a 1:1 stoichiometric ratio of BLN and NIA for 30 min by liquid-assisted grinding (EtOH solvent). The formation of salt was confirmed by FT-IR, FT-Raman, ss-NMR, PXRD and DSC. 30 mg of the ground material was dissolved in 6 mL hot CH_3NO_2 and left for slow evaporation at ambient conditions. Colorless needle morphology crystals suitable for X-ray diffraction were obtained after 3-4 d upon solvent evaporation.

BLNH$^+$–TsO$^-$ salt (1:1): BLNH$^+$–TsO$^-$ salt was obtained upon co-grinding BLN (100 mg, 0.272 mmol) and p-TsOH (46.8 mg, 0.272 mmol) in a stoichiometric ratio for 30 min by liquid-assisted grinding (EtOH solvent). The formation of salt was confirmed by FT-IR, FT-Raman, ss-NMR, PXRD and DSC. The ground material (about 30 mg) was dissolved in 6 mL hot ethyl methyl ketone and left for slow evaporation at ambient conditions. Colorless needle-shaped crystals suitable for X-ray diffraction were obtained after 3-4 d upon solvent evaporation.

BLN⁺−MSA⁻ salt (1:1): This salt was obtained in bulk upon grinding about 150 mg of a 1:1 stoichiometric ratio of BLN and MSA for 30 min by liquid-assisted grinding (EtOH solvent). The formation of salt was confirmed by FT-IR, FT-Raman, ss-NMR, PXRD and DSC. 30 mg of the ground material was dissolved in 8 mL hot toluene−EtOAc solvent mixture (1:1, v/v) and left for slow evaporation at ambient conditions. Colorless needle-shaped crystals suitable for X-ray diffraction were obtained after 3-4 d upon solvent evaporation.

BLN⁺–MSA⁻–H₂O (1:1:1): This salt hydrate was obtained upon grinding about 150 mg of a 1:1 stoichiometric ratio of BLN and MSA for 1 h by liquid-assisted grinding (H_2O solvent). The formation of salt hydrate was confirmed by FT-IR, FT-Raman, ss-NMR, PXRD and DSC. About 30 mg of the ground material was dissolved in 6 mL hot iso-propanol and left for slow evaporation at ambient conditions. Colorless needle-shaped crystals suitable for X-ray diffraction were obtained after 3-4 d upon solvent evaporation.

Vibrational spectroscopy: Thermo-Nicolet 6700 Fourier transform infrared spectrophotometer with NXR-Fourier transform Raman module (Thermo Scientific, Waltham, Massachusetts) was used to record IR and Raman spectra. IR spectra were recorded on samples dispersed in KBr pellets. Raman spectra were recorded on samples contained in standard NMR diameter tubes or on compressed samples contained in a gold-coated sample holder. Data was analyzed using the Omnic software (Thermo Scientific, Waltham, Massachusetts).

Solid-state NMR spectroscopy: Solid-state ^{13}C NMR (ss-NMR) spectroscopy provides structural information about differences in hydrogen bonding, molecular conformations, and molecular mobility in the solid state.[34] The solid-state ^{13}C NMR spectra were obtained on a Bruker Ultrashield 400 spectrometer (Bruker BioSpin, Karlsruhe, Germany) utilizing a ^{13}C resonant frequency of 100 MHz (magnetic field strength of 9.39 T). Approximately 100 mg of crystalline sample was packed into a zirconium rotor with a Kel-F cap. The cross polarization, magic angle spinning (CP-MAS) pulse sequence was used for spectral acquisition. Each sample was spun at a frequency of 5.0 ± 0.01 kHz and the magic angle setting was calibrated by the KBr method. Each data set was subjected to a 5.0 Hz line broadening factor and subsequently Fourier transformed and phase corrected to produce a

frequency domain spectrum. The chemical shifts were referenced to TMS using glycine ($\delta_{glycine} = 43.3$ ppm) as an external secondary standard.

Differential Scanning Calorimetry (DSC): DSC was performed on a Mettler-Toledo DSC 822e module. Samples were placed in crimped but vented aluminum sample pans. The typical sample size is 3-4 mg, and the temperature range is 30-250 °C @ 5 °C/min. Samples were purged by a stream of dry nitrogen flowing at 80 mL/min.

X-ray crystallography: X-ray reflections for all the BLN solid forms, except BLN^+–NIA^- salt, were collected at 100 K on Bruker SMART-APEX CCD diffractometer equipped with a graphite monochromator and Mo-Kα fine-focus sealed tube ($\lambda = 0.71073$ Å). Data reduction was performed using Bruker SAINT Software.[42] Intensities were corrected for absorption using SADABS,[43] and the structure was solved and refined using SHELX-97.[44] X-ray reflections for BLN^+–NIA^- salt was collected at 298 K on Oxford Xcalibur Gemini Eos CCD diffractometer using Mo−Kα radiation ($\lambda = 0.7107$ Å). Data reduction was performed using CrysAlisPro (version 1.171.33.55)[45] and OLEX2-1.0[46] was used to solve and refine the structures. The flexible cyclooctane ring C atoms (C33A, C33B; C34A, C34B) were disordered in one of the $BLNH^+$ cation of the BLN^+−MSA^- salt and it was modeled using the FVAR command. All non-hydrogen atoms were refined anisotropically. Hydrogen atoms on heteroatoms were located from difference electron density maps and all C−H hydrogens were fixed geometrically. Hydrogen bond geometries were determined in Platon.[47] X-Seed[48] was used to prepare packing diagrams.

Powder X-ray diffraction: Powder X-ray diffraction of all the samples were recorded on Bruker D8 Advance diffractometer (Bruker-AXS, Karlsruhe, Germany) using Cu-Kα X-radiation ($\lambda = 1.5406$ Å) at 40 kV and 30 mA power. X-ray diffraction patterns were collected over the 2θ range 5-50° at a scan rate of 1°/min. Powder Cell 2.4[49] was used for Rietveld refinement of experimental PXRD and calculated lines from the X-ray crystal structure.

Solubility and dissolution measurements: The solubility of BLN solid forms were measured using the Higuchi and Connors method[50] in 60% EtOH-water medium at ambient

conditions. First, the absorbance of a known concentration of the salt/salt hydrate/cocrystal was measured at the given λ_{max} (BLN 314 nm, BLN$^+$–SUC$^-$ 314 nm, BLN–SBA 315 nm, BLN$^+$–NIA$^-$ 315 nm, BLN$^+$–TsO$^-$ 315 nm, BLN$^+$–MSA$^-$ 314 nm, BLN$^+$–MSA$^-$–H$_2$O 314 nm) in 60% EtOH-water on Thermo Scientific Evolution 300 UV-vis spectrometer (Thermo Scientific, Waltham, MA). These absorbance values were plotted against several known concentrations to prepare the concentration vs. intensity calibration curve. From the slope of the calibration curves, molar extinction coefficients for all the BLN solid forms were calculated. An excess amount of the sample was added to 4 mL of 60% EtOH-water. The supersaturated solution was stirred at 300 rpm using a magnetic stirrer at ambient conditions. After 24 h, the suspension was filtered through Whatman's 0.45 μm syringe filter. The filtered aliquots were diluted sufficiently, and the absorbance was measured at the given λ_{max}. Intrinsic dissolution rate (IDR) measurements were carried out on a USP certified Electrolab TDT-08 L Dissolution Tester (Electrolab, Mumbai, MH, India). Dissolution experiments were performed for 45 min in 60% EtOH–water at 37 °C. Prior to IDR estimation, standard curves for all the compounds were obtained spectrophotometrically at their respective λ_{max}. The slope of the plot from the standard curve gave the molar extinction coefficient (ε) by applying the Beer−Lambert's law, which was used to determine the IDR values. For IDR measurements, 500 mg of the solid material of each solid form was taken in the intrinsic attachment and compressed to a 0.5 cm^2 pellet using a hydraulic press at a pressure of 2.5 ton/inch^2 for 4 min. The pellet was compressed to provide a flat surface on one side and the other side was sealed. Then the pellet was dipped into 500 mL of 60% EtOH−water medium at 37 °C with the paddle rotating at 150 rpm. At a specific time interval, 5 mL of the dissolution medium was withdrawn and replaced by an equal volume of fresh medium to maintain a constant volume. Samples were filtered through 0.2 μm nylon filter and assayed for drug content spectrophotometrically at λ_{max} on a Thermo-Nicolet EV300 UV−vis spectrometer. There was no interference to BLN λ_{max} (314 nm) in UV-Vis with salt/cocrystal formers which absorb strongly at 210−263 nm (Table S5). The amount of drug dissolved in each time interval was calculated using the calibration curve. The linear region of the dissolution profile was used to determine the intrinsic dissolution rate (IDR) of the compound (= slope of the curve, that is, the amount of drug dissolved divided by the

surface area of the disk (0.5 cm^2) per minute). The dissolution rates for BLN and its solid forms were computed from their IDR values.

4.7 References

1. (a) J. Bernstein, *Polymorphism in Molecular Crystals*; Clarendon, Oxford, U. K., 2002. (b) F. Fabbiani, D. Allan, S. Parsons, C. Pulham, *CrystEngComm* 2005, **7**, 179. (c) P. Sanphui, N. Goud, U. Khandavilli, S. Bhanoth, A. Nangia, *Chem. Commun.*2011, **47**, 5013. (d) J. Haleblian, W. McCrone, *J. Pharm. Sci.* 1969, **58**, 911.

2. (a) R. K. Khankari, D. J. W. Grant, *Thermochimica Acta* 1995, **248**, 61. (b) R. Banerjee, P. M. Bhatt, G. R. Desiraju, *Cryst. Growth Des.* 2006, **6**, 1468. (c) S. Roy, N. R. Goud, N. J. Babu, J. Iqbal, A. K. Kruthiventi, A. Nangia, *Cryst. Growth Des.* 2008, **8**, 4343.

3. (a) A. T. M. Serajuddin, *Adv. Drug Delivery Rev.* 2007, **59**, 603. (b) S. M. Berge, L. D. Bighley, D. C. Monkhouse, *J. Pharm. Sci.* 1977, **66**, 1. (c) P. M. Bhatt, N. V. Ravindra, R. Banerjee, G. R. Desiraju, *Chem. Commun.* 2005, 1073. (d) R. Thakuria, A. Nangia, *CrystEngComm* 2011, **13**, 1759.

4. (a) J. F. Remenar, S. L. Morissette, M. L. Peterson, B. Moulton, J. M. MacPhee, H. R. Guzmán, Ö. Almarsson, *J. Am. Chem. Soc.* 2003, **125**, 8456. (b) P. Sanphui, N. R. Goud, U. B. R. Khandavilli, A. Nangia, *Cryst. Growth Des.* 2011, **11**, 4135. (c) Ö. Almarsson, M. J. Zaworotko, *Chem. Commun.* 2004, 1889. (d) D. J. Good, N. Rodríguez-Hornedo, *Cryst. Growth Des.* 2009, **9**, 2252..

5. (a) C. Leuner, J. Dressman, *Eur. J. Pharm. Biopharm.* 2000, **50**, 47. (b) A. Serajuddin, *J. Pharm. Sci.* 1999, **88**, 1058. (c) T. Vasconcelos, B.Sarmento, P. Costa, *Drug Discovery Today* 2007, **12**, 1068.

6. (a) C. G. Smith and J. J. O'Donnell, *The Process of New Drug Discovery and Development. Informa*, Newyork, 2006. (b) J. Aaltonen, M. Allesø, S. Mirza, V. Koradia, K. C. Gordon and J. Rantanen, *Eur. J. Pharm. Biopharm.,* 2009, **71**, 23.

7. C. A. Lipinski, F.Lombardo, B. W. Dominy, P. J. Feeney, *Adv. Drug Deliv.Rev.* 2012, **64**, 4.

8. (a) S. Li, H. He, L. Parthiban, H. Yin and A. T. M. Serajuddin, *J. Pharm. Sci.,* 2005, **94**, 1396. (b) A. T. M. Serajuddin, *Adv. Drug Delivery Rev*., 2007, **59**, 603.

9. (a) J. C. Chaumeil, *Clin. Pharmacol.* 1998, **20**, 211. (b) V. Kumar, L. Wang, M. Riebe, H. H. Tung, R. K. Prud homme, *Mol. Pharmaceutics,* 2009, **6**, 1118. (c) K. Amin, R.-M. Dannenfelser, J. Zielinski, B. Wang, *J. Pharm. Sci.* 2004, **93**, 2244.(d) V.P. Torchillin, Pharm. Res. 2007, **24**, 1. (e) R.A. Rajewski, V.J. Stella, *J. Pharm. Sci.* 1996, **85**, 1142.

10. (a) S. L. Childs, G. P. Stahly, A. Park, *Mol. Pharmaceutics* 2007, **4**, 323. (b) C. B. Aakeröy, M. E. Fasulo, J. Desper, *Mol. Pharmaceutics* 2007, **4**, 317. (c) S. Mohamed, D. A. Tocher, M. Vickers, P. G. Karamertzanis, S. L. Price, *Cryst. Growth Des.* 2009, **9**, 2881. (d) B. Sarma, N. K. Nath, B. R. Bhogala, A. Nangia, *Cryst. Growth Des.* 2009, **9**, 1546. (e) B.R. Bhogala, Basavoju, S. Nangia, A. *CrystEngComm* 2005, **7**, 551.

11. S. V. Sastry, J. R. Nyshadham, J. A. Fix, *Pharm. Sci. Technol. Today*, 2000, **3**, 138.

12. T. Takagi, C. Ramachandran, M. Bermejo, S. Yamashita, L. X. Yu, G. L. Amidon, *Mol. Pharm.* 2006, **3**, 631.

13. G. A. Stephenson, A. Arurub, T. A. Woods, *J. Pharm. Sci.* 2011, **100**, 1607.

14. R.N. Jashnani, R.N. Dalby, P.R. Byron, J. *Pharm. Sci.*1993, **82**, 613.

15. S. R. Perumalla, L. Shi, C. C. Sun, *CrystEngComm*, 2012, **14**, 2389.

16. W.Q. Tong, G. Alva, D. Carlton, F. Viscomi, K. Adkison, A. Millar, O. Dhingra, *A strategic approach to the salt selection of an insoluble drug candidate, 13th AAPS Meeting, New Orleans*, 1999.

17. (a) N. Blagden, M. De Matas, P. T. Gavan, P. York, *Adv. Drug Del. Rev.* 2007, **59**, 617. (b) Ö. Almarsson, M. L. Peterson, M. Zaworotko, *Pharm. Pat. Analyst*, 2012, **1**, 313. (c) R. Thakuria, A. Delori, W. Jones, M. P. Lipert, L. Roy, N. Rodríguez-Hornedo, *Int. J. Pharm.* 2013, **453**, 101. (d) A. Llinás, J. M. Goodman, *Drug Discovery Today* 2008, **13**, 198.

18. M. Oka, K. Hino, *Drugs Future* 1992, **17**, 9. (b) B. Ebdrup, H. Rasmussen, J. Arnt, B. Glenthøj, *Expert Opinion on Investigational Drugs* 2011, **20**, 1211. (c) H. Suzuki, K. Gen, *Human Psychopharmacology* 2010, **25**, 342.

19. T. R. Insel, *Nature*, 2010, **468**, 187.

20. J. Delay, P. Deniker, J. M. Harl, *Annales Médico-Psychologiques* 1952, **110**, 112.

21. (a) E. D. Deeks, G. M. Keating, *CNS Drugs* 2010, **24**, 65. (b) C. E. Heading, *IDrugs: The Investigational Drugs Journal*, 1998, **1**, 813. (c) T. Ishibashi, H. Nishikawa, T. Une, H. Nakamura, *Folia Pharmacol. Jpn.* 2008, 132.

22. T. Kishi, Y. Matsuda, H. Nakamura, N. Iwata, *J. Psychiatr. Res*. 2013, 47, 149.

23. ChemSpider: Chemical Structure Database freely distributed by the RSC, www.chemspider.com (accessed 25 January 2014).

24. S. Huilin, S. Qiang, W. Junfang, W. Xiaomei, W. Zhefeng, Patent CN101747272 (A), 2010.

25. H. Maeda, N. Ohara, US Patent 2009/0169605 A1, 2009.

26. (a) P. Sanphui, N. R. Goud, U. B. R. Khandavilli, S. Bhanoth, A. Nangia, *Chem Commun*, 2011, **47**, 5013. (b) S. Aitipamula, P. S. Chow, R. B. H. Tan, *CrystEngComm*, 2009, **11**, 1823.

27. (a) N. Shan, F. Toda, W. Jones, *Chem. Commun.* 2002, 2372. (b) A. V. Trask, W. Jones, *Top. Curr. Chem*. 2005, **254**, 41. (c) A. Dilori, T. Friščić, W. Jones, *CrystEngComm* 2012, **14**, 2350.

28. P. P. Bag, M. Patni, C. M. Reddy, *CrystEngComm* 2011, **13**, 5650.

29. Marvin, 5.10.1, 2012, ChemAxon, http://www.chemaxon.com (accessed 25 January 2014).

30. Cruz-Cabeza, A. J. *CrystEngComm* **2012**, *14*, 6362–6365.

31. (a) D. Maddileti, R. Thakuria, S. Cherukuvada, A. Nangia, *CrystEngComm*, 2012, 14, 2367. (b) M. C. Etter, *Acc. Chem. Res*. 1990, 23, 120. (c) J. Bernstein, R. E. Davis, L. Shimoni, N. L. Chang, *Angew. Chem., Int. Ed. Engl.* 1995, **34**, 1555.

32. (a) N. Shan, F. Toda, W. Jones, *Chem. Commun*. 2002, 2372. (b) A. V. Trask, D. A. Haynes, W. D. S. Motherwell, W. Jones, *Chem. Commun.* 2006, 51. (c) T. Friščić, A. V. Trask, W. Jones, W. D. S. Motherwell, *Angew. Chem. Int. Ed*. 2006, **45**, 7546.

33. (a) R. M. Silverstein, *Spectrometric Identification of Organic Compounds*. 6th Ed. John Wiley and Sons, Inc.: New York, 2002. (b) E. Smith, G. Dent, *Modern Raman Spectroscopy, A Practical Approach*, John Wiley: New York, 2005.

34. (a) F. G. Vogt, J. S. Clawson, M. Strohmeier, A. J. Edwards, T. N. Pham, Watson, S. A. *Cryst. Growth Des.* 2008, **9**, 921. (b) A. E. Aliev, K. D. Harris, *Supramolecular*

Assembly via Hydrogen Bonds I, 2004, 1. (c) A. W. Newman, S. L. Childs, B. A. Cowans, Salt Cocrystal Form Selection, In *Preclinical Development Handbook*; John-Wiley, Hoboken, 2008, 455.

35. A.Burger, R. Ramberger, *Mikrochim. Acta II* 1979, 259.

36. J. F. Remenar, M. L. Peterson, P. W. Stephens, Z. Zhang, Y. Zimekov, M. B. Hickey, *Mol. Pharmaceutics* 2007, **4***, 386. (b) S. Karki, T. Friščić, L. Fábián, W. Jones, *CrystEngComm* 2010, **12**, 4038.

37. S. Huilin, S. Qiang, W. Junfang, W. Xiaomei, Zhefeng, Patent CN101747274 (A), 2010.

38. http://www.ich.org/fileadmin/Public_Web_Site/ICH_Products/Guidelines/Quality/Q1F/Stability_Guideline_WHO.pdf (accessed 25 January 2014).

39. J. B. Dressman, G. L. Amidon, C. Reppas, V. P. Shah, *Pharm. Res.* 1998, **15**, 11.

40. L. X. Yu, A. S. Carlin, G. L. Amidon, A. S. Hussain, *Int. J. Pharm.* 2004, **270**, 221.

41. (a) N. Schultheiss, A. Newman, *Cryst. Growth Des.* 2009, **9**, 2950. (b) M. K. Stanton, A. Bak, *Cryst. Growth Des.* 2008, **8**, 3856. (c) R. Abramowitz, S. H. Yalkowsky, *Pharm. Res.* 1990, 7, 942.

42. *SAINT-Plus*, version 6.45; Bruker AXS Inc.: Madison, Wisconsin, U.S.A., 2003.

43. SADABS, *Program for Empirical Absorption Correction of Area Detector Data*; , G. M. SheldrickUniversity of Göttingen: Göttingen, Germany, 1997.

44. (a) *SMART*, version 5.625 and *SHELX-TL*, version 6.12;, Bruker AXS Inc.: Madison, Wisconsin, USA, 2000. (b) G. M. Sheldrick, *SHELXS-97* and *SHELXL-97*; University of Göttingen: Göttingen, Germany, 1997.

45. *CrysAlis CCD and CrysAlis RED*, Ver. 1.171.33.55; Oxford Diffraction Ltd: Yarnton, Oxfordshire, U.K., 2008.

46. O. V. Dolomanov, A. J. Blake, N. R. Champness, M. Schröder, *J. Appl. Crystallogr.* 2003, **36**, 1283.

47. A. L. Spek, *PLATON, A Multipurpose Crystallographic Tool*; Utrecht University: Utrecht, Netherlands, 2002.

48. L. J. Barbour, *X-Seed*, *Graphical Interface to SHELX-97 and POV-Ray*, *Program for Better Quality of Crystallographic Figures*; University of Missouri-Columbia, Missouri, U.S.A., 1999.

49. Powder Cell, *A Program for Structure Visualization, Powder Pattern Calculation and Profile Fitting*, http://www.ccp14.ac.uk/index.html (accessed 25 January 2014).

50. T. Higuchi, K. A. Connors, *Adv. Anal. Chem. Instrum.* 1965, **4**, 117.

CHAPTER FIVE

## POLYMORPHISM IN ANTI-HYPERAMMONEMIC AGENT N-CARBMOYL-L-GLUTAMIC ACID
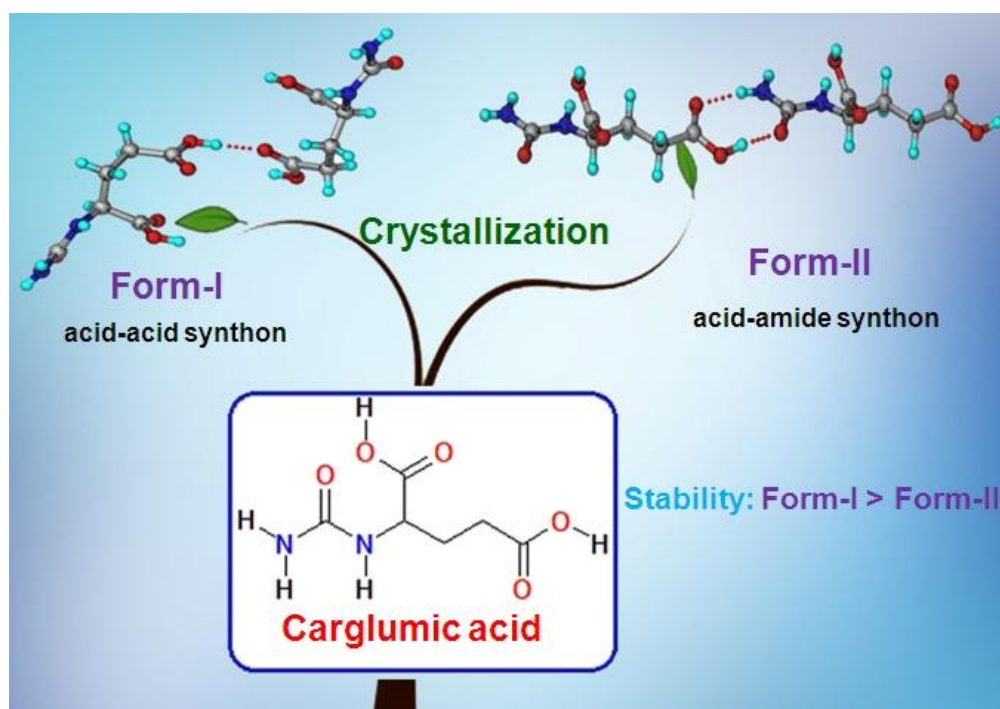
Solid form screen of anti-hyperammonemic drug carglumic acid (CGA) resulted in two polymorphs Form-I and Form-II. The crystal structure of Form-I is sustained by acid catemer synthon whereas Form-II has acid-amide heterosynthon. Slurry grinding, thermal stress, stability measurements, and DVS analysis confirm the thermodynamic stability of Form-I.

5.1 Introduction

Carglumic acid is an orphan drug used for the treatment of hyperammonaemia in patients with N-acetylglutamate synthase (NAGS) deficiency.[1] NAGS deficiency is one the most severe and rarest of the hereditary urea cycle disorders (UCDs). This rare genetic disorder results in elevated levels of ammonia in the blood, which can eventually cross the blood-brain barrier and cause neurologic problems, cerebral edema, coma, and eventually death. CGA is a structural analogue of N-acetylglutamate, the naturally occurring activator of carbamoyl phosphate synthetase (CPS) and helps to break down ammonia to reduce concentration in blood and toxic effects.[2] CGA was approved by the U.S. Food and Drug Administration (FDA) in 2010 to treat hyperammonemia because it can act as a replacement for NAG in NAGS deficient patients by activating CPS.[3] It is sold under the brand name Carbaglu which is formulated as a water-dispersible tablet and each tablet contains 200 mg of carglumic acid and excipients. CGA is an acidic drug molecule in the form of white crystalline powder having aqueous solubility of 19.1 mg/mL[4] and is practically insoluble in organic solvents, perhaps due to high density of functional groups (dicarboxylic acid and urea) in a small molecule. Studies on hyperammonemia are limited due to the rarity of the disease. The condition is particularly toxic to the central nervous system (CNS).[5] X-ray crystal structure of the analog N-acetylglutamate is reported[6] (CSD Refcode TERRUD and TERRUD01, multiple determinations of the same structure), but no crystal structure of CGA was found in the Cambridge Structural Database (ver. 5.36, November 2014 update).[7] In view of the importance of polymorphism in pharmaceuticals[8] to control physicochemical properties, solubility, stability, dissolution rate, melting point, bioavailability,[9] etc., CGA was screened by different techniques such as liquid-assisted grinding (LAG), slurry crystallization, solvent removal in rotavap, freeze drying, spray drying, and solution crystallization.[10] Two novel polymorphs named Form-I, and Form-II and a degraded derivative of CGA, hydantoin-5-propionic acid (5-HPA) are reported(5-HPA, chemical name 3-(2,5-dioxoimidazolidin-4-yl) propanoic acid).   .

5.2 Results and Discussion

Since the API is routinely exposed to various conditions ranging from production to tableting to transportation before consumption, the risk of process-induced transformations and stability of polymorphs must be properly understood for phramaceuticals.[11] Thus, a sound understanding of a polymorphic system is a prerequisite for product quality and performance. Even though strong hydrogen bonding functional groups COOH and urea are present in CGA molecule, which generally promote crystallization, we had to try a range of solvent systems and mixtures to obtain diffraction quality crystals. A majority of crystallization experiments gave microcrystalline powders which matched with the PXRD pattern of the starting material (form-I). Solubility of CGA in aqueous medium is very high but in organic solvents it is practically insoluble. This limitation narrowed down the variety of solvents which could be used for crystallization screen, and hence mostly Form-I was observed. Form-I was crystallized by slurring in EtOH, freeze drying in water (lyophilization), and spray drying from water. Novel form-II was produced upon rotovaporization of CGA in water : acetone (1:5 v/v solvent) (see Experimental Section). The above procedures were optimized to obtain reproducibly pure polymorphs I and II. A degradation derivative of CGA, 5-HPA, was serendipitously obtained upon solution crystallization of CGA from 2-butanone : propionic acid (1:1 v/v) (Scheme 5.1). The three crystal structures illustrate acid-acid catemer and dimer, amide-amide homodimer, and acid-amide heterosynthons[12] (Scheme 5.2). In this paper we describe two novel forms and one degraded form of CGA, which are fully characterized by spectroscopic (FT-IR, ^{13}C ss-NMR), thermal (DSC), field emission scanning electron microscopy (FESEM), powder X-ray diffraction (PXRD), and their structures were confirmed by single crystal X-ray diffraction. Crystallographic parameters of the novel forms and their hydrogen bonds are listed in Table 5.1 and Table 5.2.

L-Carglumic acid, CGA   Hydantoin-5-propionic acid, 5-HPA
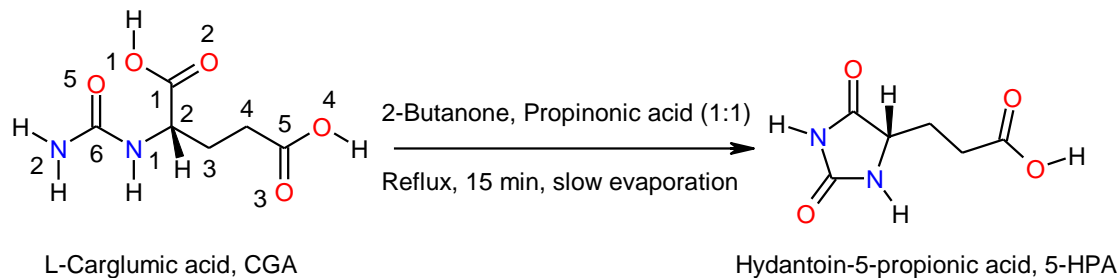
Scheme 5.1 The transformation of CGA to 5-HPA during crystallization. The natural L-glutamic acid S-configuration is shown.

acid-acid catemer   acid-acid dimer   acid-amide   amide-amide
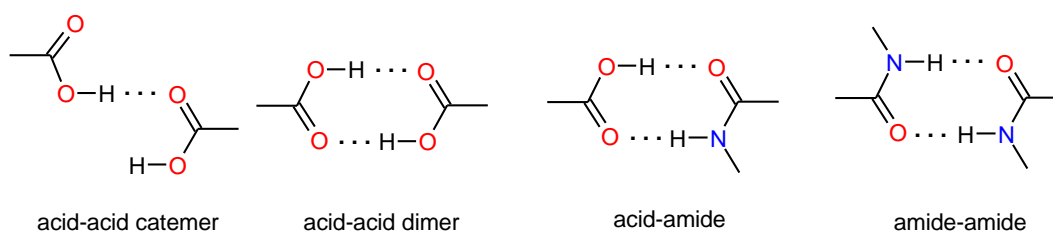
Scheme 5.2 Hydrogen bonded synthons in crystal structures.

5.2.1 Molecular Geometry

The chemical structure of CGA (Scheme 1) indicates that the conformationally flexible molecule will exhibit different torsion angles. The two symmetry-independent molecules in the asymmetric unit of Form-II are labeled A and B. The values of τ_1 (C2-C3-C4-C5) and τ_2 (C6-N1-C2-C1) are 79.7°, 81.26° in form-I, and 177.4°, −55.8° for molecule A, and 178.7, −57.6° for molecule B in form-II respectively. The main difference in the torsion angles of both Forms-I and II was observed for τ_1 in the alkyl chain portion (C2-C3-C4-C5 $\Delta\tau$ about 100°, see Table 5.3) for these conformational polymorphs.[13] The overlay diagram of the CGA molecules from Form-I and II shows conformational changes (Figure 5.1). From the molecular overlay and structural analysis we can classify both forms as conformational and synthon polymorphs. Reflections data were collected using Mo-Kα X-radiation and the S-configuration at the chiral center in the molecule was assigned based on the natural L-glutamic acid derived starting material.
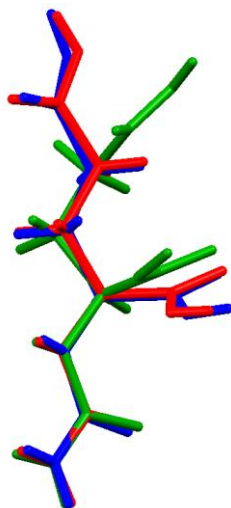
Figure 5.1 Overlay diagram of CGA molecules in form-I and II. Color code: Green = Form-I, Red = CGA-Form-IIA, Blue = CGA-Form-IIB. Note that A and B are the two symmetry-independent molecules in the crystal structure of the Form-II.

Table 5.3 Shows that difference in the torsion angle in both the forms (Form-I and Form-II).

Torsion angles (τ)	CGA-Form-I	CGA-Form-II molecule A/molecule B
C2-C3-C4-C5 (τ_1)	79.72°	177.35°/178.73°
C6-N1-C2-C1 (τ_2)	81.26°	-55.77°/-57.59°
N1-C2-C3-C4 (τ_3)	176.89°	-175.87°/-168.49°

5.2.2 Crystal Structure Analysis

Form-I: Upon crystallizing CGA of commercial pharmaceutical grade from MeOH : 2-butanone (1:1 v/v) needle shaped crystals were obtained which solved and refined in the orthorhombic space group $P2_12_12_1$. CGA molecules are connected by the acid catemer synthon of C(4) graph set notation,[14] which is stabilized by C–H···O (2.58 Å, 144º) interaction resulting in a 1D tape along [100] (Figure 5.2a). The second carboxylic acid and N-carbamoyl groups are connected through N–H···O=C (acid) (1.90 Å, 167º) and N–H···O=C (carbamoyl) (2.09 Å, 147º) H-bonds resulting in R_2^2 (11) motif.[14] Such tapes are

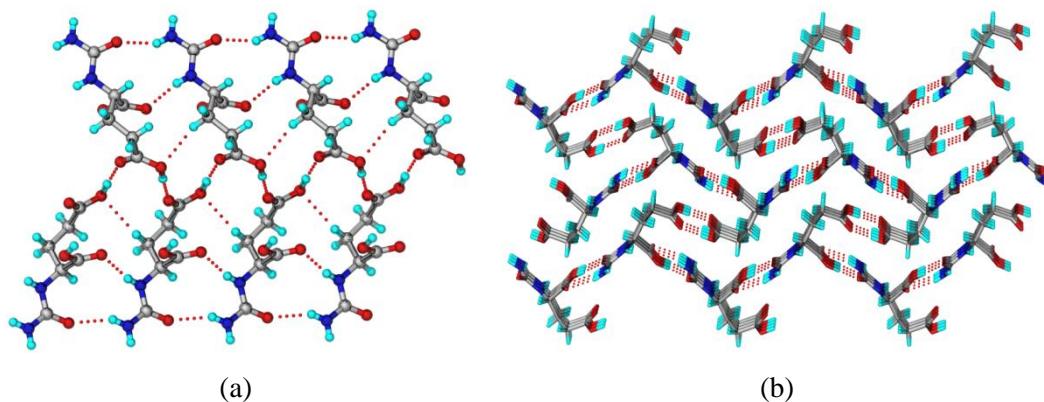inter-connected through acid-amide R_2^2 (8) heterosynthon in a corrugated sheet structure (Figure 5.2b).

(a)   (b)

Figure 5.2 (a) 1D tape formed through acid-acid C(4) catemer and supporting C–H···O and N–H···O interactions. (b)   Acid-acid C(4) chain and acid-amide R_2^2 (8) heterosynthon resulting in a corrugated structure.

Form-II: Crystallization of CGA from CH_3CN: m-cresol (1:1 v/v) mixture afforded block crystals which were solved and refined in the monoclinic space group *P2₁* with two molecules of CGA in the asymmetric unit. One of the carboxylic acid and N-carbamoyl group of CGA forms acid-amide R_2^2 (8) motif (N–H···O: 1.90 Å, 167º; 1.94 Å, 160º; O–H···O: 1.63 Å, 172º; 1.66 Å, 170º) resulting in an infinite linear chain along the [001] direction (Figure 5.3a). These chains extend in a 2D sheet parallel to the (020) plane, being connected to the other carboxylic acid and carbamoyl group through N–H···O=C (acid) (1.82 Å, 173º; 1.86 Å, 156º) and N–H···O=C (carbamoyl) (2.21 Å, 147º; 2.25 Å, 146º) bonds (Figure 5.3b). Adjacent sheets are connected through O–H···O (1.73 Å, 166º; 1.73 Å, 166º) hydrogen bonds resulting in ladder like structure, and C−H···C short contacts connect these ladders (Figure 5.3c).
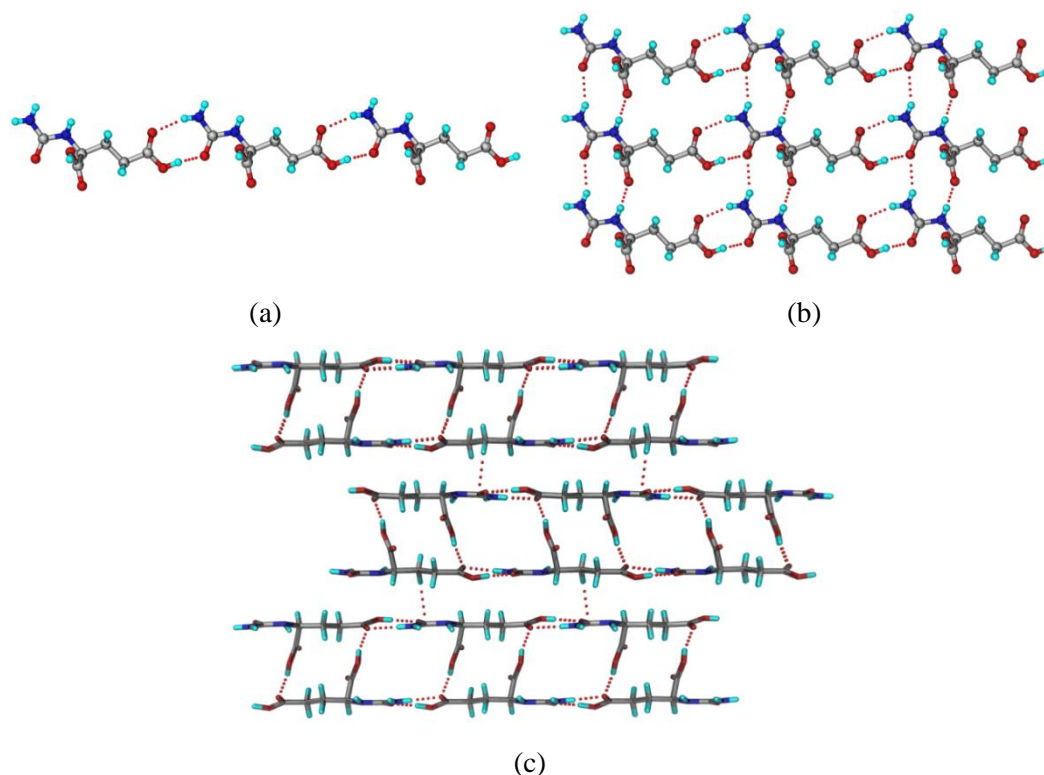
(a)　　　　　　　　　　　　　　　　　　(b)

(c)

Figure 5.3 (a) An infinite linear chain formed through acid-amide R_2^2 (8) heterosynthon. (b) Hydrogen bonded 2D sheet structure formed through N–H⋯O interactions. (c) O–H⋯O and C−H⋯π interactions in the inter-sheet region viewed down the a-axis.

Hydantoin-5-propionic acid (5-HPA): Hydantoin-5-propionic acid (5-HPA, chemical name 3-(2,5-dioxoimidazolidin-4-yl) propanoic acid) was obtained as a by-product of crystallization of CGA from 2-butanone : propionic acid (1:1 v/v). The structure was solved and refined in monoclinic space group *P2₁* with two molecules of 5-HPA in the asymmetric unit. The molecules form an infinite linear chain through acid-acid R_2^2 (8) (O–H⋯O: 1.72 Å, 171º; 1.74 Å, 172º) and amide-amide R_2^2 (8) (N–H⋯O: 1.79 Å, 171º; 1.81 Å, 161º) homosynthon. Such chains are inter-connected through N–H⋯O (1.88 Å, 168º; 1.89 Å, 176º) and C–H⋯O (2.58 Å, 161º; 2.62 Å, 144º) H-bonds in a corrugated 2D sheet, with weak C–H⋯O (2.48 Å, 139º; 2.53 Å, 137º; 2.29 Å, 145º) interactions to complete the structure (Figure 5.4).
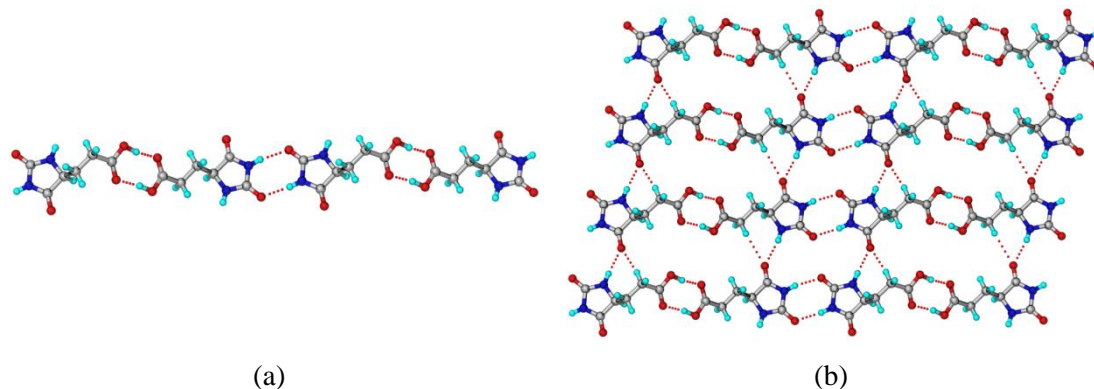
(a)   (b)

Figure 5.4 (a) Infinite linear chain formed through acid-acid R_2^2 (8) and amide-amide R_2^2 (8) homosynthons. (b) A 2D corrugated sheet structure assembled through N–H⋯O and C–H⋯O interactions.

Table 5.1 Cystallographic parameters of CGA polymorphs and 5-HPA.

	CGA–Form-I	CGA–Form-II	Hydantoin-5 propionic acid (5-HPA)
Emp form.	C6 H10 N2 O5	C6 H10 N2 O5	C6 H8 N2 O4
Form wt	190.16	190.16	172.14
Cryst syst	Orthorhombic	monoclinic	monoclinic
Sp gr	$P2_12_12_1$	$P2_1$	$P2_1$
T/K	100(2)	100(2)	298(2)
a/Å	5.1179(8)	5.3615(5)	6.2475(4)
b/Å	12.2079(18)	15.8123(15)	7.1111(6)
c/Å	12.7508(19)	9.9631(9)	17.3692(11)
α/°	90	90	90
β/°	90	90.899(2)	96.792(5)
γ/°	90	90	90
Z	4	4	4
V/Å^3	796.7(2)	844.54(14)	766.24(10)
D_{calc}/g cm^{-3}	1.585	1.496	1.492
μ/mm^{-1}	0.139	0.131	0.127
Rflns collect	8323	8820	3079
Unique rflns	1576	3335	2191
Obsd rflns	1532	3159	1973
R_1 [I>2σ(I)]	0.0264	0.0323	0.0362
wR_2 [all]	0.0632	0.0777	0.0804
GOF	1.089	1.049	1.068

Table 5.2 Hydrogen bond metrics in the crystal structures.

D–H···A	H···A (Å)	D···A (Å)	D–H···A (°)	symmetry code
		CGA–Form-I		
O1–H1···O5	1.63	2.548(1)	167	-x+1,+y+1/2,-z+1/2+1
O4–H5···O3	1.72	2.660(2)	176	x-1/2,-y+1/2+2,-z+1
N1–H6···O2	1.90	2.914(2)	167	x+1,+y,+z
N2–H2A···O5	2.09	3.009(2)	147	x+1,+y,+z
N2–H2B···O2	2.09	3.084(2)	161	-x+1,+y-1/2,-z+1/2+1
C3–H3A···O4	2.58	3.515(2)	144	x+1,+y,+z
		CGA–Form-II		
O1–H1···O8	1.73	2.662(2)	171	x,y,z
O4–H5···O5	1.66	2.587(2)	170	x,+y,+z-1
O6–H7···O3	1.73	2.664(2)	166	x-1,+y,+z
O9–H11···O10	1.63	2.558(2)	172	x,+y,+z+1
N1–H6···O2	1.82	2.841(2)	173	x+1,+y,+z
N2–H2A···O5	2.25	3.159(2)	146	x+1,+y,+z
N2–H2B···O3	1.90	2.915(2)	167	x,+y,+z+1
N3–H12···O7	1.86	2.832(2)	156	x+1,+y,+z
N4–H13A···O8	1.94	2.931(2)	160	x,+y,+z-1
N4–H13B···O10	2.21	3.119(2)	147	x+1,+y,+z
C4–H4A···O6	2.39	3.299(2)	141	x,y,z
C9–H9B···O2	2.63	3.505(2)	138	x,y,z
C10–H10A···O1	2.44	3.381(2)	145	x-1,+y,+z
		Hydantoin-5-propionic acid (5-HPA)		
O1–H1···O6	1.72	2.646(3)	171	x, y, z
O5–H7···O2	1.74	2.670(3)	172	x, y, z
N1–H5···O4	1.89	2.914(2)	176	x-1,+y,+z
N2–H6···O7	1.79	2.820(2)	171	x+1,+y, +z+1
N3–H11···O8	1.88	2.900(2)	168	x+1,+y,+z
N4–H12···O3	1.81	2.801(2)	161	x-1,+y,+z-1
C2–H2A···O1	2.29	3.239(4)	145	-x+1,+y-1/2,-z+1
C2–H2B···O4	2.58	3.618(3)	161	x-1,+y,+z
C3–H3A···O5	2.53	3.397(3)	137	-x+2,+y-1/2,-z+1
C8–H8A···O8	2.62	3.551(3)	144	x+1,+y,+z
C10–H10···O3	2.48	3.365(3)	139	-x+1,+y+1/2,-z+1

5.2.3 Spectroscopic Characterization

IR spectroscopic analysis of CGA forms showed significant differences in the vibrational patterns of their functional groups.[15] The NH_2 asymmetric stretch of $C(=O)NH_2$ in Form-I gives a strong band at 3439.9 cm^{-1} and symmetric NH_2 stretch at 3344.3 cm^{-1} with a somewhat weaker intensity, whereas for secondary NH stretch it showed peaks at 3295.4 cm^{-1}. The asymmetric and symmetric stretching frequencies of $C(=O)NH_2$ in Form-II appeared at 3454.3 cm^{-1} and 3315.3 cm^{-1}, and for secondary NH at 3247.3 cm^{-1}. The C=O stretching vibration of the carboxylic acid gave a strong absorption at 1728.5 cm^{-1} in Form-I and 1709.9 cm^{-1} in Form-II. The stretching frequencies for amide C=O resonated at 1697.3 cm^{-1} in Form-I and 1666.9 cm^{-1} in Form-II. The signature frequencies are listed in Table 5.4 and spectra are presented in Figure 5.5.
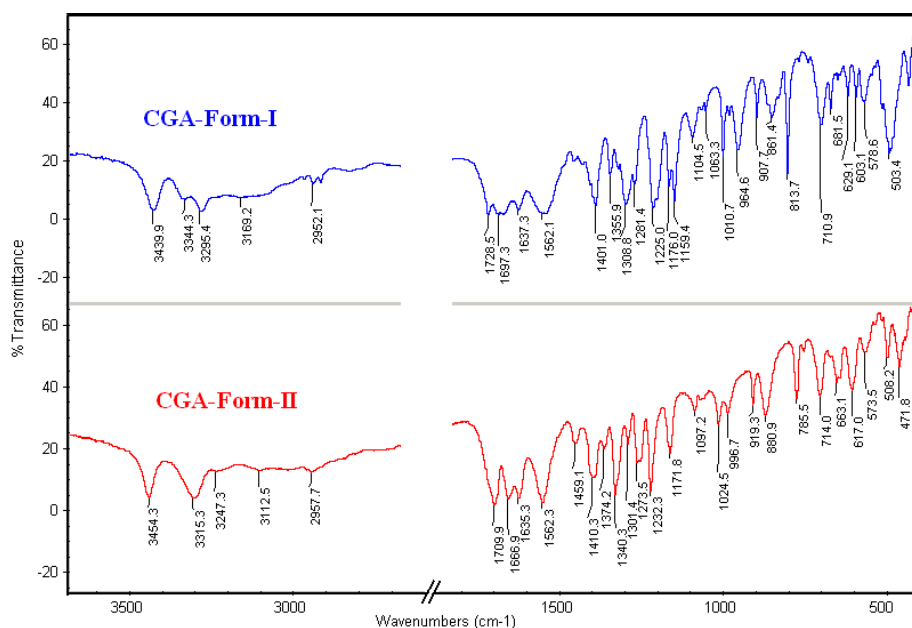

Figure 5.5 FT-IR spectral comparison of CGA forms indicate that there is significant differences in stretching frequencies between the two polymorphs.

Table 5.4 Summary of FT-IR stretching frequencies of CGA polymorphs.

Drug forms	1° and 2° N–H stretch (cm^{-1})	C–H Stretch (cm^{-1})	Carboxylic C=O stretch (cm^{-1})	Amide C=O stretch (cm^{-1})	O–H stretch (cm^{-1})
CGA-Form-I	3439.9 3344.3 3295.4	2952.1	1728.5	1697.3	3169.2
CGA-Form-II	3454.3 3315.3 3247.3	2957.7	1709.9	1666.9	3112.5

We also characterized CGA forms through solid-state NMR because this technique provides information about differences in hydrogen bonding, molecular environment, and local short range differences.[16] ^{13}C solid-state NMR spectra are presented in Figure 5.6. The chemical shift values of the alkyl chain of CGA did not exhibit significant differences for C2, C3, C4 and also for amide C6 atoms (Figure 5.6, Table 5.5). The carboxylic acid C1 and C5 atoms showed peak values at 175.4, 179.4 ppm in Form-I where as in Form-II in addition to the C1 and C5 (175.3, 179.4 ppm) peak positions two extra peaks were observed at 177.33 and 181.7 ppm, which is due to the two molecules in the asymmetric unit for Form-II (from X-ray analysis).
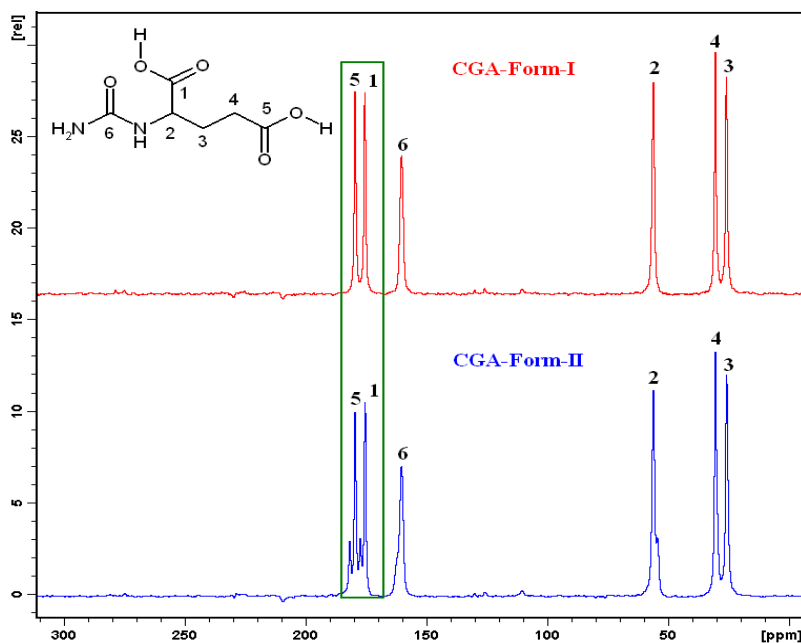
Figure 5.6 ^{13}C ss-NMR spectrum of CGA polymorphs shows that there is significant difference in chemical shifts. Multiple peaks for carboxylic C atoms in the Form-II represent the two molecules in the asymmetric unit.

Table 5.5 ^{13}C ss-NMR chemical shift values (δ, ppm) of CGA Polymorphs

Carbon No.	CGA-Form-I	CGA-Form-II
C1	175.43	175.36, 177.33
C2	55.85	55.83
C3	25.62	25.56
C4	30.35	30.31
C5	179.47	179.44, 181.67
C6	160.19	160.18

5.2.4 Powder X-ray diffraction

CGA Forms-I and II are readily distinguishable by their unique powder XRD line patterns[17] (blue lines in Figure 5.7). The experimental PXRD pattern of commercial CGA matches with the calculated pattern of CGA Form-I. Bulk material of novel Form-II prepared by rotovaporization exhibited unique powder diffraction line pattern that matches with the calculated pattern single crystal X-ray crystal structure for Form-II (Figure 5.7). The small

differences in the overlay of peaks of the experimental PXRD and the calculated lines of CGA-Form-II crystal structure may be due to temperature effect (300 K for experimental PXRD and 100 K for SC-XRD). The two polymorphs did not show any phase transformation up to heating at 160 °C in independent experiments as monitored by PXRD.
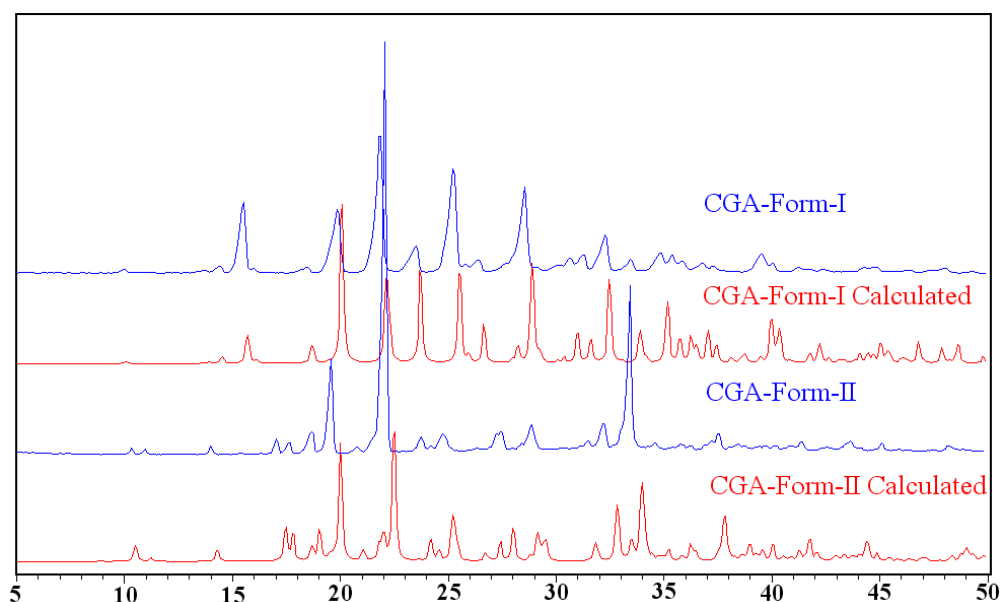

Figure 5.7 PXRD overlay of experimental patterns of the CGA forms exhibit unique powder lines and match to the calculated lines from the respective crystal structures.

5.2.5 Thermal and FESEM analysis

After confirming the bulk purity of the polymorphic materials, DSC analysis[18] was carried out to understand their thermodynamic relationship. No phase transformation was observed prior to melting at 167.9 °C for Form-I and 160.6 °C for Form-II (Figure 5.8, Table 5.6). The high melting polymorph Form-I has a higher heat of fusion (48.4 kJ/mol) while the lower melting polymorph Form-II has a lower heat of fusion (36.5 kJ/mol), and hence both the polymorphs are monotropically related.[19] Both the forms were kept at 160 °C for 40 min in programmable oven to see the thermal effect; they were stable and no phase transformations were observed confirming the DSC measurements. Thus Form-I is the stable polymorph with higher enthalpy of fusion and higher melting point. The broad endotherm for Form-II

was observed in multiple batches. Normally a broad endotherm in DSC implies that there is some other event such as, phase transformation, water evolution, occurring along with the melting process or due to low thermal conductivity of sample, kinetic effects, etc. The exact reason for a broad endotherm for Form-II but a sharp peak for Form-I is not clear at the moment. What we did observe for both Form-I and II is that heating the sample just beyond the melting point, cooling to room temperature and then re-heating did not show any DSC peak at the same temperature (Figure 5.9). This implies some kind of chemical transformation of the sample on heating.
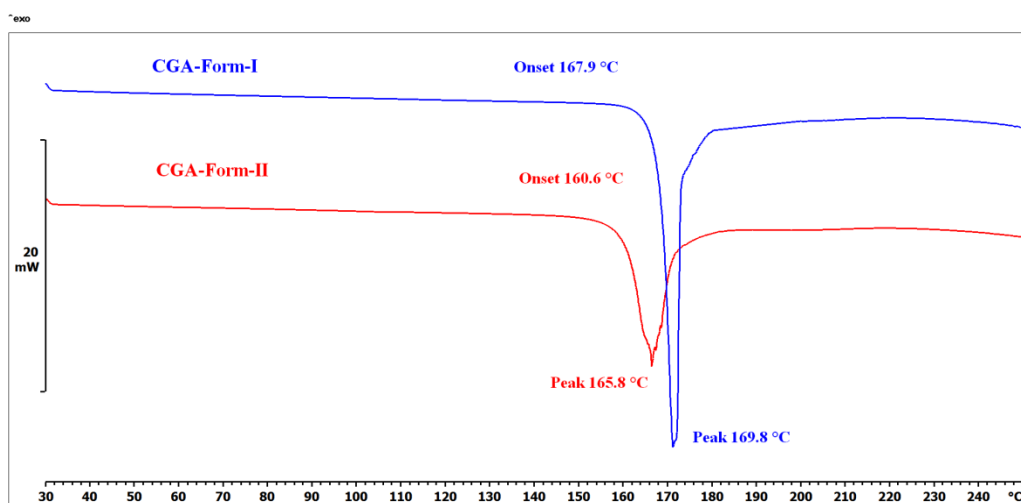

Figure 5.8 DSC thermograms of CGA Forms-I and II to show direct melting without any phase transition.
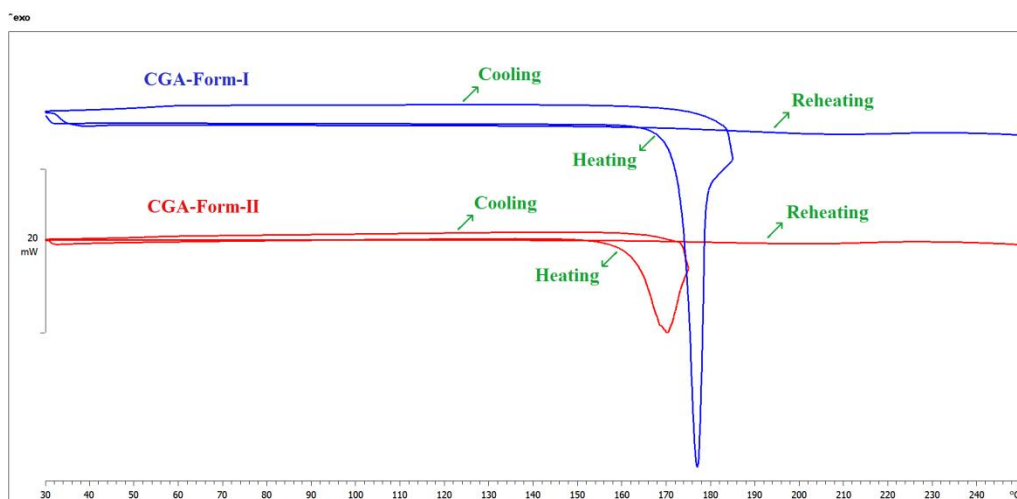
Figure 5.9 Heat-cool-heat experiments on (a) Form-I as well as (b) Form-II showed no phase transition events at the melting temperature suggesting that some kind of decomposition of CGA takes place upon heating to the melting temperature.

Table 5.6 Melting point and enthalpy values of CGA forms.

CGA Forms	M.p. (°C) T_{onset}/ T_{peak}	ΔH_{fus} kJ/mol	Packing fraction (%)	Stability relation
CGA–Form-I	167.98/169.82	48.4	73.8	Monotropic, Form-I is thermodynamic
CGA–Form-II	160.61/165.79	36.5	69.4	

Field emission scanning electron microscopy is extremely informative for pharmaceutical solids to understand their morphology at the nm scale.[20] The individual polymorphs were spread uniformly on a carbon coated copper grid and then FESEM was recorded (Figure 5.10). Form-I appeared as needle and Form-II was found to be block morphology at 20 μm magnification scale, and these observed morphologies were in excellent match with those of the single crystals mounted for X-ray diffraction.
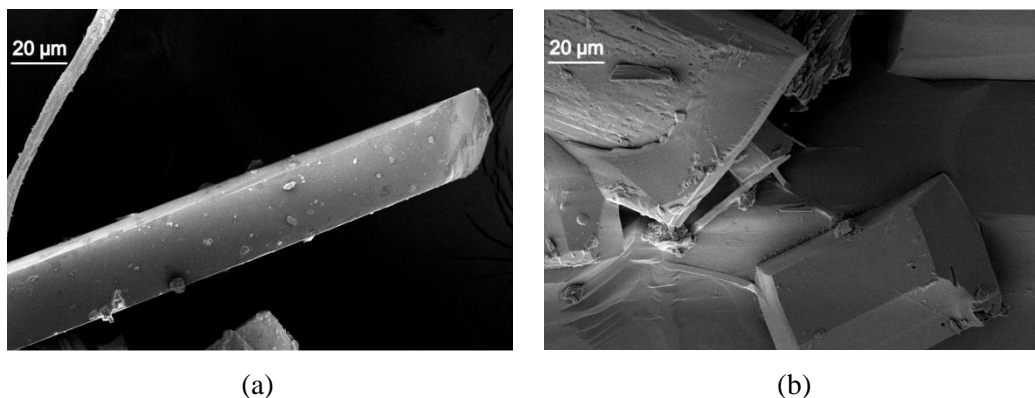
<center>(a)   (b)</center>

Figure 5.10 SEM images of CGA polymorphs (a) Form-I (b) Form-II to show the differences in morphology and bulk particles.

5.2.6 Hirshfeld surface and 2D fingerprint plots

Hirshfeld molecular surfaces[21] and the associated fingerprint plots generated using CrystalExplorer 3.0 on the basis of X-ray diffraction provides quantitative differences between polymorphs. The d_{norm} Hirshfeld surfaces are displayed using a red–white–blue color scheme, where red highlights shorter contacts, white is used for contacts around the van der Waals separation and blue is for longer contacts. The surfaces are shown as transparent to allow visualization of the orientation of the molecule and to show the conformational differences of the CGA molecules in both the Forms-I and II. Figure 5.11 presents Hirshfeld surfaces of the molecules in both the polymorphs. In Form-I, three large circular depressions (deep red) visible on the top left of the surface are indicative of hydrogen-bonding (O–H···O) contacts, and additional faint red circles one on top left and other is on right are from the N–H···O hydrogen bonds (Figure 5.11a). In general, the color intensity is high for stronger interactions, and this was observed for Form-I with shorter H-bonds (O–H···O: 1.63 Å, 167º, 1.72 Å, 176º; N–H···O: 1.90 Å, 167º, 2.09 Å, 147º). For Form-II (Figure 5.11b) there are three red regions on the left of the surface, two intense large circles due to the strong O–H···O (1.73 Å, 171º, 1.63 Å, 172º) and also from N–H···O (1.94 Å, 160º) bonds. Additional red regions at the left and right of the surface arise from the N–H···O (1.86 Å, 156º) and O–H···O (1.73 Å, 166º) contacts.
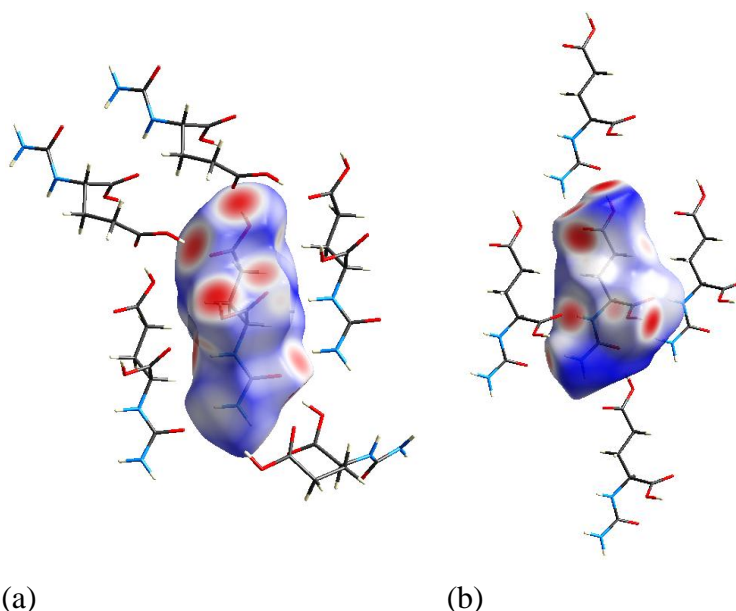
(a)   (b)

Figure 5.11 Hirshfeld surfaces with mapped d_{norm} property and neighboring molecules for (a) Form-I and (b) Form-II projected and transparency to show the conformation of the molecules in the forms.

Hirshfeld surfaces and fingerprint plots proved to be particularly suited for comparing environments of structures with $Z' > 1$ where the complex interplay between crystallographically unique molecules could be rationalized in terms of the complementary surface regions. In Figure 5.12, d_i represents the distance from the surface to the nearest atom in the molecule itself, and d_e the distance to the nearest atom outside the molecule. In Form-I, presence of long sharp spikes towards the lower left corner near $d_e + d_i \approx 1.6$ Å of the plot indicates O···H interactions and it is a characteristic for strong hydrogen bonds resulting from N−H···O and O−H···O and C−H···O hydrogen bonds (Figure 5.12). The contribution of these interactions to the Hirshfeld surfaces is 53.2% in Form-I (Figure 5.13). Two sharp spikes are present for Form-II as well, but because of two molecules in the asymmetric unit of Form-II structure, the contribution of O···H interactions increase (57.8% for molecule A and 56.6% for molecule B) (Figure 5.13). Overall there are more numerous short O···H interactions (from N−H···O, O−H···O, C−H···O) in Form-II. The wings for C−H···C interactions are slightly different for the two forms due to the different methylene CH atoms involved in C···H interactions, but their contribution is very low (2-3%) (Figure

5.13). The H··H interaction values are in a similar range (33% for Form-I and 31, 32% for Form-II). The calculated density and packing efficiency of the thermodynamic Form-I is higher (1.585 g cm^{-3}, 73.8%; vs. 1.496 g cm^{-3}, 69.4%).
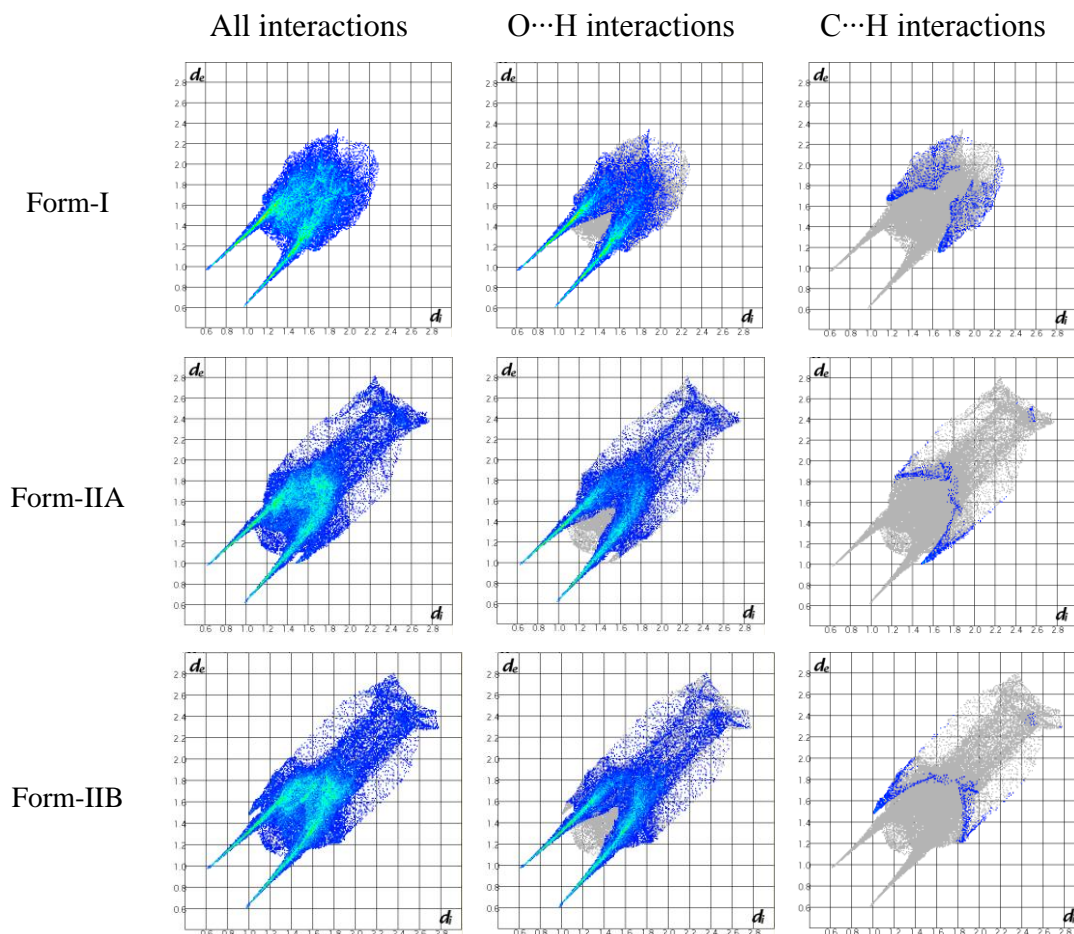

Figure 5.12 2D Hirshfeld fingerprint plots for Form-I and Form-II. Note that the A and B represent the two crystallographically independent molecules in Form-II.
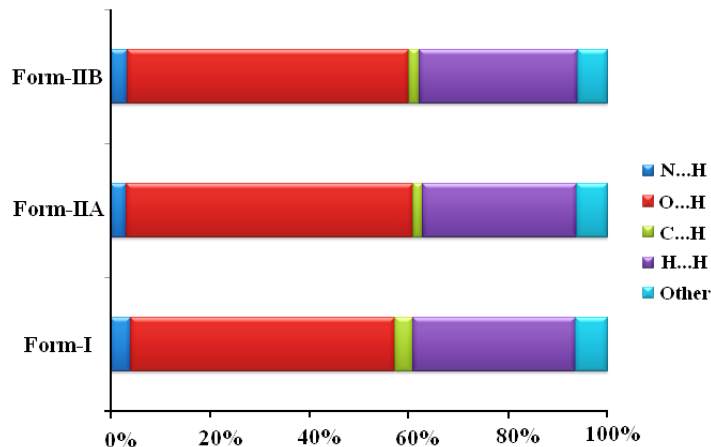
Figure 5.13 Contribution of major interactions to the Hirshfeld surface for Form-I and Form-II of CGA.

5.2.7 Grinding and Solvent Mediated Transformations

The most suitable form for drug formulation is the one which exhibits an appropriate balance between solubility and stability. Therefore, it is important to establish the stability of polymorphic systems. Solution mediated polymorphic transformation is a fast, easy, and reliable method to determine the stable polymorph under conditions relevant to pharmaceutical tablets. Hence, slurry grinding experiments were performed on CGA polymorphs in a range of solvents, e.g. water, ethanol, pentane, alkaline pH 9.0 solution, and acetic acid pH 2.4 solution. Both the polymorphs were subjected to slurry grinding separately in these solvents to understand the effect of solvent on the stability outcome of solvent-mediated processes. Upon slurry grinding in water, ethanol, and pentane pure Form-I was stable for 48 h. Pure Form-II converted into Form-I in 10-12 h in water and ethanol but in pentane it took 24 h for conversion to Form-I (Figure 5.14). Interestingly, slurry experiments on Form-I at alkaline pH 9.0 and acetic acid pH 2.4 solutions was found to convert to Form-II after 24 h, whereas Form-II under similar experimental conditions was found to be stable for 24 h. We did not observe trends such as non polar solvents preferentially give metastable form whereas polar solvents give stable forms,[22] however in our study alkaline pH 9.0 and acetic acid pH 2.4 solutions resulted in metastable Form-II. In

competitive slurry experiments, wherein a mixture of the two forms was taken in 1:1 ratio, the product was pure Form-I (in water, ethanol, and pentane) after 8-10 h of slurry (Figure 5.15 and Figure 5.16).
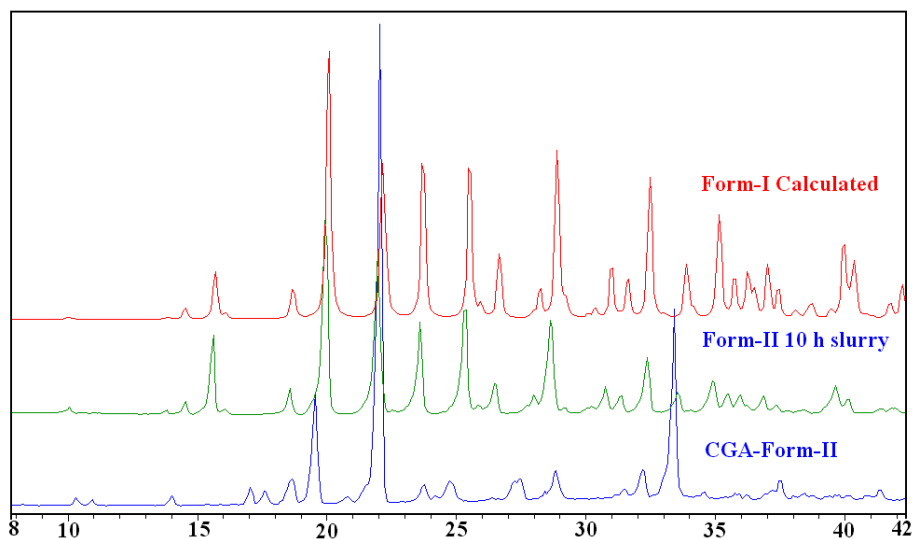
Figure 5.14 Overlay of experimental PXRD pattern of CGA-Form-II (blue) with the PXRD pattern after slurry experiment in which Form-II was found to convert into Form-I after 10 h slurry in EtOH. The calculated pattern of Form-I is shown for comparison (red).
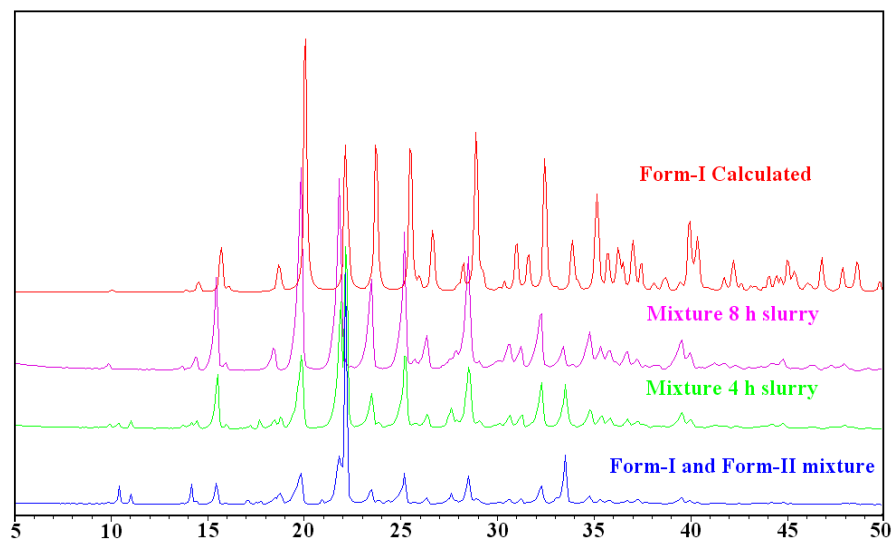
Figure 5.15 The mixture of Form-I and II (blue) was found to convert into Form-I (magenta) after slurry in EtOH solvent. The calculated PXRD pattern of Form-I (red) is shown for comparison.
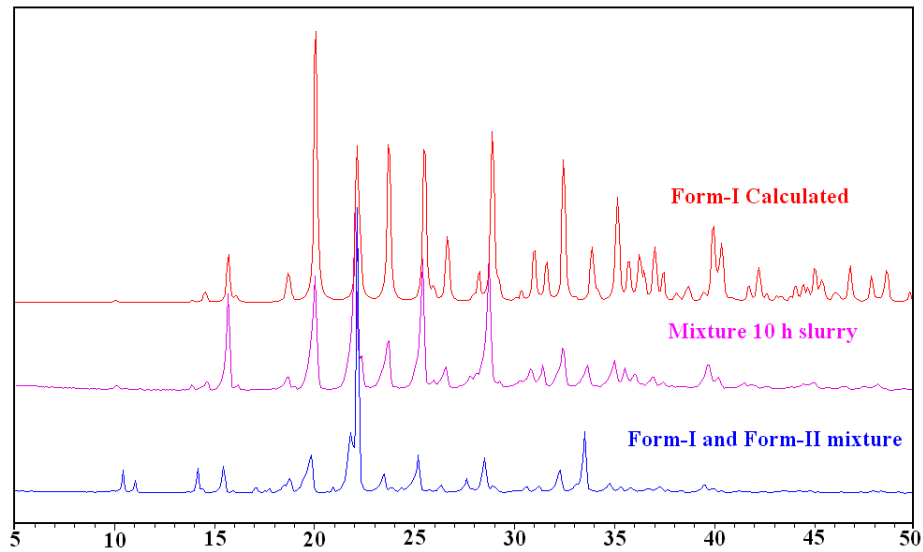
Figure 5.16 The mixture of Form-I and II (blue) was found to convert into Form-I (magenta) after slurry in pentane solvent. The calculated PXRD pattern of Form-I (red) was shown for comparison.

Processing of solids can have a major impact on solid-solid phase transformations which consequently affects the dissolution of the crystal forms. Neat grinding/liquid assisted grinding (NG/LAG) at room temperature was carried out on CGA forms up to 1 h to gain an insight into mechanically activated polymorph conversion. Grinding is one process that has been shown to cause changes in polymorphs, and such a polymorphic transformation is often detrimental to the efficacy of the formulation for example, chloramphenicol palmitate[23] and ritonavir[24] cases. NG/LAG of pure Form-II was converted into Form-I upon grinding for 60 min (Figure 5.17). However, extended NG/LAG on Form-I for 2 h did not show any effect. In addition, competitive NG/LAG experiments on a mixture of forms gave the stable Form-I after 20 min (Figure 5.18).
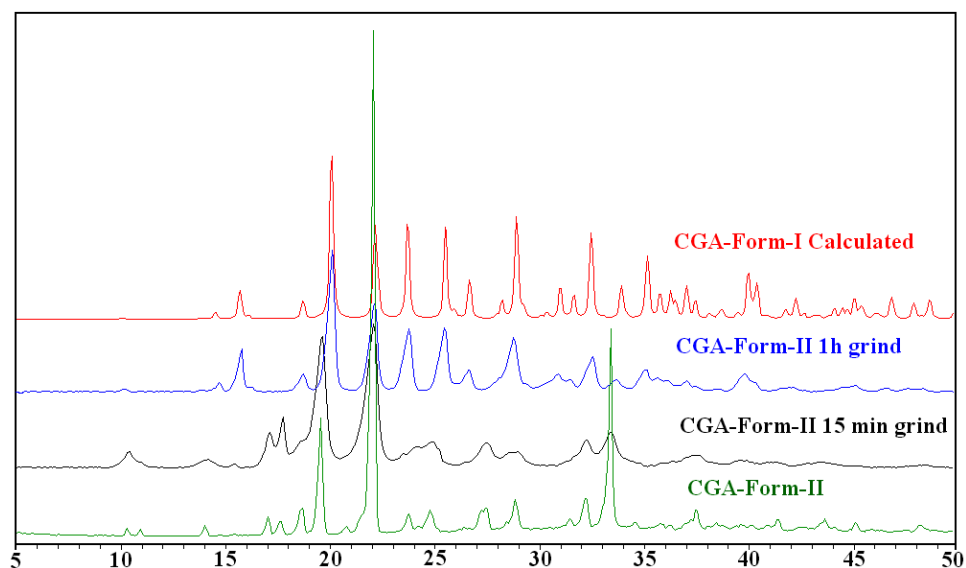

Figure 5.17 Overlay of experimental PXRD pattern of CGA-Form-II (green) with the ground material PXRD pattern of the same form, and Form-II was found to convert into Form-I after 1 h grinding. The calculated pattern of Form-I is shown for comparison (red).
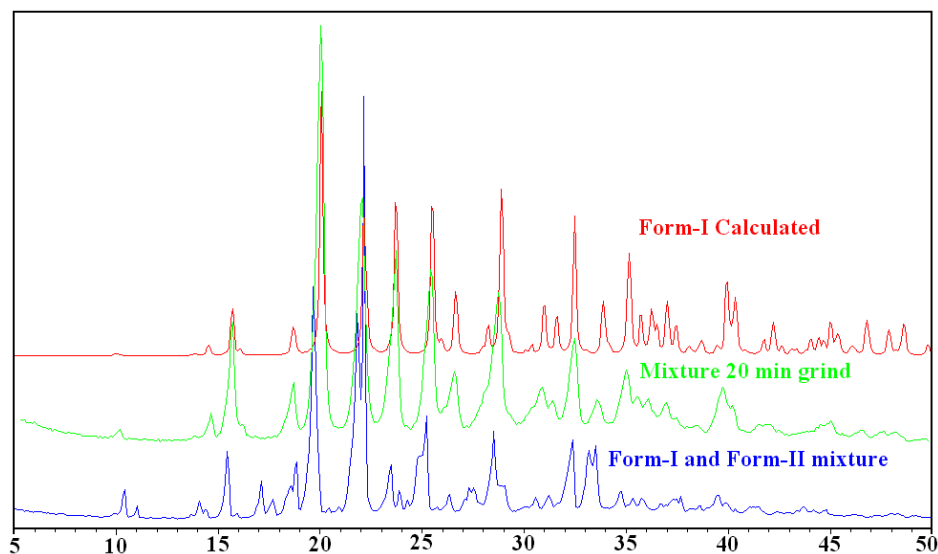
Figure 5.18 Overlay of experimental PXRD patterns of the mixture of Form-I and Form-II (blue), and the mixture was found to convert into Form-I after 20 min grinding (green). The calculated pattern of Form-I is shown for comparison (red).

5.2.8 Effect of humidity on CGA forms

Storage conditions of temperature and humidity affect the stability of pharmaceuticals.[25] In particular, hygroscopicity can have a significant impact on the physical and chemical stability of active pharmaceutical ingredients (APIs). Therefore, it is important to know the physicochemical stabilities of different forms and the kinetics of their transformation at different humidity levels. Stability study for CGA polymorphs was carried out in accelerated ICH conditions of 40 °C and 75% RH. Both forms were found to be stable (no phase transformation or hydrate formation) for the test period of 2 months based on PXRD analysis (Figure 5.19). Whereas Form-I is thermodynamically stable, the fact that there was no change in Form-II also came as a surprise. At ambient conditions of Hyderabad (35 °C and 40% RH) the polymorphs are stable for more than six months.

(a)   (b)

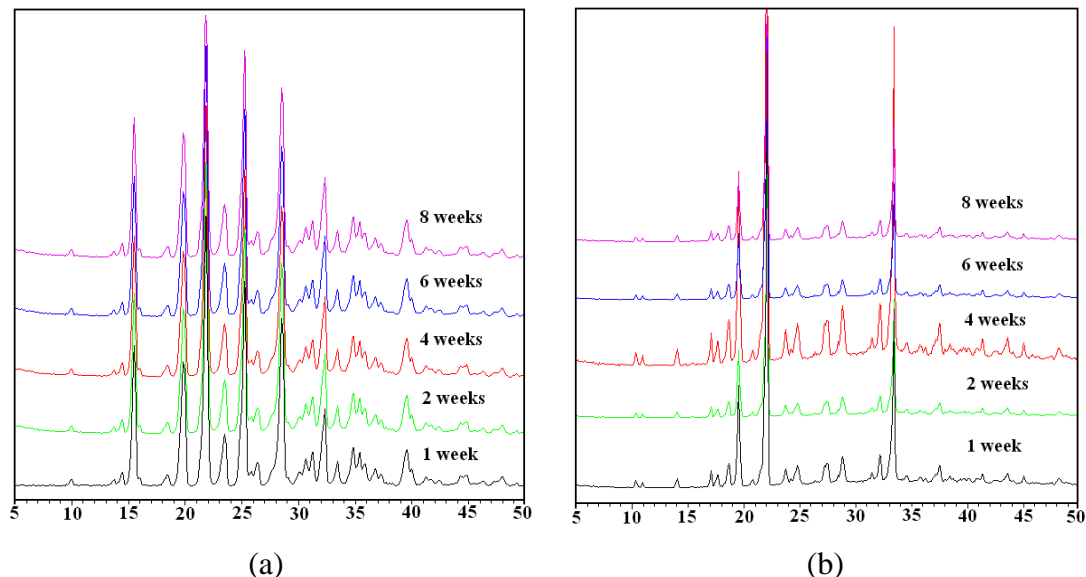**Figure 5.19** Overlay of PXRD patterns of (a) Form-I (b) Form-II after the **s**tability study at 40 °C and 75% RH shows that no form change/hydrate formation up to 2 months.

The study of hydration and dehydration of drug substances quantitatively is an important part of the investigations on polymorphs. This is achieved by measuring the water sorption-desorption isotherms on CGA polymorphs by Dynamic Vapor Sorption (DVS). Samples were subjected to a RH cycle of 10-90-10% at 40 °C (detailed in Experimental Section) and their water adsorption/ desorption behavior was analyzed. CGA-Form-II was found to adsorb 100.5% water at 90% RH and there was no significant percentage of water retention upon bringing down to 10% RH (Figure 5.20b). CGA-Form-I was found to be the least hygroscopic compared to Form-II (Figure 5.20a). Interestingly, moisture sorption profiles of both the forms showed somewhat different trends may be due to differences of the structure in the solid state. Water adsorption and desorption character of the solid materials depends on physical characteristics of the material, such as particle size, surface area, and pore size. From crystal structure analysis, both polymorphs have strong O–H···O and N–H···O hydrogen bonds, but the packing density of Form-II is lower, thereby leaving pores for water to enter uniformly during the sorption cycle (and leave during desorption), whereas the tighter packing of Form-I means that the behavior of water sorption/desorption is erratic due to lattice reorganizations as water molecules interact with the crystal surface. Hence the

DVS plots of polymorphs are different (Figure 5.20) but there is very small net gain/loss (<0.5%) of moisture by the sample.
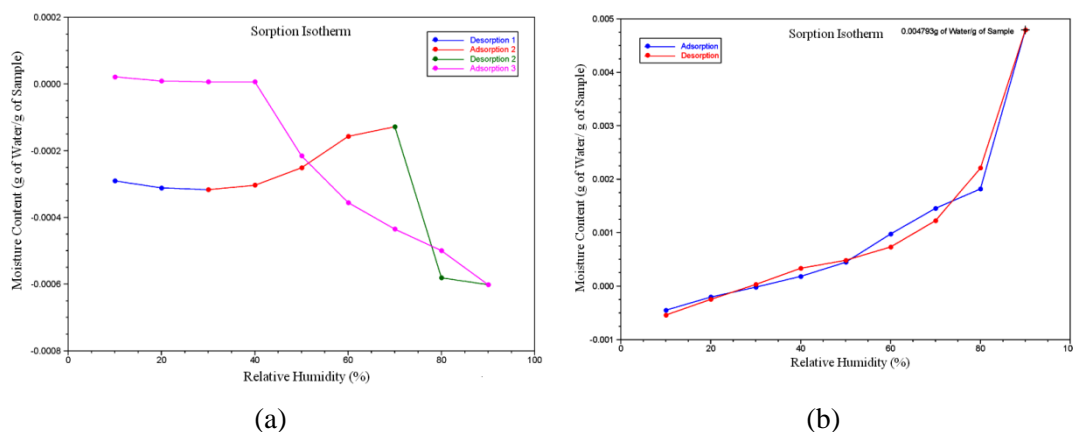

(a)   (b)

Figure 5.20 DVS isotherms of the CGA forms show the stability towards the moisture uptake (a) Form-I (b) Form-II shows negligible (0.5%) water uptake at 90% RH but there is no retention of water after desorption.

5.3 Conclusions

Polymorph screening was carried out on the anti-hyperammonemic drug carglumic acid (CGA). In our search we found that two polymorphs Form-I and Form-II, and a degraded form hydantoin-5-propionic acid (5-HPA). We were successful in getting diffraction quality single crystals for all the forms and determined their X-ray crystal structures. The procedures were optimized to obtain each polymorph in bulk quantity for PXRD and DSC/DVS analysis. The main difference in synthons of these polymorphs is acid-acid catemer synthon in Form-I and acid-amide heterosynthon in Form-II. There are significant conformational differences between these synthon polymorphs. The higher density Form-I is thermodynamically stable and the dimorphs are monotropically related. The polymorphs were fully characterized by FT-IR, ^{13}C ss-NMR, DSC, FESEM, PXRD, and DVS techniques. Thermodynamic stability and phase transformations were established and furthermore the major intermolecular interactions in the two crystal structures were quantified through Hirshfeld surface analysis. Both polymorphs were stable for 2 months at

ICH conditions of 40 ºC, 75% RH, and DVS analysis showed that Form-I is more stable to moisture than Form-II.

5.4 Experimental Section

Materials and Methods: Carglumic acid was purchased from Sigma-Aldrich (Hyderabad, India) and used without further purification. All other chemicals were of analytical or chromatographic grade. Water purified from a deionizer-cum-mixed-bed purification system (AquaDM, Bhanu, Hyderabad, India) was used in the experiments.

Preparation of CGA forms

CGA-Form-I: The commercial material obtained from Sigma-Aldrich matches to Form-I in our study which was confirmed by PXRD overlay. The bulk material in pure Form-I can also be obtained by slurry in EtOH, freeze drying in water. The bulk material was characterized by FT-IR, ^{13}C ss-NMR, PXRD and DSC. Single crystals suitable for X-ray diffraction were obtained upon dissolving 30 mg of CGA in 10 mL hot MeOH : 2-butanone (1:1 v/v) solvent mixture and left for slow evaporation at ambient conditions. Colorless needle crystals suitable for X-ray diffraction were obtained after 3-4 d upon solvent evaporation.

CGA-Form-II: Form-II was obtained in bulk upon dissolving 100 mg of CGA commercial material in 20 ml of water: acetone (1:5 v/v) solvent mixture and heated until to obtain clear saturated solution. This solution was subjected to the rotoevaporation until the complete removal of solvent and the resultant material was kept at high vacuum of 30 min to result in dry powder material. This powder material was confirmed as Form-II by FT-IR, ^{13}C ss-NMR, PXRD and DSC. Colorless single crystals were obtained upon dissolving 30 mg of CGA in 12 mL hot CH$_3$CN: m-cresol (1:1 v/v) solvent mixture and left for slow evaporation at ambient conditions. Colorless block crystals suitable for X-ray diffraction were obtained after 3-4 d upon solvent evaporation.

Hydantoin-5-propionic acid (5-HPA): The degraded form (5-HPA) of CGA was obtained upon dissolving 30 mg of CGA commercial material in 10 ml of 2-butanone: propionic acid

(1:1 v/v) solvent mixture and heated until to obtain clear solution. The solution filtered and left for slow evaporation at ambient conditions. Colorless needle crystals suitable for X-ray diffraction were obtained after 4-5 d upon solvent evaporation.

Vibrational spectroscopy: Thermo-Nicolet 6700 Fourier transform infrared spectrophotometer with NXR-Fourier transform Raman module (Thermo Fisher Scientific, Waltham, Massachusetts) was used to record IR spectra. IR spectra were recorded on samples dispersed in KBr pellets. Data was analyzed using the Omnic software (Thermo Fisher Scientific, Waltham, Massachusetts).

Solid-state NMR spectroscopy: Solid-state ^{13}C NMR (ss-NMR) spectroscopy provides structural information about differences in hydrogen bonding, molecular conformations, and molecular mobility in the solid state.[16] The solid-state ^{13}C NMR spectra were obtained on a Bruker Ultrashield 400 spectrometer (Bruker BioSpin, Karlsruhe, Germany) utilizing a ^{13}C resonant frequency of 100 MHz (magnetic field strength of 9.39 T). Approximately 100 mg of crystalline sample was packed into a zirconium rotor with a Kel-F cap. The cross polarization, magic angle spinning (CP-MAS) pulse sequence was used for spectral acquisition. Each sample was spun at a frequency of 5.0 ± 0.01 kHz and the magic angle setting was calibrated by the KBr method. Each data set was subjected to a 5.0 Hz line broadening factor and subsequently Fourier transformed and phase corrected to produce a frequency domain spectrum. The chemical shifts were referenced to TMS using glycine ($\delta_{glycine} = 43.3$ ppm) as an external secondary standard.

Differential Scanning Calorimetry (DSC): DSC was performed on a Mettler Toledo DSC 822e module. Samples were placed in crimped but vented aluminium sample pans. The typical sample size is 3-5 mg, and the temperature range is 30-250 °C @ 5 °C min^{-1}. Samples were purged by a stream of dry nitrogen flowing at 80 mL min^{-1}.

Field Emission Scanning Electron Microscope (FESEM): The shape and morphology of the CGA forms were examined on a Carl Zeiss model Merlin Compact 6027 FESEM with a beam voltage of 3.0 kV. The sample was spread on a carbon-coated copper grid. Prior to

FESEM imaging, an ultrathin layer of gold was coated in order to enhance the conductivity of the sample.

Dynamic Vapor Sorption (DVS): Dynamic vapor sorption (DVS) was used to obtain sorption–desorption kinetic data of CGA polymorphs. DVS measurements were performed using a Q5000SA vapor sorption analyzer (TA Instruments, Delaware, USA) at 40°C. About 4-10 mg of the sample was placed in a metalized quartz sample pan and subjected to relative humidity flux from 10% RH to 90% RH and back to 10% RH with a step size of 10% change in humidity. A dwell time of 60 min was set for a weight change of >0.1% in the adsorption/desorption phase at a particular RH (5 min dwell time for a weight change of <0.1%). Thus, if the weight loss/gain is >0.1% at a particular RH, the instrument maintains the same RH for 60 min and then automatically sets at the next higher/lower value. If the weight gain/loss is <0.1%, the DVS cycle (10%−90%−10%) will be completed within 2 hours, otherwise it will take a longer duration.

X-ray crystallography: X-ray reflections for Form-I and Form-II were collected at 100 K on Bruker SMART-APEX CCD diffractometer equipped with a graphite monochromator and Mo-Kα fine-focus sealed tube (λ = 0.71073 Å). Data reduction was performed using Bruker SAINT Software.[26] Intensities were corrected for absorption using SADABS,[27] and the structure was solved and refined using SHELX-97.[28] X-ray reflections for hydantoin-5-propionic acid (5-HPA) was collected at 298 K on Oxford Xcalibur Gemini Eos CCD diffractometer using Mo−Kα radiation (λ = 0.7107 Å). Data reduction was performed using CrysAlisPro (version 1.171.33.55)[29] and OLEX2-1.0[30] was used to solve and refine the structures. All non-hydrogen atoms were refined anisotropically. Hydrogen atoms on heteroatoms were located from difference electron density maps and all C−H hydrogens were fixed geometrically. Hydrogen bond geometries were determined in Platon.[31] X-Seed[32] was used to prepare packing diagrams.

Powder X-ray diffraction: Powder X-ray diffraction of all the samples were recorded on Bruker D8 Advance diffractometer (Bruker-AXS, Karlsruhe, Germany) using Cu-Kα X-radiation (λ= 1.5406 Å) at 40 kV and 30 mA power. X-ray diffraction patterns were collected over the 2θ range 5-50° at a scan rate of 1° min^{-1}. Powder Cell 2.4[33] (Federal

Institute of Materials Research and Testing, Berlin, Germany) was used for Rietveld refinement of experimental PXRD and calculated lines from the X-ray crystal structure.

5.5 References

1.   (a) L. Caldovic, H. Morizono, Y. Daikhin, I. Nissim, R. J. McCarter, M. Yudkoff, M. Tuchman, *J. Pediatr.*, 2004, **145**, 552. (b) O. Elpeleg, A. Shaag, E. Ben-Shalom, T. Schmid, C. Bachmann, *Ann. Neurol.*, 2002, **52**, 845. (c) J. V. Leonard, M. P. W. Platt, A. A. Morris, *Eur. J. Pediatr.* 2008, **167**, 305.

2. (a) J. Häberle, *Ther. Clin. Risk Manag.*, 2011, **7**, 327. (b) J. E. O'Connor, A. Jordá, S. Grisolia, *Eur. J. Pediatr.*, 1985, **143**, 196.

3.   M. Daniotti, G. la Marca, P. Fiorini, L. Filippi, *Int. J. Gen. Med.*, 2011, **4,** 21.

4. ChemSpider: Chemical structure database freely distributed by the RSC, www.chemspider.com.

5. (a) M. Abacan, A. Boneh, *Mol. Genet. Metab.*, 2013, **109**, 397. (b) C. Bachmann, S. Krähenbühl, J. P. Colombo, G. Schubiger, K. H. Jaggi, O. Tönz, *N. Engl. J. Med.*, 1981, **304**, 543. (c) J. P. Colombo JP, *Adv. Exp. Med. Biol.*, 1994, **368**, 135.

6. (a) A. J. Dobson, R. E. Gerkin, *Acta Crystallogr.*, 1997, **C53**, 73. (b) N. Kausar, B. D. Alexander, R. A. Palmer, B. S. Potter, T. J. Dines, M. Helliwell, B. Z. Chowdhry, *J. Chem. Crystallogr.*, 2010, **40**, 602.

7. Cambridge Structural Database, ver. 5.36. ConQuest 1.17, November 2014 release, November 2014 update, CCDC, www.ccdc.cam.ac.uk.

8. (a) G. R. Desiraju, *Crystal Engineering: The Design of Organic Solids*, Elsevier, Amsterdam, 1989; (b) G. R. Desiraju, *J. Chem. Sci.*, 2010, **122**, 667. (c) G. R. Desiraju, J. J. Vittal and A. Ramanan, *Crystal Engineering. A Textbook*, World Scientific, Singapore, 2011.

9. (a) L. F. Huang and W. Q. T. Tong, *Adv. Drug Del. Rev.*, 2004, **56**, 321. (b) T. L. Threlfall, *Analyst*, 1995, **120**, 2435. (c) J. Bernstein, *Polymorphism in Molecular Crystals*, Clarendon, Oxford, 2002. (d) F. Fabbiani, D. Allan, S. Parsons and C. Pulham, *CrystEngComm*, 2005, **7**, 179. (e) P. Sanphui, N. Goud, U. Khandavilli, S.

Bhanoth and A. Nangia, *Chem. Commun.*, 2011, **47**, 5013. (F) J. Haleblian and W. J. McCrone, *Pharm. Sci.*, 1969, **58**, 911.

10. (a) P. P. Bag, M. Patni and C. M. Reddy, *CrystEngComm*, 2011, **13**, 5650. (b) N. Shan, F. Toda and W. Jones, *Chem. Commun.*, 2002, 2372. (c) A. V. Trask and W. Jones, *Top. Curr. Chem*., 2005, **254,** 41. (d) A. Delori, T. Friščić and W. Jones, *CrystEngComm*, 2012, **14**, 2350.

11. K. R. Morris, U. J. Griesser, C. J. Eckhardt and J. G. Stowell, *Adv. Drug Del. Rev.*, 2001, **48**, 91.

12. (a) R. D. B. Walsh, M. W. Bradner, S. Fleischman, L. A. Morales, B. Moulton, N. Rodriguez-Hornedo and M. J. Zaworotko, *Chem. Commun.*, 2003, **2**, 186. (b) G. R. Desiraju, *Angew. Chem., Int. Ed. Engl*., 1995, **34**, 2311. (c) F. H. Allen, W. D. S. Motherwell, P. R. Raithby, G. P. Shields and R. Taylor, *New J. Chem.*, 1999, **23**, 25.

13. A. J. Cruz-Cabeza and J. Bernstein, *Chem. Rev.*, 2014, **114**, 2170.

14. (a) M. C. Etter, *Acc. Chem. Res*., 1990, **23**, 120. (b) J. Bernstein, R. E. Davis, L. Shimoni and N. L. Chang, *Angew. Chem., Int. Ed. Engl.*, 1995, **34**, 1555.

15. (a) R. M. Silverstein, *Spectrometric Identification of Organic Compounds*, 6th Ed., John Wiley, New York, 2002. (b) E. Smith and G. Dent, *Modern Raman Spectroscopy, A Practical Approach*, John Wiley, New York, 2005.

16. (a) F. G. Vogt, J. S. Clawson, M. Strohmeier, A. J. Edwards, T. N. Pham and S. A. Watson, *Cryst. Growth Des.*, 2008, **9**, 921. (b) A. E. Aliev and K. D. M. Harris, *Supramolecular Assembly via Hydrogen Bonds I*, 2004, 1. (c) A. W. Newman, S. L. Childs and B. A Cowans, Salt Cocrystal Form Selection, In *Preclinical Development Handbook*, John-Wiley, Hoboken, 2008, 455.

17. (a) H. B. Brittain, *Am. Pharm. Rev.*, 2002, **5**, 74. (b) G. P. Stahly, *Cryst. Growth Des.*, 2007, **7**, 1007.

18. (a) J. L. Ford, P. Timmins, *Pharmaceutical Thermal Analysis: Techniques and Applications*, E. Horwood, Chichester, 1989. (b) H. G. Brittain, *Polymorphism in Pharmaceutical Solids*, Marcel Dekker, New York, 1999.

19. (a) A.Burger and R. Ramberger, *Mikrochim. Acta II*, 1979, 259.

20. (a) M. Veverka, P. Simon, J. Lokaj and E. Veverkova, *Monatsh. Chem.*, 2012, **143**, 65. (b) R. Barbas, R. Prohens and C. Puigjaner, *J. Therm. Anal. Calor.*, 2007, **89**, 687. (c) J. Mensah and K. Kim, *Chem. Eng. Trans.*, 2013, **32**, 2221.

21. (a) M. A. Spackman and D. Jayatilaka, *CrystEngComm*, 2009, **11**, 19. (b) J. J. McKinnon, D. Jayatilaka and M. A. Spackman, *Chem. Commun.*, 2007, 3814. (c) J. Bernstein, *Cryst. Growth Des.*, 2011, **11**, 632. (d) F. P. A. Fabbiani, L. T. Byrne, J. J. McKinnon and M. A. Spackman, *CrystEngComm*, 2007, **9**, 728.

22. (a) V. Trask, A. W. S. Motherwell and W. Jones, *Chem. Commun.*, 2004, 890. (b) S. Aitipamula, P. S. Chow and R. Tan, *CrystEngComm*, 2010, **12**, 3691. (c) M. D. Eddleston, S. Sivachelvam and W. Jones, *CrystEngComm*, 2013, **15**, 175.

23. J. Bernstein, *NATO Sci. Ser., II Mathematics, Phys. Chem.*, 2002, **68**, 244.

24. C.-H. Gu, V. Young Jr. and D. J. W. Grant, *J. Pharm. Sci.*, 2001, **90**, 1878.

25. (a) N. V. Phadnis and R. Suryanarayanan, *J. Pharm. Sci*., 1997, **86**, 1256. (b) M. Otsuka, R. Teraoka and Y. Matsuda, *Pharm. Res.*, 1991, **8**, 1066. (c) Y. Hu, A. Erxleben, B. K. Hodnett, B. Li, P. McArdle, Å. C. Rasmuson and A. G. Ryder, *Cryst. Growth Des.*, 2013, **13**, 3404. (d) M. Otsuka, M. Onoe and Y. Matsuda, *Pharm. Res.* 1993, **10**, 577.

26. *SAINT-Plus*, version 6.45; Bruker AXS Inc., Madison, Wisconsin, U.S.A., 2003.

27. SADABS, *Program for Empirical Absorption Correction of Area Detector Data*; G. M. Sheldrick, University of Göttingen: Göttingen, Germany, 1997.

28. (a) *SMART*, version 5.625 and *SHELX-TL*, version 6.12, Bruker AXS Inc.: Madison, Wisconsin, USA, 2000. (b) G. M. Sheldrick, *SHELXS-97* and *SHELXL-97*; University of Göttingen: Göttingen, Germany, 1997.

29. *CrysAlis CCD and CrysAlis RED*, Ver. 1.171.33.55; Oxford Diffraction Ltd: Yarnton, Oxfordshire, U.K., 2008.

30. O. V. Dolomanov, A. J. Blake, N. R. Champness and M. Schröder, *J. Appl. Crystallogr.*, 2003, **36**, 1283.

31. A. L. Spek, *PLATON, A Multipurpose Crystallographic Tool*; Utrecht University: Utrecht, Netherlands, 2002.

32. L. J. Barbour, *X-Seed*, *Graphical Interface to SHELX-97 and POV-Ray*, *Program for Better Quality of Crystallographic Figures*; University of Missouri-Columbia, Missouri, U.S.A., **1999**.

33. Powder Cell, A Program for Structure Visualization, Powder Pattern Calculation and Profile Fitting, http://www.ccp14.ac.uk/index.html, **2013**.

SOLUBILITY AND STABILITY OF BLONANSERIN SALT POLYMORPHS
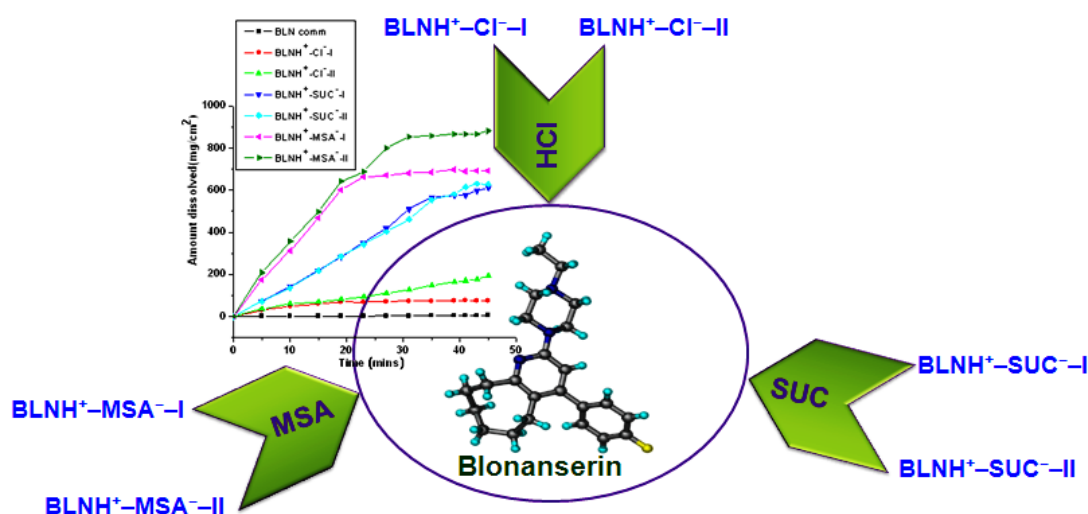
Salt polymorphs were obtained for the antipsychotic BCS class II drug Blonanserin (BLN) with GRAS molecules. Crystal structures of the salt forms were stabilized by N^+–$H{\cdots}O^-$ ionic H-bond. Out of three dimorphic pairs, $BLNH^+$–SUC^-–Form-II exhibited the highest solubility (468.8 mg/mL, 293 times) and dissolution rate (61 times) in 60% EtOH−water medium compared to the parent drug and showed good stability for 3 months in accelerated ICH conditions (40 °C, 75% RH).

6.1 Introduction

Pharmaceutical salts are important in the process of drug development, as converting acidic or basic active pharmaceutical ingredients (APIs) into a salt via a simple neutralisation reaction has the ability to change the physicochemical properties of API. Potential counterions are chosen for salt formation based on pKa differences[1] and counterion toxicity, preferably molecules from generally regarded as safe GRAS list.[2] Salt formation of the drug molecules alter the properties such as crystallinity, low hygroscopicity, good chemical stability, high melting point, high water solubility, high dissolution rate and good bioavailability.[3] However, the relative importance of these properties may vary from drug to drug. Within the pharmaceutical research and development field, the selection of a suitable solid-state form represents a crucial step. Selecting a solid-state form comprises several decisions, mainly the selection of a salt form and the selection of a polymorph or pseudo-polymorph of the respective salt. Although the choice of salt form can have a significant impact on the physicochemical properties of drug candidates,[4] the importance of this impact can differ from one molecule to another. For instance, even if the high solubility salt form found to be unstable, changing from a crystalline form to the amorphous form or other crystalline polymorph will have detrimental effect, and may even result in product failure. Hence, in recent times various solid forms were screened particularly for low soluble drugs with diverse salt formers.[3] This becomes especially clear when trends in the usage of pharmaceutical salts today are compared to the situation in the 1980s,[5] a period in which mostly hydrochlorides were used as pharmaceutical salts. Hydrochlorides have not been replaced simply by another salt form, instead a broad variety of salt forms are now being used. This is because there is no universal answer to the question as to which salt form may be most useful for a specific drug. This reflects the increased need to optimize a broader variety of parameters relevant for a specific drug.

In this context, we have screened for salt polymorphs of the Blonanserin (BLN). BLN is a relatively new antipsychotic agent having dopamine D2 and serotonin 5-HT2 receptor antagonist properties.[6] It was invented by Dainippon Sumitomo Pharma and launched in 2008 under the brand name Lonasen[7] in Japan and Korea for the treatment of schizophrenia.[8]

BLN is effective towards positive symptoms of schizophrenia (such as hallucinations and delusions) and negative symptoms of schizophrenia (such as flat affect and hypobulia).[7] The crystal structure of blonanserin was reported by Suzuki et al.[9] This compound is structurally unrelated to existing antipsychotics such as haloperidol, chlorpromazine and risperidone (Scheme 6.1). Compared to many other antipsychotics, blonanserin has improved tolerability profile, lacking side effects such as extrapyramidal symptoms, excessive sedation and hypotension.[10] A usual maintenance dose of Lonasen is 8–16 mg per day, and the highest dose is 24 mg per day. Generally salt forms of drugs are preferred due to higher solubility, improved stability, and ease of filtration.[3] After the study of various salts of BLN in chapter 4 we found that few salts found to exhibit polymorphic behaviour. Our main intention of the work was to understand the behaviour of BLN salt polymorphs towards solubility, dissolution, stability and also to explore phase transformations behaviour.
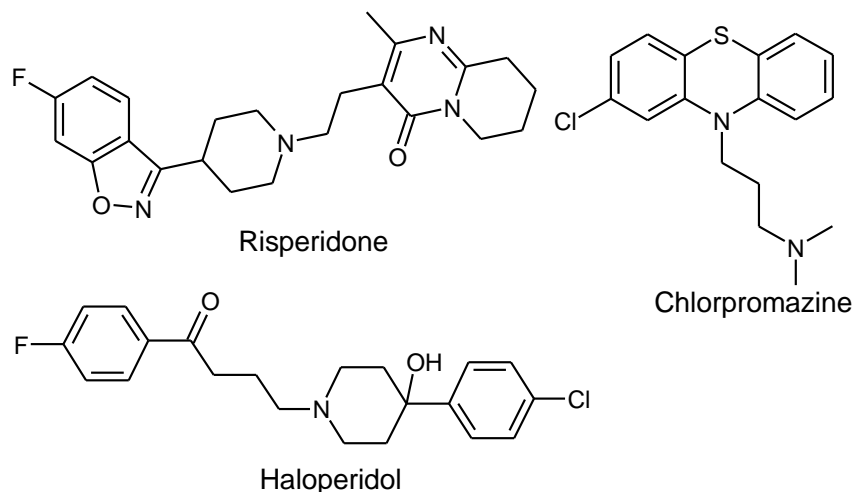
Scheme 6.1 Chemical structures of the various antipsychotic drugs.

6.2 Design and Preparation of Blonanserin Salt Polymorphs

Almost an estimated 50% of drug molecules used in medicinal therapy are administered as salts, however studies on salt polymorphs are insignificant as compared to single component (such as APIs) ones. With the back ground of low solubility (0.033 mg/L)[11] of BLN which belongs to Biopharmaceutics Classification System (BCS) class II (low solubility, high

permeability), we have screened for various salts of the drug to address the issue. All the salts obtained were found to exhibit improved solubility and dissolution with good stability (discussed in chapter 4). However, salts BLN with hydrochloric acid (HCl), succinic acid (SUC), and methane sulfonic acid (MSA) were found to exhibit polymorphic behavior (BLNH$^+$–Cl$^-$ –Form-I and Form-II; BLNH$^+$–SUC$^-$–Form-I and Form-II; BLNH$^+$–MSA$^-$– Form-I and Form-II). Hence, it is important to have sound knowledge of the behaviour of the salt polymorphs towards towards solubility, dissolution, stability and thermal effects because each form can show different properties. This is particularly important because uncertainty about accidental phase transformations to the stable crystalline modification during dissolution or upon storage is detrimental in the late stage. With this back ground we have prepared the salt forms (BLNH$^+$–Cl$^-$ –Form-I and Form-II; BLNH$^+$–SUC$^-$–Form-I and Form-II; BLNH$^+$–MSA$^-$–Form-I and Form-II) and a BLNH$^+$–Cl$^-$ monohydrate by various methods such as liquid assisted grinding, dehydration, slurry crystallization, heating and optimized the conditions to obtained the forms in a reproducible manner (see experimental section). All the salt formers (HCl, SUC, and MSA) were selected from GRAS list and chemical structures were presented in Scheme 6.2.
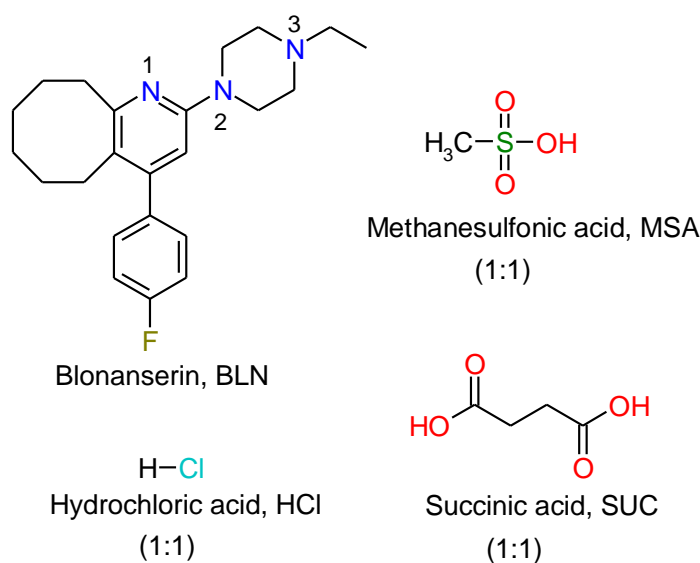
Scheme 6.2 Chemical structures of Blonanserin and salt formers which resulted salt polymorphs. The stoichiometry of API: salt former ratio is mentioned in brackets.

6.3 Results and Discussion

BLN (Scheme 6.2) is a weak basic drug and salt formation was carried out with acidic salt formers. We were successful in getting diffraction quantity single crystals for $BLNH^+–Cl^-$ –Form-I, $BLNH^+–Cl^-$ monohydrate, $BLNH^+–SUC^-$–Form-I and $BLNH^+–MSA^-$–Form-I. We were unsuccessful so far in getting suitable single crystals for Form-II of salts $BLNH^+–Cl^-$, $BLNH^+–SUC^-$ and $BLNH^+–MSA^-$, however these forms were characterized by other techniques such as FT-IR, Raman, PXRD, etc. Structural analysis of the forms revealed that proton transferred from acidic salt formers to the piperazine N_3 position of BLN. BLN salt polymorphs ($BLNH^+–Cl^-$ –Form-I and Form-II; $BLNH^+–SUC^-$–Form-I and Form-II; $BLNH^+–MSA^-$–Form-I and Form-II) and a $BLNH^+–Cl^-$ monohydrate were produced in bulk quantity by various methods in their pure forms for other studies (detailed in experimental section). Salt forms were characterized by spectroscopic (FT-IR, FT-Raman, ss-NMR), thermal (DSC, TGA and HSM), and X-ray diffraction techniques. Further, for all the salt forms solubility, dissolution studies were carried out in 60% EtOH−water medium, relative stability and stability towards international conference on harmonisation (ICH) conditions[12] were established. Crystallographic data of the X-ray crystal structures and hydrogen bonding parameters are listed in Table 6.1 and 6.2.

Table 6.1 Crystallographic parameters of BLN salt forms.

	$BLNH^+–Cl^-$–Form-I	$BLNH^+–Cl^-$ monohydrate	$BLNH^+–SUC^-$–Form-I	$BLNH^+–MSA^-$–Form-I
Emp form.	$C_{23}H_{31}Cl_1F_1N_3$	$C_{23}H_{33}Cl_1F_1N_3O_1$	C27 H36 F N3 O4	C24 H34 F N3 O3 S
Form wt	403.96	421.97	485.59	463.60
Cryst syst	Triclinic	Monoclinic	Orthorhombic	Triclinic
Sp gr	$P\bar{1}$	$P2_1/c$	$P2_12_12_1$	$P\bar{1}$
T/K	100(2)	100(2)	100(2)	100(2)
a/Å	7.485(10)	17.0708(14)	8.9999(9)	12.6945(9)
b/Å	8.578(9)	11.9644(10)	13.0762(13)	13.7444(9)
c/Å	16.794(18)	11.0576(9)	21.704(2)	14.4954(10)
α/°	82.718(17)	90	90	98.5020(10)
β/°	85.478(17)	106.1890(10)	90	98.8410(10)
γ/°	84.883(11)	90	90	105.9490(10)
Z	2	4	4	4
V/Å^3	1063(2)	2168.9(3)	2554.2(4)	2354.3(3)
D_{calc}/g cm^{-3}	1.262	1.292	1.263	1.308
μ/mm^{-1}	0.202	0.204	0.090	0.176
Rflns collect	9615	8198	26650	24415
Unique rflns	2863	3511	5015	9148
Obsd rflns	4082	4199	4715	8046
R_1 [$I>2\sigma(I)$]	0.0741	0.0499	0.0339	0.0464
wR_2 [all]	0.1953	0.1075	0.0762	0.1121
GOF	1.047	1.025	1.032	1.041

Table 6.2 Hydrogen bonds in BLN salt forms.

D–H···A	H···A (Å)	D···A (Å)	D–H···A (°)	symmetry code
BLNH⁺–Cl⁻ –Form-I				
N3–H3···Cl1	2.15	3.088(5)	160	x+1, y, z
C6–H6A···F1	2.57	3.412(3)	143	−x, −y+1, −z
C18–H18B···Cl1	2.88	3.619(3)	132	x+1, y, z
C19–H19B···N2	2.50	3.490(6)	174	−x+1, −y+1, −z+1
C20–H20A···Cl1	2.93	3.613(5)	127	x, y, z
C20–H20B···Cl1	2.76	3.624(6)	146	−x+1, −y, −z+1
C22–H22A···Cl1	2.64	3.502(6)	146	−x+1, −y, −z+1
BLNH⁺–Cl⁻ monohydrate				
O1–H1A···Cl1	2.42	3.237(2)	150	−x+1, y+1/2, −z+1/2
O1–H1B···Cl1	2.28	3.179(2)	161	−x+1, −y+1, −z+1
N3–H3···Cl1	2.14	3.069(2)	177	x, y, z
C6–H6A···F1	2.50	3.402(3)	151	−x+2, −y+2, −z
C20–H20B···O1	2.30	3.149(3)	143	−x+1, y−1/2, −z+1/2
BLNH⁺–SUC⁻–Form-I				
O1–H1···O4	1.60	2.5460(16)	174	−x, −1/2+y,1/2−z
N3–H3···O3	2.49	3.1894(17)	128	1−x, −1/2+y,1/2−z
N3–H3···O4	1.71	2.6676(17)	171	1−x, −1/2+y,1/2−z
C2–H2···O3	2.52	3.3369(19)	144	1−x, −1/2+y,1/2−z
C10–H10···F1	2.54	3.516(2)	150	x,+y+1, z
C16–H16···O4	2.48	3.556(2)	172	−x+1/2+1, −y,+z+1/2
C19–H19B···O3	2.65	3.176(2)	109	x+1,+y,+z
C20–H20B···O2	2.46	3.246(2)	136	1+x,y,z
C21–H21A···O3	2.59	3.2322(19)	122	1+x,y,z
C26–H26B···F1	2.51	3.530(2)	158	−x+1/2+1, −y,+z−1/2
BLNH⁺–MSA⁻–Form-I				
N3–H3···O3	1.66	2.675(2)	169	−x+2, −y+1, −z+1
N6–H6···O6	1.66	2.677(2)	169	x, y, z
C6–H6B···O1	2.45	3.413(2)	170	1−x,1−y,1−z
C10–H10B···O6	2.57	3.538(2)	174	x, −1+y,z
C14–H14···F2	2.54	3.118(3)	120	1+x,1+y, −1+z
C18–H18A···O2	2.52	3.406(3)	152	−1+x,y,z
C21–H21B···O5	2.41	3.226(2)	132	x, y, z
C23–H23A···O3	2.57	3.419(3)	135	x, y, z
C31–H31B···O5	2.53	3.475(3)	166	−x,1−y,1−z
C43–H43B···O4	2.57	3.399(2)	144	1−x,1−y,1−z
C45–H45A···O1	2.61	3.211(2)	115	−x+1, −y, −z+1
C46–H46A···O2	2.39	3.374(2)	151	1−x, −y,1−z
C48–H48B···O6	2.49	3.369(3)	138	−x+1, −y, −z+1

6.3.1 Crystal Structural Description

BLNH$^+$–Cl$^-$ –Form-I: Crystallization of blonanserin hydrochloride (BLN HCl) from benzene afforded block shaped crystals of the salt in $P\bar{1}$ space group. The N-ethyl piperazine N$_3$ of BLN base is protonated in the salt structure (N$^+$–H···Cl$^-$ 2.15 Å, 160°). Molecules are connected by activated C–H···Cl$^-$ interactions (CH donors adjacent to ammonium cation) of a neighboring BLN molecule in a dimer motif (2.64 Å, 146°; 2.76 Å, 146°) along the *b*-axis. The protonoted molecules extend through a R_2^2 (18) ring[13] assembled via C–H···F interactions (2.57 Å, 143°) between inversion related molecules (Figure 6.1).
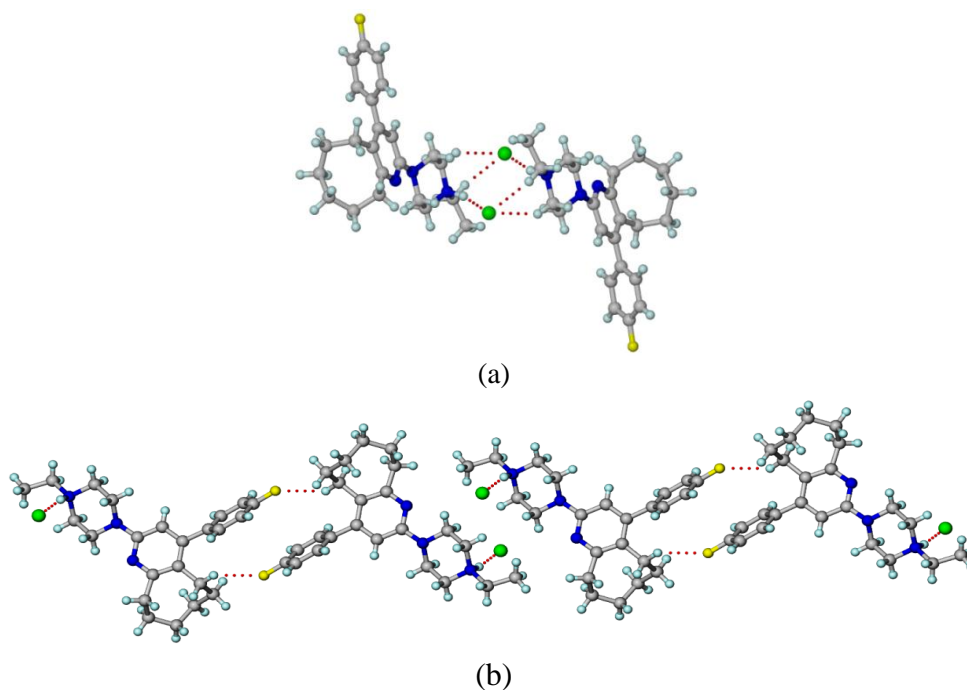

(a)

(b)

Figure 6.1 (a) Blonanserin molecules are connected through N$^+$–H···Cl$^-$ and C–H···Cl$^-$ interactions along the *b*-axis. (b) R_2^2 (18) ring motif of C–H···F interactions and close packing of such units.

BLNH⁺–Cl⁻ monohydrate: Crystallization of blonanserin hydrochloride from nitromethane afforded a monohydrate of the salt in $P2_1/c$ space group. It is likely that atmospheric moisture was included in the crystal lattice since no special care was taken to scrupulously exclude water during the crystallization experiment. Now a water molecule connects BLN molecules through O–H···Cl⁻ hydrogen bonds (2.42 Å, 150º; 2.28 Å, 161º) in a chain along the *c*-axis. Similar to the salt structure, adjacent BLN molecules are connected by C–H···F dimers (2.50 Å, 151º) (Figure 6.2).
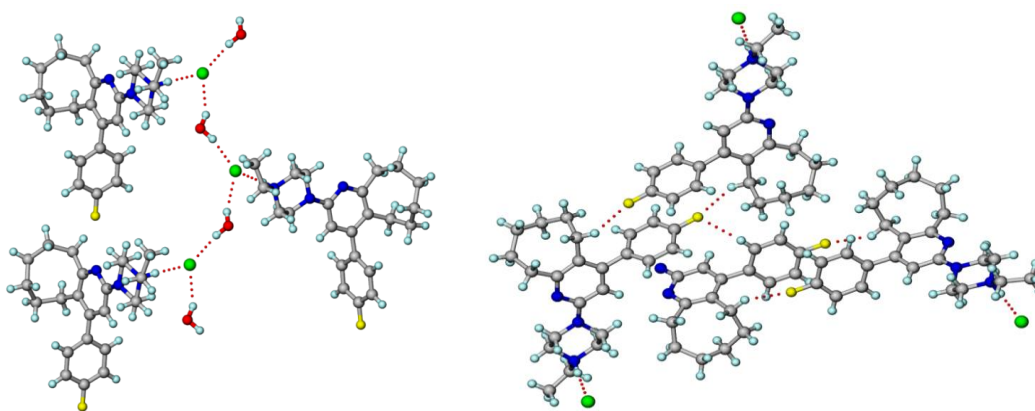

Figure 6.2 (a) Water molecules and chloride ions form a channel along *c*-axis and are flanked by BLN molecules. (b) Adjacent BLN molecules are connected by bifurcated C–H···F interactions.

BLNH⁺–SUC⁻–Form-I: Single crystals of Form-I were obtained upon crystallizing the ground material of salt formers (BLN and SUC) from EtOAc−ethyl methyl ketone. The X-ray crystal structure was solved and refined in space group $P2_12_12_1$ with a proton being transferred from one of the carboxylic acid groups of SUC to the piperazine N_3 position of BLN as observed in BLNH⁺–Cl⁻ –Form-I. SUC⁻ anions connect through O–H···O⁻ (1.60 Å, 174º) hydrogen bonds forming a channel along the [010] axis, and BLNH⁺ cations were arranged in an alternate fashion on both sides of this channel through N⁺–H···O⁻ (1.71 Å, 171º) hydrogen bonds. CH donors adjacent to the protonated ammonium cation form auxiliary C–H···O (2.46 Å, 136º; 2.65 Å, 109º) interactions with COO⁻ and COOH groups of

SUC⁻ anions in R_2^2 (7) and R_3^2 (9) ring motifs. Adjacent channels were connected by auxiliary C–H···O (2.48 Å, 172º) and bifurcated C–H···F (2.51 Å, 158º; 2.54 Å, 150º) interactions (Figure 6.3).
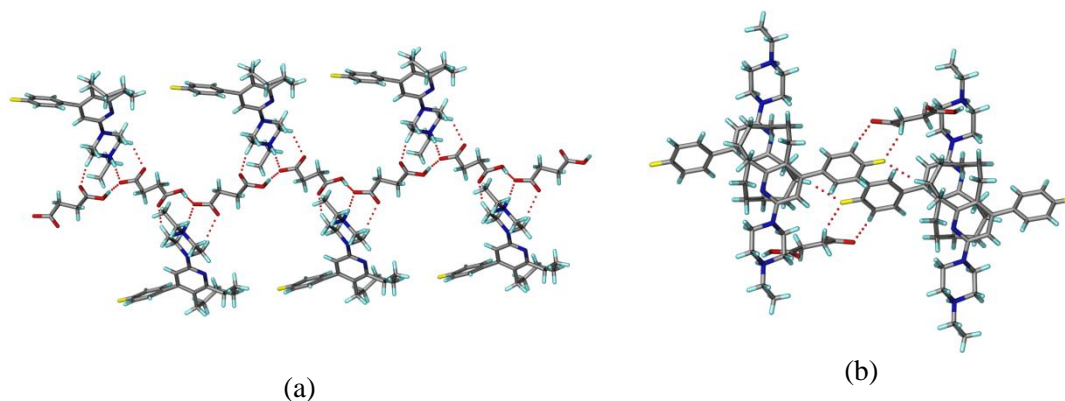

(a)

(b)

Figure 6.3 (a) SUC⁻ anions form a channel along the *b*-axis and BLNH⁺ cations are flanked through N⁺–H···O⁻ and C–H···O interactions. (b) Adjacent channels are connected by auxiliary C–H···O and C–H···F interactions.

BLN⁺−MSA⁻–Form-I: Single crystals of Form-I were obtained when the ground material (BLN and MSA) was crystallized from toluene−EtOAc (1:1, v/v), and the crystal structure of BLNH⁺−MSA⁻–Form-I (2 symmetry-independent ions of each component) was solved in $P\bar{1}$ space group. The flexible cyclooctane ring C atoms (C33A, C33B; C34A, C34B) are disordered in one of the BLNH⁺ cations (shown in ball and stick). Protonation occurred at the piperazine N₃ of BLNH⁺, similar to other salts (N⁺−H···O⁻ 1.66 Å, 169º; 1.66 Å, 169º). BLNH⁺ cations are connected through C–H···π interactions to form a dimeric motif. Symmetry-independent BLNH⁺ cations are connected by MSA⁻ anions in a 1D tape via N⁺−H···O⁻ (1.66 Å, 169º; 1.66 Å, 169º) and C−H···O (2.41 Å, 132º; 2.39 Å, 151º; 2.61 Å, 115º) H-bonds (Figure 6.4).

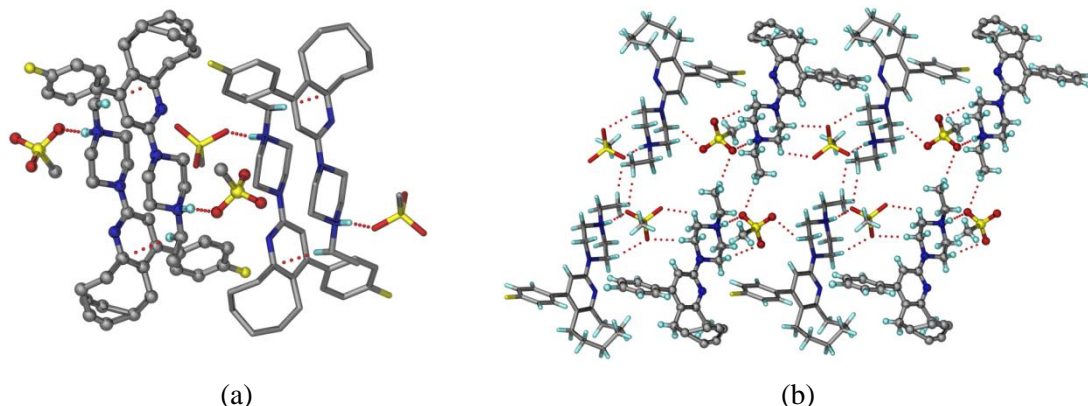<center>(a)   (b)</center>

Figure 6.4 (a) BLNH$^+$ cations form a dimeric motif through C−H···π interactions. Hydrogen atoms which are not involved in H-bonding are removed for clarity. (b) N$^+$−H···O$^-$ and C−H···O H-bonds in BLNH$^+$−MSA$^-$ anhydrous salt. Crystallographic independent ions are shown in ball-stick and capped-stick representation.

6.3.2 Spectroscopic Characterization

Spectroscopic methods such as IR and Raman are excellent tools in characterization of solid forms which is based on molecular functionalities and bonding interactions by probing vibrations of atoms.[14] BLN has no good functional groups except C–F, tertiary amine N and pyridine N, hence shifts in the vibrational frequencies with respect to the starting materials was used in identifying the formation of salt forms. Generally, neutral carboxylic acid (–COOH) exhibits a strong C=O stretching band around 1700 cm^{-1} and a weaker C–O stretch around 1200 cm^{-1}, while for a carboxylate anion (–COO$^-$) two characteristic coupled carbonyl absorption bands appear around 1600 cm^{-1} for asymmetric and 1400 cm^{-1} for symmetric stretching. Stretching frequencies for carboxylate group was found at 1605.5 cm^{-1} (asymmetric), 1413.2 cm^{-1} (symmetric) in BLNH$^+$–SUC$^-$–Form-I, and 1604.6 cm^{-1} (asymmetric), 1411.8 cm^{-1} (symmetric) in BLNH$^+$–SUC$^-$–Form-II. In both the forms stretching frequencies for carboxylic acid was found at 1709.5 cm^{-1} in BLNH$^+$–SUC$^-$–Form-I and at 1711.1 cm^{-1} in BLNH$^+$–SUC$^-$–Form-II, which indicate that salt former SUC (a dicarboxylic acid) has transferred one proton and left other carboxylic group unionized in both polymorphs. Similarly, formation of BLNH$^+$–MSA$^-$ salt polymorphs was identified based on the changes in the stretching frequencies of salt former MSA. In general, S=O

exhibits stretching frequency in the range of 1060-1020 cm^{-1}. The shift in the stretching frequency of S=O (1048.4 cm^{-1}) in MSA to the 1037.0 cm^{-1} in BLNH$^+$–MSA$^-$–Form-I and to 1043.1 cm^{-1} in BLNH$^+$–MSA$^-$–Form-II indicate the formation of salt polymorphs (Figure 6.5, Table 6.3). Similarly, all the salt forms were characterized by Raman spectroscopy significant Raman frequencies are summarized in Table 6.3 and spectra showed in Figure 6.6. The identity of BLNH$^+$–Cl$^-$–Form-I and BLNH$^+$–Cl$^-$–Form-II was confirmed by ^{13}C solid state-NMR which showed significant difference in both the forms (Figure 6.7). More number of peaks in BLNH$^+$–Cl$^-$–Form-II may be due to the presence of more than one molecule in the asymmetric unit.
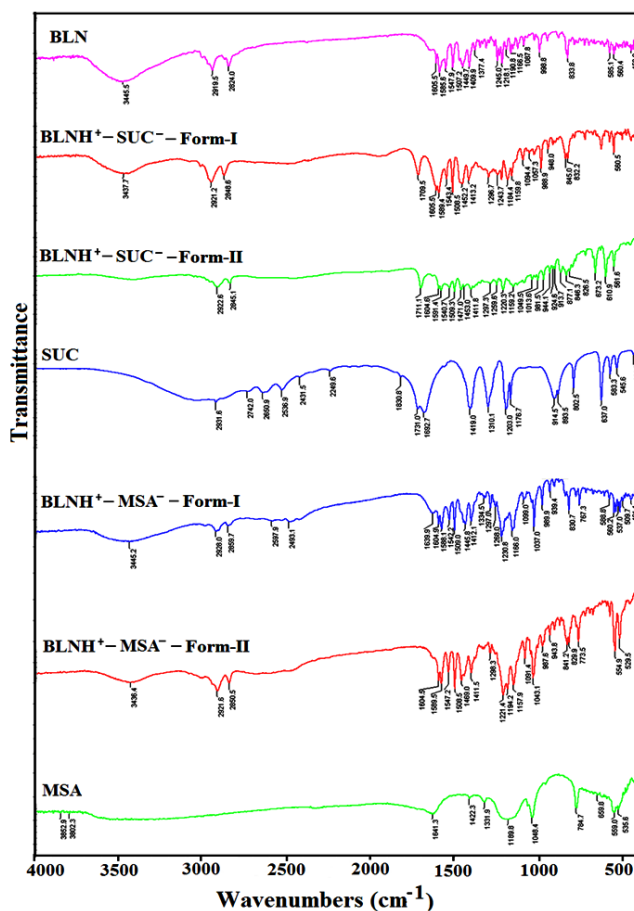

Figure 6.5 FT-IR spectral comparison of BLN salt forms with its individual components.
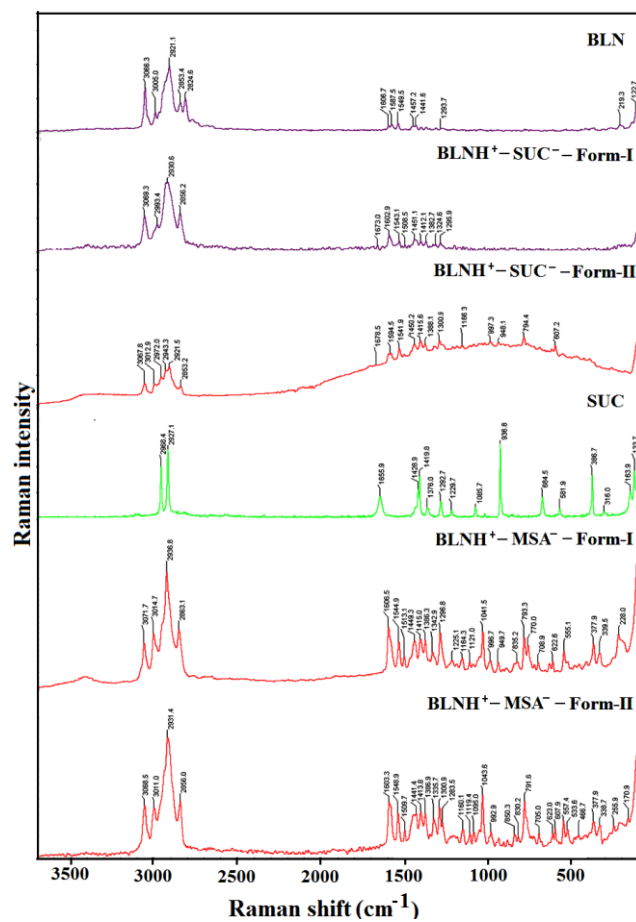
Figure 6.6 FT-Raman spectral comparison of BLN salt forms with its individual components.
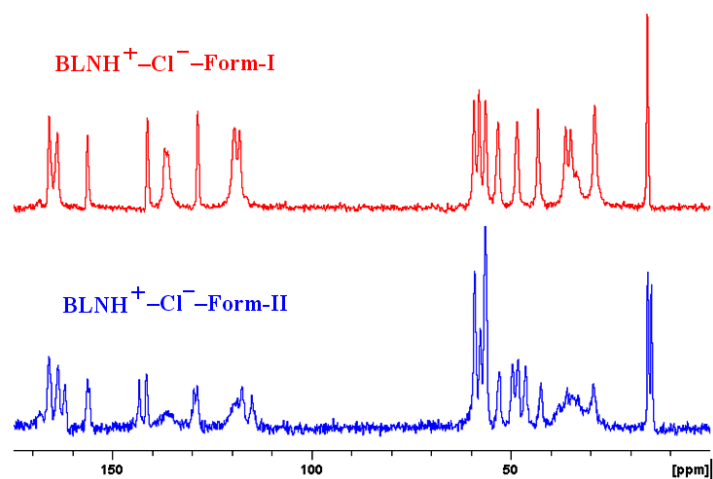
Figure 6.7 ^{13}C ss-NMR of BLNH$^+$–Cl$^-$–Form-I (red) and BLNH$^+$–Cl$^-$–Form-I (blue) of BLN salt forms. There appear to be differences in short range order and molecular packing in both the polymorphs as shown by ss-NMR spectra.

Table 6.3 FT-IR and Raman frequencies of BLN salt forms and starting components (cm^{-1}).

INFRARED						
compound	C–H Stretch	C–F stretch	Carboxylic C=O stretch	–COO$^-$ asym stretch	–COO$^-$ sym stretch	S=O stretch
BLN	2919.5	1245.0	-	-	-	-
SUC	-	-	1731.0	-	-	-
BLNH$^+$–SUC$^-$–Form-I	2921.2	1243.7	-	1605.5	1413.2	-
BLNH$^+$–SUC$^-$–Form-II	2922.6	1259.6	-	1604.6	1411.8	-
MSA	-	-	-	-	-	1048.4
BLNH$^+$–MSA$^-$–Form-I	2928.0	1230.8	-	-	-	1037.0
BLNH$^+$–MSA$^-$–Form-II	2921.6	1221.4	-	-	-	1043.1
RAMAN						
BLN	2921.1	1293.7	-	-	-	-
SUC	2927.1	-	1655.9	-	-	-
BLNH$^+$–SUC$^-$–Form-I	2930.6	1295.9	-	1673.0	1412.1	-
BLNH$^+$–SUC$^-$–Form-II	2921.5	1300.9	-	1678.5	1415.6	-
MSA	2936.8	1296.8	-	-	-	1041.5
BLNH$^+$–MSA$^-$–Form-I	2931.4	1300.9	-	-	-	1043.6
BLNH$^+$–MSA$^-$–Form-II	2921.1	1293.7	-	-	-	-

6.3.3 Powder X-ray diffraction

Powder X-ray diffraction has become an important tool for rapid identification and to establish the formation of novel solid forms such as cocrystals, polymorphs, salts, etc. in pharmaceutical industry.[15] Novel salt forms were prepared in bulk by liquid-assisted grinding (LAG) or slurry crystallization or by heating in the programmable oven or dehydration, and found that unique powder line pattern for each salt form (Figure 6.8a and Figure 6.9). We were successful in getting diffraction quality single crystals for all Form-I of salt forms ($BLNH^+$–Cl^-, $BLNH^+$–SUC^-, $BLNH^+$–MSA^-) but for Form-II of all salt forms we were unsuccessful to get diffraction quality crystals even after numerous crystallization experiments; however these were characterized by their unique powder line pattern. The experimental PXRD pattern of the all Form-I of salt forms were found excellent match with their respective calculated line diffraction pattern from crystal structures which confirm the bulk solid phase purity and homogeneity of the crystalline phase. PXRD lines of dimorphs of salt forms ($BLNH^+$–Cl^-, $BLNH^+$–SUC^-, $BLNH^+$–MSA^-) exhibited unique diffraction line pattern and can be distinguished easily between the forms (Figure 6.8a and Figure 6.9). The conversion of $BLNH^+$–Cl^- –Form-I to $BLNH^+$–Cl^- –Form-II of $BLNH^+$–Cl^- salt forms was confirmed through variable temperature powder X-ray diffraction (VTPXRD) measurement , which showed transition from $BLNH^+$–Cl^- –Form-I to $BLNH^+$–Cl^- –Form-II at 190–205 ℃ (Figure 6.8b). It was further supported by DSC and HSM (as discussed below).
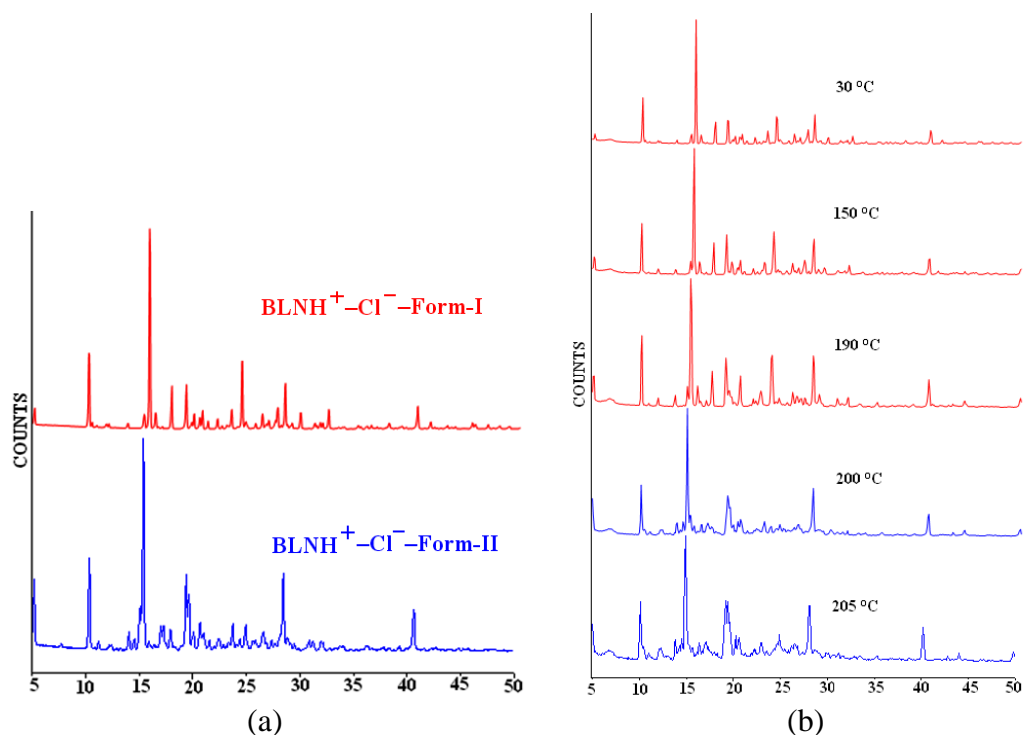
Figure 6.8 (a) PXRD comparison of BLNH⁺–Cl⁻–Form-I (red) and BLNH⁺–Cl⁻–Form-II (blue) show clear differences in diffraction peaks. (b) VTPXRD pattern of BLNH⁺–Cl⁻–Form-I (red) to show transformation to BLNH⁺–Cl⁻–Form-II (blue) upon heating.
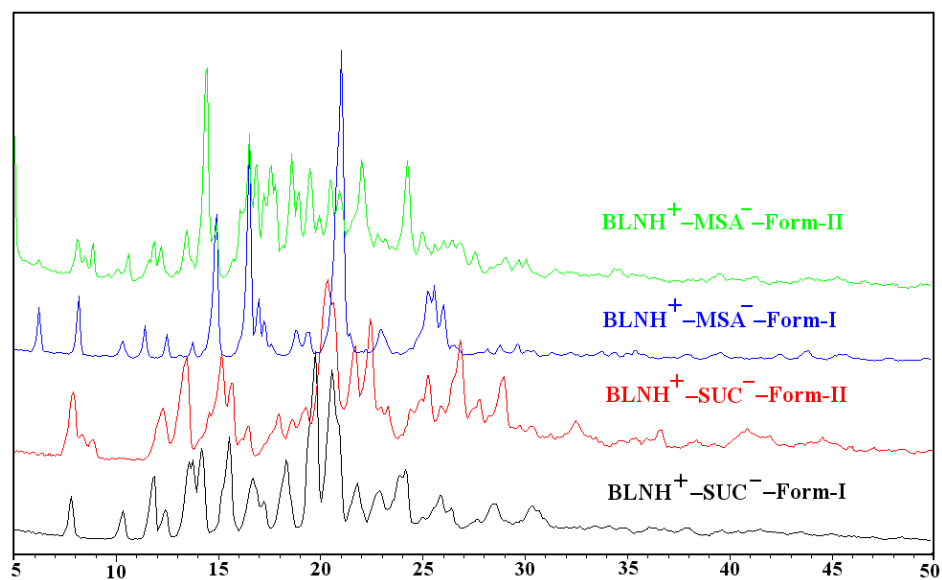
Figure 6.9 Overlay of experimental PXRD patterns of the BLN salt forms shows that each form exhibits unique powder lines.

6.3.4 Thermal Analysis

DSC has diverse advantages especially for polymorphs from which we can establish the sample purity, polymorphic transition temperatures and heat of fusion of each phase.[16] DSC of BLNH$^+$–Cl$^-$–Form-I showed an endothermic phase transition at 200 °C followed by melting endotherm at 255 °C (Figure 6.10a, red trace). TGA of the sample (Figure 6.10a, blue trace) showed no weight loss over the transition temperature range, which indicated the possible existence of a high temperature phase (BLNH$^+$–Cl$^-$–Form-II). No reversible phase transition was observed in a DSC heat–cool–heat cycle, which indicated that this high temperature phase (BLNH$^+$–Cl$^-$–Form-II) survived the temperature regime of the experiment (Figure 6.10b). The bulk material of BLNH$^+$–Cl$^-$–Form-II was obtained upon heating BLNH$^+$–Cl$^-$–Form-I to in separate experiment by salt bath at 220 °C. DSC of the resultant material of BLNH$^+$–Cl$^-$–Form-II showed a single melting endotherm at 255 °C (Figure 6.10a, green trace). The endotherm at 200 °C in the BLNH$^+$–Cl$^-$–Form-I is due to phase transformation of the BLNH$^+$–Cl$^-$–Form-I to BLNH$^+$–Cl$^-$–Form-II and the endotherm at 255 °C is the melting of the later form. Hence, from the heat of transition rule these forms (BLNH$^+$–Cl$^-$–Form-I and BLNH$^+$–Cl$^-$–Form-II) found to be enantiotropically related.[17] The transformation of BLNH$^+$–Cl$^-$–Form-I to the BLNH$^+$–Cl$^-$–Form-II was visualized on a hot stage microscope (HSM) as a solid-to-solid transformation event without the intermediacy of a melt transition at 200 ºC. The formation of flake like crystals of BLNH$^+$–Cl$^-$–Form-II from plate crystals of BLNH$^+$–Cl$^-$–Form-I was visualized in HSM snapshots (Figure 6.11). Numerous attempts to grow diffraction quality single crystals of BLNH$^+$–Cl$^-$–Form-II were unsuccessful due to their fragile nature. DSC on BLNH$^+$–SUC$^-$–Form-I showed characteristic melting endotherm at 148.9 °C without any phase transition, where as BLNH$^+$–SUC$^-$–Form-II exhibited endothermic transition at 125.0 °C and immediately followed by recrystallization to the other polymorph (BLNH$^+$–SUC$^-$–Form-I) which subsequently melts upon further heating (Figure 6.12a). At present in this case it is difficult to say whether an enantiotropic or monotropic[16] relationship is present between these two

forms. Similarly, DSC on BLNH$^+$–MSA$^-$–Form-I showed melting endotherm at 210.2 °C without any phase transition, where as BLNH$^+$–MSA$^-$–Form-II exhibited a small exothermic peak corresponding to polymorphic transformation to BLNH$^+$–MSA$^-$–Form-I at temperature 162.1 °C, and followed by melting of latter form at 210.3 °C upon further heating (Figure 6.12b). The transition is exothermic, which means that the two forms concerned are monotropically related to one another.

Crystallization of BLNH$^+$–Cl$^-$ salt from nitromethane afforded a monohydrate form and it was obtained in bulk by water assisted grinding of BLNH$^+$–Cl$^-$–Form-I. DSC and TGA plots of BLNH$^+$–Cl$^-$ monohydrate (Figure 6.13) exhibited water loss in a broad temperature range of 45–110 °C. The evolved vapor weight is consistent with one water molecule stoichiometry (obs. 4.19%, calc. 4.26%). Controlled dehydration of BLNH$^+$–Cl$^-$ monohydrate at 120 °C for 30 minutes resulted in the formation of BLNH$^+$–Cl$^-$–Form-I as analyzed by PXRD. Further heating up to 200 °C resulted in the formation of BLNH$^+$–Cl$^-$– Form-II, consistent with the endotherm at 180 ℃ in the DSC (Figure 6.13). But, the transformation to BLNH$^+$–Cl$^-$–Form-II is at lower temperature, compared to a sharp endotherm at 200 ℃ for BLNH$^+$–Cl$^-$–Form-I to BLNH$^+$–Cl$^-$–Form-II phase transition in Figure 6.10a. The kinetics of BLNH$^+$–Cl$^-$–Form-I to BLNH$^+$–Cl$^-$–Form-II phase transformation could be influenced by water in the crystal structure of the monohydrate leading to transformation at lower temperature.
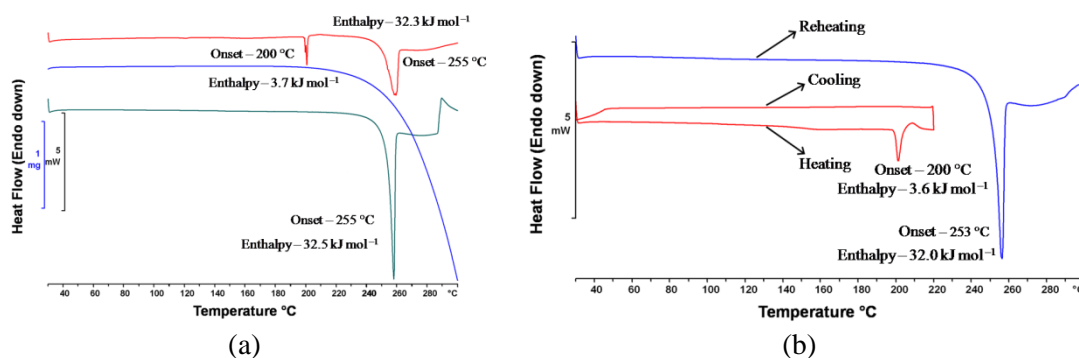

(a) (b)

Figure 6.10 (a) DSC of the BLNH$^+$–Cl$^-$–Form-I (red) and the BLNH$^+$–Cl$^-$–Form-II (green). The former showed phase transition (at 200 °C) before melting whereas the latter polymorph is stable to temperature changes in the range studied. TGA of BLNH$^+$–Cl$^-$–Form-I (blue)

showed no weight loss over the phase transition temperature. (b) Heat–cool–heat DSC of BLNH$^+$–Cl$^-$–Form-I to show phase transition to the high temperature form (BLNH$^+$–Cl$^-$–Form-II).

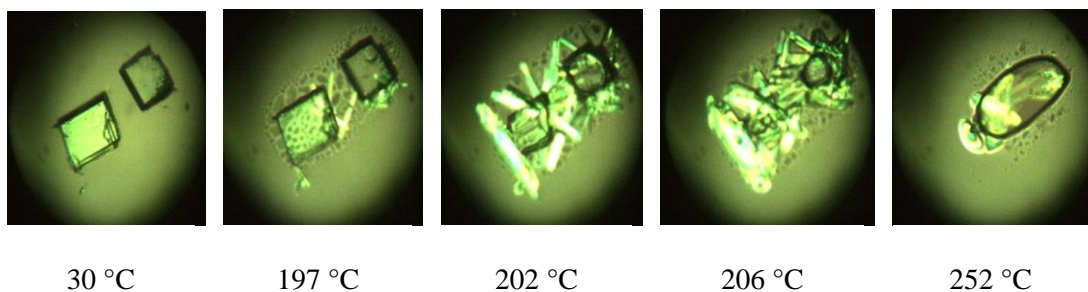| 30 °C | 197 °C | 202 °C | 206 °C | 252 °C |

Figure 6.11 HSM snapshots of BLNH$^+$–Cl$^-$–Form-I to show the transformation at about 200 ºC and melting of the transformed phase at 252 ºC. The plate crystal morphology of BLNH$^+$–Cl$^-$–Form-I converted to flake like crystals of BLNH$^+$–Cl$^-$–Form-II before melting.
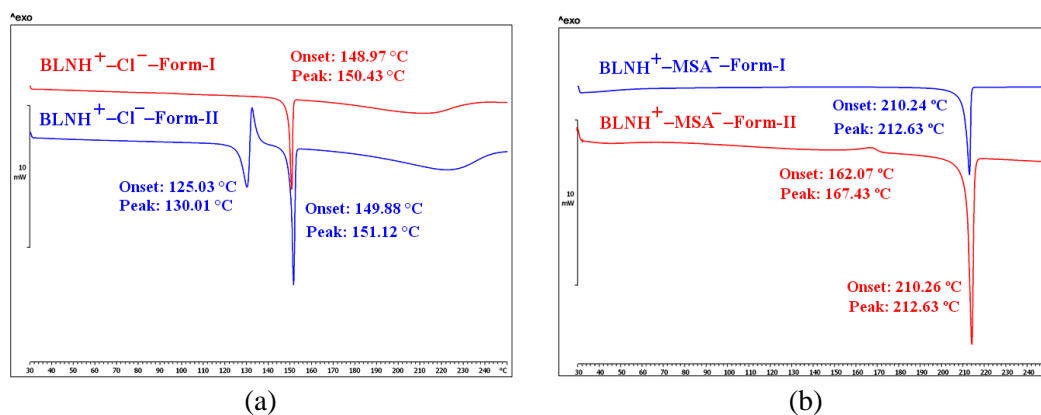

Figure 6.12 DSC thermograms of (a) BLN$^+$–SUC$^-$ salt polymorphs and (b) BLN$^+$–MSA$^-$ salt polymorphs.
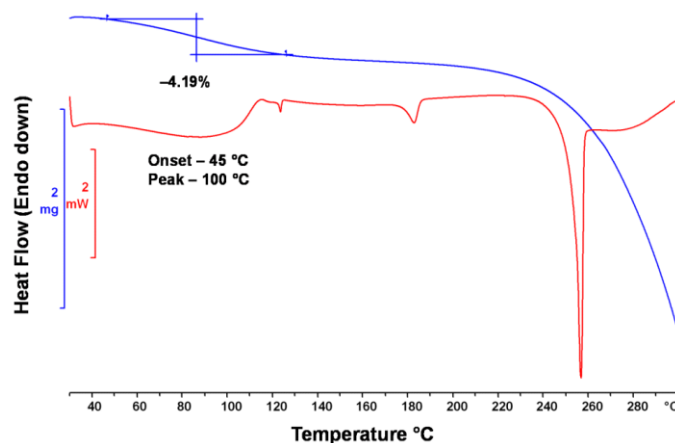
Figure 6.13 DSC (red) and TGA (blue) of BLNH$^+$–Cl$^-$ monohydrate. Weight loss in TGA is consistent with one water molecule for the endotherm at about 100 °C in DSC. The thermal behavior of dehydrated monohydrate to give the BLNH$^+$–Cl$^-$–Form-I and then its transformation to BLNH$^+$–Cl$^-$–Form-II polymorph is slightly different from that of BLNH$^+$–Cl$^-$–Form-I (phase transition endotherm to BLNH$^+$–Cl$^-$–Form-II at 180 ºC here compared to 200 ºC in Figure 6.10a).

6.3.5 Solid Form Stability

The relative stability of BLNH$^+$–Cl$^-$–Form-I, Form-II, and BLNH$^+$–Cl$^-$ monohydrate were established by grinding and slurry[18] experiments. Both the BLNH$^+$–Cl$^-$–Form-I and the BLNH$^+$–Cl$^-$ monohydrate were stable after one hour of dry grinding in a mortar-pestle in independent experiments which was established through FT-IR and PXRD. However, the BLNH$^+$–Cl$^-$–Form-II was converted to BLNH$^+$–Cl$^-$–Form-I upon grinding (Figure 6.14). Addition of a few drops of water to BLNH$^+$–Cl$^-$ salt forms (BLNH$^+$–Cl$^-$–Form-I or Form-II) during grinding gave the BLNH$^+$–Cl$^-$ monohydrate. Thus the relative stability of BLNH$^+$–Cl$^-$–Form-I , II and BLNH$^+$–Cl$^-$ monohydrate were found be BLNH$^+$–Cl$^-$ monohydrate > BLNH$^+$–Cl$^-$–Form-I > BLNH$^+$–Cl$^-$–Form-II. With the similar experiments relative stability order of BLNH$^+$–SUC$^-$ and BLNH$^+$–MSA$^-$ salt forms were established. Neat grinding (NG) of pure BLNH$^+$–SUC$^-$–Form-I showed complete conversion to BLNH$^+$–Cl$^-$–Form-II after 1h, whereas no effect on BLNH$^+$–SUC$^-$–Form-II under similar experimental conditions over extended period of 1-2 h. Further, slurry grinding (in water and ethanol) of BLNH$^+$–SUC$^-$–

Form-I also converted into BLNH$^+$–SUC$^-$–Form-II at ambient conditions of stirring for overnight. Hence relative stability order for both the forms were found to be BLNH$^+$–SUC$^-$–Form-II > BLNH$^+$–SUC$^-$ –Form-I. Similarly, upon neat grinding of pure BLNH$^+$–MSA$^-$–Form-II for 30 min showed that transformation of BLNH$^+$–MSA$^-$–Form-II to BLNH$^+$–MSA$^-$–Form-I which was monitored by PXRD (Figure 6.15). With these observations the relative stability order of the BLNH$^+$–MSA$^-$ salt forms found to be BLNH$^+$–MSA$^-$–Form-I > BLNH$^+$–MSA$^-$–Form-II.
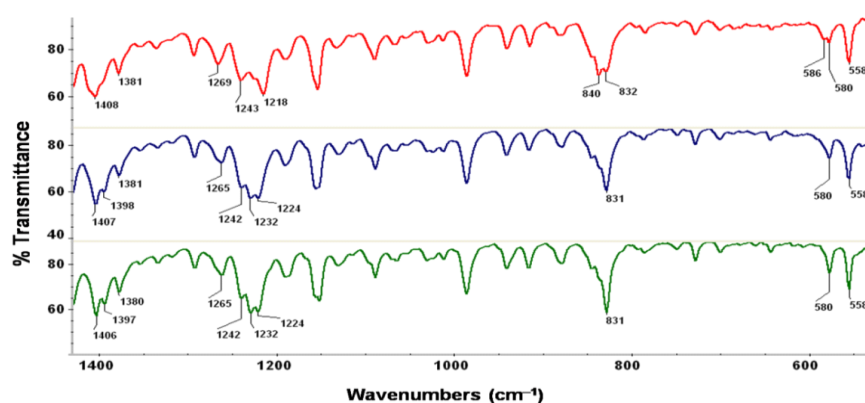
Figure 6.14 FT-IR spectra to show transformation of BLNH$^+$–Cl$^-$–Form-II (red, top) to BLNH$^+$–Cl$^-$–Form-I (green, bottom) after grinding for 1 h. The ground material of the BLNH$^+$–Cl$^-$–Form-II (blue, middle) shows peaks characteristic of BLNH$^+$–Cl$^-$–Form-I with respect to C–N (1400 cm^{-1}), C–F (1230 cm^{-1}) and C–H (830, 580 cm^{-1}) vibrations.

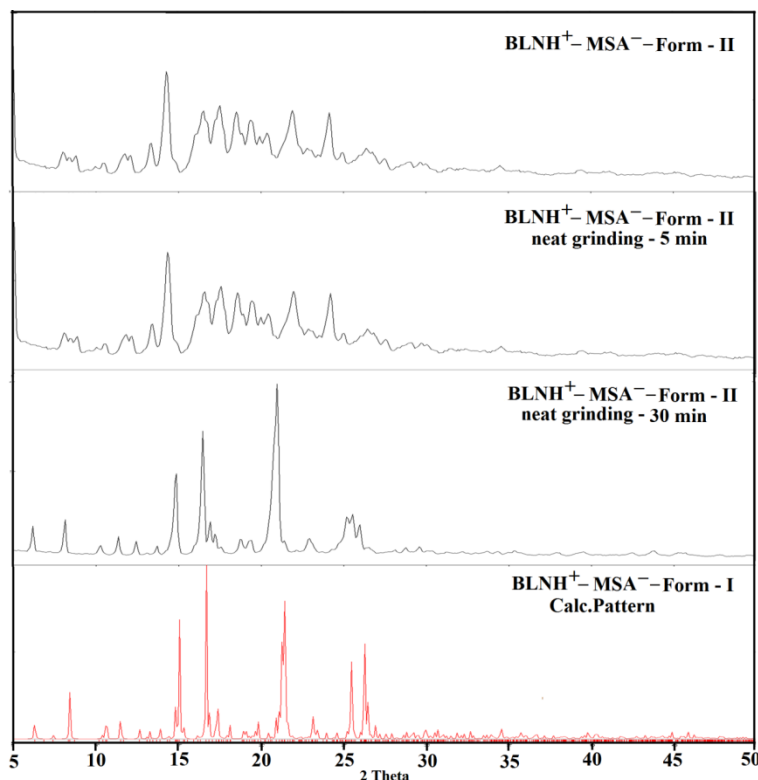**Figure 6.15** Overlay of experimental PXRD patterns represent the conversion of BLNH⁺–MSA⁻–Form-II (top) to BLNH⁺–MSA⁻–Form-I after neat grinding of BLNH⁺–MSA⁻–Form-II for 30 min. The calculated pattern of BLNH⁺–MSA⁻–Form-I (red) showed for comparison.

Stability studies on BLN salt forms were carried out in accelerated ICH conditions[12] of 40°C temperature and 75% relative humidity. Powder XRD was recorded on all the solid forms at regular intervals up to 3 months. Based on the characteristic peak positions, stability of the samples to the set humidity conditions was assessed. BLNH⁺–Cl⁻–Form-I, Form-II and BLNH⁺–SUC⁻–Form-I, Form-II were found to be stable throughout the 3 months period of stability test (Figure 6.16 and chapter 4 Figure 4.14). However, BLNH⁺–MSA⁻–Form-I and BLNH⁺–MSA⁻–Form-II were found to convert into monohydrate form (BLNH⁺–MSA⁻–H₂O) upon similar conditions within 4 weeks and 48 h respectively based on the changes in powder XRD pattern (Figure 6.17 and chapter 4 Figure 4.12). From the ICH stability studies we found that BLNH⁺–Cl⁻ salt Forms-I and II and BLNH⁺–SUC⁻ salt Forms-I and II

exhibited good stability as that of the reference drug but with the added advantage of higher solubility/dissolution (discussed later) compared to BLN.
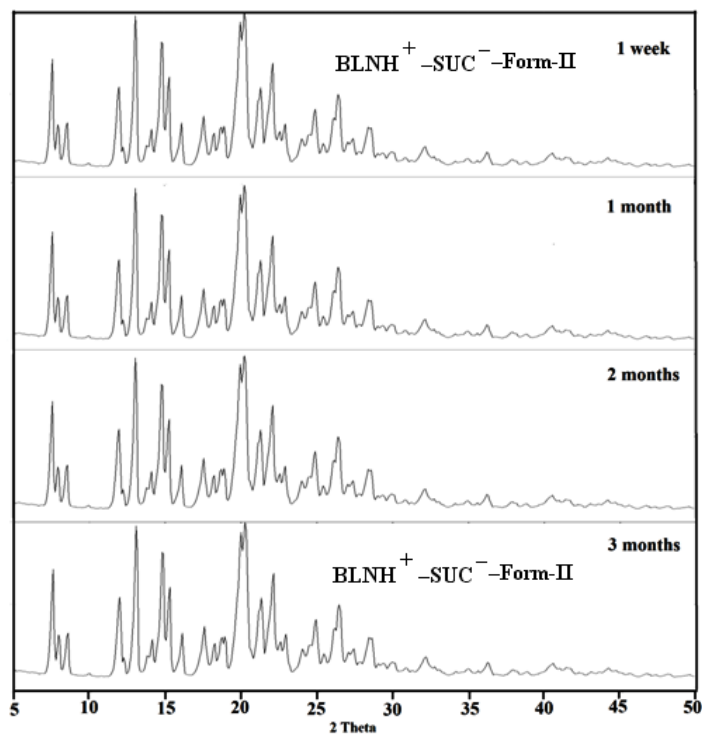

Figure 6.16 Overlay of PXRD patterns from the stability study of $BLNH^+–SUC^-–$Form-II at 40 °C and 75% RH showed that no polymorphic conversion/hydrate formation up to 3 months.
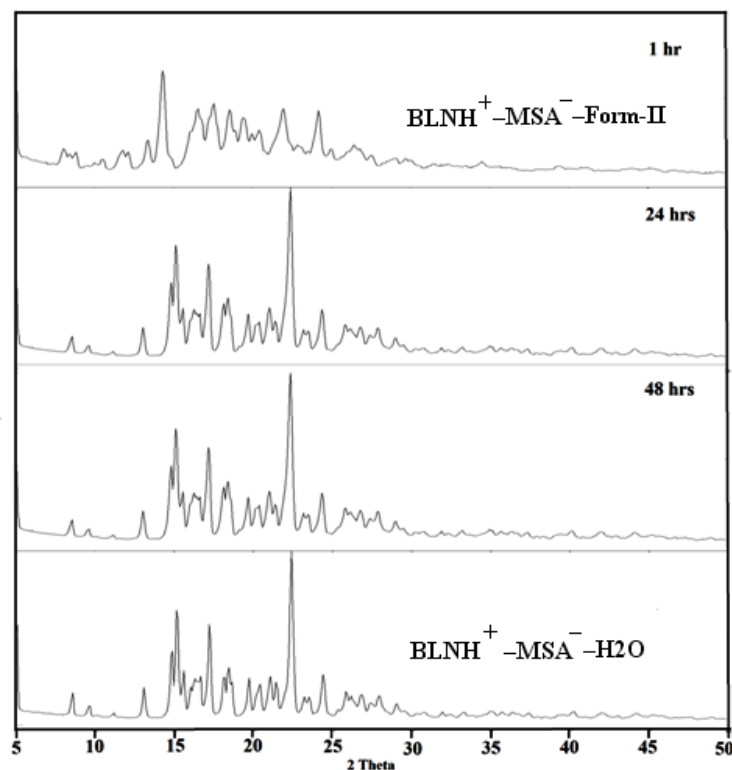
Figure 6.17 Overlay of PXRD patterns from the stability study of BLNH$^+$–MSA$^-$–Form-II at 40 °C and 75% RH showed that transformation of BLNH$^+$–MSA$^-$–Form-II to BLNH$^+$–MSA$^-$ monohydrate after 48 h.

6.3.6 Solubility and Dissolution

The search for more soluble and bioavailable drug forms is a current challenge in pharmaceutical development. Blonanserin base is practically insoluble in water (0.033 mg/L). Surprisingly BLNH$^+$–Cl$^-$ salt (Form-I) too is very insoluble in water (0.112 mg/L).[11] The equilibrium solubility of values of all the salt forms BLN were therefore measured in 60% EtOH–water medium. The solubility values (at 24 h) of BLN free base and BLN HCl salt are of 1.6 mg/mL and 119.2 mg/mL, respectively, as measured by UV-Vis spectra calibration curves.[19] The solubility value of BLNH$^+$–Cl$^-$ salt actually corresponds to its monohydrate form since the undissolved material after 24 h of the solubility experiment is the monohydrate. The transformation of BLNH$^+$–Cl$^-$ salt to its monohydrate form was also checked in controlled experiment and found that transformation occurred in 1 h. BLNH$^+$–

SUC⁻–Form-I was found to convert into BLNH⁺–SUC⁻–Form-II upon slurry for 24 h in equilibrium solubility conditions. Hence, solubility of BLNH⁺–SUC⁻–Form-I could not be determined where as the solubility of BLNH⁺–SUC⁻–Form-II found to be 468.8 mg/mL. Similarly, under slurry conditions of solubility experiments BLNH⁺–MSA⁻–Form-I and BLNH⁺–MSA⁻–Form-II found to convert into BLNH⁺–MSA⁻ salt hydrate form as discussed in the chapter 4.

Further, IDR experiments on BLN salt forms were performed in 60% EtOH−water medium for 45 min by the rotating disk intrinsic dissolution rate (DIDR) method[20] at 37 °C. All the salt forms exhibited improved dissolution rate compared to the parent drug and were stable until the end of the IDR experimental conditions. Only the exception was found to be with BLNH⁺–MSA⁻ salt forms which were converted into monohydrate form as expected. The extent of salt forms dissolved over 30 min were BLNH⁺–MSA⁻–Form-II 73%, BLNH⁺–MSA⁻–Form-I 68 %, BLNH⁺–SUC⁻–Form-I 51%, BLNH⁺–SUC⁻–Form-II 50%, BLNH⁺–Cl⁻–Form-II 10%, BLNH⁺–Cl⁻–Form-I 8% and BLN 0.5% (Figure 6.18). Dissolution curves for all the salt polymorphic systems were displayed in Figure 6.18 and the calculated IDR values presented in Table 6.4. In Figure X, BLNH⁺–MSA⁻ salt forms exhibited faster dissolution for the first 23-25 min, after 25 min curves became stagnant may be due to the conversion of BLNH⁺–MSA⁻ salt forms to BLNH⁺–MSA⁻ salt hydrate. The calculated IDR values of the salt forms followed the order BLNH⁺–MSA⁻–Form-II > BLNH⁺–MSA⁻–Form-I > BLNH⁺–SUC⁻–Form-I ≈ BLNH⁺–SUC⁻–Form-II > BLNH⁺–Cl⁻–Form-II > BLNH⁺–Cl⁻–Form-I > BLN. In this chapter we have spotlighted screening of BLN salt polymorphs and found that BLNH⁺–SUC⁻–Form-II found to be high soluble and excellent stability candidate in anhydrous salt forms of BLN for formulation purpose.
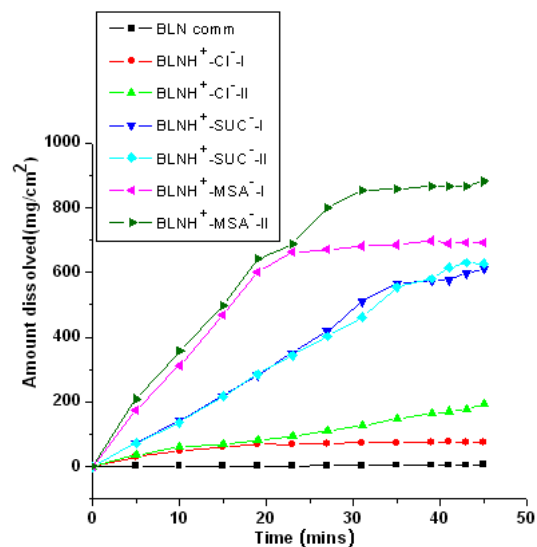
Figure 6.18 IDR curves of BLN salt polymorphs.

Table 6.4 Molar extinction coefficient values and IDR values of BLN salt forms in 60% ethanol−water.

Drug/ salt former	Solubility of salt former in water (mg/mL)	Drug/Salt form	ε (mL mg^{-1} cm^{-1})	IDR in 60% EtOH−water (mg cm^{-2} min^{-1})
BLN	3.3×10^{-5}	BLN	9.92536	0.20
HCl	673.0	BLNH$^+$–Cl$^-$–Form-I	42.9814	4.04 (x20.2)
HCl	673.0	BLNH$^+$–Cl$^-$–Form-II	42.2712	4.57 (x22.85)
SUC	83.5	BLNH$^+$–SUC$^-$–Form-I	9.48963	12.32 (x61.9)
SUC	83.5	BLNH$^+$–SUC$^-$–Form-II	9.79721	12.12 (x60.6)
MSA	1000.0	BLNH$^+$–MSA$^-$–Form-I	10.44853	26.28 (x132.0)
MSA	1000.0	BLNH$^+$–MSA$^-$–Form-II	10.02674	27.01 (x135.1)

6.4 Conclusions

Blonanserin belongs to BCS class II having poor aqueous solubility which is used for schizophrenia. Various salt screening techniques such as liquid assisted grinding, dehydration, slurry crystallization, heating and solvent evaporative crystallization with GRAS molecules resulted dimorphs for $BLNH^+–Cl^-$, $BLNH^+–SUC^-$, $BLNH^+–MSA^-$ and a $BLNH^+–Cl^-$ monohydrate. These novel salt forms were characterized by spectroscopic (FT-IR, FT-Raman, ss-NMR), thermal (DSC, TGA and HSM), and X-ray diffraction techniques. Structural analysis revealed that proton transferred from salt former to the piperazine N_3 atom of BLN and sustained by $N^+–H \cdots O^-$ ionic H-bond. Stability at ICH conditions (40 °C, 75% RH) showed that dimorphs of $BLNH^+–MSA^-$ (Form-I and II) were found convert into $BLNH^+–MSA^-$ monohydrated form, where as dimorphs of $BLNH^+–Cl^-$ (Form-I and II) and $BLNH^+–SUC^-$ (Form-I and II) were found to be stable for 3 months. The relative stability studies resulted that stability order for $BLNH^+–Cl^-$ salt forms as $BLNH^+–Cl^-$ monohydrate > $BLNH^+–Cl^-$–Form-I > $BLNH^+–Cl^-$–Form-II, for $BLNH^+–MSA^-$ salt forms $BLNH^+–MSA^-$–Form-I > $BLNH^+–MSA^-$–Form-II, and for $BLNH^+–SUC^-$ salt forms $BLNH^+–SUC^-$–Form-II > $BLNH^+–SUC^-$ –Form-I. In this chapter we have spotlighted screening of polymorphs for salts and found that $BLNH^+–SUC^-$–Form-II found to be promising candidate for formulation purpose with twin advantages of high solubility (468.8 mg/mL, 293 times) and excellent stability. Further, this chapter highlights the proper selection of suitable polymorphic form of a salt as one of the most important activities that critically affect the successful development of a drug candidate.

6.5 Experimental Section

Materials and Methods: Blonanserin base and blonanserin hydrochloride were purchased from Shanghai Shibo Chemical Co. Ltd., China, and were used without further purification. The salt formers (purity >99.8%) were purchased from Sigma-Aldrich, Hyderabad, India. All other chemicals were of analytical or chromatographic grade. Water purified from a deionizer-cum-mixed-bed purification system (AquaDM, Bhanu, Hyderabad, India) was used in the experiments.

Preparation of BLN salt forms

BLNH$^+$–Cl$^-$–Form-I: About 50 mg of blonanserin hydrochloride was dissolved in 8 mL hot benzene and left for slow evaporation at room temperature. Colorless block crystals were obtained after a few days upon solvent evaporation.

^{1}H NMR (CDCl$_3$, δ, Hz): 1.34 (4H, t, *J* 5), 1.39 (4H, m), 1.50 (3H, t, *J* 8), 1.75 (4H, m), 2.57 (4H, t, *J* 5), 2.87 (4H, t, *J* 6), 3.10 (2H, q, *J* 7), 6.31 (1H, s), 7.08 (2H, t, *J* 8), 7.18 (2H, dd, *J* 8, 5), 12.81 (1H, s).

BLNH$^+$–Cl$^-$–Form-II: The bulk material of BLNH$^+$–Cl$^-$–Form-II was obtained upon heating BLNH$^+$–Cl$^-$–Form-I in the programmable oven at 200 °C for 20 min. The resultant material was characterized by various techniques like FT-IR, PXRD, DSC, and ^{13}Css-NMR. We were unsuccessful in getting the diffraction quality single crystals even after number of trails.

BLNH$^+$–Cl$^-$ monohydrate: About 50 mg of BLNH$^+$–Cl$^-$–Form-I was dissolved in 5 mL hot nitromethane and left for slow evaporation at room temperature. The bulk material of monohydrate form was obtained in bulk by water assisted grinding of BLNH$^+$–Cl$^-$–Form-I. Colorless plate crystals obtained after a few days of solvent evaporation which were identified as a monohydrate.

BLN$^+$–SUC$^-$–Form-I: This salt form was obtained by co-grinding BLN (100 mg, 0.272 mmol) and SUC (32.1 mg, 0.272 mmol) in stoichiometric ratio for 30 min by adding catalytic amount (two or three drops) of EtOH solvent. The formation of salt form was confirmed by FT-IR, FT-Raman, PXRD and DSC. Colorless single crystals suitable for X-ray diffraction were obtained upon dissolving 30 mg of ground material in 8 mL hot EtOAc-ethyl methyl ketone (1:1 v/v) solvent mixture and left for slow evaporation.

BLN$^+$–SUC$^-$–Form-II: The bulk material of BLN$^+$–SUC$^-$–Form-II was obtained by slurry crystallization of 200 mg BLN$^+$–SUC$^-$–Form-I in 10 mL water: ethanol (3:2 v/v) solvent

mixture for 24h. After 24 h the resultant precipitate was filtered and identified as BLN^+–SUC^-–Form-II with various techniques such as FT-IR, Raman, PXRD and DSC. We were unsuccessful in getting the diffraction quality single crystals so far even after numerous trails.

BLN^+−MSA^-–Form-I: This salt form was obtained in bulk upon grinding about 150 mg of a 1:1 stoichiometric ratio of BLN and MSA for 30 min by liquid-assisted grinding (EtOH solvent). The formation of salt was confirmed by FT-IR, FT-Raman, PXRD and DSC. 30 mg of the ground material was dissolved in 8 mL hot toluene−EtOAc solvent mixture (1:1, v/v) and left for slow evaporation at ambient conditions. Colorless needle-shaped crystals suitable for X-ray diffraction were obtained after 3-4 d upon solvent evaporation.

BLN^+−MSA^-–Form-II: The bulk material of BLN^+−MSA^-–Form-II was obtained upon dehydration of $BLNH^+$–MSA^-–H_2O salt hydrate. Salt hydrate was kept in the programmable oven at 100 °C for 30 min and the resultant material was found to be BLN^+−MSA^-–Form-II analyzed by FT-IR, Raman, PXRD and DSC. Single crystals for X-ray diffraction were not harvested even after many crystallization experiments.

Spectroscopy: Thermo-Nicolet 6700 Fourier transform infrared spectrophotometer with NXR-Fourier transform Raman module (Thermo Scientific, Waltham, Massachusetts) was used to record IR and Raman spectra. IR spectra were recorded on samples dispersed in KBr pellets. Raman spectra were recorded on samples contained in standard NMR diameter tubes or on compressed samples contained in a gold-coated sample holder. Data was analyzed using the Omnic software (Thermo Scientific, Waltham, Massachusetts). Solution and solid state NMR spectra were recorded on a Bruker Avance spectrometer at 400 MHz. ss-NMR experiments were carried out on Bruker 4 mm double resonance CPMAS probe in zirconia rotors at 5.0 kHz with a cross-polarization contact time of 2.5 ms and a recycle delay of 8 s. ^{13}C-CPMAS spectra recorded at 100 MHz were referenced to methylene carbon of glycine and then the chemical shifts were recalculated to the TMS scale ($\delta_{glycine}$ = 43.3 ppm).

Thermal Analysis: DSC was performed on a Mettler Toledo DSC 822e module and calibrated with Indium (T_m = 156.60 °C; ΔH_f = 28.45 J g^{-1}) and Zinc (T_m = 419.50 °C; ΔH_f =

107.50 J g^{-1}) as per the manufacturer's specifications. TGA was performed on a Mettler Toledo TGA/SDTA 851e module calibrated with indium (T_m = 156.60 °C) and aluminum (T_m = 660.30 °C). The temperature range used for both DSC and TGA is 30–300 °C @ 5 °C/min. The typical sample size is 3-5 mg for DSC and 8-12 mg for TGA. Samples were placed in crimped but vented aluminum pans for DSC and open alumina pans for TGA and were purged by a stream of nitrogen flowing at 80 mL/min.

X-ray crystallography: X-ray reflections for BLN salt forms were collected at 100 K on Bruker SMART-APEX CCD diffractometer equipped with a graphite monochromator and Mo-Kα fine-focus sealed tube (λ = 0.71073 Å). Data reduction was performed using Bruker SAINT Software.[21] Intensities were corrected for absorption using SADABS,[22] and the structure was solved and refined using SHELX-97.[23] All non-hydrogen atoms were refined anisotropically. Hydrogen atoms on heteroatoms were located from difference electron density maps and all C−H hydrogens were fixed geometrically. Hydrogen bond geometries were determined in Platon.[24] X-Seed[25] was used to prepare packing diagrams.

Powder X-ray Diffraction: Powder X-ray diffraction of all the samples were recorded on Bruker D8 Advance diffractometer using Cu-Kα X-radiation (λ = 1.5406 Å) at 40 kV and 30 mA. Diffraction patterns were collected over 2θ range of 5-50° at scan rate of 1° min^{-1}. Powder Cell 2.4[26] was used for Rietveld refinement. VT-PXRD was performed on the same instrument equipped with a variable temperature stage (TTK450 chamber, working temperature range –190 °C to 450 °C). The sample was packed in a Cr–plated copper holder and heated from 30 °C to 210 °C at 5 °C/min. Scans were taken at selected temperatures over 2θ range of 5-50°, using a step size of 0.08° 2θ and time/step of 1 sec.

Solubility and dissolution measurements: The solubility of BLN salt forms were measured using the Higuchi and Connors method[27] in 60% EtOH-water medium at ambient conditions. Prior to solubility measurements, standard curves of the compounds were obtained at the given λ_{max} (314-315 nm) spectrophotometrically using a Thermo Scientific Evolution 300 UV-Vis spectrometer (Thermo Scientific, Waltham, MA). Absorbance values were plotted against several known concentrations to prepare the concentration vs. intensity calibration curve. From the slope of the calibration curves, molar extinction coefficients for salt forms

were calculated. Excess amount of powdered compound was added to 5 mL of 60% EtOH–water solution to result in a suspension which was stirred at room temperature for 24 h. The suspension was then filtered through 2.5 μm Whatman filter paper. The concentration of the solution thus obtained was determined with appropriate dilution using the pre-determined standard curves.

Intrinsic dissolution rate (IDR) measurements were carried out on a USP certified Electrolab TDT-08 L Dissolution Tester (Electrolab, Mumbai, MH, India). Dissolution experiments were performed for 45 min in 60% EtOH–water at 37 °C. Prior to IDR estimation, standard curves for all the compounds were obtained spectrophotometrically at their respective λ_{max}. The slope of the plot from the standard curve gave the molar extinction coefficient (ε) by applying the Beer−Lambert's law, which was used to determine the IDR values. For IDR measurements, 500 mg of the solid material of each salt form was taken in the intrinsic attachment and compressed to a 0.5 cm^2 pellet using a hydraulic press at a pressure of 2.5 ton/inch^2 for 4 min. The pellet was compressed to provide a flat surface on one side and the other side was sealed. Then the pellet was dipped into 500 mL of 60% EtOH−water medium at 37 °C with the paddle rotating at 150 rpm. At a specific time interval, 5 mL of the dissolution medium was withdrawn and replaced by an equal volume of fresh medium to maintain a constant volume. Samples were filtered through 0.2 μm nylon filter and assayed for drug content spectrophotometrically at λ_{max} on a Thermo-Nicolet EV300 UV−vis spectrometer. There was no interference to BLN λ_{max} (314 nm) in UV-Vis with salt formers (HCl, SUC and MSA) which absorb strongly at 210−263 nm. The amount of drug dissolved in each time interval was calculated using the calibration curve. The linear region of the dissolution profile was used to determine the intrinsic dissolution rate (IDR) of the compound (= slope of the curve, that is, the amount of drug dissolved divided by the surface area of the disk (0.5 cm^2) per minute). The dissolution rates for BLN and its salt forms were computed from their IDR values.

6.6 References

1. (a) S. L. Childs, G. P. Stahly, A. Park, *Mol. Pharmaceutics* 2007, **4**, 323. (b) C. B. Aakeröy, M. E. Fasulo, J. Desper, *Mol. Pharmaceutics* 2007, **4**, 317.(c) A. J. Cruz-Cabeza, *CrystEngComm* 2012, **14**, 6362.

2. US-FDA GRAS chemical list, http://www.fda.gov/Food/IngredientsPackagingLabeling/FoodAdditivesIngredients/ucm091048.htm (accessed 20 February 2015).

3. (a) T. M. Serajuddin, *Adv. Drug Delivery Rev.* 2007, **59**, 603. (b) P. M. Bhatt, N. V. Ravindra, R. Banerjee, G. R. Desiraju, *Chem. Commun.* 2005, 1073. (c) R. Thakuria, A. Nangia, *CrystEngComm* 2011, **13**, 1759. (d) P. L. Gould, *Int. J. Pharm.*, 1986, **33**, 201.(e) D. Maddileti, B. Swapna, A. Nangia, *Cryst. Growth Des.* 2014, **14**, 2557.(e) S. Domingos, V. André, S. Quaresma, I. C. Martins, M. F. Minas da Piedade, M. T. Duarte, *J. Pharm. Pharmacol.*2015, DOI: 10.1111/jphp.12384.

4. (a) A.T.M. Serajuddin, M. Pudipeddi, Salt selection strategies, in: P.H. Stahl, C.G. Wermuth (Eds.), *Handbook of Pharmaceutical Salts: Properties, Selection, and Use*, Wiley-VCH, Weinheim, 2002, pp. 135–160. (b) P.H. Stahl, Salt selection, in: R. Hilfiker (Ed.), *Polymorphism in pharmaceutical industry*, John Wiley and Sons, Weinheim, 2006, pp. 309–322. (c) R. J. Bastin, M. J. Bowker, B. J. Slater, *Org. Process Res. Dev.*, 2000, **4**, 427. (d) S. M. Berge, L. D. Bighley, D. C. Monkhouse, *J. Pharm. Sci.* 1977, **66**, 1.

5. G. S. Paulekuhn, J. B. Dressmann, C. Saal, *J. Med. Chem.*, 2007, **50**, 6665.

6. M. Oka, K. Hino, *Drugs Fut.,* 1992, **17**, 9.

7. Dainippon Sumitomo Pharma Co., Ltd. (2008), Lonasen®, http://www.ds-pharma.com/news/pdf/ene20080421.pdf

8. (a) E.D. Deeks, G.M. Keating, *CNS Drugs,* 2010, **24**, 65. (b) E. Garcia, M. Robert, F. Peris, H. Nakamura, N. Sato, Y. Terazawa, *CNS Drugs,* 2009, **23**, 615.

9. K. Suzuki, Y. Hiyama, T. Une, I. Fujiwara, *Anal. Sci.*, 2002, 1**8**, 1289.

10. C. E. Heading, *IDrugs: The Investigational Drugs Journal*, 1998, **1**, 813.

11. ChemSpider: Chemical Structure Database freely distributed by the RSC, www.chemspider.com (accessed 20 February 2015).

12. http://www.ich.org/fileadmin/Public_Web_Site/ICH_Products/Guidelines/Quality/Q 1F/Stability_Guideline_WHO.pdf (accessed 20 February 2015).

13. (a) M. C. Etter, *Acc. Chem. Res*. 1990, **23**, 120. (b) J. Bernstein, R. E. Davis, L. Shimoni, N. L. Chang, *Angew. Chem., Int. Ed. Engl.* 1995, **34**, 1555.

14. (a) R. M. Silverstein, *Spectrometric Identification of Organic Compounds*. 6th Ed. John Wiley and Sons, Inc.: New York, 2002. (b) E. Smith, G. Dent, *Modern Raman Spectroscopy, A Practical Approach*, John Wiley: New York, 2005.

15. (a) J. F. Remenar, M. L. Peterson, P. W. Stephens, Z. Zhang, Y. Zimekov, M. B. Hickey, *Mol. Pharmaceutics* 2007, **4***, 386. (b) S. Karki, T. Friščić, L. Fábián, W. Jones, *CrystEngComm* 2010, **12**, 4038.

16. (a) J. L. Ford, P. Timmins, *Pharmaceutical Thermal Analysis*, Techniques and Applications. New York: Horwood, E.; Chichester, 1989. (b) H. G. Brittain, *Polymorphism in Pharmaceutical Solids*, Marcel Dekker, New York, 1999.

17. A.Burger, R. Ramberger, *Mikrochim. Acta II* 1979, 259.

18. (a) S. R. Byrn, R. R. Pfeiffer, J. G. Stowell, ed., *Solid-state Chemistry of Drugs*, SSCI Inc., 1999. (b) G. G. Z. Zhang, D. Law, E. A. Schmitt, Y. Qiu, *Adv. Drug. Deliv. Rev*., 2004, **56**, 371.

19. (a) P. Schneider, S. S. Hosseiny, M. Szczotka, V. Jordan, K. Schlitter, *Phytochem. Lett*., 2009, **2**, 85.

20. L. X. Yu, A. S. Carlin, G. L. Amidon, A. S. Hussain, *Int. J. Pharm.* 2004, **270**, 221.

21. *SAINT-Plus*, version 6.45; Bruker AXS Inc.: Madison, Wisconsin, U.S.A., 2003.

22. SADABS, *Program for Empirical Absorption Correction of Area Detector Data*; , G. M. SheldrickUniversity of Göttingen: Göttingen, Germany, 1997.

23. (a) *SMART*, version 5.625 and *SHELX-TL*, version 6.12;, Bruker AXS Inc.: Madison, Wisconsin, USA, 2000. (b) G. M. Sheldrick, *SHELXS-97* and *SHELXL-97*; University of Göttingen: Göttingen, Germany, 1997.

24. A. L. Spek, *PLATON, A Multipurpose Crystallographic Tool*, Utrecht University: Utrecht, Netherlands, 2002.

25. L. J. Barbour, *X-Seed*, *Graphical Interface to SHELX-97 and POV-Ray*, *Program for Better Quality of Crystallographic Figures*; University of Missouri-Columbia, Missouri, U.S.A., 1999.

26. Powder Cell, A Program for Structure Visualization, Powder Pattern Calculation and Profile Fitting, http://www.ccp14.ac.uk/index.html, 2013.

27. T. Higuchi, K. A. Connors, *Adv. Anal. Chem. Instrum*. 1965, **4**, 117.

CHAPTER SEVEN

CONCLUSIONS AND FUTURE PROSPECTS

This thesis deals with the identification, characterization and application of various single and multicomponent solid forms of Active pharmaceutical Ingredients (APIs). Extensive studies on various solid forms such as cocrystals (Chapter 2), drug polymorphs (Chapter 3 and 5), salts (Chapter 4), and salt polymorphs (Chapter 6) of several APIs were carried out with the intent of understanding the solid form diversity and to address the various problems associated with the APIs.

Febuxostat (FEB), which is used to treat hyperuricemia in patients with gout, is a low aqueous soluble (12.9 mg/L) drug. In chapter 2, our aim was to improve the aqueous solubility and stability of FEB through cocrystals using appropriate GRAS coformers. The justification for making cocrystals of FEB comes from the fact that its sodium salt (of the carboxylic acid functionality) is known to precipitate with uric acid forming sodium urate crystals, which cause acute pain at the joints, thus justifying the need to study cocrystals as a potential alternative to salts. In addition to the crystal structure of a guest-free form of FEB, five new cocrystals are reported for the first time. Furthermore, the extensive polymorphism characteristic of this API appears to be controlled in that no polymorphic cocrystals were observed in our study. The crystal structure of FEB has COOH$\cdots$N$\equiv$C hydrogen bond whereas the cocrystal structures are sustained by acid–amide (urea and nicotinamide cocrystals) and acid–acid synthons (para-aminobenzoic acid cocrystal). We report that FEB–NIC cocrystal as a preferable candidate for further development because it exhibits both good dissolution rate (36.6 times faster than FEB) and high stability under ICH conditions of 75% RH at 40 °C. In short, we have highlighted that cocrystals represent a viable alternative for an ionizable API to improve solubility wherein salt formation is not an option.

In chapter 3, an exhaustive polymorphic screen of the well-known antibiotic drug Trimethoprim (TMP) resulted in four anhydrous polymorphs (Forms 1, 2, 3, and 4) and a TMP hemihydrate form. The polymorphs were characterized by spectroscopic (FT-IR and Raman, ^{15}N ss-NMR), thermal (DSC, HSM), field emission scanning electron microscopy (FESEM), and powder X-ray diffraction (PXRD). Crystal structure analysis of Form 1 and 2 showed that both the structures are sustained by N–H⋯N$_{arom}$ hydrogen bonds and the main difference is R_2^2 (8) type I and type II motifs in Form 1, and R_2^2 (8) type III and R_3^2 (8) motifs in Form 2. Thus Form 1 and Form 2 can be classified as synthon and packing polymorphs. The major intermolecular interactions were quantified by Hirshfeld surface analysis and the stability order was rationalized by the percentage of strong H bond contribution. Based on DSC thermograms, the relative thermodynamic relationships (enantiotropic or monotropic) of TMP polymorphic pairs were evaluated. DVS analysis revealed that all the TMP forms show negligible moisture uptake (< 0.3 %) even at high RH conditions. All the polymorphs were found to be stable for a test period of three months in accelerated ICH conditions of 40 ºC and 75% RH, except Form 3 which converted to Form 2. From slurry and grinding experiments Form 2, Form 3 and Form 4 found to be metastable with Form 1 being stable, and the stability order of the polymorphs follows the order Form 3 < Form 4 < Form 2 < Form 1 (most stable). We, therefore, establish from our extensive experimentation that TMP Form 1 is the most stable modification for drug formulation.

The main objective of chapter 4 is to address the poor aqueous solubility of antipsychotic drug Blonanserin (BLN). Liquid-assisted grinding and solvent evaporative crystallization of BLN with GRAS coformers resulted in four salts (BLNH$^+$–SUC$^-$, BLNH$^+$–NIA$^-$, BLNH$^+$–TsO$^-$ and BLNH$^+$–MSA$^-$), one salt hydrate (BLNH$^+$–MSA$^-$–H$_2$O), and one cocrystal (BLN–SBA) of higher solubility and dissolution rate. All the novel solid forms were characterized by thermal, spectroscopic and X-ray diffraction techniques. In all the crystal structures proton transferred to the piperazine N$_3$ atom of BLN and sustained by N$^+$–H⋯O$^-$ ionic H-bond, except in BLN–SBA which has neutral COOH⋯N (tertiary amine) H-bond. All the solid forms were stable in the laboratory storage conditions of ambient temperature and humidity over six months. These solid forms were tested in accelerated stability ICH conditions at 40 ºC and 75% RH and were found to be stable except BLNH$^+$–MSA$^-$ which converted to its monohydrate BLNH$^+$–MSA$^-$–H$_2$O after

one month. $BLNH^+–MSA^-–H_2O$ salt hydrate exhibited the highest solubility (742.9 mg/mL, 464 times) and dissolution rate (126 times) in 60% EtOH−water. Thus, we establish $BLNH^+–MSA^-–H_2O$ salt hydrate as a potential lead for further development in drug formulation of Blonanserin as a stable, soluble salt.

In chapter 5, polymorph screening was carried out on the anti-hyperammonemic drug N-Carbmoyl-L-glutamic acid (CGA). It was fully characterised and particular emphasis on stability relationship between polymorphs was highlighted. We found two polymorphs, Form-I and Form-II, and a degraded form hydantoin-5-propionic acid (5-HPA) from our screening experiments. We were successful in getting diffraction quality single crystals for all the forms and determined their X-ray crystal structures. The procedures were optimized to obtain each polymorph in bulk quantity for PXRD and DSC/DVS analysis. The main difference in synthons of these polymorphs is acid-acid catemer synthon in Form-I and acid-amide heterosynthon in Form-II. There are significant conformational differences between these synthon polymorphs hence, these forms can be called as conformational and synthon polymorphs. The higher density Form-I is thermodynamically stable and the dimorphs are monotropically related. The polymorphs were fully characterized by FT-IR, ^{13}C ss-NMR, DSC, FESEM, PXRD, and DVS techniques. Thermodynamic stability and phase transformations were established and furthermore the major intermolecular interactions in the two crystal structures were quantified through Hirshfeld surface analysis. Both polymorphs were stable for 2 months at ICH conditions of 40 ºC and 75% RH. DVS analysis showed that Form-I is more stable to moisture than Form-II. Slurry grinding, thermal stress, stability and DVS studies confirm the thermodynamic stability of Form-I and hence best candidate for formulation.

Polymorphism studies on multicomponent solids such as salts are comparatively smaller to single component ones in spite of vast applications of salts. In this context, in chapter 6, the intension was to understand the differences in solubility, dissolution and stability behaviour of Blonanserin (BLN) salt polymorphs. Various salt screening techniques such as liquid assisted grinding, dehydration, slurry crystallization, heating and solvent evaporative crystallization with GRAS molecules resulted dimorphs for $BLNH^+–Cl^-$, $BLNH^+–SUC^-$, $BLNH^+–MSA^-$ and a $BLNH^+–Cl^-$ monohydrate. These novel salt forms were characterized by spectroscopic (FT-IR, FT-Raman, ss-NMR), thermal (DSC, TGA

and HSM), and X-ray diffraction techniques. Structural analysis revealed that proton transferred from salt former to the piperazine N_3 atom of BLN and sustained by N^+–H···O^- ionic H-bond. Stability experiments at ICH conditions (40 °C, 75% RH) showed that dimorphs of $BLNH^+$–MSA^- (Form-I and II) were found to convert into $BLNH^+$–MSA^- monohydrated form, whereas dimorphs of $BLNH^+$–Cl^- (Form-I and II) and $BLNH^+$–SUC^- (Form-I and II) were found to be stable for 3 months. The relative stability studies gave the stability order: for $BLNH^+$–Cl^- salt, $BLNH^+$–Cl^- monohydrate > $BLNH^+$–Cl^-–Form-I > $BLNH^+$–Cl^-–Form-II, for $BLNH^+$–MSA^- salt, $BLNH^+$–MSA^-–Form-I > $BLNH^+$–MSA^-–Form-II, and for $BLNH^+$–SUC^- salt, $BLNH^+$–SUC^-–Form-II > $BLNH^+$–SUC^-–Form-I. In this chapter we have spotlighted screening of polymorphs for salts and found $BLNH^+$–SUC^-–Form-II as a promising candidate for formulation purpose with twin advantages of high solubility (468.8 mg/mL, 293 times) and excellent stability. Further, this chapter highlights the importance of selection of suitable polymorphic form of a salt as one of the most important activities that critically affect the successful development of a drug candidate.

In general for an ionisable drug salt formation is the first choice, however if making a salt form is detrimental for some reason then the cocrystallisation technique offers new avenues in addressing the issues associated with drug molecules. The recent release of guidelines on pharmaceutical cocrystals by US-FDA (in 2013) and EMA (in 2014), though contradictory, illustrates the importance of cocrystals in pharmaceutical field. EMA considers a drug cocrystal to be a 'New Active Substance (NAS)', if it differs in properties from parent drug, contrast to US-FDA which holds it to be a 'drug product intermediate' but not a new drug form. Together, there is an opportunity to exploit cocrystals to modulate physical properties of drugs as well as to safeguard intellectual property and commercial interests both in innovator and generic industry. For the drugs namely dapagliflozin, escitalopram and valproic acid, the marketed solid forms (dapagliflozin propylene glycol monohydrate, escitalopram oxalic acid oxalate and valproic acid sodium valproate respectively) come under the broad definition of cocrystals worked out by an Indo-US group in 2012. Thus, the future is bright for cocrystals and new research will see growth in the unexplored areas of designing ternary and higher-order structures, cocrystals between neutral and ionic species, thermodynamics of cocrystallization, etc. Making salt for a drug molecule is almost regular activity in pharmaceutical industry and to some extent in academics, however the

studies on polymorphic forms of the salts are comparatively limited, chapter 6 provides insight into the various properties of polymorphic salts. On the other hand, despite the long history of polymorphism in single component systems and prominent research area in the pharmaceutical industry, however it is still a challenge for some drug molecules and hence exploring various polymorphs is never ending and ever green process. In essence, studies and understanding of various solid forms that govern the physicochemical behaviour of pharmaceutical solids will lead to better medicines and also avoid pit-falls in drug commercialization.

ABOUT THE AUTHOR

D. Maddileti, son of Mr. D. Bichaiah and Mrs. D. Balamma, was born in Bavai Pally, Mahaboob Nagar, Telangana State, India. He received primary education at Zilla Parishad High School (ZPHS), Wanaparthy and secondary education at Andhra Pradesh Social Welfare Residential School (APSWRS), Madanapuram, Mahaboob Nagar. He completed Intermediate (M. P. C.) at APSWR Jr College for Boys, Shaik Pet, Hyderabad. He pursued Bachelor of Science (B.Sc., M. P. C) at Gayathri Degree College, Wanaparthy, Mahaboob Nagar, and Master of Science (M. Sc., Chemistry) at Indian Institute of Technology (IIT), Delhi. He qualified GATE examination in February 2008. In December 2008, he was awarded 'Junior Research Fellowship' (JRF) by Council for Scientific and Industrial Research (CSIR), New Delhi, upon qualifying CSIR-UGC-JRF National Entrance Examination. Then he joined (in 2009) Prof. Ashwini Nangia's Research Group, School of Chemistry, University of Hyderabad, as a PhD Student and was upgraded as a 'Senior Research Fellow' (SRF) in 2011.

LIST OF PUBLICATIONS

1. Blonanserin HCl Salt and its Monohydrate.
   D. Maddileti, Ranjit Thakuria, Suryanarayan Cherukuvada, and Ashwini Nangia. *CrystEngComm,* **2012**, *14*, 2367–2372.

2. Structural Motifs in Phenylbismuth Heterocyclic Carboxylates-Secondary Interactions leading to Oligomers.
   O. Anjaneyulu, **D. Maddileti**, and K. C. Kumara Swamy.
   Dalton Trans., **2012**, *41*, 1004–1012.

3. Soluble Cocrystals of the Xanthine Oxidase Inhibitor Febuxostat.
   D. Maddileti, S. K. Jayabun, and Ashwini Nangia.
   Cryst. Growth Des., **2013**, *13*, 3188–3196.

4. High Solubility Crystalline Pharmaceutical Forms of Blonanserin.
   D. Maddileti, Battini Swapna, and Ashwini Nangia.
   Cryst. Growth Des., **2014***, 14*, 2557–2570.

5. Cocrystals of the Tuberculosis Drug Isoniazid: Polymorphism, Isostructurality, and Stability.
   Battini Swapna, **D. Maddileti**, and Ashwini Nangia.
   Cryst. Growth Des., **2014***, 14,* 5991−6005.

6. Tetramorphs of the Antibiotic Drug Trimethoprim: Characterization and Stability.
   D. Maddileti, Battini Swapna, and Ashwini Nangia.
   Cryst. Growth Des., **2015***, 15*, 1745–1756.

7. Improved Stability of Fixed Dose Combination of Anti TB Drugs via Cocrystals.
   Sudhir Mittapalli, **D. Maddileti**, Battini Swapna, Suryanarayan Cherukuvada, and Ashwini Nangia.

Indian Patent, **2014**, Application No. 5833/CHE/2014.

8. Polymorphism in anti-hyperammonemic agent N-Carbmoyl-L-glutamic Acid.
   D. Maddileti, and Ashwini Nangia.
   *CrystEngComm,***2015**, DOI: 10.1039/C5CE00116A.

9. Solubility and Stability of Blonanserin Salt Polymorphs.
   D. Maddileti, CH. Sharath Chandra, Divya Kuravi, Battini Swapna, and Ashwini Nangia.
   (Manuscript under preparation).

10. Pharmacological Evaluation of N-Oxide Metabolites of Antipsychotic Drugs for Type 2 Diabetes.
    D. Maddileti, M. K. Chaithanya Mannava, Battini Swapna, Ruchi Tejpal, K. Durga Bhavani, U. B. Rao Khandavilli, Kusuma, V. Lavanya, K. Kanakaraju, K. Vishwanadh, Srikanth R Medipelli, and Ashwini Nangia.
    (Patent to be filed).

PARTICIPATION IN SYMPOSIA & CONFERENCES

1. Participated in "**5th Singapore India Collaborative and Cooperative Chemistry symposium**" held in University of Hyderabad, Hyderabad, February 20-21, 2009.

2. Participated in "**Symposium on Modern Trends in Inorganic Chemistry (MTIC-XIV)**" at University of Hyderabad, Hyderabad, December 10-13, 2011.

3. Participated in the "**International Conference on the Chemistry of Organic Solid state (ICCOSS) XX**" held at Indian Institute of Science, Bengalore, June 26-30, 2011.

4. Presented a poser entitled **"Blonanserin HCl salt and its monohydrate"** at the 2nd Indo-US Bilateral Meeting on "**The Evolving Role of Solid State Chemistry in Pharmaceutical Science**" held at Gurgaon, New Delhi, February 2-4, 2012.

5. Participated in "**Bruker Symposium on Pharmaceutical Solids**" at Hyderabad, by Bruker AXS GmbH, Germany and Bruker AXS, India, May 10, 2012.

6. Delivered an oral presentation entitled **"Soluble Cocrystals of the Xanthine Oxidase Inhibitor Febuxostat**" at "**Annual in House Symposium Chemfest 2013**" held at University of Hyderabad, Hyderabad, February 15-16, 2013.

7. Presented a poser entitled "**High Solubility Crystalline Pharmaceutical Forms of Blonanserin**" in "**8th CRSI-RSC Joint Symposium in Chemistry and 16th CRSI National Symposium in Chemistry**" at IIT Bombay, Bombay, February 6-9, 2014.